*International Tables for Crystallography* (2006). Vol. C, Chapter 4.4, pp. 430–487.

# 4.4. Neutron techniques

By I. S. Anderson, P. J. Brown, J. M. Carpenter, G. Lander, R. Pynn, J. M. Rowe, O. Schärpf, V. F. Sears and B. T. M. Willis

## 4.4.1. Production of neutrons (By J. M. Carpenter and G. Lander)

The production of neutrons of sufficient intensity for scattering experiments is a 'big-machine' operation; there is no analogue to the small laboratory X-ray unit. The most common sources of neutrons, and those responsible for the great bulk of today's successful neutron scattering programs, are the nuclear reactors. These are based on the continuous, self-sustaining fission reaction. Research-reactor design emphasizes power density, that is the highest power within a small 'leaky' volume, whereas power reactors generate large amounts of power over a large core volume. In research reactors, fuel rods are of highly enriched $^{235}$U. Neutrons produced are distributed in a fission spectrum centred about 1 MeV: Most of the neutrons within the reactor are moderated (*i.e.* slowed down) by collisions in the cooling liquid, normally $D_2O$ or $H_2O$, and are absorbed in fuel to propagate the reaction. As large a fraction as possible is allowed to leak out as fast neutrons into the surrounding moderator ($D_2O$ and Be are best) and to slow down to equilibrium with this moderator. The neutron spectrum is Maxwellian with a mean energy of ~300 K (= 25 meV), which for neutrons corresponds to 1.8 Å since

$$E_n\,(\text{meV}) = 81.8/\lambda^2\ (\text{Å}^2).$$

Neutrons are extracted in beams through holes that penetrate the moderator.

There are two points to remember: (*a*) neutrons are neutral so that we cannot *focus* the beams and (*b*) the spectrum is broad and continuous; there is no analogy to the characteristic wavelength found with X-ray tubes, or to the high directionality of synchrotron-radiation sources.

Neutron production and versatility in reactors reached a new level with the construction of the High-Flux Reactor at the French-German-English Institut Laue-Langevin (ILL) in Grenoble, France. An overview of the reactor and beam-tube assembly is shown in Fig. 4.4.1.1. To shift the spectrum in energy, both a cold source (25 l of liquid deuterium at 25 K) and a hot source (graphite at 2400 K) have been inserted into the $D_2O$ moderator. Special beam tubes view these sources allowing a range of wavelengths from ~ 0.3 to ~17 Å to be used. Over 30 instruments are in operation at the ILL, which started in 1972.

The second method of producing neutrons, which historically predates the discovery of fission, is with charged particles ($\alpha$ particles, protons, *etc.*) striking a target nuclei. The most powerful source of neutrons of this type uses proton beams. These are accelerated in short bursts (< 1 μs) to 500–1000 MeV, and after striking the target produce an instantaneous supply of high-energy 'evaporation' neutrons. These extend up in energy close to that of the incident proton beam. Shielding for spallation sources tends to be even more massive than that for reactors. The targets, usually tungsten or uranium and typically much smaller than a reactor core, are surrounded by hydrogenous moderators such as polyethylene (often at different temperatures) to produce the 'slow' neutrons ($E_n$ < 10 eV) used in scattering experiments. The moderators are very different from those of reactors; they are designed to slow down neutrons rapidly and to let them leak out, rather than to store them for a long time. If the accelerated

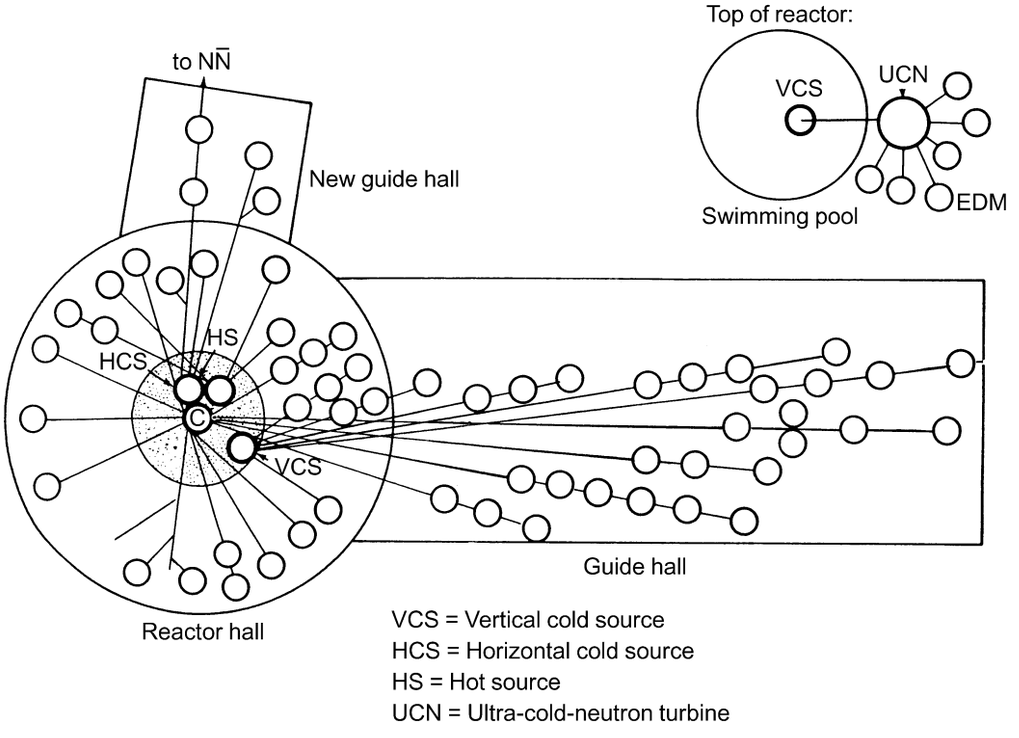


Fig. 4.4.1.1. A plane view of the installation at the Institut Laue–Langevin, Grenoble. Note especially the guide tubes exiting from the reactor that transport the neutron beams to a variety of instruments; these guide tubes are made of nickel-coated glass from which the neutrons are totally internally reflected.

particle pulse is short enough, the duration of the moderated neutron pulses is roughly inversely proportional to the neutron speed.

These accelerator-driven pulsed sources are pulsed at frequencies of between 10 and 100 Hz.

There are two fundamental differences between a reactor and a pulsed source.

(1) *All* experiments at a pulsed source must be performed with time-of-flight techniques. The pulsed source produces neutrons in bursts of 1 to 50 μs duration, depending on the energy, spaced about 10 to 100 ms apart, so that the duty cycle is low but there is very high neutron intensity within each pulse. The time-of-flight technique makes it possible to exploit that high intensity. With the de Broglie relationship, for neutrons

$$\lambda\,(\text{Å}) = 0.3966\,t\,(\mu s)/L\,(\text{cm}),$$

where $t$ is the flight time in μs and $L$ is the total flight path in cm.

(2) The spectral characteristics of pulsed sources are somewhat different from reactors in that they have a much larger component of higher-energy (above 100 meV) neutrons than the thermal spectrum at reactors. The exploitation of this new energy regime accompanied by the short pulse duration is one of the great opportunities presented by spallation sources.

Fig. 4.4.1.2 illustrates the essential difference between experiments at a steady-state source (left panel) and a pulsed source (right panel). We confine the discussion here to diffraction. If the time over which useful information is gathered is equivalent to the full period of the source $\Delta t$ (the case suggested by the lower-right figure), the *peak flux* of the pulsed source is the effective parameter to compare with the flux of the steady-state source. Often this is not the case, so one makes a comparison in terms of *time-averaged flux* (centre panel). For the pulsed source, this is lowered from the peak flux by the duty cycle, but with the time-of-flight method one uses a large interval of the spectrum (shaded area). For the steady-state source, the time-averaged flux is high, but only a small wavelength slice (stippled area) is used in the experiment. It is the *integrals* of the two areas which must be compared; for the pulsed sources now being designed, the integral is generally favourable compared with present-day reactors. Finally, one can see from the central panel that high-energy neutrons (100–1000 meV) are especially plentiful at the pulsed sources. These various features can be exploited in the design of different kinds of experiments at pulsed sources.

### 4.4.2. Beam-definition devices (By I. S. Anderson and O. Schärpf)

#### 4.4.2.1. *Introduction*

Neutron scattering, when compared with X-ray scattering techniques developed on modern synchrotron sources, is flux limited, but the method remains unique in the resolution and range of energy and momentum space that can be covered. Furthermore, the neutron magnetic moment allows details of microscopic magnetism to be examined, and polarized neutrons can be exploited through their interaction with both nuclear and electron spins.

Owing to the low primary flux of neutrons, the beam definition devices that play the role of defining the beam conditions (direction, divergence, energy, polarization, *etc.*) have to be highly efficient. Progress in the development of such devices not only results in higher-intensity beams but also allows new techniques to be implemented.

The following sections give a (non-exhaustive) review of commonly used beam-definition devices. The reader should keep in mind the fact that neutron scattering experiments are typically carried out with large beams (1 to 50 $\text{cm}^2$) and divergences between 5 and 30 mrad.

#### 4.4.2.2. *Collimators*

A collimator is perhaps the simplest neutron optical device and is used to define the direction and divergence of a neutron beam. The most rudimentary collimator consists of two slits or pinholes

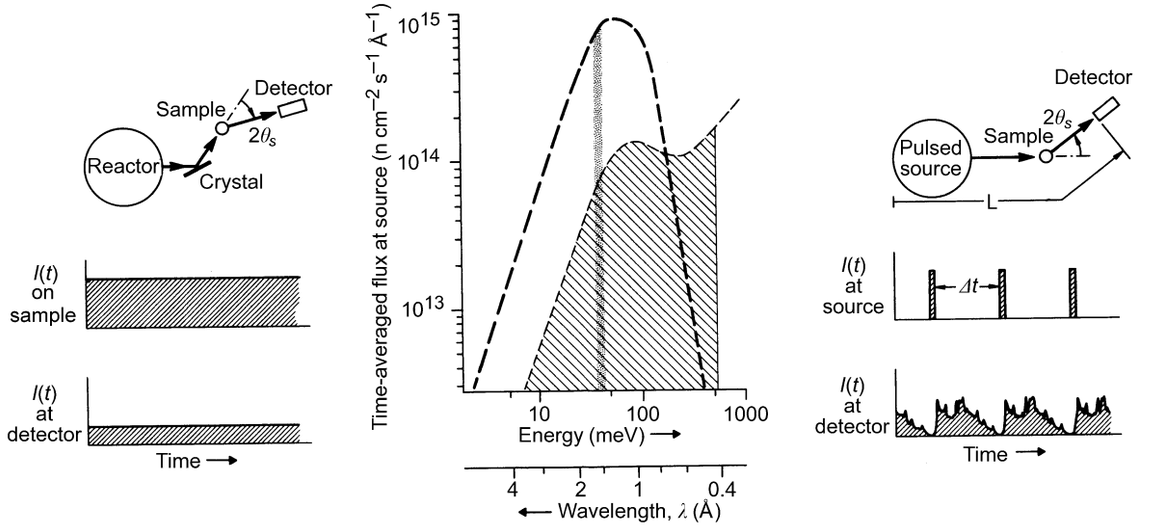


Fig. 4.4.1.2. Schematic diagram for performing diffraction experiments at steady-state and pulsed neutron sources. On the left we see the familiar monochromator crystal allowing a constant (in time) beam to fall on the sample (centre left), which then diffracts the beam through an angle $2\theta_s$ into the detector. The signal in the latter is also constant in time (lower left). On the right, the pulsed source allows a wide spectrum of neutrons to fall on the sample in sharp pulses separated by $\Delta t$ (centre right). The neutrons are then diffracted by the sample through $2\theta_s$ and their time of arrival in the detector is analysed (lower right). The centre figure shows the time-averaged flux at the source. At a reactor, we make use of a narrow band of neutrons (heavy shading), here chosen with $\lambda = 1.5$ Å. At a pulsed source, we use a wide spectral band, here chosen from 0.4 to 3 Å and each one is identified by its time-of-flight. For the experimentalist, an important parameter is the integrated area of the two-shaded areas. Here they have been made identical.

cut into an absorbing material and placed one at the beginning and one at the end of a collimating distance $L$. The maximum beam divergence that is transmitted with this configuration is

$$\alpha_{\max} = (a_1 + a_2)/L, \qquad (4.4.2.1)$$

where $a_1$ and $a_2$ are the widths of the slits or pinholes.

Such a device is normally used for small-angle scattering and reflectometry. In order to avoid parasitic scattering by reflection from slit edges, very thin sheets of a highly absorbing material, *e.g.* gadolinium foils, are used as the slit material. Sometimes wedge-formed cadmium plates are sufficient. In cases where a very precise edge is required, cleaved single-crystalline absorbers such as gallium gadolinium garnet (GGG) can be employed.

To avoid high intensity losses when the distances are large, sections of neutron guide can be introduced between the collimators, as in, for example, small-angle scattering instruments with variable collimation. In this case, for maximum intensity at a given resolution (divergence), the collimator length should be equal to the camera length, *i.e.* the sample–detector distance (Schmatz, Springer, Schelten & Ibel, 1974).

As can be seen from (4.4.2.1), the beam divergence from a simple slit or pinhole collimator depends on the aperture size. In order to collimate (in one dimension) a beam of large cross section within a reasonable distance $L$, Soller collimators, composed of a number of equidistant neutron absorbing blades, are used. To avoid losses, the blades must be as thin and as flat as possible. If their surfaces do not reflect neutrons, which can be achieved by using blades with rough surfaces or materials with a negative scattering length, such as foils of hydrogen-containing polymers (Mylar is commonly used) or paper coated with neutron-absorbing paint containing boron or gadolinium (Meister & Weckerman, 1973; Carlile, Hey & Mack, 1977), the angular dependence of the transmission function is close to the ideal triangular form, and transmissions of 96% of the theoretical value can be obtained with 10′ collimation. If the blades of the Soller collimator are coated with a material whose critical angle of reflection is equal to $\alpha_{\max}/2$ (for one particular wavelength), then a square angular transmission function is obtained instead of the normal triangular function, thus doubling the theoretical transmission (Meardon & Wroe, 1977).

Soller collimators are often used in combination with single-crystal monochromators to define the wavelength resolution of an instrument but the Soller geometry is only useful for one-dimensional collimation. For small-angle scattering applications, where two-dimensional collimation is required, a converging 'pepper pot' collimator can be used (Nunes, 1974; Glinka, Rowe & LaRock, 1986).

Cylindrical collimators with radial blades are sometimes used to reduce background scattering from the sample environment. This type of collimator is particularly useful with position-sensitive detectors and may be oscillated about the cylinder axis to reduce the shadowing effect of the blades (Wright, Berneron & Heathman, 1981).

### 4.4.2.3. *Crystal monochromators*

Bragg reflection from crystals is the most widely used method for selecting a well defined wavelength band from a white neutron beam. In order to obtain reasonable reflected intensities and to match the typical neutron beam divergences, crystals that reflect over an angular range of 0.2 to 0.5° are typically employed. Traditionally, mosaic crystals have been used in preference to perfect crystals, although reflection from a mosaic crystal gives rise to an increase in beam divergence with a concomitant broadening of the selected wavelength band. Thus, collimators are often used together with mosaic monochromators to define the initial and final divergences and therefore the wavelength spread.

Because of the beam broadening produced by mosaic crystals, it was soon recognised that elastically deformed perfect crystals and crystals with gradients in lattice spacings would be more suitable candidates for focusing applications since the deformation can be modified to optimize focusing for different experimental conditions (Maier-Leibnitz, 1969).

Perfect crystals are used commonly in high-energy-resolution backscattering instruments, interferometry and Bonse–Hart cameras for ultra-small-angle scattering (Bonse & Hart, 1965).

An ideal mosaic crystal is assumed to comprise an agglomerate of independently scattering domains or mosaic blocks that are more or less perfect, but small enough that primary extinction does not come into play, and the intensity reflected by each block may be calculated using the kinematic theory (Zachariasen, 1945; Sears, 1997). The orientation of the mosaic blocks is distributed inside a finite angle, called the mosaic spread, following a distribution that is normally assumed to be Gaussian. The ideal neutron mosaic monochromator is not an ideal mosaic crystal but rather a mosaic crystal that is sufficiently thick to obtain a high reflectivity. As the crystal thickness increases, however, secondary extinction becomes important and must be accounted for in the calculation of the reflectivity. The model normally used is that developed by Bacon & Lowde (1948), which takes into account strong secondary extinction and a correction factor for primary extinction (Freund, 1985). In this case, the mosaic spread (usually defined by neutron scatterers as the full width at half maximum of the reflectivity curve) is not an intrinsic crystal property, but increases with wavelength and crystal thickness and can become quite appreciable at longer wavelengths.

Ideal monochromator materials should have a large scattering-length density, low absorption, incoherent and inelastic cross sections, and should be available as large single crystals with a suitable defect concentration. Relevant parameters for some typical neutron monochromator crystals are given in Table 4.4.2.1.

In principle, higher reflectivities can be obtained in neutron monochromators that are designed to operate in reflection geometry, but, because reflection crystals must be very large when takeoff angles are small, transmission geometry may be used. In that case, the optimization of crystal thickness can only be achieved for a small wavelength range.

Nickel has the highest scattering-length density, but, since natural nickel comprises several isotopes, the incoherent cross section is quite high. Thus, isotopic $^{58}$Ni crystals have been grown as neutron monochromators despite their expense. Beryllium, owing to its large scattering-length density and low incoherent and absorption cross sections, is also an excellent candidate for neutron monochromators, but the mosaic structure of beryllium is difficult to modify, and the availability of good-quality single crystals is limited (Mücklich & Petzow, 1993). These limitations may be overcome in the near future, however, by building composite monochromators from thin beryllium blades that have been plastically deformed (May, Klimanek & Magerl, 1995).

Pyrolytic graphite is a highly efficient neutron monochromator if only a medium resolution is required (the minimum mosaic spread is of the order of 0.4°), owing to high reflectivities, which may exceed 90% (Shapiro & Chesser, 1972), but its use is limited to wavelengths above 1.5Å, owing to the rather large $d$ spacing of the 002 reflection. Whenever better resolution at

Table 4.4.2.1. *Some important properties of materials used for neutron monochromator crystals (in order of increasing unit-cell volume)*

| Material | Structure | Lattice constant(s) at 300 K $a, c$ (Å) | Unit-cell volume $V_0(10^{-24}$ cm$^3)$ | Coherent scattering length $b$ ($10^{-12}$ cm) | Square of scattering-length density $10^{-21}$ cm$^{-4}$ | Ratio of incoherent to total scattering cross section $\sigma_{\rm inc}/\sigma_s$ | Absorption cross section $\sigma_{\rm abs}$ (barns)* (at $\lambda = 1.8$ Å) | Atomic mass $A$ | Debye temperature $\theta_D$ (K) | $A\theta_D^2$ ($10^6$ K$^2$) |
|---|---|---|---|---|---|---|---|---|---|---|
| Beryllium | h.c.p | $a$ : 2.2856<br>$c$ : 3.5832 | 16.2 | 0.779 (1) | 9.25 | $6.5 \times 10^{-4}$ | 0.0076 (8) | 9.013 | 1188 | 12.7 |
| Iron | b.c.c. | $a$ : 2.8664 | 23.5 | 0.954 (6) | 6.59 | 0.033 | 2.56 (3) | 55.85 | 411 | 9.4 |
| Zinc | h.c.p. | $a$ : 2.6649<br>$c$ : 4.9468 | 30.4 | 0.5680 (5) | 1.50 | 0.019 | 1.11 (2) | 65.38 | 253 | 4.2 |
| Pyrolytic graphite | layer hexag. | $a$ : 2.461<br>$c$ : 6.708 | 35.2 | 0.66484 (13) | 5.71 | $< 2 \times 10^{-4}$ | 0.00350 (7) | 12.01 | 800 | 7.7 |
| Niobum | b.c.c. | 3.3006 | 35.9 | 0.7054 (3) | 1.54 | $4 \times 10^{-4}$ | 1.15 (5) | 92.91 | 284 | 7.5 |
| Nickel ($^{58}$Ni) | f.c.c. | 3.5241 | 43.8 | 1.44 (1) | 17.3 | 0 | 4.6 (3) | 58.71 | 417 | 9.9 |
| Copper | f.c.c. | 3.6147 | 47.2 | 0.7718 (4) | 4.28 | 0.065 | 3.78 (2) | 63.54 | 307 | 6.0 |
| Aluminium | f.c.c. | 4.0495 | 66.4 | 0.3449 (5) | 0.43 | $5.6 \times 10^{-3}$ | 0.231 (3) | 26.98 | 402 | 4.4 |
| Lead | f.c.c. | 4.9502 | 121 | 0.94003 (14) | 0.97 | $2.7 \times 10^{-4}$ | 0.171 (2) | 207.21 | 87 | 1.6 |
| Silicon | diamond | 5.4309 | 160 | 0.41491 (10) | 0.43 | $6.9 \times 10^{-3}$ | 0.171 (3) | 28.09 | 543 | 8.3 |
| Germanium | diamond | 5.6575 | 181 | 0.81929 (7) | 1.31 | 0.020 | 2.3 (2) | 72.60 | 290 | 6.1 |

* 1 barn= $10^{-28}$ m$^2$.

shorter wavelengths is required, copper (220 and 200) or germanium (311 and 511) monochromators are frequently used. The advantage of copper is that the mosaic structure can be easily modified by plastic deformation at high temperature. As with most face-centred cubic crystals, it is the (111) slip planes that are functional in generating the dislocation density needed for the desired mosaic spread, and, depending on the required orientation, either isotropic or anisotropic mosaics can be produced (Freund, 1976). The latter is interesting for vertical focusing applications, where a narrow vertical mosaic is required regardless of the resolution conditions.

Although both germanium and silicon are attractive as monochromators, owing to the absence of second-order neutrons for odd-index reflections, it is difficult to produce a controlled uniform mosaic spread in bulk samples by plastic deformation at high temperature because of the difficulty in introducing a spatially homogenous microstructure in large single crystals (Freund, 1975). Recently this difficulty has been overcome by building up composite monochromators from a stack of thin wafers, as originally proposed by Maier-Leibnitz (1967; Frey, 1974).

In practice, an artificial mosaic monochromator can be built up in two ways. In the first approach, illustrated in Fig. 4.4.2.1(*a*), the monochromator comprises a stack of crystalline wafers, each of which has a mosaic spread close to the global value required for the entire stack. Each wafer in the stack must be plastically deformed (usually by alternated bending) to produce the correct mosaic spread. For certain crystal orientations, the plastic deformation may result in an anisotropic mosaic spread. This method has been developed in several laboratories to construct germanium monochromators (Vogt, Passell, Cheung & Axe, 1994; Schefer *et al.*, 1996).

In the second approach, shown in Fig. 4.4.2.1(*b*), the global reflectivity distribution is obtained from the contributions of several stacked thin crystalline wafers, each with a rather narrow mosaic spread compared with the composite value but slightly misoriented with respect to the other wafers in the stack. If the misorientation of each wafer can be correctly controlled, this technique has the major advantage of producing monochromators with a highly anisotropic mosaic structure. The shape of the reflectivity curve can be chosen at will (Gaussian, Lorentzian, rectangular), if required. Moreover, because the initial mosaicity required is small, it is not necessary to use mosaic wafers and therefore for each wafer to undergo a long and tedious plastic deformation process. Recently, this method has been applied successfully to construct copper monochromators (Hamelin, Anderson, Berneron, Escoffier, Foltyn & Hehn, 1997), in which individual copper wafers were cut in a cylindrical form and then slid across one another to produce the required mosaic spread in the scattering plane. This technique looks very promising for the production of anisotropic mosaic monochromators.

The reflection from a mosaic crystal is visualized in Fig. 4.4.2.2(*b*). An incident beam with small divergence is transformed into a broad exit beam. The range of **k** vectors, $\Delta k$, selected in this process depends on the mosaic spread, $\eta$, and the incoming and outgoing beam divergences, $\alpha_1$ and $\alpha_2$.

$$\Delta k/k = \Delta\tau/\tau + \alpha\cot\theta, \tag{4.4.2.2}$$

where $\tau$ is the magnitude of the crystal reciprocal-lattice vector ($\tau = 2\pi/d$) and $\alpha$ is given by

$$\alpha = \sqrt{\frac{\alpha_1^2\alpha_2^2 + \alpha_1^2\eta^2 + \alpha_2^2\eta^2}{\alpha_1^2 + \alpha_2^2 + 4\eta^2.}} \tag{4.4.2.3}$$

The resolution can therefore be defined by collimators, and the highest resolution is obtained in backscattering, where the wavevector spread depends only on the intrinsic $\Delta d/d$ of the crystal.

In some applications, the beam broadening produced by mosaic crystals can be detrimental to the instrument performance. An interesting alternative is a gradient crystal, *i.e.* a single crystal with a smooth variation of the interplanar lattice spacing along a defined crystallographic direction. As shown in Fig. 4.4.2.2(*c*), the diffracted phase-space element has a different shape from that obtained from a mosaic crystal. Gradients in $d$ spacing can be produced in various ways,

including thermal gradients (Alefeld, 1972), vibrating crystals by piezoelectric excitation (Hock, Vogt, Kulda, Mursic, Fuess & Magerl, 1993), and mixed crystals with concentration gradients, *e.g.* Cu–Ge (Freund, Guinet, Maréschal, Rustichelli & Vanoni, 1972) and Si–Ge (Maier-Leibnitz & Rustichelli, 1968; Magerl, Liss, Doll, Madar & Steichele, 1994).

Both vertically and horizontally focusing assemblies of mosaic crystals are employed to make better use of the neutron flux when making measurements on small samples. Vertical focusing can lead to intensity gain factors of between two and five without affecting resolution (real-space focusing) (Riste, 1970; Currat, 1973). Horizontal focusing changes the $k$-space volume that is selected by the monochromator through the variation in Bragg angle across the monochromator surface ($k$-space focusing) (Scherm, Dolling, Ritter, Schedler, Teuchert & Wagner, 1977). The orientation of the diffracted $k$-space volume can be modified by variation of the horizontal curvature, so that the resolution of the monochromator may be optimized with respect to a particular sample or experiment without loss of illumination. Monochromatic focusing can be achieved. Furthermore, asymmetrically cut crystals may be used, allowing focusing effects in real space and $k$ space to be decoupled (Scherm & Kruger, 1994).

Traditionally, focusing monochromators consist of rectangular crystal plates mounted on an assembly that allows the orientation of each crystal to be varied in a correlated manner (Bührer, 1994). More recently, elastically deformed perfect crystals (in particular silicon) have been exploited as focusing elements for monochromators and analysers (Magerl & Wagner, 1994).

Since thermal neutrons have velocities that are of the order of km $s^{-1}$, their wavelengths can be Doppler shifted by diffraction from moving crystals. The $k$-space representation of the diffraction from a crystal moving perpendicular to its lattice planes is shown in Fig. 4.4.2.3(*a*). This effect is most commonly used in backscattering instruments on steady-state sources to vary the energy of the incident beam. Crystal velocities of 9–10 m $s^{-1}$ are practically achievable, corresponding to energy variations of the order of $\pm$ 60 μeV.

The Doppler shift is also important in determining the resolution of the rotating-crystal time-of-flight (TOF) spectrom-

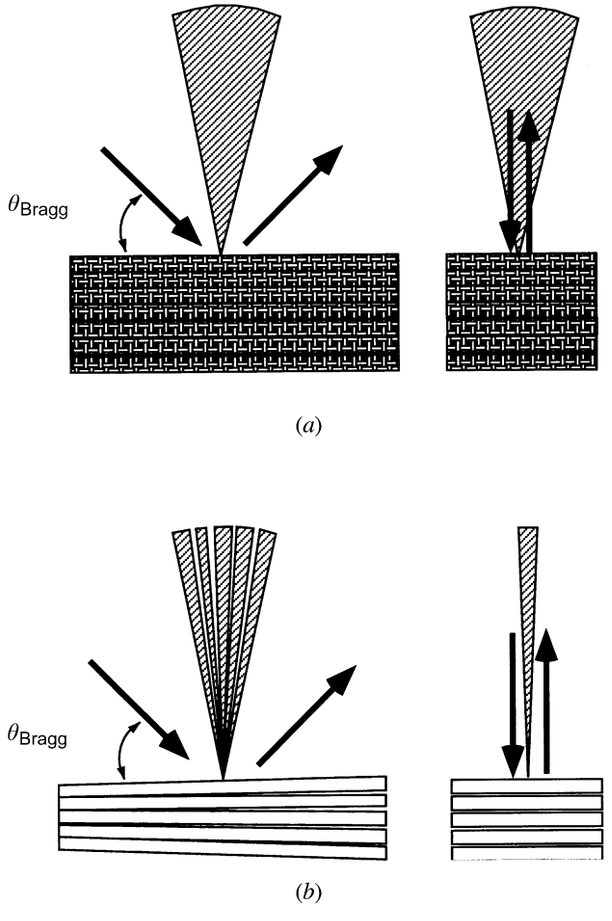


Fig. 4.4.2.1. Two methods by which artificial mosaic monochromators can be constructed: (*a*) out of a stack of crystalline wafers, each with a mosaicity close to the global value. The increase in divergence due to the mosaicity is the same in the horizontal (left picture) and the vertical (right picture) directions; (*b*) out of several stacked thin crystalline wafers each with a rather narrow mosaic but slightly misoriented in a perfectly controlled way. This allows the shape of the reflectivity curve to be rectangular, Gaussian, Lorentzian, *etc.*, and highly anisotropic, *i.e.* vertically narrow (right picture) and horizontally broad (left figure).

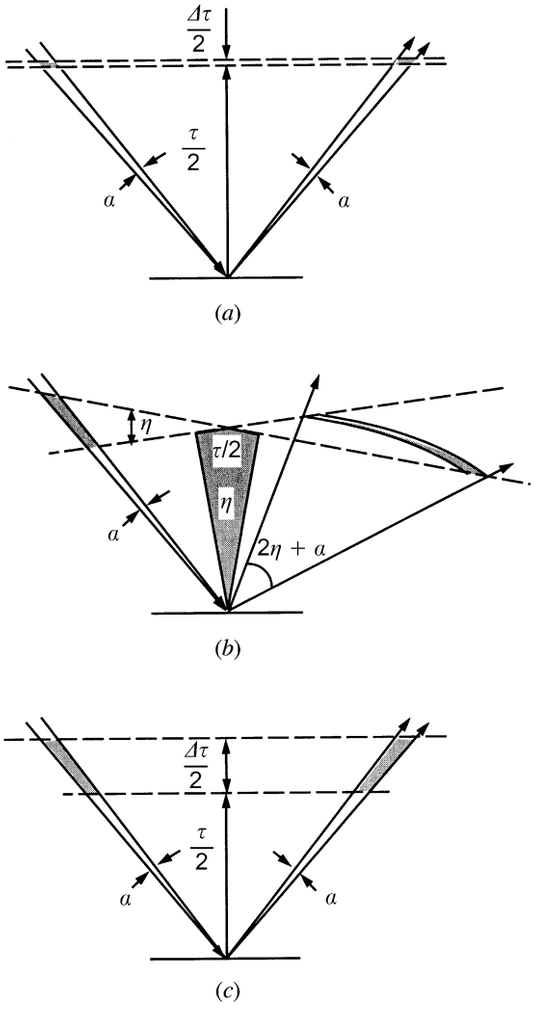


Fig. 4.4.2.2. Reciprocal-lattice representation of the effect of a monochromator with reciprocal-lattice vector $\tau$ on the reciprocal-space element of a beam with divergence $\alpha$. (*a*) For an ideal crystal with a lattice constant width $\Delta\tau$; (*b*) for a mosaic crystal with mosaicity $\eta$, showing that a beam with small divergence, $\alpha$, is transformed into a broad exit beam with divergence $2\eta + \alpha$; (*c*) for a gradient crystal with interplanar lattice spacing changing over $\Delta\tau$, showing that the divergence is not changed in this case.

eter, first conceived by Brockhouse (1958). A pulse of monochromatic neutrons is obtained when the reciprocal-lattice vector of a rotating crystal bisects the angle between two collimators. Effectively, the neutron **k** vector is changed in both direction and magnitude, depending on whether the crystal is moving towards or away from the neutron. For the rotating crystal, both of these situations occur simultaneously for different halves of the crystal, so that the net effect over the beam cross section is that a wider energy band is reflected than from the crystal at rest, and that, depending on the sense of rotation, the beam is either focused or defocused in time (Meister & Weckerman, 1972).

The Bragg reflection of neutrons from a crystal moving parallel to its lattice planes is illustrated in Fig. 4.4.2.3(*b*). It can be seen that the moving crystal selects a larger $\Delta k$ than the crystal at rest, so that the reflected intensity is higher. Furthermore, it is possible under certain conditions to orientate the diffracted phase-space volume orthogonal to the diffraction vector. In this way, a monochromatic divergent beam can be obtained from a collimated beam with a larger energy spread. This provides an elegant means of producing a divergent beam with a sufficiently wide momentum spread to be scanned by the Doppler crystal of a backscattering instrument (Schelten & Alefeld, 1984).

Finally, an alternative method of scanning the energy of a monochromator in backscattering is to apply a steady but uniform temperature variation. The monochromator crystal must have a reasonable thermal expansion coefficient, and care has to be taken to ensure a uniform temperature across the crystal.

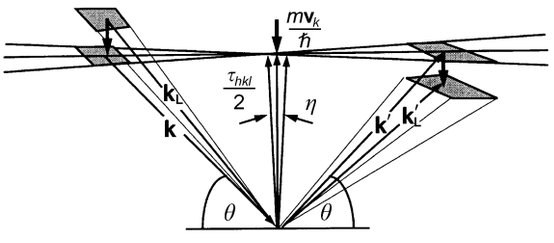


(*a*)

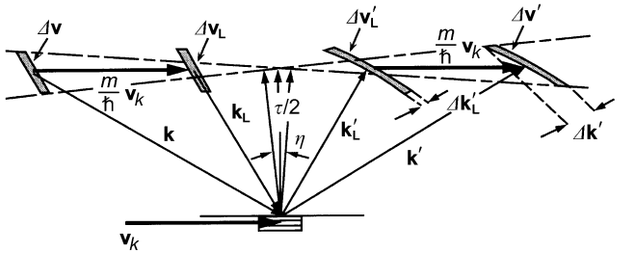


(*b*)

Fig. 4.4.2.3. Momentum-space representation of Bragg scattering from a crystal moving (*a*) perpendicular and (*b*) parallel to the diffracting planes with a velocity $\mathbf{v}_k$. The vectors $\mathbf{k}_L$ and $\mathbf{k}'_L$ refer to the incident and reflected wavevectors in the laboratory frame of reference. In (*a*), depending on the direction of $\mathbf{v}_k$, the reflected wavevector is larger or smaller than the incident wavevector, $\mathbf{k}_L$. In (*b*), a larger incident reciprocal-space volume, $\Delta\mathbf{v}_L$, is selected by the moving crystal than would have been selected by the crystal at rest. The reflected reciprocal-space element, $\Delta\mathbf{v}'_L$, has a large divergence, but can be arranged to be normal to $\mathbf{k}'_L$, hence improving the resolution $\Delta\mathbf{k}'_L$.

Table 4.4.2.2. *Neutron scattering-length densities, $Nb_{coh}$, for some commonly used materials*

| Material | $Nb$ ($10^{-6}$ Å$^{-2}$) |
|---|---|
| $^{58}$Ni | 13.31 |
| Diamond | 11.71 |
| Nickel | 9.40 |
| Quartz | 3.64 |
| Germanium | 3.62 |
| Silver | 3.50 |
| Aluminium | 2.08 |
| Silicon | 2.08 |
| Vanadium | −0.27 |
| Titanium | −1.95 |
| Manganese | −2.95 |

### 4.4.2.4. *Mirror reflection devices*

The refractive index, $n$, for neutrons of wavelength $\lambda$ propagating in a nonmagnetic material of atomic density $N$ is given by the expression

$$n^2 = 1 - \frac{\lambda^2 Nb_{\rm coh}}{\pi,} \qquad (4.4.2.4)$$

where $b_{\rm coh}$ is the mean coherent scattering length. Values of the scattering-length density $Nb_{\rm coh}$ for some common materials are listed in Table 4.4.2.2, from which it can be seen that the refractive index for most materials is slightly less than unity, so that total external reflection can take place. Thus, neutrons can be reflected from a smooth surface, but the critical angle of reflection, $\gamma_c$, given by

$$\gamma_c = \lambda \sqrt{\frac{Nb_{\rm coh}}{\pi}}, \qquad (4.4.2.5)$$

is small, so that reflection can only take place at grazing incidence. The critical angle for nickel, for example, is $0.1^\circ$ Å$^{-1}$.

Because of the shallowness of the critical angle, reflective optics are traditionally bulky, and focusing devices tend to have long focal lengths. In some cases, however, depending on the beam divergence, a long mirror can be replaced by an equivalent stack of shorter mirrors.

#### 4.4.2.4.1. *Neutron guides*

The principle of mirror reflection is the basis of neutron guides, which are used to transmit neutron beams to instruments that may be situated up to 100 m away from the source (Christ & Springer, 1962; Maier-Leibnitz & Springer, 1963). A standard neutron guide is constructed from boron glass plates assembled to form a rectangular tube, the dimensions of which may be up to 200 mm high by 50 mm wide. The inner surface of the guide is coated with approximately 1200 Å of either nickel, $^{58}$Ni ($\gamma_c = 0.12^\circ$ Å$^{-1}$), or a 'supermirror' (described below). The guide is usually evacuated to reduce losses due to absorption and scattering of neutrons in air.

Theoretically, a neutron guide that is fully illuminated by the source will transmit a beam with a square divergence of full width $2\gamma_c$ in both the horizontal and vertical directions, so that the transmitted solid angle is proportional to $\lambda^2$. In practice, owing to imperfections in the assembly of the guide system, the divergence profile is closer to Gaussian than square at the end of a long guide. Since the neutrons may undergo a large number of reflections in the guide, it is important to achieve a high reflectivity. The specular reflectivity is determined by the surface roughness, and typically values in the range 98.5 to 99% are

achieved. Further transmission losses occur due to imperfections in the alignment of the sections that make up the guide.

The great advantage of neutron guides, in addition to the transport of neutrons to areas of low background, is that they can be multiplexed, *i.e.* one guide can serve many instruments. This is achieved either by deflecting only a part of the total cross section to a given instrument or by selecting a small wavelength range from the guide spectrum. In the latter case, the selection device (usually a crystal monochromator) must have a high transmission at other wavelengths.

If the neutron guide is curved, the transmission becomes wavelength dependent, as illustrated in Fig. 4.4.2.4. In this case, one can define a characteristic wavelength, $\lambda^*$, given by the relation $\theta^* = \sqrt{2a/\rho}$, so that

$$\lambda^* = \sqrt{\frac{\pi}{Nb_{\rm coh}}}\sqrt{\frac{2a}{\rho}} \qquad (4.4.2.6)$$

(where $a$ is the guide width and $\rho$ the radius of curvature), for which the theoretical transmission drops to 67%. For wavelengths less than $\lambda^*$, neutrons can only be transmitted by 'garland' reflections along the concave wall of the curved guide. Thus, the guide acts as a low-pass energy filter as long as its length is longer than the direct line-of-sight length $L_1 = \sqrt{8a\rho}$. For example, a 3 cm wide nickel-coated guide whose characteristic wavelength is 4 Å (radius of curvature 1300 m) must be at least 18 m long to act as a filter. The line-of-sight length can be reduced by subdividing the guide into a number of narrower channels, each of which acts as a miniguide. The resulting device, often referred to as a neutron bender, since deviation of the beam is achieved more rapidly, is used in beam deviators (Alefeld *et al.*, 1988) or polarizers (Hayter, Penfold & Williams, 1978). A microbender was devised by Marx (1971) in which the channels were made by evaporating alternate layers of aluminium (transmission layer) and nickel (mirror layer) onto a flexible smooth substrate.

Tapered guides can be used to reduce the beam size in one or two dimensions (Rossbach *et al.*, 1988), although, since mirror reflection obeys Liouville's theorem, focusing in real space is achieved at the expense of an increase in divergence. This fact can be used to calculate analytically the expected gain in neutron flux at the end of a tapered guide (Anderson, 1988). Alternatively, focusing can be achieved in one dimension using a bender in which the individual channel lengths are adjusted to create a focus (Freund & Forsyth, 1979).

#### 4.4.2.4.2. *Focusing mirrors*

Optical imaging of neutrons can be achieved using ellipsoidal or torroidal mirrors, but, owing to the small critical angle of reflection, the dimensions of the mirrors themselves and the radii of curvature must be large. For example, a 4 m long toroidal mirror has been installed at the IN15 neutron spin echo spectrometer at the Institut Laue–Langevin, Grenoble (Hayes *et al.*, 1996), to focus neutrons with wavelengths greater than 15Å. The mirror has an in-plane radius of curvature of 408.75 m, and the sagittal radius is 280 mm. A coating of $^{65}$Cu is used to obtain a high critical angle of reflection while maintaining a low surface roughness. Slope errors of less than $2.5 \times 10^{-5}$ rad (r.m.s.) combined with a surface roughness of less than 3Å allow a minimum resolvable scattering vector of about $5 \times 10^{-4}$ Å$^{-1}$ to be reached.

For best results, the slope errors and the surface roughness must be low, in particular in small-angle scattering applications, since diffuse scattering from surface roughness gives rise to a halo around the image point. Owing to its low thermal expansion coefficient, highly polished Zerodur is often chosen as substrate.

#### 4.4.2.4.3. *Multilayers*

Schoenborn, Caspar & Kammerer (1974) first pointed out that multibilayers, comprising alternating thin films of different scattering-length densities ($Nb_{\rm coh}$) act like two-dimensional crystals with a $d$ spacing given by the bilayer period. With modern deposition techniques (usually sputtering), uniform films of thickness ranging from about twenty to a few hundred ångströms can be deposited over large surface areas of the order of 1 m$^2$. Owing to the rather large $d$ spacings involved, the Bragg reflection from multilayers is generally at grazing incidence, so that long devices are required to cover a typical beam width, or a stacked device must be used. However, with judicious choice of the scattering-length contrast, the surface and interface roughness, and the number of layers, reflectivities close to 100% can be reached.

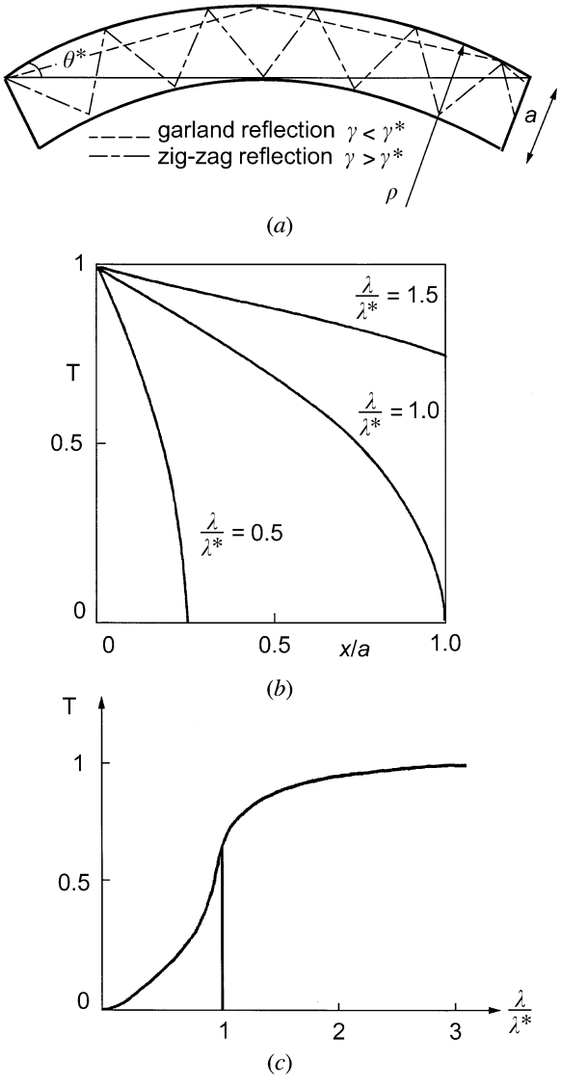


Fig. 4.4.2.4. In a curved neutron guide, the transmission becomes $\lambda$ dependent: (*a*) the possible types of reflection (garland and zig-zag), the direct line-of-sight length, the critical angle $\theta^*$, which is related to the characteristic wavelength $\lambda^* = \theta^*\sqrt{\pi/Nb_{\rm coh}}$; (*b*) transmission across the exit of the guide for different wavelengths, normalized to unity at the outside edge; (*c*) total transmission of the guide as a function of $\lambda$.

Fig. 4.4.2.5 illustrates how variation in the bilayer period can be used to produce a monochromator (the minimum $\Delta\lambda/\lambda$ that can be achieved is of the order of 0.5%), a broad-band device, or a 'supermirror', so called because it is composed of a particular sequence of bilayer thicknesses that in effect extends the region of total mirror reflection beyond the ordinary critical angle (Turchin, 1967; Mezei, 1976; Hayter & Mook, 1989). Supermirrors have been produced that extend the critical angle of nickel by a factor, $m$, of between three and four with reflectivities better than 90%. Such high reflectivities enable supermirror neutron guides to be constructed with flux gains, compared with nickel guides, close to the theoretical value of $m^2$.

The choice of the layer pairs depends on the application. For non-polarizing supermirrors and broad-band devices (Høghøj, Anderson, Ebisawa & Takeda, 1996), the Ni/Ti pair is commonly used, either pure or with some additions to relieve strain and stabilize interfaces (Elsenhans *et al.*, 1994) or alter the magnetism (Anderson & Høghøj, 1996), owing to the high contrast in scattering density, while for narrow-band monochromators a low contrast pair such as W/Si is more suitable.

#### 4.4.2.4.4. *Capillary optics*

Capillary neutron optics, in which hollow glass capillaries act as waveguides, are also based on the concept of total external reflection of neutrons from a smooth surface. The advantage of capillaries, compared with neutron guides, is that the channel sizes are of the order of a few tens of micrometres, so that the radius of curvature can be significantly decreased for a given characteristic wavelength [see equation (4.4.2.6)]. Thus, neutrons can be efficiently deflected through large angles, and the device can be more compact.

Two basic types of capillary optics exist, and the choice depends on the beam characteristics required. Polycapillary fibres are manufactured from hollow glass tubes several centimetres in diameter, which are heated, fused and drawn multiple times until bundles of thousands of micrometre-sized channels are formed having an open area of up to 70% of the cross section. Fibre outer diameters range from 300 to 600 μm and contain hundreds or thousands of individual channels with inner diameters between 3 and 50 μm. The channel cross section is usually hexagonal, though square channels have been produced, and the inner channel wall surface roughness is typically less than 10 Å r.m.s., giving rise to very high reflectivities. The principal limitations on transmission efficiency are the open area, the acceptable divergence (note that the critical angle for glass is 1 mrad $\text{Å}^{-1}$) and reflection losses due to absorption and scattering. A typical optical device will comprise hundreds or thousands of fibres threaded through thin screens to produce the required shape.

Fig. 4.4.2.6 shows typical applications of polycapillary devices. In Fig. 4.4.2.6(*a*), a polycapillary lens is used to refocus neutrons collected from a divergent source. The half lens depicted in Fig. 4.4.2.6(*b*) can be used either to produce a nearly parallel (divergence $= 2\gamma_c$) beam from a divergent source or (in the reverse sense) to focus a nearly parallel beam, *e.g.* from a neutron guide. The size of the focal point depends on the channel size, the beam divergence, and the focal length of the lens. For example, a polycapillary lens used in a prompt $\gamma$-activation analysis instrument at the National Institute of Standards and Technology to focus a cold neutron beam from a neutron guide results in a current density gain of 80 averaged over the focused beam size of 0.53 mm (Chen *et al.*, 1995).

Fig. 4.4.2.6(*c*) shows another simple application of polycapillaries as a compact beam bender. In this case, such a bender may be more compact than an equivalent multichannel guide bender, although the accepted divergence will be less. Furthermore, as with curved neutron guides, owing to the wavelength dependence of the critical angle the capillary curvature can be used to filter out thermal or high-energy neutrons.

It should be emphasized that the applications depicted in Fig. 4.4.2.6 obey Liouville's theorem, in that the density of neutrons in phase space is not changed, but the shape of the phase-space volume is altered to meet the requirements of the experiment,

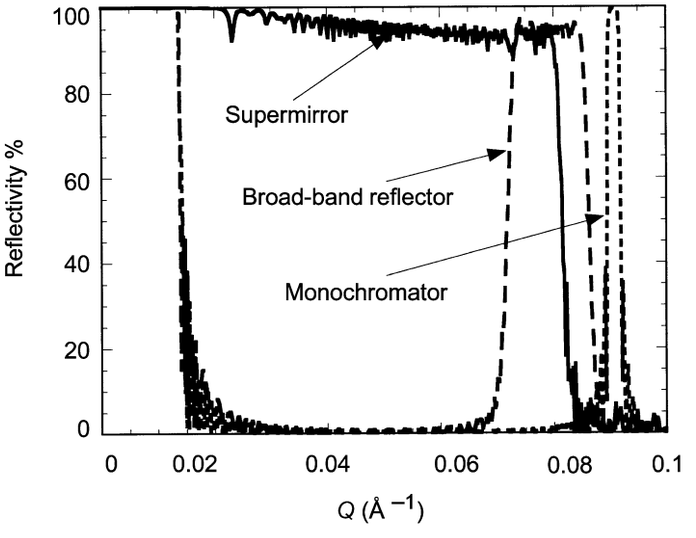


Fig. 4.4.2.5. Illustration of how a variation in the bilayer period can be used to produce a monochromator, a broad-band device, or a supermirror.

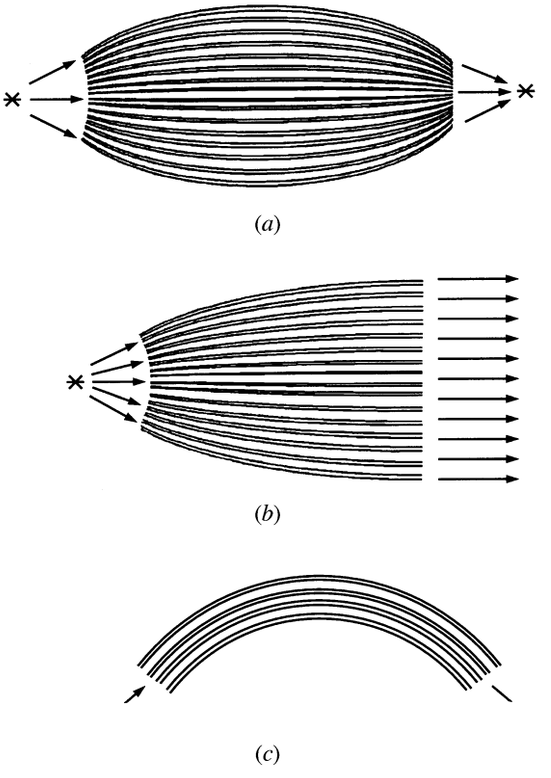


Fig. 4.4.2.6. Typical applications of polycapillary devices: (*a*) lens used to refocus a divergent beam; (*b*) half-lens to produce a nearly parallel beam or to focus a nearly parallel beam; (*c*) a compact bender.

*i.e.* there is a simple trade off between beam dimension and divergence.

The second type of capillary optic is a monolithic configuration. The individual capillaries in monolithic optics are tapered and fused together, so that no external frame assembly is necessary (Chen-Mayer *et al.*, 1996). Unlike the multifibre devices, the inner diameters of the channels that make up the monolithic optics vary along the length of the component, resulting in a smaller more compact design.

Further applications of capillary optics include small-angle scattering (Mildner, 1994) and lenses for high-spatial-resolution area detection.

#### 4.4.2.5. *Filters*

Neutron filters are used to remove unwanted radiation from the beam while maintaining as high a transmission as possible for the neutrons of the required energy. Two major applications can be identified: removal of fast neutrons and $\gamma$-rays from the primary beam and reduction of higher-order contributions ($\lambda/n$) in the secondary beam reflected from crystal monochromators. In this section, we deal with non-polarizing filters, *i.e.* those whose transmission and removal cross sections are independent of the neutron spin. Polarizing filters are discussed in the section concerning polarizers.

Filters rely on a strong variation of the neutron cross section with energy, usually either the wavelength-dependent scattering cross section of polycrystals or a resonant absorption cross section. Following Freund (1983), the total cross section determining the attenuation of neutrons by a crystalline solid can be written as a sum of three terms,

$$\sigma = \sigma_{\rm abs} + \sigma_{\rm tds} + \sigma_{\rm Bragg}. \qquad (4.4.2.7)$$

Here, $\sigma_{\rm abs}$ is the true absorption cross section, which, at low energy, away from resonances, is proportional to $E^{-1/2}$. The temperature-dependent thermal diffuse cross section, $\sigma_{\rm tds}$, describing the attenuation due to inelastic processes, can be split into two parts depending on the neutron energy. At low energy, $E \ll k_b\Theta_D$, where $k_b$ is Boltzmann's constant and $\Theta_D$ is the characteristic Debye temperature, single-phonon processes dominate, giving rise to a cross section, $\sigma_{\rm sph}$, which is also proportional to $E^{-1/2}$. The single-phonon cross section is proportional to $T^{7/2}$ at low temperatures and to $T$ at higher temperatures. At higher energies, $E \geq k_b\Theta_D$, multiphonon and multiple-scattering processes come into play, leading to a cross section, $\sigma_{\rm mph}$, that increases with energy and temperature. The third contribution, $\sigma_{\rm Bragg}$, arises due to Bragg scattering in single- or polycrystalline material. At low energies, below the Bragg cut-off ($\lambda > 2d_{\rm max}$), $\sigma_{\rm Bragg}$ is zero. In polycrystalline materials, the cross section rises steeply above the Bragg cut-off and oscillates with increasing energy as more reflections come into play. At still higher energies, $\sigma_{\rm Bragg}$ decreases to zero.

In single-crystalline material above the Bragg cut-off, $\sigma_{\rm Bragg}$ is characterized by a discrete spectrum of peaks whose heights and widths depend on the beam collimation, energy resolution, and the perfection and orientation of the crystal. Hence a monocrystalline filter has to be tuned by careful orientation.

The resulting attenuation cross section for beryllium is shown in Fig. 4.4.2.7. Cooled polycrystalline beryllium is frequently used as a filter for neutrons with energies less than 5 meV, since there is an increase of nearly two orders of magnitude in the attenuation cross section for higher energies. BeO, with a Bragg cut-off at approximately 4 meV, is also commonly used.

Pyrolytic graphite, being a layered material with good crystalline properties along the $c$ direction but random orientation perpendicular to it, lies somewhere between a polycrystal and a single crystal as far as its attenuation cross section is concerned. The energy-dependent cross section for a neutron beam incident along the $c$ axis of a pyrolytic graphite filter is shown in Fig. 4.4.2.8, where the attenuation peaks due to the $00\xi$ reflections can be seen. Pyrolytic graphite serves as an efficient second- or third-order filter (Shapiro & Chesser, 1972) and can be 'tuned' by slight misorientation away from the $c$ axis.

Further examples of typical filter materials (*e.g.* silicon, lead, bismuth, sapphire) can be found in the paper by Freund (1983).

Resonant absorption filters show a large increase in their attenuation cross sections at the resonant energy and are therefore used as selective filters for that energy. A list of typical filter materials and their resonance energies is given in Table 4.4.2.3.

#### 4.4.2.6. *Polarizers*

Methods used to polarize a neutron beam are many and varied, and the choice of the best technique depends on the instrument and the experiment to be performed. The main parameter that has to be considered when describing the effectiveness of a given polarizer is the polarizing efficiency, defined as

$$P = (N_+ - N_-)/(N_+ + N_-), \qquad (4.4.2.8)$$

where $N_+$ and $N_-$ are the numbers of neutrons with spin parallel (+) or antiparallel (−) to the guide field in the outgoing beam. The second important factor, the transmission of the wanted spin state, depends on various factors, such as acceptance angles, reflection, and absorption.

##### 4.4.2.6.1. *Single-crystal polarizers*

The principle by which ferromagnetic single crystals are used to polarize and monochromate a neutron beam simultaneously is shown in Fig. 4.4.2.9. A field **B**, applied perpendicular to the scattering vector $\boldsymbol{\kappa}$, saturates the atomic moments $\mathbf{M}_\nu$ along the field direction. The cross section for Bragg reflection in this geometry is

$$(\mathrm{d}\sigma/\mathrm{d}\Omega) = F_N(\boldsymbol{\kappa})^2 + 2F_N(\boldsymbol{\kappa})F_M(\boldsymbol{\kappa})(\mathbf{P}\cdot\boldsymbol{\mu}) + F_M(\boldsymbol{\kappa})^2, \quad (4.4.2.9)$$

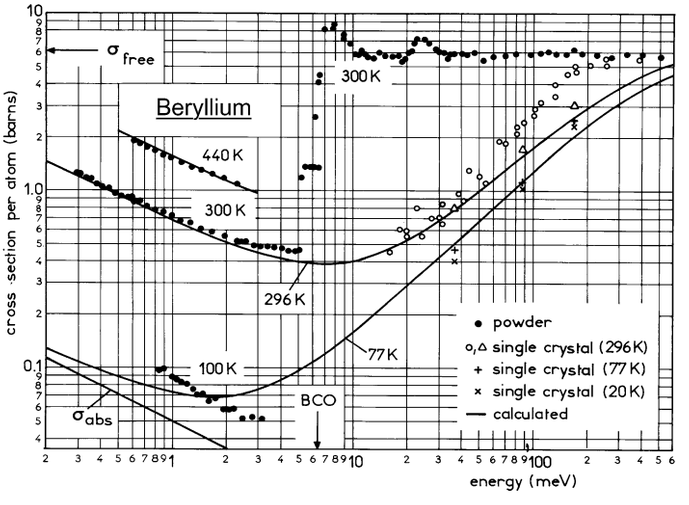


Fig. 4.4.2.7. Total cross section for beryllium in the energy range where it can be used as a filter for neutrons with energy below 5 meV (Freund, 1983).

Table 4.4.2.3. *Characteristics of some typical elements and isotopes used as neutron filters*

| Element or isotope | Resonance (eV) | $\sigma_s$ (resonance) (barns) | $\lambda$ (Å) | $\sigma_s(\lambda)$ (barns) | $\frac{\sigma_s(\lambda/2)}{\sigma_s(\lambda)}$ |
|---|---|---|---|---|---|
| In | 1.45 | 30000 | 0.48 | 94 | 319 |
| Rh | 1.27 | 4500 | 0.51 | 76 | 59.2 |
| Hf | 1.10 | 5000 | 0.55 | 58 | 86.2 |
| $^{240}$Pu | 1.06 | 115000 | 9.55 | 145 | 793 |
| Ir | 0.66 | 4950 | 0.70 | 183 | 27.0 |
| $^{229}$Th | 0.61 | 6200 | 0.73 | $<100$ | $>62.0$ |
| Er | 0.58 | 1500 | 0.75 | 127 | 11.8 |
| Er | 0.46 | 2300 | 0.84 | 125 | 18.4 |
| Eu | 0.46 | 10100 | 0.84 | 1050 | 9.6 |
| $^{231}$Pa | 0.39 | 4900 | 0.92 | 116 | 42.2 |
| $^{239}$Pu | 0.29 | 5200 | 1.06 | 700 | 7.4 |

1 barn $= 10^{-28}$ m$^2$.

where $F_N(\boldsymbol{\kappa})$ is the nuclear structure factor and $F_M(\boldsymbol{\kappa}) = [(\gamma/2)r_0] \sum_\nu M_\nu f(hkl) \exp[2\pi(hx + ky + lz)]$ is the magnetic structure factor, with $f(hkl)$ the magnetic form factor of the magnetic atom at the position $(x, y, z)$ in the unit cell. The vector $\mathbf{P}$ describes the polarization of the incoming neutron with respect to $\mathbf{B}$; $\mathbf{P} = 1$ for $+$ spins and $\mathbf{P} = -1$ for $-$ spins and $\boldsymbol{\mu}$ is a unit vector in the direction of the atomic magnetic moments. Hence, for neutrons polarized parallel to $\mathbf{B}$ $(\mathbf{P} \cdot \boldsymbol{\mu} = 1)$, the diffracted intensity is proportional to $[F_N(\boldsymbol{\kappa}) + F_M(\boldsymbol{\kappa})]^2$, while, for neutrons polarized antiparallel to $\mathbf{B}$ $(\mathbf{P} \cdot \boldsymbol{\mu} = -1)$, the diffracted intensity is proportional to $[F_N(\boldsymbol{\kappa}) - F_M(\boldsymbol{\kappa})]^2$. The polarizing efficiency of the diffracted beam is then

$$P = \pm 2F_N(\boldsymbol{\kappa})F_M(\boldsymbol{\kappa})/[F_N(\boldsymbol{\kappa})^2 + F_M(\boldsymbol{\kappa})^2], \qquad (4.4.2.10)$$

which can be either positive or negative and has a maximum value for $|F_N(\boldsymbol{\kappa})| = |F_M(\boldsymbol{\kappa})|$. Thus, a good single-crystal polarizer, in addition to possessing a crystallographic structure in which $F_N$ and $F_M$ are matched, must be ferromagnetic at room temperature and should contain atoms with large magnetic moments. Furthermore, large single crystals with 'controllable' mosaic should be available. Finally, the structure factor for the required reflection should be high, while those for higher-order reflections should be low.

None of the three naturally occurring ferromagnetic elements (iron, cobalt, nickel) makes efficient single-crystal polarizers. Cobalt is strongly absorbing and the nuclear scattering lengths of iron and nickel are too large to be balanced by their weak magnetic moments. An exception is $^{57}$Fe, which has a rather low nuclear scattering length, and structure-factor matching can be achieved by mixing $^{57}$Fe with Fe and 3% Si (Reed, Bolling & Harmon, 1973).

In general, in order to facilitate structure-factor matching, alloys rather than elements are used. The characteristics of some alloys used as polarizing monochromators are presented in Table 4.4.2.4. At short wavelengths, the 200 reflection of $Co_{0.92}Fe_{0.08}$ is used to give a positively polarized beam [$F_N(\boldsymbol{\kappa})$ and $F_M(\boldsymbol{\kappa})$ both positive], but the absorption due to cobalt is high. At longer wavelengths, the 111 reflection of the Heusler alloy $Cu_2MnAl$ (Delapalme, Schweizer, Couderchon & Perrier de la Bathie, 1971; Freund, Pynn, Stirling & Zeyen, 1983) is commonly used, since it has a higher reflectivity and a larger $d$ spacing than $Co_{0.92}Fe_{0.08}$. Since for the 111 reflection $F_N \approx -F_M$, the diffracted beam is negatively polarized. Unfortunately, the structure factor of the 222 reflection is higher than that of the 111 reflection, leading to significant higher-order contamination of the beam.

Other alloys that have been proposed as neutron polarizers are $Fe_{3-x}Mn_xSi$, $^7Li_{0.5}Fe_{2.5}O_4$ (Bednarski, Dobrzynski & Steinsvoll, 1980), $Fe_3Si$ (Hines *et al.*, 1976), $Fe_3Al$ (Pickart & Nathans, 1961), and $HoFe_2$ (Freund & Forsyth, 1979).

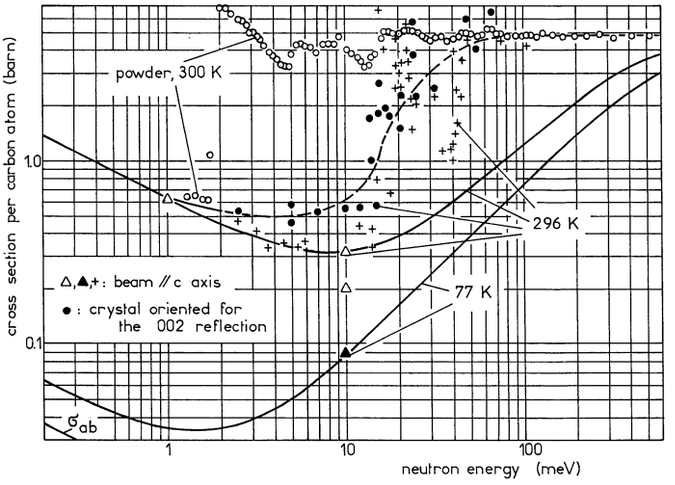


Fig. 4.4.2.8. Energy-dependent cross section for a neutron beam incident along the $c$ axis of a pyrolytic graphite filter. The attenuation peaks due to the $00\xi$ reflections can be seen.

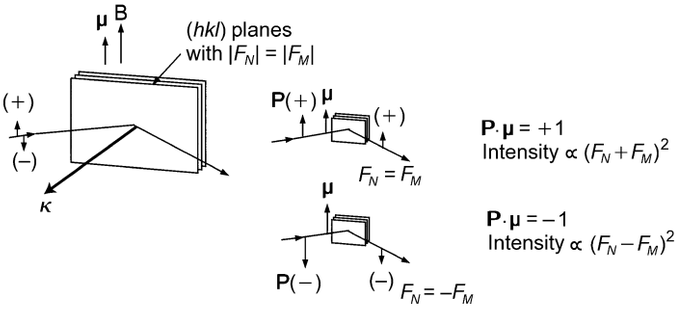


Fig. 4.4.2.9. Geometry of a polarizing monochromator showing the lattice planes $(hkl)$ with $|F_N| = |F_M|$, the direction of $\mathbf{P}$ and $\boldsymbol{\mu}$, the expected spin direction and intensity.

Table 4.4.2.4. *Properties of polarizing crystal monochromators (Williams, 1988)*

| | $Co_{0.92}Fe_{0.08}$ | $Cu_2MnAl$ | $Fe_3Si$ | $^{57}Fe$:Fe | $HoFe_2$ |
|---|---|---|---|---|---|
| Matched reflection $\|F_N\| \sim \|F_M\|$ | 200 | 111 | 111 | 110 | 620 |
| $d$ spacing (Å) | 1.76 | 3.43 | 3.27 | 2.03 | 1.16 |
| Take-off angle $2\theta_B$ at 1Å (°) | 33.1 | 16.7 | 17.6 | 28.6 | 50.9 |
| Cut-off wavelength, $\lambda_{max}$ (Å) | 3.5 | 6.9 | 6.5 | 4.1 | 2.3 |

#### 4.4.2.6.2. *Polarizing mirrors*

For a ferromagnetic material, the neutron refractive index is given by

$$n_{\pm}^2 = 1 - \lambda^2 N(b_{coh} \pm p)/\pi, \qquad (4.4.2.11)$$

where the magnetic scattering length, $p$, is defined by

$$p = 2\mu(B - H)m\pi/h^2N. \qquad (4.4.2.12)$$

Here, $m$ and $\mu$ are the neutron mass and magnetic moment, $B$ is the magnetic induction in an applied field $H$, and $h$ is Planck's constant.

The $-$ and $+$ signs refer, respectively, to neutrons whose moments are aligned parallel and antiparallel to $B$. The refractive index depends on the orientation of the neutron spin with respect to the film magnetization, thus giving rise to two critical angles of total reflection, $\gamma_-$ and $\gamma_+$. Thus, reflection in an angular range between these two critical angles gives rise to polarized beams in reflection and in transmission. The polarization efficiency, $P$, is defined in terms of the reflectivity $r_+$ and $r_-$ of the two spin states,

$$P = (r_+ - r_-)/(r_+ + r_-). \qquad (4.4.2.13)$$

The first polarizers using this principle were simple cobalt mirrors (Hughes & Burgy, 1950), while Schaerpf (1975) used FeCo sheets to build a polarizing guide. It is more common these days to use thin films of ferromagnetic material deposited onto a substrate of low surface roughness (*e.g.* float glass or polished silicon). In this case, the reflection from the substrate can be eliminated by including an antireflecting layer made from, for example, Gd–Ti alloys (Drabkin *et al.*, 1976). The major limitation of these polarizers is that grazing-incidence angles must be used and the angular range of polarization is small. This limitation can be partially overcome by using multilayers, as described above, in which one of the layer materials is ferromagnetic. In this case, the refractive index of the ferromagnetic material is matched for one spin state to that of the non-magnetic material, so that reflection does not occur. A polarizing supermirror made in this way has an extended angular range of polarization, as indicated in Fig. 4.4.2.10. It should be noted that modern deposition techniques allow the refractive index to be adjusted readily, so that matching is easily achieved. The scattering-length densities of some commonly used layer pairs are given in Table 4.4.2.5

Polarizing multilayers are also used in monochromators and broad-band devices. Depending on the application, various layer pairs have been used: Co/Ti, Fe/Ag, Fe/Si, Fe/Ge, Fe/W, FeCoV/TiN, FeCoV/TiZr, $^{63}Ni_{0.66}{}^{54}Fe_{0.34}$/V and the range of fields used to achieve saturation varies from about 100 to 500 Gs.

Polarizing mirrors can be used in reflection or transmission with polarization efficiencies reaching 97%, although, owing to the low incidence angles, their use is generally restricted to wavelengths above 2 Å.

Various devices have been constructed that use mirror polarizers, including simple reflecting mirrors, $V$-shaped transmission polarizers (Majkrzak, Nunez, Copley, Ankner & Greene, 1992), cavity polarizers (Mezei, 1988), and benders (Hayter, Penfold & Williams, 1978; Schaerpf, 1989). Perhaps the best known device is the polarizing bender developed by Schärpf. The device consists of 0.2 mm thick glass blades coated on both sides with a Co/Ti supermirror on top of an antireflecting Gd/Ti coating designed to reduce the scattering of the unwanted spin state from the substrate to a very low $Q$ value. The device is quite compact (typically 30 cm long for a beam cross section up to $6 \times 5$ cm) and transmits over 40% of an unpolarized beam with the collimation from a nickel-coated guide for wavelengths above 4.5 Å. Polarization efficiencies of over 96% can be achieved with these benders.

#### 4.4.2.6.3. *Polarizing filters*

Polarizing filters operate by selectively removing one of the neutron spin states from an incident beam, allowing the other spin state to be transmitted with only moderate attenuation. The spin selection is obtained by preferential absorption or scattering, so the polarizing efficiency usually increases with the thickness of the filter, whereas the transmission decreases. A compromise must therefore be made between polarization, $P$, and transmission, $T$. The 'quality factor' often used is $P\sqrt{T}$ (Tasset & Resouche, 1995).

The total cross sections for a generalized filter may be written as

$$\sigma_{\pm} = \sigma_0 \pm \sigma_p, \qquad (4.4.2.14)$$

where $\sigma_0$ is a spin-independent cross section and $\sigma_p = (\sigma_+ + \sigma_-)/2$ is the polarization cross section. It can be

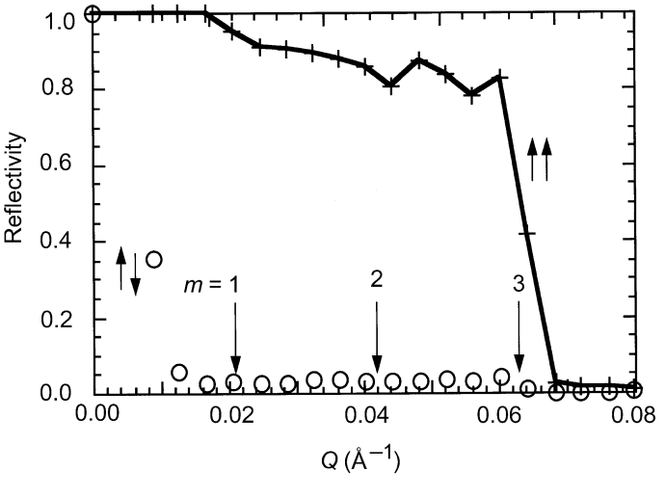


Fig. 4.4.2.10. Measured reflectivity curve of an FeCoV/TiZr polarizing supermirror with an extended angular range of polarization of three times that of $\gamma_c$(Ni) for neutrons without spin flip, ↑↑, and with spin flip, ↑↓.

Table 4.4.2.5. *Scattering-length densities for some typical materials used for polarizing multilayers*

| Magnetic layer | $N(b+p)$ ($10^{-6}$ Å$^{-2}$) | $N(b-p)$ ($10^{-6}$ Å$^{-2}$) | $Nb$ ($10^{-6}$ Å$^{-2}$) | Nonmagnetic layer |
|---|---|---|---|---|
| Fe | 13.04 | 3.08 | 3.64 | Ge |
| | | | 3.50 | Ag |
| | | | 3.02 | W |
| | | | 2.08 | Si |
| | | | 2.08 | Al |
| Fe:Co (50:50) | 10.98 | −0.52 | −0.27 | V |
| | | | −1.95 | Ti |
| Ni | 10.86 | 7.94 | | |
| Fe:Co:V (49:49:2) | 10.75 | −0.63 | −0.27 | V |
| | | | −1.95 | Ti |
| Fe:Co:V (50:48:2) | 10.66 | −0.64 | −0.27 | V |
| | | | −1.95 | Ti |
| Fe:Ni (50:50) | 10.53 | 6.65 | | |
| Co | 6.65 | −2.00 | −1.95 | Ti |
| Fe:Co:V (52:38:10) | 6.27 | 2.12 | 2.08 | Si |
| | | | 2.08 | Al |

For the non-magnetic layer we have only listed the simple elements that give a close match to the $N(b-p)$ value of the corresponding magnetic layer. In practice excellent matching can be achieved by using alloys (*e.g.* $Ti_xZr_y$ alloys allow Nb values between −1.95 and $3.03 \times 10^{-6}$Å$^{-2}$ to be selected) or reactive sputtering (*e.g.*$TiN_x$).

shown (Williams, 1988) that the ratio $\sigma_p/\sigma_0$ must be $\geq 0.65$ to achieve $|P| > 0.95$ and $T > 0.2$.

Magnetized iron was the first polarizing filter to be used (Alvarez & Bloch, 1940). The method relies on the spin-dependent Bragg scattering from a magnetized polycrystalline block, for which $\sigma_p$ approaches 10 barns near the Fe cut-off at 4 Å (Steinberger & Wick, 1949). Thus, for wavelengths in the range 3.6 to 4 Å, the ratio $\sigma_p/\sigma_0 \simeq 0.59$, resulting in a theoretical polarizing efficiency of 0.8 for a transmittance of $\sim 0.3$. In practice, however, since iron cannot be fully saturated, depolarization occurs, and values of $P \simeq 0.5$ with $T \sim 0.25$ are more typical.

Resonance absorption polarization filters rely on the spin dependence of the absorption cross section of polarized nuclei at their nuclear resonance energy and can produce efficient polarization over a wide energy range. The nuclear polarization is normally achieved by cooling in a magnetic field, and filters based on $^{149}$Sm ($E_r = 0.097$ eV) (Freeman & Williams, 1978) and $^{151}$Eu ($E_r = 0.32$ and 0.46 eV) have been successfully tested. The $^{149}$Sm filter has a polarizing efficiency close to 1 within a small wavelength range (0.85 to 1.1 Å), while the transmittance is about 0.15. Furthermore, since the filter must be operated at temperatures of the order of 15 mK, it is very sensitive to heating by $\gamma$-rays.

Broad-band polarizing filters, based on spin-dependent scattering or absorption, provide an interesting alternative to polarizing mirrors or monochromators, owing to the wider range of energy and scattering angle that can be accepted. The most promising such filter is polarized $^3$He, which operates through the huge spin-dependent neutron capture cross section that is totally dominated by the resonance capture of neutrons with antiparallel spin. The polarization efficiency of an $^3$He neutron spin filter of length $l$ can be written as

$$P_n(\lambda) = \tanh[\mathcal{O}(\lambda)P_{\rm He}], \qquad (4.4.2.15)$$

where $P_{\rm He}$ is the $^3$He polarization, and $\mathcal{O}(\lambda) = [^3\mathrm{He}]l\sigma_0(\lambda)$ is the dimensionless effective absorption coefficient, also called the opacity (Surkau *et al.*, 1997). For gaseous $^3$He, the opacity can be written in more convenient units as

$$\mathcal{O}' = p[\mathrm{bar}] \times l[\mathrm{cm}] \times \lambda[\text{Å}], \qquad (4.4.2.16)$$

where $p$ is the $^3$He pressure (1 bar = $10^5$ Pa) and $\mathcal{O} = 7.33 \times 10^{-2}\mathcal{O}'$. Similarly, the residual transmission of the spin filter is given by

$$T_n(\lambda) = \exp[-\mathcal{O}(\lambda)]\cosh[\mathcal{O}(\lambda)P_{\rm He}]. \qquad (4.4.2.17)$$

It can be seen that, even at low $^3$He polarization, full neutron polarization can be achieved in the limit of large absorption at the cost of the transmission.

$^3$He can be polarized either by spin exchange with optically pumped rubidium (Bouchiat, Carver & Varnum, 1960; Chupp, Coulter, Hwang, Smith & Welsh, 1996; Wagshul & Chupp, 1994) or by pumping of metastable $^3$He$^*$ atoms followed by metastable exchange collisions (Colegrove, Schearer & Walters, 1963). In the former method, the $^3$He gas is polarized at the required high pressure, whereas $^3$He$^*$ pumping takes place at a pressure of about 1 mbar, followed by a polarization conserving compression by a factor of nearly 10 000. Although the polarization time constant for Rb pumping is of the order of several hours compared with fractions of a second for $^3$He$^*$ pumping, the latter requires several 'fills' of the filter cell to achieve the required pressure.

An alternative broad-band spin filter is the polarized proton filter, which utilizes the spin dependence of nuclear scattering. The spin-dependent cross section can be written as (Lushchikov, Taran & Shapiro, 1969)

$$\sigma_\pm = \sigma_1 + \sigma_2 P_{\rm H}^2 \mp \sigma_3 P_{\rm H}, \qquad (4.4.2.18)$$

where $\sigma_1$, $\sigma_2$, and $\sigma_3$ are empirical constants. The viability of the method relies on achieving a high nuclear polarization $P_{\rm H}$. A polarization $P_{\rm H} = 0.7$ gives $\sigma_p/\sigma_0 \approx 0.56$ in the cold-neutron region. Proton polarizations of the order of 0.8 are required for a useful filter (Schaerpf & Stuesser, 1989). Polarized proton filters can polarize very high energy neutrons even in the eV range.

#### 4.4.2.6.4. *Zeeman polarizer*

The reflection width of perfect silicon crystals for thermal neutrons and the Zeeman splitting ($\Delta E = 2\mu B$) of a field of about 10 kGs are comparable and therefore can be used to polarize a neutron beam. For a monochromatic beam (energy $E_0$) in a strong magnetic field region, the result of the Zeeman splitting will be a separation into two polarized subbeams, one polarized along **B** with energy $E_0 + \mu B$, and the other polarized antiparallel to **B** with energy $E_0 - \mu B$. The two polarized beams can be selected by rocking a perfect crystal in the field region $B$ (Forte & Zeyen, 1989).

### 4.4.2.7. *Spin-orientation devices*

Polarization is the state of spin orientation of an assembly of particles in a target or beam. The beam polarization vector **P** is defined as the vector average of this spin state and is often described by the density matrix $\rho = \frac{1}{2}(1 + \sigma\mathbf{P})$. The polarization is then defined as $\mathbf{P} = \mathrm{Tr}(\rho\sigma)$. If the polarization vector is inclined to the field direction in a homogenous magnetic field, **B**, the polarization vector will precess with the classical Larmor frequency $\omega_L = |\gamma|B$. This results in a precessing spin polarization. For most experiments, it is sufficient to consider the linear polarization vector in the direction of an applied magnetic field. If, however, the magnetic field direction changes along the path of the neutron, it is also possible that the direction of **P** will change. If the frequency, $\Omega$, with which the magnetic field changes is such that

$$\Omega = \mathrm{d}(\mathbf{B}/|\mathbf{B}|)/\,\mathrm{d}t \ll \omega_L, \qquad (4.4.2.19)$$

then the polarization vector follows the field rotation adiabatically. Alternatively, when $\Omega \gg \omega_L$, the magnetic field changes so rapidly that **P** cannot follow, and the condition is known as non-adiabatic fast passage. All spin-orientation devices are based on these concepts.

#### 4.4.2.7.1. *Maintaining the direction of polarization*

A polarized beam will tend to become depolarized during passage through a region of zero field, since the field direction is ill defined over the beam cross section. Thus, in order to keep the polarization direction aligned along a defined quantization axis, special precautions must be taken.

The simplest way of maintaining the polarization of neutrons is to use a guide field to produce a well defined field **B** over the whole flight path of the beam. If the field changes direction, it has to fulfil the adiabatic condition $\Omega \ll \omega_L$, *i.e.* the field changes must take place over a time interval that is long compared with the Larmor period. In this case, the polarization follows the field direction adiabatically with an angle of deviation $\Delta\theta \leq 2\arctan(\Omega/\omega_L)$ (Schärpf, 1980).

Alternatively, some instruments (*e.g.* zero-field spin-echo spectrometers and polarimeters) use polarized neutron beams in regions of zero field. The spin orientation remains constant in a zero-field region, but the passage of the neutron beam into and out of the zero-field region must be well controlled. In order to provide a well defined region of transition from a guide-field region to a zero-field region, a non-adiabatic fast passage through the windings of a rectangular input solenoid can be used, either with a toroidal closure of the outside field or with a $\mu$-metal closure frame. The latter serves as a mirror for the coil ends, with the effect of producing the field homogeneity of a long coil but avoiding the field divergence at the end of the coil.

#### 4.4.2.7.2. *Rotation of the polarization direction*

The polarization direction can be changed by the adiabatic change of the guide-field direction so that the direction of the polarization follows it. Such a rotation is performed by a spin turner or spin rotator (Schärpf & Capellmann, 1993; Williams, 1988).

Alternatively, the direction of polarization can be rotated relative to the guide field by using the property of precession described above. If a polarized beam enters a region where the field is inclined to the polarization axis, then the polarization vector **P** will precess about the new field direction. The precession angle will depend on the magnitude of the field and the time spent in the field region. By adjustment of these two parameters together with the field direction, a defined, though wavelength-dependent, rotation of **P** can be achieved. A simple device uses the non-adiabatic fast passage through the windings of two rectangular solenoids, wound orthogonally one on top of the other. In this way, the direction of the precession field axis is determined by the ratio of the currents in the two coils, and the sizes of the fields determine the angle $\varphi$ of the precession. The orientation of the polarization vector can therefore be defined in any direction.

In order to produce a continuous rotation of the polarization, *i.e.* a well defined precession, as required in neutron spin-echo (NSE) applications, precession coils are used. In the simplest case, these are long solenoids where the change of the field integral over the cross section can be corrected by Fresnel coils (Mezei, 1972). More recently, Zeyen & Rem (1996) have developed and implemented optimal field-shape (OFS) coils. The field in these coils follows a cosine squared shape that results from the optimization of the line integral homogeneity. The OFS coils can be wound over a very small diameter, thereby reducing stray fields drastically.

#### 4.4.2.7.3. *Flipping of the polarization direction*

The term 'flipping' was originally applied to the situation where the beam polarization direction is reversed with respect to a guide field, *i.e.* it describes a transition of the polarization direction from parallel to antiparallel to the guide field and *vice versa*. A device that produces this 180° rotation is called a $\pi$ flipper. A $\pi/2$ flipper, as the name suggests, produces a 90° rotation and is normally used to initiate precession by turning the polarization at 90° to the guide field.

The most direct wavelength-independent way of producing such a transition is again a non-adiabatic fast passage from the region of one field direction to the region of the other field direction. This can be realized by a current sheet like the Dabbs foil (Dabbs, Roberts & Bernstein, 1955), a Kjeller eight (Abrahams, Steinsvoll, Bongaarts & De Lange, 1962) or a cryoflipper (Forsyth, 1979).

Alternatively, a spin flip can be produced using a precession coil, as described above, in which the polarization direction makes a precession of just $\pi$ about a direction orthogonal to the guide field direction (Mezei, 1972). Normally, two orthogonally wound coils are used, where the second, correction, coil serves to compensate the guide field in the interior of the precession coil. Such a flipper is wavelength dependent and can be easily tuned by varying the currents in the coils.

Another group of flippers uses the non-adiabatic transition through a well defined region of zero field. Examples of this type of flipper are the two-coil flipper of Drabkin, Zabidarov, Kasman & Okorokov (1969) and the line-shape flipper of Korneev & Kudriashov (1981).

Historically, the first flippers used were radio-frequency coils set in a homogeneous magnetic field. These devices are wavelength dependent, but may be rendered wavelength independent by replacing the homogeneous magnetic field with a gradient field (Egorov, Lobashov, Nazarento, Porsev & Serebrov, 1974).

In some devices, the flipping action can be combined with another selection function. The wavelength-dependent magnetic wiggler flipper proposed by Agamalyan, Drabkin & Sbitnev (1988) in combination with a polarizer can be used as a polarizing monochromator (Majkrzak & Shirane, 1982). Badurek & Rauch (1978) have used flippers as choppers to pulse a polarized beam.

In neutron resonance spin echo (NRSE) (Gähler & Golub, 1987), the precession coil of the conventional spin-echo configuration is replaced by two resonance spin flippers separated by a large zero-field region. The radio-frequency field of amplitude $B_1$ is arranged orthogonal to the DC field, $B_0$, with a frequency $\omega = \omega_L$, and an amplitude defined by the relation $\omega_1 \tau = \pi$, where $\tau$ is the flight time in the flipper coil and $\omega_1 = \gamma B_1$. In this configuration, the neutron spin precesses through an angle $\pi$ about the resonance field in each coil and leaves the coil with a phase angle $\varphi$. The total phase angle after passing through both coils, $\varphi = 2\omega L/v$, depends on the velocity $v$ of the neutron and the separation $L$ between the two coils. Thus, compared with conventional NSE, where the phase angle comes from the precession of the neutron spin in a strong magnetic field compared with a static flipper field, in NRSE the neutron spin does not precess, but the flipper field rotates. Effectively, the NRSE phase angle $\varphi$ is a factor of two larger than the NSE phase angle for the same DC field $B_0$. Furthermore, the resolution is determined by the precision of the RF frequencies and the zero-field flight path $L$ rather than the homogeneity of the line integral of the field in the NSE precession coil.

#### 4.4.2.8. *Mechanical choppers and selectors*

Thermal neutrons have relatively low velocities (a 4 Å neutron has a reciprocal velocity of approximately $1000\,\mu s\,m^{-1}$), so that mechanical selection devices and simple flight-time measurements can be used to make accurate neutron energy determinations.

Disc choppers rotating at speeds up to 20 000 revolutions per minute about an axis that is parallel to the neutron beam are used to produce a well defined pulse of neutrons. The discs are made from absorbing material (at least where the beam passes) and comprise one or more neutron-transparent apertures or slits. For polarized neutrons, these transparent slits should not be metallic, as the eddy currents in the metal moving in even a weak guide field will strongly depolarize the beam. The pulse frequency is determined by the number of apertures and the rotation frequency, while the duty cycle is given by the ratio of open time to closed time in one rotation. Two such choppers rotating in phase can be used to monochromate and pulse a beam simultaneously (Egelstaff, Cocking & Alexander, 1961). In practice, more than two choppers are generally used to avoid frame overlap of the incident and scattered beams. The time resolution of disc choppers (and hence the energy resolution of the instrument) is determined by the beam size, the aperture size and the rotation speed. For a realistic beam size, the rotation speed limits the resolution. Therefore, in modern instruments, it is normal to replace a single chopper with two counter-rotating choppers (Hautecler *et al.*, 1985; Copley, 1991). The low duty cycle of a simple disc chopper can be improved by replacing the single slit with a series of slits either in a regular sequence (Fourier chopper) (Colwell, Miller & Whittemore, 1968; Hiismäki, 1997) or a pseudostatistical sequence (pseudostatistical chopper) (Hossfeld, Amadori & Scherm, 1970), with duty cycles of 50 and 30%, respectively.

The Fermi chopper is an alternative form of neutron chopper that simultaneously pulses and monochromates the incoming beam. It consists of a slit package, essentially a collimator, rotating about an axis that is perpendicular to the beam direction (Turchin, 1965). For optimum transmission at the required wavelength, the slits are usually curved to provide a straight collimator in the neutron frame of reference. The curvature also eliminates the 'reverse burst', *i.e.* a pulse of neutrons that passes when the chopper has rotated by 180°.

A Fermi chopper with straight slits in combination with a monochromator assembly of wide horizontal divergence can be used to time focus a polychromatic beam, thus maintaining the energy resolution while improving the intensity (Blanc, 1983).

Velocity selectors are used when a continuous beam is required with coarse energy resolution. They exist in either multiple disc configurations or helical channels rotating about an axis parallel to the beam direction (Dash & Sommers, 1953). Modern helical channel selectors are made up of lightweight absorbing blades slotted into helical grooves on the rotation axis (Wagner, Friedrich & Wille, 1992). At higher energies where no suitable absorbing material is available, highly scattering polymers [poly(methyl methacrylate)] can be used for the blades, although in this case adequate shielding must be provided. The neutron wavelength is determined by the rotation speed, and resolutions, $\Delta\lambda/\lambda$, ranging from 5% to practically 100% ($\lambda/2$ filter) can be achieved. The resolution is fixed by the geometry of the device, but can be slightly improved by tilting the rotation axis or relaxed by rotating in the reverse direction for shorter wavelengths. Transmissions of up to 94% are typical.

### 4.4.3. Resolution functions (By R. Pynn and J. M. Rowe)

In a *Gedanken* neutron scattering experiment, neutrons of wavevector $\mathbf{k}_I$ impinge on a sample and the wavevector, $\mathbf{k}_F$, of the scattered neutrons is determined. A number of different types of spectrometer are used to achieve this goal (*cf.* Pynn, 1984). In each case, finite instrumental resolution is a result of uncertainties in the definition of $\mathbf{k}_I$ and $\mathbf{k}_F$. Propagation directions for neutrons are generally defined by Soller collimators for which the transmission as a function of divergence angle generally has a triangular shape. Neutron monochromatization may be achieved either by Bragg reflection from a (usually) mosaic crystal or by a time-of-flight method. In the former case, the mosaic leads to a spread of $|k_I|$ while, in the latter, pulse length and uncertainty in the lengths of flight paths (including sample size and detector thickness) produce a similar effect. Calculations of instrumental resolution are generally lengthy and lack of space prohibits their detailed presentation here. In the following paragraphs, the concepts involved are indicated and references to original articles are provided.

In resolution calculations for neutron spectrometers, it is usually assumed that the uncertainty of the neutron wavevector does not vary spatially across the neutron beam, although this reasoning may not apply to the case of small samples and compact spectrometers. To calculate the resolution of the spectrometer in the large-beam approximation, one writes the measured intensity $I$ as

$$I \propto \int \mathrm{d}^3k_i \int \mathrm{d}^3k_f P_i(\mathbf{k}_i) S(\mathbf{k}_i \rightarrow \mathbf{k}_f) P_f(\mathbf{k}_f), \qquad (4.4.3.1)$$

where $P_i(\mathbf{k}_i)$ is the probability that a neutron of wavevector $\mathbf{k}_i$ is incident on the sample, $P_f(\mathbf{k}_f)$ is the probability that a neutron of wavevector $\mathbf{k}_f$ is transmitted by the analyser system and $S(\mathbf{k}_i \rightarrow \mathbf{k}_f)$ is the probability that the sample scatters a neutron from $\mathbf{k}_i$ to $\mathbf{k}_f$. The fluctuation spectrum of the sample, $S(\mathbf{k}_i \rightarrow \mathbf{k}_f)$, does not depend separately on $\mathbf{k}_i$ and $\mathbf{k}_f$ but rather on the scattering vector $\mathbf{Q}$ and energy transfer $\hbar\omega$ defined by the conservation equations

$$\mathbf{Q} = \mathbf{k}_i - \mathbf{k}_f; \quad \hbar\omega = \frac{\hbar^2}{2m}(k_i^2 - k_f^2), \qquad (4.4.3.2)$$

where $m$ is the neutron mass.

A number of methods of calculating the distribution functions $P_i(\mathbf{k}_i)$ and $P_f(\mathbf{k}_f)$ have been proposed. The method of independent distributions was used implicitly by Stedman (1968) and in more detail by Bjerrum Møller & Nielson (MN) (Nielsen & Bjerrum Møller, 1969; Bjerrum Møller & Nielsen, 1970) for three-axis spectrometers. Subsequently, the method has been extended to perfect-crystal monochromators (Pynn, Fujii & Shirane, 1983) and to time-of-flight spectrometers (Steinsvoll, 1973; Robinson, Pynn & Eckert, 1985). The method involves separating $P_i$ and $P_f$ into a product of independent distribution functions each of which can be convolved separately with the fluctuation spectrum $S(\mathbf{Q}, \omega)$ [*cf.* equation (4.4.3.1)]. Extremely simple results are obtained for the widths of scans through a phonon dispersion surface for spectrometers where the energy of scattered neutrons is analysed (Nielson & Bjerrum Møller, 1969). For diffractometers, the width of a scan through a Bragg peak may also be obtained (Pynn *et al.*, 1983), yielding a result equivalent to that given by Caglioti, Paoletti & Ricci (1960). In this case, however, the singular nature of the Bragg scattering process introduces a correlation between the distribution functions that contribute to $P_i$ and $P_f$ and the calculation is less transparent than it is for phonons.

A somewhat different approach, which does not explicitly separate the various contributions to the resolution, was proposed by Cooper & Nathans (CN) (Cooper & Nathans, 1967, 1968; Cooper, 1968). Minor errors were corrected by several authors (Werner & Pynn, 1971; Chesser & Axe, 1973). The CN method calculates the instrumental resolution function $R(\mathbf{Q} - \mathbf{Q}_0, \omega - \omega_0)$ as

$$R(\Delta\mathbf{Q}, \Delta\omega) = R_0 \exp -\tfrac{1}{2} \sum_{\alpha,\beta} M_{\alpha\beta} X_\alpha X_\beta, \qquad (4.4.3.3)$$

where $X_1$, $X_2$, and $X_3$ are the three components of $\Delta\mathbf{Q}$, $X_4 = \Delta\omega$, and $\mathbf{Q}_0$ and $\omega_0$ are obtained from (4.4.3.2) by replacing $\mathbf{k}_i$ and $\mathbf{k}_f$ by $\mathbf{k}_I$ and $\mathbf{k}_F$, respectively. The matrix $\boldsymbol{M}$ is given in explicit form by several authors (Cooper & Nathans, 1967, 1968; Cooper, 1968; Werner & Pynn, 1971; Chesser & Axe, 1973) and the normalization $R_0$ has been discussed in detail by Dorner (1972). [A refutation (Tindle, 1984) of Dorner's work is incorrect.] Equation (4.4.3.3) implies that contours of constant transmission for the spectrometer [$R(\Delta\mathbf{Q}, \Delta\omega) = \text{constant}$] are ellipsoids in the four-dimensional $\mathbf{Q}$–$\omega$ space. Optimum resolution (focusing) is achieved by a scan that causes the resolution function to intersect the feature of interest in $S(\mathbf{Q}, \omega)$ (*e.g.* Bragg peak or phonon dispersion surface) for the minimum scan interval. The optimization of scans for a diffractometer has been considered by Werner (1971).

The MN and CN methods are equivalent. Using the MN formalism, it can be shown that

$$\boldsymbol{M} = (\boldsymbol{A})^{-1} \quad \text{with} \quad A_{\alpha\beta} = \sum_j \chi_{j\alpha} \chi_{j\beta}, \qquad (4.4.3.4)$$

where the $\chi_{j\alpha}$ are the components of the standard deviations of independent distributions (labelled by index $j$) defined by Bjerrum Møller & Nielsen (1970). In the limit $Q \rightarrow 0$, the matrices $\boldsymbol{M}$ and $\boldsymbol{A}$ are of rank three and other methods must be used to calculate the resolution ellipsoid (Mitchell, Cowley & Higgins, 1984). Nevertheless, the MN method may be used even in this case to calculate widths of scans.

To obtain the resolution function of a diffractometer (in which there is no analysis of scattered neutron energy) from the CN form for $\boldsymbol{M}$, it is sufficient to set to zero those contributions that arise from the mosaic of the analyser crystal. For elastic Bragg scattering, the problem is further simplified because $X_4$ [*cf.* equation (4.4.3.3)] is zero. The spectrometer resolution function is then an ellipsoid in $\mathbf{Q}$ space.

For the measurement of integrated intensities (of Bragg peaks for example), the normalization $R_0$ in (4.4.3.3) is required in order to obtain the Lorentz factor. The latter has been calculated for an arbitrary scan of a three-axis spectrometer (Pynn, 1975) and the results may be modified for a diffractometer as described in the preceding paragraph.

## 4.4.4. Scattering lengths for neutrons (By V. F. Sears)

The use of neutron diffraction for crystal-structure determinations requires a knowledge of the scattering lengths and the corresponding scattering and absorption cross sections of the elements and, in some cases, of individual isotopes. This information is needed to calculate unit-cell structure factors and to correct for effects such as absorption, self-shielding, extinction, thermal diffuse scattering, and detector efficiency (Bacon, 1975; Sears, 1989). Table 4.4.4.1 lists the best values of the neutron scattering lengths and cross sections that are available at the time of writing (January 1995). We begin by summarizing the basic relationships between the scattering lengths and cross sections of the elements and their isotopes that have been used in the compilation of this table. More background information can be found in, for example, the book by Sears (1989).

### 4.4.4.1. *Scattering lengths*

The scattering of a neutron by a single bound nucleus is described within the Born approximation by the Fermi pseudopotential,

$$V(\mathbf{r}) = \left(\frac{2\pi\hbar^2}{m}\right) b\delta(\mathbf{r}), \qquad (4.4.4.1)$$

in which $\mathbf{r}$ is the position of the neutron relative to the nucleus, $m$ the neutrons mass, and $b$ the bound scattering length. The neutron has spin $\mathbf{s}$ and the nucleus spin $\mathbf{I}$ so that, if $I \neq 0$, the Fermi pseudopotential and, hence, the bound scattering length will be spin dependent. Since $s = 1/2$, the most general rotationally invariant expression for $b$ is

$$b = b_c + \frac{2b_i}{\sqrt{I(I+1)}} \mathbf{s} \cdot \mathbf{I}, \qquad (4.4.4.2)$$

in which the coefficients $b_c$ and $b_i$ are called the bound coherent and incoherent scattering lengths. If $I = 0$, then $b_i = 0$ by convention.

Table 4.4.4.1. *Bound scattering lengths, b, in fm and cross sections, σ, in barns (1 barn = 100 fm²) of the elements and their isotopes*

$Z$: atomic number; $A$: mass number; $I(\pi)$: spin (parity) of the nuclear ground state; $c$: % natural abundance (for radioisotopes, the half-life is given instead in annums); $b_c$: bound coherent scattering length; $b_i$: bound incoherent scattering length; $\sigma_c$: bound coherent scattering cross section; $\sigma_i$: bound incoherent scattering cross section; $\sigma_s$: total bound scattering cross section; $\sigma_a$: absorption cross section for 2200 m s$^{-1}$ neutrons ($E$ = 25.30 meV, $k$ = 3.494 Å$^{-1}$, $\lambda$ = 1.798 Å); $i = \sqrt{-1}$.

| Element | $Z$ | $A$ | $I(\pi)$ | $c$ | $b_c$ | $b_i$ | $\sigma_c$ | $\sigma_i$ | $\sigma_s$ | $\sigma_a$ |
|---|---|---|---|---|---|---|---|---|---|---|
| H | 1 | | | | −3.7390(11) | | 1.7568(10) | 80.26(6) | 82.02(6) | 0.3326(7) |
| | | 1 | 1/2(+) | 99.985 | −3.7406(11) | 25.274(9) | 1.7583(10) | 80.27(6) | 82.03(6) | 0.3326(7) |
| | | 2 | 1(+) | 0.015 | 6.671(4) | 4.04(3) | 5.592(7) | 2.05(3) | 7.64(3) | 0.000519(7) |
| | | 3 | 1/2(+) | (12.32a) | 4.792(27) | −1.04(17) | 2.89(3) | 0.14(4) | 3.03(5) | 0 |
| He | 2 | | | | 3.26(3) | | 1.34(2) | 0.00 | 1.34(2) | 0.00747(1) |
| | | 3 | 1/2(+) | 0.00014 | 5.74(7) | −2.5(6) | 4.42(10) | 1.6(4) | 6.0(4) | 5333.(7.) |
| | | | | | −1.483(2)$i$ | +2.568(3)$i$ | | | | |
| | | 4 | 0(+) | 99.99986 | 3.26(3) | 0 | 1.34(2) | 0 | 1.34(2) | 0 |
| Li | 3 | | | | −1.90(2) | | 0.454(14) | 0.92(3) | 1.37(3) | 70.5(3) |
| | | 6 | 1(+) | 7.5 | 2.00(11) | −1.89(5) | 0.51(5) | 0.46(2) | 0.97(7) | 940.(4.) |
| | | | | | −0.261(1)$i$ | 0.257(11)$i$ | | | | |
| | | 7 | 3/2(−) | 92.5 | −2.22(2) | −2.49(5) | 0.619(11) | 0.78(3) | 1.40(3) | 0.0454(3) |
| Be | 4 | 9 | 3/2(−) | 100 | 7.79(1) | 0.12(3) | 7.63(2) | 0.0018(9) | 7.63(2) | 0.0076(8) |
| B | 5 | | | | 5.30(4) | | 3.54(5) | 1.70(12) | 5.24(11) | 767.(8.) |
| | | | | | 0.213(2)$i$ | | | | | |
| | | 10 | 3(+) | 20.0 | −0.1(3) | −4.7(3) | 0.144(8) | 3.0(4) | 3.1(4) | 3835.(9.) |
| | | | | | 1.066(3)$i$ | 1.231(3)$i$ | | | | |
| | | 11 | 3/2(−) | 80.0 | 6.65(4) | −1.3(2) | 5.56(7) | 0.22(6) | 5.78(9) | 0.0055(33) |
| C | 6 | | | | 6.6460(12) | | 5.550(2) | 0.001(4) | 5.551(3) | 0.00350(7) |
| | | 12 | 0(+) | 98.90 | 6.6511(16) | 0 | 5.559(3) | 0 | 5.559(3) | 0.00353(7) |
| | | 13 | 1/2(−) | 1.10 | 6.19(9) | −0.52(9) | 4.81(14) | 0.034(12) | 4.84(14) | 0.00137(4) |
| N | 7 | | | | 9.36(2) | | 11.01(5) | 0.50(12) | 11.51(11) | 1.90(3) |
| | | 14 | 1(+) | 99.63 | 9.37(2) | 2.0(2) | 11.03(5) | 0.5(1) | 11.53(11) | 1.91(3) |
| | | 15 | 1/2(−) | 0.37 | 6.44(3) | −0.02(2) | 5.21(5) | 0.00005(10) | 5.21(5) | 0.000024(8) |
| O | 8 | | | | 5.803(4) | | 4.232(6) | 0.000(8) | 4.232(6) | 0.00019(2) |
| | | 16 | 0(+) | 99.762 | 5.803(4) | 0 | 4.232(6) | 0 | 4.232(6) | 0.00010(2) |
| | | 17 | 5/2(+) | 0.038 | 5.78(12) | 0.18(6) | 4.20(22) | 0.004(3) | 4.20(22) | 0.236(10) |
| | | 18 | 0(+) | 0.200 | 5.84(7) | 0 | 4.29(10) | 0 | 4.29(10) | 0.00016(1) |
| F | 9 | 19 | 1/2(+) | 100 | 5.654(10) | −0.082(9) | 4.017(17) | 0.0008(2) | 4.018(14) | 0.0096(5) |
| Ne | 10 | | | | 4.566(6) | | 2.620(7) | 0.008(9) | 2.628(6) | 0.039(4) |
| | | 20 | 0(+) | 90.51 | 4.631(6) | 0 | 2.695(7) | 0 | 2.695(7) | 0.036(4) |
| | | 21 | 3/2(+) | 0.27 | 6.66(19) | ±0.6(1) | 5.6(3) | 0.05(2) | 5.7(3) | 0.67(11) |
| | | 22 | 0(+) | 9.22 | 3.87(1) | 0 | 1.88(1) | 0 | 1.88(1) | 0.046(6) |
| Na | 11 | 23 | 3/2(+) | 100 | 3.63(2) | 3.59(3) | 1.66(2) | 1.62(3) | 3.28(4) | 0.530(5) |
| Mg | 12 | | | | 5.375(4) | | 3.631(5) | 0.08(6) | 3.71(4) | 0.063(3) |
| | | 24 | 0(+) | 78.99 | 5.66(3) | 0 | 4.03(4) | 0 | 4.03(4) | 0.050(5) |
| | | 25 | 5/2(+) | 10.00 | 3.62(14) | 1.48(10) | 1.65(13) | 0.28(4) | 1.93(14) | 0.19(3) |
| | | 26 | 0(+) | 11.01 | 4.89(15) | 0 | 3.00(18) | 0 | 3.00(18) | 0.0382(8) |
| Al | 13 | 27 | 5/2(+) | 100 | 3.449(5) | 0.256(10) | 1.495(4) | 0.0082(7) | 1.503(4) | 0.231(3) |
| Si | 14 | | | | 4.1491(10) | | 2.1633(10) | 0.004(8) | 2.167(8) | 0.171(3) |
| | | 28 | 0(+) | 92.23 | 4.107(6) | 0 | 2.120(6) | 0 | 2.120(6) | 0.177(3) |
| | | 29 | 1/2(+) | 4.67 | 4.70(10) | 0.09(9) | 2.78(12) | 0.001(2) | 2.78(12) | 0.101(14) |
| | | 30 | 0(+) | 3.10 | 4.58(8) | 0 | 2.64(9) | 0 | 2.64(9) | 0.107(2) |
| P | 15 | 31 | 1/2(+) | 100 | 5.13(1) | 0.2(2) | 3.307(13) | 0.005(10) | 3.312(16) | 0.172(6) |
| S | 16 | | | | 2.847(1) | | 1.0186(7) | 0.007(5) | 1.026(5) | 0.53(1) |
| | | 32 | 0(+) | 95.02 | 2.804(2) | 0 | 0.9880(14) | 0 | 0.9880(14) | 0.54(4) |
| | | 33 | 3/2(+) | 0.75 | 4.74(19) | 1.5(1.5) | 2.8(2) | 0.3(6) | 3.1(6) | 0.54(4) |
| | | 34 | 0(+) | 4.21 | 3.48(3) | 0 | 1.52(3) | 0 | 1.52(3) | 0.227(5) |
| | | 36 | 0(+) | 0.02 | 3.(1.) $E$ | 0 | 1.1(8) | 0 | 1.1(8) | 0.15(3) |

Table 4.4.4.1. *Bound scattering lengths (cont.)*

| Element | $Z$ | $A$ | $I(\pi)$ | $c$ | $b_c$ | $b_i$ | $\sigma_c$ | $\sigma_i$ | $\sigma_s$ | $\sigma_a$ |
|---|---|---|---|---|---|---|---|---|---|---|
| Cl | 17 | | | | 9.5770(8) | | 11.526(2) | 5.3(5) | 16.8(5) | 33.5(3) |
| | | 35 | 3/2(+) | 75.77 | 11.65(2) | 6.1(4) | 17.06(6) | 4.7(6) | 21.8(6) | 44.1(4) |
| | | 37 | 3/2(+) | 24.23 | 3.08(6) | 0.1(1) | 1.19(5) | 0.001(3) | 1.19(5) | 0.433(6) |
| Ar | 18 | | | | 1.909(6) | | 0.458(3) | 0.22(2) | 0.683(4) | 0.675(9) |
| | | 36 | 0(+) | 0.337 | 24.90(7) | 0 | 77.9(4) | 0 | 77.9(4) | 5.2(5) |
| | | 38 | 0(+) | 0.063 | 3.5(3.5) | 0 | 1.5(3.1) | 0 | 1.5(3.1) | 0.8(2) |
| | | 40 | 0(+) | 99.600 | 1.830(6) | 0 | 0.421(3) | 0 | 0.421(3) | 0.660(9) |
| K | 19 | | | | 3.67(2) | | 1.69(2) | 0.27(11) | 1.96(11) | 2.1(1) |
| | | 39 | 3/2(+) | 93.258 | 3.74(2) | 1.4(3) | 1.76(2) | 0.25(11) | 2.01(11) | 2.1(1) |
| | | 40 | 4(−) | 0.012 | 3.(1.) *E* | | 1.1(8) | 0.5(5) | 1.6(9) | 35.(8.) |
| | | 41 | 3/2(+) | 6.730 | 2.69(8) | 1.5(1.5) | 0.91(5) | 0.3(6) | 1.2(6) | 1.46(3) |
| Ca | 20 | | | | 4.70(2) | | 2.78(2) | 0.05(3) | 2.83(2) | 0.43(2) |
| | | 40 | 0(+) | 96.941 | 4.80(2) | 0 | 2.90(2) | 0 | 2.90(2) | 0.41(2) |
| | | 42 | 0(+) | 0.647 | 3.36(10) | 0 | 1.42(8) | 0 | 1.42(8) | 0.68(7) |
| | | 43 | 7/2(−) | 0.135 | −1.56(9) | 0.31(4) | 0.5(5) *E* | | 0.8(5) | 6.2(6) |
| | | 44 | 0(+) | 2.086 | 1.42(6) | 0 | 0.25(2) | 0 | 0.25(2) | 0.88(5) |
| | | 46 | 0(+) | 0.004 | 3.6(2) | 0 | 1.6(2) | 0 | 1.6(2) | 0.74(7) |
| | | 48 | 0(+) | 0.187 | 0.39(9) | 0 | 0.019(9) | 0 | 0.019(9) | 1.09(14) |
| Sc | 21 | 45 | 7/2(−) | 100 | 12.29(11) | −6.0(3) | 19.0(3) | 4.5(5) | 23.5(6) | 27.5(2) |
| Ti | 22 | | | | −3.370(13) | | 1.427(11) | 2.63(3) | 4.06(3) | 6.43(6) |
| | | 46 | 0(+) | 8.2 | 4.725(5) | 0 | 2.80(6) | 0 | 2.80(6) | 0.59(18) |
| | | 47 | 5/2(−) | 7.4 | 3.53(7) | −3.5(2) | 1.57(6) | 1.5(2) | 3.1(2) | 1.7(2) |
| | | 48 | 0(+) | 73.8 | −5.86(2) | 0 | 4.32(3) | 0 | 4.32(3) | 8.30(9) |
| | | 49 | 7/2(−) | 5.4 | 0.98(5) | 5.1(2) | 0.12(1) | 3.3(3) | 3.4(3) | 2.2(3) |
| | | 50 | 0(+) | 5.2 | 5.88(10) | 0 | 4.34(15) | 0 | 4.34(15) | 0.179(3) |
| V | 23 | | | | −0.3824(12) | | 0.01838(12) | 5.08(6) | 5.10(6) | 5.08(2) |
| | | 50 | 6(+) | 0.250 | 7.6(6) | | 7.3(1.1) | 0.5(5) *E* | 7.8(1.0) | 60.(40.) |
| | | 51 | 7/2(−) | 99.750 | −0.402(2) | 6.435(4) | 0.0203(2) | 5.07(6) | 5.09(6) | 4.9(1) |
| Cr | 24 | | | | 3.635(7) | | 1.660(6) | 1.83(2) | 3.49(2) | 3.05(8) |
| | | 50 | 0(+) | 4.35 | −4.50(5) | 0 | 2.54(6) | 0 | 2.54(6) | 15.8(2) |
| | | 52 | 0(+) | 83.79 | 4.920(10) | 0 | 3.042(12) | 0 | 3.042(12) | 0.76(6) |
| | | 53 | 3/2(−) | 9.50 | −4.20(3) | 6.87(10) | 2.22(3) | 5.93(17) | 8.15(17) | 18.1(1.5) |
| | | 54 | 0(+) | 2.36 | 4.55(10) | 0 | 2.60(11) | 0 | 2.60(11) | 0.36(4) |
| Mn | 25 | 55 | 5/2(−) | 100 | −3.750(18) | 1.79(4) | 1.77(2) | 0.40(2) | 2.17(3) | 13.3(2) |
| Fe | 26 | | | | 9.45(2) | | 11.22(5) | 0.40(11) | 11.62(10) | 2.56(3) |
| | | 54 | 0(+) | 5.8 | 4.2(1) | 0 | 2.2(1) | 0 | 2.2(1) | 2.25(18) |
| | | 56 | 0(+) | 91.7 | 9.94(3) | 0 | 12.42(7) | 0 | 12.42(7) | 2.59(14) |
| | | 57 | 1/2(−) | 2.2 | 2.3(1) | 0.66(6) | | 0.3(3) *E* | 1.0(3) | 2.48(30) |
| | | 58 | 0(+) | 0.3 | 15.(7.) | 0 | 28.(26.) | 0 | 28.(26.) | 1.28(5) |
| Co | 27 | 59 | 7/2(−) | 100 | 2.49(2) | −6.2(2) | 0.779(13) | 4.8(3) | 5.6(3) | 37.18(6) |
| Ni | 28 | | | | 10.3(1) | | 13.3(3) | 5.2(4) | 18.5(3) | 4.49(16) |
| | | 58 | 0(+) | 68.27 | 14.4(1) | 0 | 26.1(4) | 0 | 26.1(4) | 4.6(3) |
| | | 60 | 0(+) | 26.10 | 2.8(1) | 0 | 0.99(7) | 0 | 0.99(7) | 2.9(2) |
| | | 61 | 3/2(−) | 1.13 | 7.60(6) | ±3.9(3) | 7.26(11) | 1.9(3) | 9.2(3) | 2.5(8) |
| | | 62 | 0(+) | 3.59 | −8.7(2) | 0 | 9.5(4) | 0 | 9.5(4) | 14.5(3) |
| | | 64 | 0(+) | 0.91 | −0.37(7) | 0 | 0.017(7) | 0 | 0.017(7) | 1.52(3) |
| Cu | 29 | | | | 7.718(4) | | 7.485(8) | 0.55(3) | 8.03(3) | 3.78(2) |
| | | 63 | 3/2(−) | 69.17 | 6.43(15) | 0.22(2) | 5.2(2) | 0.006(1) | 5.2(2) | 4.50(2) |
| | | 65 | 3/2(−) | 30.83 | 10.61(19) | 1.79(10) | 14.1(5) | 0.40(4) | 14.5(5) | 2.17(3) |
| Zn | 30 | | | | 5.60(5) | | 4.054(7) | 0.077(7) | 4.131(10) | 1.11(2) |
| | | 64 | 0(+) | 48.6 | 5.22(4) | 0 | 3.42(5) | 0 | 3.42(5) | 0.93(9) |
| | | 66 | 0(+) | 27.9 | 5.97(5) | 0 | 4.48(8) | 0 | 4.48(8) | 0.62(6) |
| | | 67 | 5/2(−) | 4.1 | 7.56(8) | −1.50(7) | 7.18(15) | 0.28(3) | 7.46(15) | 6.8(8) |
| | | 68 | 0(+) | 18.8 | 6.03(3) | 0 | 4.57(5) | 0 | 4.57(5) | 1.1(1) |
| | | 70 | 0(+) | 0.6 | 6.(1.) *E* | 0 | 4.5(1.5) | 0 | 4.5(1.5) | 0.092(5) |

Table 4.4.4.1. *Bound scattering lengths (cont.)*

| Element | $Z$ | $A$ | $I(\pi)$ | $c$ | $b_c$ | $b_i$ | $\sigma_c$ | $\sigma_i$ | $\sigma_s$ | $\sigma_a$ |
|---|---|---|---|---|---|---|---|---|---|---|
| Ga | 31 | | | | 7.288(2) | | 6.675(4) | 0.16(3) | 6.83(3) | 2.75(3) |
| | | 69 | 3/2(−) | 60.1 | 7.88(2) | −0.85(5) | 7.80(4) | 0.091(11) | 7.89(4) | 2.18(5) |
| | | 71 | 3/2(−) | 39.9 | 6.40(3) | −0.82(4) | 5.15(5) | 0.084(8) | 5.23(5) | 3.61(10) |
| Ge | 32 | | | | 8.185(20) | | 8.42(4) | 0.18(7) | 8.60(6) | 2.20(4) |
| | | 70 | 0(+) | 20.5 | 10.0(1) | 0 | 12.6(3) | 0 | 12.6(3) | 3.0(2) |
| | | 72 | 0(+) | 27.4 | 8.51(10) | 0 | 9.1(2) | 0 | 9.1(2) | 0.8(2) |
| | | 73 | 9/2(+) | 7.8 | 5.02(4) | 3.4(3) | 3.17(5) | 1.5(3) | 4.7(3) | 15.1(4) |
| | | 74 | 0(+) | 36.5 | 7.58(10) | 0 | 7.2(2) | 0 | 7.2(2) | 0.4(2) |
| | | 76 | 0(+) | 7.8 | 8.21(1.5) | 0 | 8.(3.) | 0 | 8.(3.) | 0.16(2) |
| As | 33 | 75 | 3/2(−) | 100 | 6.58(1) | −0.69(5) | 5.44(2) | 0.060(10) | 5.50(2) | 4.5(1) |
| Se | 34 | | | | 7.970(9) | | 7.98(2) | 0.33(6) | 8.30(6) | 11.7(2) |
| | | 74 | 0(+) | 0.9 | 0.8(3.0) | 0 | 0.1(6) | 0 | 0.1(6) | 51.8(1.2) |
| | | 76 | 0(+) | 9.0 | 12.2(1) | 0 | 18.7(3) | 0 | 18.7(3) | 85.(7.) |
| | | 77 | 1/2(−) | 7.6 | 8.25(8) | ±0.6(1.6) | 8.6(2) | 0.05(26) | 8.65(16) | 42.(4.) |
| | | 78 | 0(+) | 23.5 | 8.24(9) | 0 | 8.5(2) | 0 | 8.5(2) | 0.43(2) |
| | | 80 | 0(+) | 49.6 | 7.48(3) | 0 | 7.03(6) | 0 | 7.03(6) | 0.61(5) |
| | | 82 | 0(+) | 9.4 | 6.34(8) | 0 | 5.05(13) | 0 | 5.05(13) | 0.044(3) |
| Br | 35 | | | | 6.795(15) | | 5.80(3) | 0.10(9) | 5.90(9) | 6.9(2) |
| | | 79 | 3/2(−) | 50.69 | 6.80(7) | −1.1(2) | 5.81(12) | 0.15(6) | 5.96(13) | 11.0(7) |
| | | 81 | 3/2(−) | 49.31 | 6.79(7) | 0.6(1) | 5.79(12) | 0.05(2) | 5.84(12) | 2.7(2) |
| Kr | 36 | | | | 7.81(2) | | 7.67(4) | 0.01(14) | 7.68(13) | 25.(1.) |
| | | 78 | 0(+) | 0.35 | | 0 | | 0 | | 6.4(9) |
| | | 80 | 0(+) | 2.25 | | 0 | | 0 | | 11.8(5) |
| | | 82 | 0(+) | 11.6 | | 0 | | 0 | | 29.(20.) |
| | | 83 | 9/2(+) | 11.5 | | 185(30.) | | | | |
| | | 84 | 0(+) | 57.0 | | 0 | | 0 | | 0.113(15) |
| | | 86 | 0(+) | 17.3 | 8.1(2) | 0 | 8.2(4) | 0 | 8.2(4) | 0.003(2) |
| Rb | 37 | | | | 7.09(2) | | 6.32(4) | 0.5(4) | 6.8(4) | 0.38(4) |
| | | 85 | 5/2(−) | 72.17 | 7.03(10) | 6.2(2) | 0.5(5) | *E* | 6.7(5) | 0.48(1) |
| | | 87 | 3/2(−) | 27.83 | 7.23(12) | 6.6(2) | 0.5(5) | *E* | 7.1(5) | 0.12(3) |
| Sr | 38 | | | | 7.02(2) | | 6.19(4) | 0.06(11) | 6.25(10) | 1.28(6) |
| | | 84 | 0(+) | 0.56 | 7.(1.) *E* | 0 | 6.(2.) | 0 | 6.(2.) | 0.87(7) |
| | | 86 | 0(+) | 9.86 | 5.67(5) | 0 | 4.04(7) | 0 | 4.04(7) | 1.04(7) |
| | | 87 | 9/2(+) | 7.00 | 7.40(7) | 6.88(13) | 0.5(5) | *E* | 7.4(5) | 16.(3.) |
| | | 88 | 0(+) | 82.58 | 7.15(6) | 0 | 6.42(11) | 0 | 6.42(11) | 0.058(4) |
| Y | 39 | 89 | 1/2(−) | 100 | 7.75(2) | 1.1(3) | 7.55(4) | 0.15(8) | 7.70(9) | 1.28(2) |
| Zr | 40 | | | | 7.16(3) | | 6.44(5) | 0.02(15) | 6.46(14) | 0.185(3) |
| | | 90 | 0(+) | 51.45 | 6.4(1) | 0 | 5.1(2) | 0 | 5.1(2) | 0.011(5) |
| | | 91 | 5/2(+) | 11.32 | 8.7(1) | −1.08(15) | 9.5(2) | 0.15(4) | 9.7(2) | 1.17(10) |
| | | 92 | 0(+) | 17.19 | 7.4(2) | 0 | 6.9(4) | 0 | 6.9(4) | 0.22(6) |
| | | 94 | 0(+) | 17.28 | 8.2(2) | 0 | 8.4(4) | 0 | 8.4(4) | 0.0499(24) |
| | | 96 | 0(+) | 2.76 | 5.5(1) | 0 | 3.8(1) | 0 | 3.8(1) | 0.0229(10) |
| Nb | 41 | 93 | 9/2(+) | 100 | 7.054(3) | −0.139(10) | 6.253(5) | 0.0024(3) | 6.255(5) | 1.15(5) |
| Mo | 42 | | | | 6.715(2) | | 5.67(3) | 0.04(5) | 5.71(4) | 2.48(4) |
| | | 92 | 0(+) | 14.84 | 6.91(8) | 0 | 6.00(14) | 0 | 6.00(14) | 0.019(2) |
| | | 94 | 0(+) | 9.25 | 6.80(7) | 0 | 5.81(12) | 0 | 5.81(12) | 0.015(2) |
| | | 95 | 5/2(+) | 15.92 | 6.91(6) | 6.00(10) | 0.5(5) | *E* | 6.5(5) | 13.1(3) |
| | | 96 | 0(+) | 16.68 | 6.20(6) | 0 | 4.83(9) | 0 | 4.83(9) | 0.5(2) |
| | | 97 | 5/2(+) | 9.55 | 7.24(8) | 6.59(15) | 0.5(5) | *E* | 7.1(5) | 2.5(2) |
| | | 98 | 0(+) | 24.13 | 6.58(7) | 0 | 5.44(12) | 0 | 5.44(12) | 0.127(6) |
| | | 100 | 0(+) | 9.63 | 6.73(7) | 0 | 5.69(12) | 0 | 5.69(12) | 0.4(2) |
| Tc | 43 | | | | | | | | | |
| | | 99 | 9/2(+) | $(2.13\times10^5$a) | 6.8(3) | 5.8(5) | 0.5(5) | *E* | 6.3(7) | 20.(1.) |

Table 4.4.4.1. *Bound scattering lengths (cont.)*

| Element | $Z$ | $A$ | $I(\pi)$ | $c$ | $b_c$ | $b_i$ | $\sigma_c$ | $\sigma_i$ | $\sigma_s$ | $\sigma_a$ |
|---|---|---|---|---|---|---|---|---|---|---|
| Ru | 44 | | | | 7.03(3) | | 6.21(5) | 0.4(1) | 6.6(1) | 2.56(13) |
| | | 96 | 0(+) | 5.5 | 0 | 0 | 0.28(2) | | | |
| | | 98 | 0(+) | 1.9 | 0 | 0 | <8.0 | | | |
| | | 99 | 5/2(+) | 12.7 | 6.9(1.0) | | | | | |
| | | 100 | 0(+) | 12.6 | 0 | 0 | 4.8(6) | | | |
| | | 101 | 5/2(+) | 17.0 | 3.3(9) | | | | | |
| | | 102 | 0(+) | 31.6 | 0 | 0 | 1.17(7) | | | |
| | | 104 | 0(+) | 18.7 | 0 | 0 | 0.31(2) | | | |
| Rh | 45 | 103 | 1/2(−) | 100 | 5.88(4) | 4.34(6) | 0.3(3) | *E* | 4.6(3) | 144.8(7) |
| Pd | 46 | | | | 5.91(6) | | 4.39(9) | 0.093(9) | 4.48(9) | 6.9(4) |
| | | 102 | 0(+) | 1.02 | 7.7(7) *E* | 0 | 7.5(1.4) | 0 | 7.5(1.4) | 3.4(3) |
| | | 104 | 0(+) | 11.14 | 7.7(7) *E* | 0 | 7.5(1.4) | 0 | 7.5(1.4) | 0.6(3) |
| | | 105 | 5/2(+) | 22.33 | 5.5(3) | −2.6(1.6) | 3.8(4) | 0.8(1.0) | 4.6(1.1) | 20.(3.) |
| | | 106 | 0(+) | 27.33 | 6.4(4) | 0 | 5.1(6) | 0 | 5.1(6) | 0.304(29) |
| | | 108 | 0(+) | 26.46 | 4.1(3) | 0 | 2.1(3) | 0 | 2.1(3) | 8.5(5) |
| | | 110 | 0(+) | 11.72 | 7.7(7)*E* | 0 | 7.5(1.4) | 0 | 7.5(1.4) | 0.226(31) |
| Ag | 47 | | | | 5.922(7) | | 4.407(10) | 0.58(3) | 4.99(3) | 63.3(4) |
| | | 107 | 1/2(−) | 51.839 | 7.555(11) | 1.00(13) | 7.17(2) | 0.13(3) | 7.30(4) | 37.6(1.2) |
| | | 109 | 1/2(−) | 48.161 | 4.165(11) | −1.60(13) | 2.18(1) | 0.32(5) | 2.50(5) | 91.0(1.0) |
| Cd | 48 | | | | 4.87(5) | | 3.04(6) | 3.46(13) | 6.50(12) | 2520.(50.) |
| | | | | | −0.70(1)*i* | | | | | |
| | | 106 | 0(+) | 1.25 | 5.(2.) *E* | 0 | 3.1(2.5) | 0 | 3.1(2.5) | 1. |
| | | 108 | 0(+) | 0.89 | 5.4(1) | 0 | 3.7(1) | 0 | 3.7(1) | 1.1(3) |
| | | 110 | 0(+) | 12.51 | 5.9(1) | 0 | 4.4(1) | 0 | 4.4(1) | 11.(1.) |
| | | 111 | 1/2(+) | 12.81 | 6.5(1) | 5.3(2) | 0.3(3) | *E* | 5.6(4) | 24(3.) |
| | | 112 | 0(+) | 24.13 | 6.4(1) | 0 | 5.1(2) | 0 | 5.1(2) | 2.2(5) |
| | | *113 | 1/2(+) | 12.22 | −8.0(2) | 12.1(4) | 0.3(3) *E* | 12.4(5) | | 20600(400.) |
| | | | | | −5.73(11)*i* | | | | | |
| | | 114 | 0(+) | 28.72 | 7.5(1) | 0 | 7.1(2) | 0 | 7.1(2) | 0.34(2) |
| | | 116 | 0(+) | 7.47 | 6.3(1) | 0 | 5.0(2) | 0 | 5.0(2) | 0.075(13) |
| In | 49 | | | 4.065(20) | 2.08(2) | 0.54(11) | 2.62(11) | 193.8(1.5) | | |
| | | | | | −0.0539(4)*i* | | | | | |
| | | 113 | 9/2(+) | 43 | 5.39(6) | ±0.017(1) | 3.65(8) | 0.000037(5) | 3.65(8) | 12.0(1.1) |
| | | 115 | 9/2(+) | 957 | 4.01(2) | −2.1(2) | 2.02(2) | 0.55(11) | 2.57(11) | 202(2.) |
| | | | | | −0.0562(6)*i* | | | | | |
| Sn | 50 | | | | 6.225(2) | | 4.870(3) | 0.022(5) | 4.892(6) | 0.626(9) |
| | | 112 | 0(+) | 1.0 | 6.1(1.) *E* | 0 | 4.5(1.5) | 0 | 4.5(1.5) | 1.01(11) |
| | | 114 | 0(+) | 0.7 | 6.2(3) | 0 | 4.8(5) | 0 | 4.8(5) | 0.114(30) |
| | | 115 | 1/2(+) | 0.4 | 6.(1.) *E* | 4.5(1.5) | 0.3(3) *E* | 4.8(1.5) | 30(7.) | |
| | | 116 | 0(+) | 14.7 | 5.93(5) | 0 | 4.42(7) | 0 | 4.42(7) | 0.14(3) |
| | | 117 | 1/2(+) | 7.7 | 6.48(5) | 5.28(8) | 0.3(3) *E* | 5.6(3) | 2.3(5) | |
| | | 118 | 0(+) | 24.3 | 6.07(5) | 0 | 4.63(8) | 0 | 4.63(8) | 0.22(5) |
| | | 119 | 1/2(+) | 8.6 | 6.12(5) | 4.71(8) | 0.3(3) *E* | 5.0(3) | 2.2(5) | |
| | | 120 | 0(+) | 32.4 | 6.49(5) | 0 | 5.29(8) | 0 | 5.29(8) | 0.14(3) |
| | | 122 | 0(+) | 4.6 | 5.74(5) | 0 | 4.14(7) | 0 | 4.14(7) | 0.18(2) |
| | | 124 | 0(+) | 5.6 | 5.97(5) | 0 | 4.48(8) | 0 | 4.48(8) | 0.133(5) |
| Sb | 51 | | | | 5.57(3) | | 3.90(4) | 0.00(7) | 3.90(6) | 4.91(5) |
| | | 121 | 7/2(+) | 57.3 | 5.71(6) | −0.05(15) | 4.10(9) | 0.0003(19) | 4.10(9) | 5.75(12) |
| | | 123 | 5/2(+) | 42.7 | 5.38(7) | −0.10(15) | 3.64(9) | 0.001(4) | 3.64(9) | 3.8(2) |
| Te | 52 | | | | 5.80(3) | | 4.23(4) | 0.09(1) | 4.32(4) | 4.05(5) |
| | | 120 | 0(+) | 0.096 | 5.3(5) | 0 | 3.5(7) | 0 | 3.4(7) | 2.3(3) |
| | | 122 | 0(+) | 2.60 | 3.8(2) | 0 | 1.8(2) | 0 | 1.8(2) | 3.4(5) |
| | | 123 | 1/2(+) | 0.908 | −0.05(25) | −2.04(9) | 0.002(3) | 0.52(5) | 0.52(5) | 418(30.) |
| | | | | | −0.116(8)*i* | | | | | |
| | | 124 | 0(+) | 4.816 | 7.96(10) | 0 | 8.0(2) | 0 | 8.0(2) | 6.8(1.3) |
| | | 125 | 1/2(+) | 7.14 | 5.02(8) | −0.26(13) | 3.17(10) | 0.008(8) | 3.18(10) | 1.55(16) |
| | | 126 | 0(+) | 18.95 | 5.56(7) | 0 | 3.88(10) | 0 | 3.88(10) | 1.04(15) |
| | | 128 | 0(+) | 31.69 | 5.89(7) | 0 | 4.36(10) | 0 | 4.36(10) | 0.215(8) |
| | | 130 | 0(+) | 33.80 | 6.02(7) | 0 | 4.55(11) | 0 | 4.55(11) | 0.29(6) |

Table 4.4.4.1. *Bound scattering lengths (cont.)*

| Element | $Z$ | $A$ | $I(\pi)$ | $c$ | $b_c$ | $b_i$ | $\sigma_c$ | $\sigma_i$ | $\sigma_s$ | $\sigma_a$ |
|---|---|---|---|---|---|---|---|---|---|---|
| I | 53 | 127 | 5/2(+) | 100 | 5.28(2) | 1.58(15) | 3.50(3) | 0.31(6) | 3.81(7) | 6.15(6) |
| Xe | 54 | | | | 4.92(3) | | 3.04(4) | | | 23.9(1.2) |
| | | 124 | 0(+) | 0.10 | | 0 | | 0 | | 165.(20.) |
| | | 126 | 0(+) | 0.09 | | 0 | | 0 | | 3.5(8) |
| | | 128 | 0(+) | 1.91 | | 0 | | 0 | | < 8. |
| | | 129 | 1/2(+) | 26.4 | | | | | | 21.(5.) |
| | | 130 | 0(+) | 4.1 | | 0 | | 0 | | < 26. |
| | | 131 | 3/2(+) | 21.2 | | | | | | 85.(10.) |
| | | 132 | 0(+) | 26.9 | | 0 | | 0 | | 0.45(6) |
| | | 134 | 0(+) | 10.4 | | 0 | | 0 | | 0.265(20) |
| | | 136 | 0(+) | 8.9 | | 0 | | 0 | | 0.26(2) |
| Cs | 55 | 133 | 7/2(+) | 100 | 5.42(2) | 1.29(15) | 3.69(3) | 0.21(5) | 3.90(6) | 29.0(1.5) |
| Ba | 56 | | | | 5.07(3) | | 3.23(4) | 0.15(11) | 3.38(10) | 1.1(1) |
| | | 130 | 0(+) | 0.11 | −3.6(6) | 0 | 1.6(5) | 0 | 1.6(5) | 30(5.) |
| | | 132 | 0(+) | 0.10 | 7.8(3) | 0 | 7.6(6) | 0 | 7.6(6) | 7.0(8) |
| | | 134 | 0(+) | 2.42 | 5.7(1) | 0 | 4.08(14) | 0 | 4.08(14) | 2.0(1.6) |
| | | 135 | 3/2(+) | 6.59 | 4.67(10) | | 2.74(12) | 0.5(5) *E* | 3.2(5) | 5.8(9) |
| | | 136 | 0(+) | 7.85 | 4.91(8) | 0 | 3.03(10) | 0 | 3.03(10) | 0.68(17) |
| | | 137 | 3/2(+) | 11.23 | 6.83(10) | | 5.86(17) | 0.5(5) *E* | 6.4(5) | 3.6(2) |
| | | 138 | 0(+) | 71.70 | 4.84(8) | 0 | 2.94(10) | 0 | 2.94(10) | 0.27(14) |
| La | 57 | | | | 8.24(4) | | 8.53(8) | 1.13(19) | 9.66(17) | 8.97(5) |
| | | 138 | 5(+) | 0.09 | 8.(2.) *E* | 8.(4.) | 0.5(5) *E* | 8.5(4.0) | 57.(6.) | |
| | | 139 | 7/2(+) | 99.91 | 8.24(4) | 3.0(2) | 8.53(8) | 1.13(15) | 9.66(17) | 8.93(4) |
| Ce | 58 | | | | 4.84(2) | | 2.94(2) | 0.00(10) | 2.94(10) | 0.63(4) |
| | | 136 | 0(+) | 0.19 | 5.80(9) | 0 | 4.23(13) | 0 | 4.23(13) | 7.3(1.5) |
| | | 138 | 0(+) | 0.25 | 6.70(9) | 0 | 5.64(15) | 0 | 5.64(15) | 1.1(3) |
| | | 140 | 0(+) | 88.48 | 4.84(9) | 0 | 2.94(11) | 0 | 2.94(11) | 0.57(4) |
| | | 142 | 0(+) | 11.08 | 4.75(9) | 0 | 2.84(11) | 0 | 2.84(11) | 0.95(5) |
| Pr | 59 | 141 | 5/2(+) | 100 | 4.58(5) | −0.35(3) | 2.64(6) | 0.015(3) | 2.66(6) | 11.5(3) |
| Nd | 60 | | | | 7.69(5) | | 7.43(10) | 9.2(8) | 16.6(8) | 50.5(1.2) |
| | | 142 | 0(+) | 27.16 | 7.7(3) | 0 | 7.5(6) | 0 | 7.5(6) | 18.7(7) |
| | | 143 | 7/2(−) | 12.18 | 14.2(5) *E* | ±21.1(6) | 25.(7.) | 55.(7.) | 80.(2.) | 334.(10.) |
| | | 144 | 0(+) | 23.80 | 2.8(3) | 0 | 1.0(2) | 0 | 1.0(2) | 3.6(3) |
| | | 145 | 7/2(−) | 8.29 | 14.2(5) | *E* | 25.(7.) | 5.(5.) *E* | 30.(9.) | 42.(2.) |
| | | 146 | 0(+) | 17.19 | 8.7(2) | 0 | 9.5(4) | 0 | 9.5(4) | 1.4(1) |
| | | 148 | 0(+) | 5.75 | 5.7(3) | 0 | 4.1(4) | 0 | 4.1(4) | 2.5(2) |
| | | 150 | 0(+) | 5.63 | 5.3(2) | 0 | 3.5(3) | 0 | 3.5(3) | 1.2(2) |
| Pm | 61 | | | | | | | | | |
| | | 147 | 7/2(+) | (2.62a) | 12.6(4) | ±3.2(2.5) | 20.0(1.3) | 1.3(2.0) | 21.3(1.5) | 168.4(3.5) |
| Sm | 62 | | | | 0.80(2)<br>−1.65(2)*i* | | 0.422(9) | 39.(3.) | 39.(3.) | 5922.(56.) |
| | | 144 | 0(+) | 3.1 | −3.(4.) *E* | 0 | 1.(3.) | 0 | 1.(3.) | 0.7(3) |
| | | 147 | 7/2(−) | 15.1 | 14(3.) | ±11.(7.) | 25.(11.) | 14.(19.) | 39(16.) | 57(3.) |
| | | 148 | 0(+) | 11.3 | −3.(4.) *E* | 0 | 1.(3.) | 0 | 1.(3.) | 2.4(6) |
| | | *149 | 7/2(−) | 13.9 | −19.2(1)<br>−11.7(1)*i* | ±31.4(6)<br>−10.3(1)*i* | 63.5(6) | 137.(5.) | 200.(5.) | 42080.(400.) |
| | | 150 | 0(+) | 7.4 | 14(3.) | 0 | 25(11.) | 0 | 25(11.) | 104(4.) |
| | | 152 | 0(+) | 26.6 | −5.0(6) | 0 | 3.1(8) | 0 | 3.1(8) | 206.(6.) |
| | | 154 | 0(+) | 22.6 | 9.3(1.0) | 0 | 11.(2.) | 0 | 11.(2.) | 8.4(5) |
| Eu | 63 | | | | 7.22(2)<br>−1.26(1)*i* | | 6.75(4) | 2.5(4) | 9.2(4) | 4530.(40.) |
| | | *151 | 5/2(+) | 47.8 | 6.13(14)<br>−2.53(3)*i* | ±4.5(4)<br>−2.14(2)*i* | 5.5(2) | 3.1(4) | 8.4(4) | 9100(100.) |
| | | 153 | 5/2(+) | 52.2 | 8.22(12) | ±3.2(9) | 8.5(2) | 1.3(7) | 9.8(7) | 312.(7.) |

Table 4.4.4.1.*Bound scattering lengths (cont.)*

| Element | $Z$ | $A$ | $I(\pi)$ | $c$ | $b_c$ | $b_i$ | $\sigma_c$ | $\sigma_i$ | $\sigma_s$ | $\sigma_a$ |
|---|---|---|---|---|---|---|---|---|---|---|
| Gd | 64 | | | | 6.5(5)<br>−13.82(3)*i* | | 29.3(8) | 151.(2.) | 180.(2.) | 49700.(125.) |
| | | 152 | 0(+) | 0.2 | 10.(3.) *E* | 0 | 13.(8.) | 0 | 13.(8.) | 735.(20.) |
| | | 154 | 0(+) | 2.1 | 10.(3.) *E* | 0 | 13.(8.) | 0 | 13.(8.) | 85.(12.) |
| | | *155 | 3/2(−) | 14.8 | 6.0(1)<br>−17.0(1)*i* | ±5.(5.) *E*<br>−13.16(9)*i* | 40.8(4.) | 25.(6.) | 66.(6.) | 61100.(400.) |
| | | 156 | 0(+) | 20.6 | 6.3(4) | 0 | 5.0(6) | 0 | 5.0(6) | 1.5(1.2) |
| | | *157 | 3/2(−) | 15.7 | −1.14(2)<br>−71.9(2)*i* | ±5.(5.) *E*<br>−55.8(2)*i* | 650(4.) | 394.(7.) | 1044.(8.) | 259000.(700.) |
| | | 158 | 0(+) | 24.8 | 9.(2.) | 0 | 10.(5.) | 0 | 10.(5.) | 2.2(2) |
| | | 160 | 0(+) | 21.8 | 9.15(5) | 0 | 10.52(11) | 0 | 10.52(11) | 0.77(2) |
| Tb | 65 | 159 | 3/2(+) | 100 | 7.38(3) | −0.17(7) | 6.84(6) | 0.004(3) | 6.84(6) | 23.4(4) |
| Dy | 66 | | | | 16.9(2)<br>−0.276(4)*i* | | 35.9(8) | 54.4(1.2) | 90.3(9) | 994.(13.) |
| | | 156 | 0(+) | 0.06 | 6.1(5) | 0 | 4.7(8) | 0 | 4.7(8) | 33.(3.) |
| | | 158 | 0(+) | 0.10 | 6.(4.) *E* | 0 | 5.(6.) | 0 | 5.(6.) | 43.(6.) |
| | | 160 | 0(+) | 2.34 | 6.7(4) | 0 | 5.6(7) | 0 | 5.6(7) | 56.(5.) |
| | | 161 | 5/2(+) | 19.0 | 10.3(4) | ±4.9(8) | 13.3(1.0) | 3.(1.) | 16.(1.) | 600.(25.) |
| | | 162 | 0(+) | 25.5 | −1.4(5) | 0 | 0.25(18) | 0 | 0.25(18) | 194.(10.) |
| | | 163 | 5/2(−) | 24.9 | 5.0(4) | 1.3(3) | 3.1(5) | 0.21(10) | 3.3(5) | 124.(7.) |
| | | 164 | 0(+) | 28.1 | 49.4(5)<br>−0.79(1)*i* | 0 | 307.(3.) | 0 | 307.(3.) | 2840.(40.) |
| Ho | 67 | 165 | 7/2(−) | 100 | 8.01(8) | −1.70(8) | 8.06(16) | 0.36(3) | 8.42(16) | 64.7(1.2) |
| Er | 68 | | | | 7.79(2) | | 7.63(4) | 1.1(3) | 8.7(3) | 159.(4.) |
| | | 162 | 0(+) | 0.14 | 8.8(2) | 0 | 9.7(4) | 0 | 9.7(4) | 19.(2.) |
| | | 164 | 0(+) | 1.56 | 8.2(2) | 0 | 8.4(4) | 0 | 8.4(4) | 13.(2.) |
| | | 166 | 0(+) | 33.4 | 10.6(2) | 0 | 14.1(5) | 0 | 14.1(5) | 19.6(1.5) |
| | | 167 | 7/2(+) | 22.9 | 3.0(3) | 1.0(3) | 1.1(2) | 0.13(8) | 1.2(2) | 659.(16.) |
| | | 168 | 0(+) | 27.1 | 7.4(4) | 0 | 6.8(7) | 0 | 6.9(7) | 2.74(8) |
| | | 170 | 0(+) | 14.9 | 9.6(5) | 0 | 11.6(1.2) | 0 | 11.6(1.2) | 5.8(3) |
| Tm | 69 | 169 | 1/2(+) | 100 | 7.07(3) | 0.9(3) | 6.28(5) | 0.10(7) | 6.38(9) | 100.(2.) |
| Yb | 70 | | | | 12.43(3) | | 19.42(9) | 4.0(2) | 23.05(18) | 34.8(8) |
| | | 168 | 0(+) | 0.14 | −4.07(2)<br>−0.62(1)*i* | 0 | 2.13(2) | 0 | 2.13(2) | 2230.(40.) |
| | | 170 | 0(+) | 3.06 | 6.77(10) | 0 | 5.8(2) | 0 | 5.8(2) | 11.4(1.0) |
| | | 171 | 1/2(−) | 143 | 9.66(10) | −5.59(17) | 11.7(2) | 3.9(2) | 15.6(3) | 48.6(2.5) |
| | | 172 | 0(+) | 21.9 | 9.43(10) | 0 | 11.2(2) | 0 | 11.2(2) | 0.8(4) |
| | | 173 | 5/2(−) | 16.1 | 9.56(7) | −5.3(2) | 11.5(2) | 3.5(3) | 15.0(4) | 17.1(1.3) |
| | | 174 | 0(+) | 31.8 | 19.3(1) | 0 | 46.8(5) | 0 | 46.8(5) | 69.4(5.0) |
| | | 176 | 0(+) | 12.7 | 8.72(10) | 0 | 9.6(2) | 0 | 9.6(2) | 2.85(5) |
| Lu | 71 | | | | 7.21(3) | | 6.53(5) | 0.7(4) | 7.2(4) | 74.(2.) |
| | | 175 | 7/2(+) | 97.39 | 7.24(3) | ±2.2(7) | 6.59(5) | 0.6(4) | 7.2(4) | 21.(3.) |
| | | *176 | 7(−) | 2.61 | 6.1(1)<br>−0.57(1)*i* | ±3.0(4)<br>+0.61(1)*i* | 4.7(2) | 1.2(3) | 5.9(4) | 2065.(35.) |
| Hf | 72 | | | | 7.77(14) | | 7.6(3) | 2.6(5) | 10.2(4) | 104.1(0.5) |
| | | 174 | 0(+) | 0.2 | 10.9(1.1) | 0 | 15.(3.) | 0 | 15.(3.) | 561.(35.) |
| | | 176 | 0(+) | 5.2 | 6.61(18) | 0 | 5.5(3) | 0 | 5.5(3) | 23.5(3.1) |
| | | 177 | 7/2(−) | 18.6 | 0.8(1.0) *E* | ±0.9(1.3) | 0.1(2) | 0.1(3) | 0.2(2) | 373.(10.) |
| | | 178 | 0(+) | 27.1 | 5.9(2) | 0 | 4.4(3) | 0 | 4.4(3) | 84.(4.) |
| | | 179 | 9/2(+) | 13.7 | 7.46(16) | ±1.06(8) | 7.0(3) | 0.14(2) | 7.1(3) | 41.(3.) |
| | | 180 | 0(+) | 35.2 | 13.2(3) | 0 | 21.9(1.0) | 0 | 21.9(1.0) | 13.04(7) |
| Ta | 73 | | | | 6.91(7) | | 6.00(12) | 0.01(17) | 6.01(12) | 20.6(5) |
| | | *180 | 9(−) | 0.012 | 7.(2.) *E* | 6.2(3.5) | 0.5(5) | *E* | 7.(4.) | 563.(60.) |
| | | 181 | 7/2(+) | 99.988 | 6.91(7) | −0.29(3) | 6.00(12) | 0.011(2) | 6.01(12) | 20.5(5) |

Table 4.4.4.1. *Bound scattering lengths (cont.)*

| Element | $Z$ | $A$ | $I(\pi)$ | $c$ | $b_c$ | $b_i$ | $\sigma_c$ | $\sigma_i$ | $\sigma_s$ | $\sigma_a$ |
|---|---|---|---|---|---|---|---|---|---|---|
| W | 74 | | | | 4.86(2) | | 2.97(2) | 1.63(6) | 4.60(6) | 18.3(2) |
| | | 180 | 0(+) | 0.1 | 5.(3.) *E* | 0 | 3.(4.) | 0 | 3.(4.) | 30.(20.) |
| | | 182 | 0(+) | 26.3 | 6.97(14) | 0 | 6.10(7) | 0 | 6.10(7) | 20.7(5) |
| | | 183 | 1/2(−) | 14.3 | 6.53(4) | | 5.36(7) | 0.3(3) *E* | 5.7(3) | 10.1(3) |
| | | 184 | 0(+) | 30.7 | 7.48(6) | 0 | 7.03(11) | 0 | 7.03(11) | 1.7(1) |
| | | 186 | 0(+) | 28.6 | −0.72(4) | 0 | 0.065(7) | 0 | 0.065(7) | 37.9(0.6) |
| Re | 75 | | | | 9.2(2) | | 10.6(5) | 0.9(6) | 11.5(3) | 89.7(1.0) |
| | | 185 | 5/2(+) | 37.40 | 9.0(3) | ±2.0(1.8) | 10.2(7) | 0.5(9) | 10.7(6) | 112.(2.) |
| | | 187 | 5/2(+) | 62.60 | 9.3(3) | ±2.8(1.1) | 10.9(7) | 1.0(8) | 11.9(4) | 76.4(1.0) |
| Os | 76 | | | | 10.7(2) | | 14.4(5) | 0.3(8) | 14.7(6) | 16.0(4) |
| | | 184 | 0(+) | 0.02 | 10.(2.) *E* | 0 | 13.(5.) | 0 | 13.(5.) | 3000.(150.) |
| | | 186 | 0(+) | 1.58 | 11.6(1.7) | 0 | 17.(5.) | 0 | 17.(5.) | 80.(13.) |
| | | 187 | 1/2(−) | 1.6 | 10.(2.) *E* | 13.(5.) | 0.3(3) | *E* | 13.(5.) | 320(10.) |
| | | 188 | 0(+) | 13.3 | 7.6(3) | 0 | 7.3(6) | 0 | 7.3(6) | 4.7(5) |
| | | 189 | 3/2(−) | 16.1 | 10.7(3) | | 14.4(8) | 0.5(5) *E* | 14.9(9) | 25(4.) |
| | | 190 | 0(+) | 26.4 | 11.0(3) | 0 | 15.2(9) | 0 | 15.2(8) | 13.1(3) |
| | | 192 | 0(+) | 41.0 | 11.5(4) | 0 | 16.6(1.2) | 0 | 16.6(1.2) | 2.0(1) |
| Ir | 77 | | | | 10.6(3) | | 14.1(8) | 0.(3.) | 14.(3.) | 425.3(2.4) |
| | | 191 | 3/2(+) | 37.3 | | | | | | 954.(10.) |
| | | 193 | 3/2(+) | 62.7 | | | | | | 111.(5.) |
| Pt | 78 | | | | 9.60(1) | | 11.58(2) | 0.13(11) | 11.71(11) | 10.3(3) |
| | | 190 | 0(+) | 0.01 | 9.0(1.0) | 0 | 10.(2.) | 0 | 10.(2.) | 152.(4.) |
| | | 192 | 0(+) | 0.79 | 9.9(5) | 0 | 12.3(1.2) | 0 | 12.3(1.2) | 10.0(2.5) |
| | | 194 | 0(+) | 32.9 | 10.55(8) | 0 | 14.0(2) | 0 | 14.0(2) | 1.44(19) |
| | | 195 | 1/2(−) | 33.8 | 8.83(9) | −1.00(17) | 9.8(2) | 0.13(4) | 9.9(2) | 27.5(1.2) |
| | | 196 | 0(+) | 25.3 | 9.89(8) | 0 | 12.3(2) | 0 | 12.3(2) | 0.72(4) |
| | | 198 | 0(+) | 7.2 | 7.8(1) | 0 | 7.7(2) | 0 | 7.6(2) | 3.66(19) |
| Au | 79 | 197 | 3/2(+) | 100 | 7.63(6) | −1.84(10) | 7.32(12) | 0.43(5) | 7.75(13) | 98.65(9) |
| Hg | 80 | | | | 12.692(15) | | 20.24(5) | 6.6(1) | 26.8(1) | 372.3(4.0) |
| | | 196 | 0(+) | 0.2 | 30.3(1.0) | 0 | 115(8.) | 0 | 115(8.) | 3080(180.) |
| | | 198 | 0(+) | 10.1 | | 0 | | 0 | | 2.0(3) |
| | | 199 | 1/2(−) | 17.0 | 16.9(4) | ±15.5(8) | 36.(2.) | 30.(3.) | 66.(2.) | 2150.(48.) |
| | | 200 | 0(+) | 23.1 | | 0 | | 0 | | <60. |
| | | 201 | 3/2(−) | 13.2 | | | 7.8(2.0) | | | |
| | | 202 | 0(+) | 29.6 | | 0 | | 0 | | 4.89(5) |
| | | 204 | 0(+) | 6.8 | | 0 | | 0 | | 0.43(10) |
| Tl | 81 | | | | 8.776(5) | | 9.678(11) | 0.21(15) | 9.89(15) | 3.43(6) |
| | | 203 | 1/2(+) | 29.524 | 6.99(16) | 1.06(14) | 6.14(28) | 0.14(4) | 6.28(28) | 11.4(2) |
| | | 205 | 1/2(+) | 70.476 | 9.52(7) | −0.242(17) | 11.39(17) | 0.007(1) | 11.40(17) | 0.104(17) |
| Pb | 82 | | | | 9.405(3) | | 11.115(7) | 0.0030(7) | 11.118(7) | 0.171(2) |
| | | 204 | 0(+) | 1.4 | 9.90(10) | 0 | 12.3(2) | 0 | 12.3(2) | 0.65(7) |
| | | 206 | 0(+) | 24.1 | 9.22(5) | 0 | 10.68(12) | 0 | 10.68(12) | 0.0300(8) |
| | | 207 | 1/2(−) | 22.1 | 9.28(4) | 0.14(6) | 10.82(9) | 0.002(2) | 10.82(9) | 0.699(10) |
| | | 208 | 0(+) | 52.4 | 9.50(2) | 0 | 11.34(5) | 0 | 11.34(5) | 0.00048(3) |
| Bi | 83 | 209 | 9/2(−) | 100 | 8.532(2) | 0.259(15) | 9.148(4) | 0.0084(10) | 9.156(4) | 0.0338(7) |
| Po | 84 | | | | | | | | | |
| At | 85 | | | | | | | | | |
| Rn | 86 | | | | | | | | | |
| Fr | 87 | | | | | | | | | |
| Ra | 88 | | | | | | | | | |
| | | 226 | 0(+) | $(1.60\times10^3$a) | 10.0(1.0) | 0 | 13.(3.) | 0 | 13.(3.) | 12.8(1.5) |

Table 4.4.4.1. *Bound scattering lengths (cont.)*

| Element | $Z$ | $A$ | $I(\pi)$ | $c$ | $b_c$ | $b_i$ | $\sigma_c$ | $\sigma_i$ | $\sigma_s$ | $\sigma_a$ |
|---|---|---|---|---|---|---|---|---|---|---|
| Ac | 89 | | | | | | | | | |
| Th | 90 | 232 | 0(+) | 100 | 10.31(3) | 0 | 13.36(8) | 0 | 13.36(8) | 7.37(6) |
| Pa | 91 | | | | | | | | | |
| | | 231 | 3/2(−) | ($3.28\times10^4$a) | 9.1(3) | 1 | 0.4(7) | 0.1(3.3) | 10.5(3.2) | 200.6(2.3) |
| U | 92 | | | | 8.417(5) | | 8.903(11) | 0.005(16) | 8.908(11) | 7.57(2) |
| | | 233 | 5/2(+) | ($1.59\times10^5$a) | 10.1(2) | ±1.(3.) | 12.8(5) | 0.1(6) | 12.9(3) | 574.7(1.0) |
| | | 234 | 0(+) | 0.005 | 12.4(3) | 0 | 19.3(9) | 0 | 19.3(9) | 100.1(1.3) |
| | | 235 | 7/2(−) | 0.720 | 10.47(3) | ±1.3(6) | 13.78(11) | 0.2(2) | 14.0(2) | 680.9(1.1) |
| | | 238 | 0(+) | 99.275 | 8.402(5) | 0 | 8.871(11) | 0 | 8.871(11) | 2.68(2) |
| Np | 93 | | | | | | | | | |
| | | 237 | 5/2(+) | ($2.14\times10^6$a) | 10.55(10) | | 14.0(3) | 0.5(5)*E* | 14.5(6) | 175.9(2.9) |
| Pu | 94 | | | | | | | | | |
| | | 238 | 0(+) | (87.74a) | 14.1(5) | 0 | 25.0(1.8) | 0 | 25.0(1.8) | 558.(7.) |
| | | 239 | 1/2(+) | ($2.41\times10^4$a) | 7.7(1) | ±1.3(1.9) | 7.5(2) | 0.2(6) | 7.7(6) | 1017.3(2.1) |
| | | 240 | 0(+) | ($6.56\times10^3$a) | 3.5(1) | 0 | 1.54(9) | 0 | 1.54(9) | 289.6(1.4) |
| | | 242 | 0(+) | ($3.76\times10^5$a) | 8.1(1) | 0 | 8.2(2) | 0 | 8.2(2) | 18.5(5) |
| Am | 95 | | | | | | | | | |
| | | 243 | 5/2(−) | ($7.37\times10^3$a) | 8.3(2) | ±2.(7.) | 8.7(4) | 0.3(2.6) | 9.0(2.6) | 75.3(1.8) |
| Cm | 96 | | | | | | | | | |
| | | 244 | 0(+) | (18.10a) | 9.5(3) | 0 | 11.3(7) | 0 | 11.3(7) | 16.2(1.2) |
| | | 246 | 0(+) | ($4.7\times10^3$a) | 9.3(2) | 0 | 10.9(5) | 0 | 10.9(5) | 1.36(17) |
| | | 248 | 0(+) | ($3.5\times10^5$a) | 7.7(2) | 0 | 7.5(4) | 0 | 7.5(4) | 3.00(26) |

### 4.4.4.2. *Scattering and absorption cross sections*

When a thermal neutron collides with a nucleus, it may be either scattered or absorbed. By absorption, we mean reactions such as $(n,\gamma)$, $(n,p)$, or $(n,\alpha)$, in which there is no neutron in the final state. The effect of absorption can be included by allowing the bound scattering length to be complex,

$$b = b' - ib''. \tag{4.4.4.3}$$

The total bound scattering cross section is then given by

$$\sigma_s = 4\pi\langle|b|^2\rangle, \tag{4.4.4.4}$$

in which $\langle\,\rangle$ denotes a statistical average over the neutron and nuclear spins and the absorption cross section is given by

$$\sigma_a = \frac{4\pi}{k}\langle b''\rangle, \tag{4.4.4.5}$$

where $k = 2\pi/\lambda$ is the wavevector of the incident neutron and $\lambda$ is the wavelength.

If the neutron and/or the nucleus is unpolarized, then the total bound scattering cross section is of the form

$$\sigma_s = \sigma_c + \sigma_i, \tag{4.4.4.6}$$

in which $\sigma_c$ and $\sigma_i$ are called the bound coherent and incoherent scattering cross sections and are given by

$$\sigma_c = 4\pi|b_c|^2, \quad \sigma_i = 4\pi|b_i|^2. \tag{4.4.4.7}$$

Also,

$$b_c = \langle b\rangle, \tag{4.4.4.8}$$

so that the absorption cross section is given by

$$\sigma_a = \frac{4\pi}{k}\, b_c''. \tag{4.4.4.9}$$

The absorption cross section is therefore uniquely determined by the imaginary part of the bound coherent scattering length. It is only when the neutron and the nucleus are both polarized that the imaginary part of the bound incoherent scattering length contributes to the value of $\sigma_a$.

For most nuclides, the scattering lengths and, hence, the scattering cross sections are constant in the thermal-neutron region, and the absorption cross sections are inversely proportional to $k$. Since $k$ is proportional to the neutron velocity $v$, the absorption is said to obey a $1/v$ law. By convention, absorption cross sections are tabulated for a velocity $v = 2200\ \mathrm{m\,s^{-1}}$, which corresponds to a wavevector $k = 3.494\ \mathrm{\AA^{-1}}$, a wavelength $\lambda = 1.798$ Å, or an energy $E = 25.30$ meV.

The only major deviations from the $1/v$ law are for a few heavy nuclides (specifically, $^{113}$Cd, $^{149}$Sm, $^{151}$Eu, $^{155}$Gd, $^{157}$Gd, $^{176}$Lu, and $^{180}$Ta), which have an $(n,\gamma)$ resonance at thermal-neutron energies. For these nuclides (which are indicated by the symbol * in Table 4.4.4.1), the scattering lengths and cross sections are strongly energy dependent. The scattering lengths of the resonant rare-earth nuclides have been tabulated as a function of energy by Lynn & Seeger (1990).

### 4.4.4.3. *Isotope effects*

The coefficients $b_c$ and $b_i$ in (4.4.4.2) for the bound scattering length depend on the particular isotope under consideration, and this provides an additional source of incoherence in the scattering of neutrons by a mixture of isotopes. If $\langle\,\rangle$ is now taken to denote an average over both the spin and isotope distributions, then the expressions (4.4.4.8) for $b_c$, (4.4.4.4) for $\sigma_s$, and (4.4.4.5) for

$\sigma_a$ also apply to a mixture of isotopes. Hence, if $c_l$ denotes the mole fraction of isotopes of type $l$, so that

$$\sum_l c_l = 1, \tag{4.4.4.10}$$

then, for an isotopic mixture,

$$b_c = \sum_l c_l b_{cl}, \tag{4.4.4.11}$$

$$\sigma_s = \sum_l c_l \sigma_{sl}, \tag{4.4.4.12}$$

and

$$\sigma_a = \sum_l c_l \sigma_{al}. \tag{4.4.4.13}$$

The bound coherent scattering cross section of the mixture is given, as before, by

$$\sigma_c = 4\pi|b_c|^2, \tag{4.4.4.14}$$

while the bound incoherent scattering cross section is defined as

$$\sigma_i = \sigma_s - \sigma_c. \tag{4.4.4.15}$$

Hence, it follows that

$$\sigma_i \equiv 4\pi|b_i|^2 = \sigma_i(\text{spin}) + \sigma_i(\text{isotope}), \tag{4.4.4.16}$$

in which the contribution from spin incoherence is given by

$$\sigma_i(\text{spin}) = \sum_l c_l \sigma_{il} = 4\pi \sum_l c_l |b_{il}|^2, \tag{4.4.4.17}$$

and that from isotope incoherence is given by

$$\sigma_i(\text{isotope}) = 4\pi \sum_{l<l'} c_l c_{l'} |b_{cl} - b_{cl'}|^2. \tag{4.4.4.18}$$

Note that for a mixture of isotopes only the magnitude of $b_i$ is defined by (4.4.4.16), and its sign is arbitrary. However, for the individual isotopes, both the magnitude and sign (or complex phase) of $b_i$ are defined in (4.4.4.2).

### 4.4.4.4. *Correction for electromagnetic interactions*

The effective bound coherent scattering length that describes the interaction of a neutron with an atom includes additional contributions from electromagnetic interactions (Bacon, 1975; Sears, 1986*a*, 1996). For a neutral atom with atomic number $Z$, this quantity is of the form

$$b_c(q) = b_c(0) - b_e[Z - f(q)], \tag{4.4.4.19}$$

where $q$ is the wavevector transfer in the collision, $b_c(0)$ and $b_e$ are constants, and $f(q)$ is the atomic scattering factor (Section 6.1.1). The latter quantity is the Fourier transform of the electron number density and is normalized such that $f(0) = Z$.

The main contribution to $b_c(0)$ is from the nuclear interaction between the neutron and the nucleus but there is also a small electrostatic contribution ($\leq$0.5%) arising from the neutron electric polarizability. The coefficient $b_e$ is called the neutron–electron scattering length and has the value $-1.32\ (4) \times 10^{-3}$ fm (Koester, Waschkowksi & Meier, 1988). This quantity is due mainly to the Foldy interaction with a small additional contribution ($\sim$10%) from the intrinsic charge distribution of the neutron.

The correction of the bound coherent scattering length for electromagnetic interactions requires a knowledge of the atomic scattering factor $f(q)$. Tables 6.1.1.1 and 6.1.1.3 provide accurate values of $f(q)$ obtained from relativistic Hartree–Fock calculations for all the atoms and chemically important ions in the Periodic Table. Alternatively, since the correction is small ($\sim$1%), one can often use the approximate analytical expression (Sears, 1986*a*, 1996)

$$f(q) = \frac{Z}{\sqrt{1 + 3(q/q_0)^2}} \tag{4.4.4.20}$$

with $q_0 = \gamma Z^{1/3}$. The value $\gamma = 1.90 \pm 0.07$ Å$^{-1}$ provides a good fit to the Hartree–Fock results in Table 6.1.1.1 for $Z \geq 20$.

### 4.4.4.5. *Measurement of scattering lengths*

The development of modern neutron-optical techniques during the past 25 years has produced a dramatic increase in the accuracy with which scattering lengths can be measured (Koester, 1977; Klein & Werner, 1983; Werner & Klein, 1986; Sears, 1989; Koester, Rauch & Seymann, 1991). The measurements employ a number of effects – mirror reflection, prism refraction, gravity refractometry, Christiansen filter, and interferometry – all of which are based on the fact that the neutron index of refraction, $n$, is uniquely determined by $b_c(0)$ through the relation

$$n^2 = 1 - \frac{4\pi}{k^2} \rho b_c(0), \tag{4.4.4.21}$$

in which $\rho$ is the number of atoms per unit volume. Apart from a small ($\leq$0.01%) local-field correction (Sears, 1985, 1989), this expression is exact.

In methods based on diffraction, such as Bragg reflection by powders or dynamical diffraction by perfect crystals, the measured quantity is the unit-cell structure factor $|F_{hkl}|$. This quantity depends on $b_c(q)$ in which $q$ is equal to the magnitude of the reciprocal-lattice vector corresponding to the relevant Bragg planes, *i.e.*

$$q = 2k \sin\theta_{hkl}, \tag{4.4.4.22}$$

where $\theta_{hkl}$ is the Bragg angle. In dynamical diffraction measurements, it is usual for the authors to correct their results for electromagnetic interactions so that the published quantity is again $b_c(0)$. In the past, this correction has not usually been made for the scattering lengths obtained from Bragg reflection by powders. However, these latter measurements are accurate only to $\pm$2 or 3% so that the correction is then relatively unimportant.

The essential point is that all the bound coherent scattering lengths in Table 4.4.4.1 with the experimental uncertainties less than 1% represent $b_c(0)$ and should therefore be corrected for electromagnetic interactions before being used in the interpretation of neutron diffraction experiments. Failure to make this correction will introduce systematic errors of 0.5 to 2% in the unit-cell structure factors at large $q$, and corresponding errors of 1 to 4% in the calculated intensities.

Expression (4.4.4.21) assumed that the neutrons and/or the nuclei are unpolarized. If the neutrons and the nuclei are both polarized then $b_c(0)$ is replaced by $\langle b(0)\rangle$, which depends on both the coherent and incoherent scattering lengths. If the coherent scattering length is known, neutron-optical experiments with polarized neutrons and nuclei can then be used to determine the incoherent scattering length (Glättli & Goldman, 1987).

### 4.4.4.6. *Compilation of scattering lengths and cross sections*

The bound scattering lengths and cross sections of almost all the elements in the Periodic Table, as well as those of the individual isotopes, are listed in Table 4.4.4.1. As in earlier versions of this table (Sears, 1984, 1986*b*, 1992*a,b*), our primary aim, has been to take the best current values of the bound coherent and incoherent neutron scattering lengths and to

Table 4.4.5.1. $\langle j_0 \rangle$ *form factors for 3d transition elements and their ions*

| Atom or ion | *A* | *a* | *B* | *b* | *C* | *c* | *D* | *e* |
|---|---|---|---|---|---|---|---|---|
| Sc | 0.2512 | 90.030 | 0.3290 | 39.402 | 0.4235 | 14.322 | −0.0043 | 0.2029 |
| $Sc^{+}$ | 0.4889 | 51.160 | 0.5203 | 14.076 | −0.0286 | 0.179 | 0.0185 | 0.1217 |
| $Sc^{2+}$ | 0.5048 | 31.403 | 0.5186 | 10.990 | −0.0241 | 1.183 | 0.0000 | 0.0578 |
| Ti | 0.4657 | 33.590 | 0.5490 | 9.879 | −0.0291 | 0.323 | 0.0123 | 0.1088 |
| $Ti^{+}$ | 0.5093 | 36.703 | 0.5032 | 10.371 | −0.0263 | 0.311 | 0.0116 | 0.1125 |
| $Ti^{2+}$ | 0.5091 | 24.976 | 0.5162 | 8.757 | −0.0281 | 0.916 | 0.0015 | 0.0589 |
| $Ti^{3+}$ | 0.3571 | 22.841 | 0.6688 | 8.931 | −0.0354 | 0.483 | 0.0099 | 0.0575 |
| V | 0.4086 | 28.811 | 0.6077 | 8.544 | −0.0295 | 0.277 | 0.0123 | 0.0970 |
| $V^{+}$ | 0.4444 | 32.648 | 0.5683 | 9.097 | −0.2285 | 0.022 | 0.2150 | 0.1111 |
| $V^{2+}$ | 0.4085 | 23.853 | 0.6091 | 8.246 | −0.1676 | 0.041 | 0.1496 | 0.0593 |
| $V^{3+}$ | 0.3598 | 19.336 | 0.6632 | 7.617 | −0.3064 | 0.030 | 0.2835 | 0.0515 |
| $V^{4+}$ | 0.3106 | 16.816 | 0.7198 | 7.049 | −0.0521 | 0.302 | 0.0221 | 0.0433 |
| Cr | 0.1135 | 45.199 | 0.3481 | 19.493 | 0.5477 | 7.354 | −0.0092 | 0.1975 |
| $Cr^{+}$ | −0.0977 | 0.047 | 0.4544 | 26.005 | 0.5579 | 7.489 | 0.0831 | 0.1114 |
| $Cr^{2+}$ | 1.2024 | −0.005 | 0.4158 | 20.548 | 0.6032 | 6.956 | −1.2218 | 0.0572 |
| $Cr^{3+}$ | −0.3094 | 0.027 | 0.3680 | 17.035 | 0.6559 | 6.524 | 0.2856 | 0.0436 |
| $Cr^{4+}$ | −0.2320 | 0.043 | 0.3101 | 14.952 | 0.7182 | 6.173 | 0.2042 | 0.0419 |
| Mn | 0.2438 | 24.963 | 0.1472 | 15.673 | 0.6189 | 6.540 | −0.0105 | 0.1748 |
| $Mn^{+}$ | −0.0138 | 0.421 | 0.4231 | 24.668 | 0.5905 | 6.655 | −0.0010 | 0.1242 |
| $Mn^{2+}$ | 0.4220 | 17.684 | 0.5948 | 6.0050 | 0.0043 | −0.609 | −0.0219 | 0.0589 |
| $Mn^{3+}$ | 0.4198 | 14.283 | 0.6054 | 5.469 | 0.9241 | −0.009 | −0.9498 | 0.0392 |
| $Mn^{4+}$ | 0.3760 | 12.566 | 0.6602 | 5.133 | −0.0372 | 0.563 | 0.0011 | 0.0393 |
| Fe | 0.0706 | 35.008 | 0.3589 | 15.358 | 0.5819 | 5.561 | −0.0114 | 0.1398 |
| $Fe^{+}$ | 0.1251 | 34.963 | 0.3629 | 15.514 | 0.5223 | 5.591 | −0.0105 | 0.1301 |
| $Fe^{2+}$ | 0.0263 | 34.960 | 0.3668 | 15.943 | 0.6188 | 5.594 | −0.0119 | 0.1437 |
| $Fe^{3+}$ | 0.3972 | 13.244 | 0.6295 | 4.903 | −0.0314 | 0.350 | 0.0044 | 0.0441 |
| $Fe^{4+}$ | 0.3782 | 11.380 | 0.6556 | 4.592 | −0.0346 | 0.483 | 0.0005 | 0.0362 |
| Co | 0.4139 | 16.162 | 0.6013 | 4.780 | −0.1518 | 0.021 | 0.1345 | 0.1033 |
| $Co^{+}$ | 0.0990 | 33.125 | 0.3645 | 15.177 | 0.5470 | 5.008 | −0.0109 | 0.0983 |
| $Co^{2+}$ | 0.4332 | 14.355 | 0.5857 | 4.608 | −0.0382 | 0.134 | 0.0179 | 0.0711 |
| $Co^{3+}$ | 0.3902 | 12.508 | 0.6324 | 4.457 | −0.1500 | 0.034 | 0.1272 | 0.0515 |
| $Co^{4+}$ | 0.3515 | 10.778 | 0.6778 | 4.234 | −0.0389 | 0.241 | 0.0098 | 0.0390 |
| Ni | −0.0172 | 35.739 | 0.3174 | 14.269 | 0.7136 | 4.566 | −0.0143 | 0.1072 |
| $Ni^{+}$ | 0.0705 | 35.856 | 0.3984 | 13.804 | 0.5427 | 4.397 | −0.0118 | 0.0738 |
| $Ni^{2+}$ | 0.0163 | 35.883 | 0.3916 | 13.223 | 0.6052 | 4.339 | −0.0133 | 0.0817 |
| $Ni^{3+}$ | 0.0012 | 35.000 | 0.3468 | 11.987 | 0.6667 | 4.252 | −0.0148 | 0.0883 |
| $Ni^{4+}$ | −0.0090 | 35.861 | 0.2776 | 11.790 | 0.7474 | 4.201 | −0.0163 | 0.0966 |
| Cu | 0.0909 | 34.984 | 0.4088 | 11.443 | 0.5128 | 3.825 | −0.0124 | 0.0513 |
| $Cu^{+}$ | 0.0749 | 34.966 | 0.4147 | 11.764 | 0.5238 | 3.850 | −0.0127 | 0.0591 |
| $Cu^{2+}$ | 0.0232 | 34.969 | 0.4023 | 11.564 | 0.5882 | 3.843 | −0.0137 | 0.0532 |
| $Cu^{3+}$ | 0.0031 | 34.907 | 0.3582 | 10.914 | 0.6531 | 3.828 | −0.0147 | 0.0665 |
| $Cu^{4+}$ | −0.0132 | 30.682 | 0.2801 | 11.163 | 0.7490 | 3.817 | −0.0165 | 0.0767 |

compute from them a consistent set of bound scattering cross sections. In the present version, we have used the values of the coherent and incoherent scattering lengths recommended by Koester, Rauch & Seymann (1991), supplemented with a few more recently measured values, and have computed from them the corresponding scattering cross sections. The trailing digits in parentheses give the standard errors calculated from the errors in the input data using the statistical theory of error propagation (Young, 1962). The imaginary parts of the scattering lengths, which are appreciable only for strongly absorbing nuclides, were calculated from the measured absorption cross sections (Mughabghab, Divadeenam & Holden, 1981; Mughabghab, 1984) and are listed beneath the real parts of Table 4.4.4.1.

In a few cases, where the scattering lengths have not yet been measured directly, the available scattering cross-section data (Mughabghab, Divadeenam & Holden, 1981; Mughabghab, 1984) were used to obtain the scattering lengths. Equations (4.4.4.11), (4.4.4.12), and (4.4.4.13) were used, where necessary, to fill gaps in Table 4.4.4.1. For some elements, these relations indicated inconsistencies in the data. In such cases, appropriate adjustments in the values of some of the quantities were made. In almost all cases, such adjustments were comparable with the stated errors. Finally, for some elements, it was necessary to estimate arbitrarily the scattering lengths of one or two isotopes in order to be able to complete the table. Such estimates are indicated by the letter '*E*' and were usually made only for isotopes of low natural abundance where the estimated values have only a marginal effect on the final results. Apart from the inclusion of new data for Ti and Mn, the values listed in Table 4.4.4.1 are the same as in Sears (1992*b*).

### 4.4.5. Magnetic form factors (By P. J. Brown)

The form factors used in the calculations of the cross sections for magnetic scattering of neutrons are defined in Subsection 6.1.2.3 as

$$\langle j_l(k) \rangle = \int_0^\infty U^2(r) j_l(kr) 4\pi r^2 \, \mathrm{d}r, \qquad (4.4.5.1)$$

Table 4.4.5.2. $\langle j_0 \rangle$ *form factors for 4d atoms and their ions*

| Atom or ion | *A* | *a* | *B* | *b* | *C* | *c* | *D* | *e* |
|---|---|---|---|---|---|---|---|---|
| Y | 0.5915 | 67.608 | 1.5123 | 17.900 | −1.1130 | 14.136 | 0.0080 | 0.3272 |
| Zr | 0.4106 | 59.996 | 1.0543 | 18.648 | −0.4751 | 10.540 | 0.0106 | 0.3667 |
| $Zr^{+}$ | 0.4532 | 59.595 | 0.7834 | 21.436 | −0.2451 | 9.036 | 0.0098 | 0.3639 |
| Nb | 0.3946 | 49.230 | 1.3197 | 14.822 | −0.7269 | 9.616 | 0.0129 | 0.3659 |
| $Nb^{+}$ | 0.4572 | 49.918 | 1.0274 | 15.726 | −0.4962 | 9.157 | 0.0118 | 0.3403 |
| Mo | 0.1806 | 49.057 | 1.2306 | 14.786 | −0.4268 | 6.987 | 0.0171 | 0.4135 |
| $Mo^{+}$ | 0.3500 | 48.035 | 1.0305 | 15.060 | −0.3929 | 7.479 | 0.0139 | 0.3510 |
| Tc | 0.1298 | 49.661 | 1.1656 | 14.131 | −0.3134 | 5.513 | 0.0195 | 0.3869 |
| $Tc^{+}$ | 0.2674 | 48.957 | 0.9569 | 15.141 | −0.2387 | 5.458 | 0.0160 | 0.3412 |
| Ru | 0.1069 | 49.424 | 1.1912 | 12.742 | −0.3176 | 4.912 | 0.0213 | 0.3597 |
| $Ru^{+}$ | 0.4410 | 33.309 | 1.4775 | 9.553 | −0.9361 | 6.722 | 0.0176 | 0.2608 |
| Rh | 0.0976 | 49.882 | 1.1601 | 11.831 | −0.2789 | 4.127 | 0.0234 | 0.3263 |
| $Rh^{+}$ | 0.3342 | 29.756 | 1.2209 | 9.438 | −0.5755 | 5.332 | 0.0210 | 0.2574 |
| Pd | 0.2003 | 29.363 | 1.1446 | 9.599 | −0.3689 | 4.042 | 0.0251 | 0.2453 |
| $Pd^{+}$ | 0.5033 | 24.504 | 1.9982 | 6.908 | −1.5240 | 5.513 | 0.0213 | 0.1909 |

Table 4.4.5.3. $\langle j_0 \rangle$ *form factors for rare-earth ions*

| Ion | *A* | *a* | *B* | *b* | *C* | *c* | *D* | *e* |
|---|---|---|---|---|---|---|---|---|
| $Ce^{2+}$ | 0.2953 | 17.685 | 0.2923 | 6.733 | 0.4313 | 5.383 | −0.0194 | 0.0845 |
| $Nd^{2+}$ | 0.1645 | 25.045 | 0.2522 | 11.978 | 0.6012 | 4.946 | −0.0180 | 0.0668 |
| $Nd^{3+}$ | 0.0540 | 25.029 | 0.3101 | 12.102 | 0.6575 | 4.722 | −0.0216 | 0.0478 |
| $Sm^{2+}$ | 0.0909 | 25.203 | 0.3037 | 11.856 | 0.6250 | 4.237 | −0.0200 | 0.0408 |
| $Sm^{3+}$ | 0.0288 | 25.207 | 0.2973 | 11.831 | 0.6954 | 4.212 | −0.0213 | 0.0510 |
| $Eu^{2+}$ | 0.0755 | 25.296 | 0.3001 | 11.599 | 0.6438 | 4.025 | −0.0196 | 0.0488 |
| $Eu^{3+}$ | 0.0204 | 25.308 | 0.3010 | 11.474 | 0.7005 | 3.942 | −0.0220 | 0.0356 |
| $Gd^{2+}$ | 0.0636 | 25.382 | 0.3033 | 11.212 | 0.6528 | 3.788 | −0.0199 | 0.0486 |
| $Gd^{3+}$ | 0.0186 | 25.387 | 0.2895 | 11.142 | 0.7135 | 3.752 | −0.0217 | 0.0489 |
| $Tb^{2+}$ | 0.0547 | 25.509 | 0.3171 | 10.591 | 0.6490 | 3.517 | −0.0212 | 0.0342 |
| $Tb^{3+}$ | 0.0177 | 25.510 | 0.2921 | 10.577 | 0.7133 | 3.512 | −0.0231 | 0.0512 |
| $Dy^{2+}$ | 0.1308 | 18.316 | 0.3118 | 7.665 | 0.5795 | 3.147 | −0.0226 | 0.0315 |
| $Dy^{3+}$ | 0.1157 | 15.073 | 0.3270 | 6.799 | 0.5821 | 3.020 | −0.0249 | 0.0146 |
| $Ho^{2+}$ | 0.0995 | 18.176 | 0.3305 | 7.856 | 0.5921 | 2.980 | −0.0230 | 0.1240 |
| $Ho^{3+}$ | 0.0566 | 18.318 | 0.3365 | 7.688 | 0.6317 | 2.943 | −0.0248 | 0.0068 |
| $Er^{2+}$ | 0.1122 | 18.122 | 0.3462 | 6.911 | 0.5649 | 2.761 | −0.0235 | 0.0207 |
| $Er^{3+}$ | 0.0586 | 17.980 | 0.3540 | 7.096 | 0.6126 | 2.748 | −0.0251 | 0.0171 |
| $Tm^{2+}$ | 0.0983 | 18.324 | 0.3380 | 6.918 | 0.5875 | 2.662 | −0.0241 | 0.0404 |
| $Tm^{3+}$ | 0.0581 | 15.092 | 0.2787 | 7.801 | 0.6854 | 2.793 | −0.0224 | 0.0351 |
| $Yb^{2+}$ | 0.0855 | 18.512 | 0.2943 | 7.373 | 0.6412 | 2.678 | −0.0213 | 0.0421 |
| $Yb^{3+}$ | 0.0416 | 16.095 | 0.2849 | 7.834 | 0.6961 | 2.672 | −0.0229 | 0.0344 |

Table 4.4.5.4 $\langle j_0 \rangle$ *form factors for actinide ions*

| Ion | *A* | *a* | *B* | *b* | *C* | *c* | *D* | *e* |
|---|---|---|---|---|---|---|---|---|
| $U^{3+}$ | 0.5058 | 23.288 | 1.3464 | 7.003 | −0.8724 | 4.868 | 0.0192 | 0.1507 |
| $U^{4+}$ | 0.3291 | 23.548 | 1.0836 | 8.454 | −0.4340 | 4.120 | 0.0214 | 0.1757 |
| $U^{5+}$ | 0.3650 | 19.804 | 3.2199 | 6.282 | −2.6077 | 5.301 | 0.0233 | 0.1750 |
| $Np^{3+}$ | 0.5157 | 20.865 | 2.2784 | 5.893 | −1.8163 | 4.846 | 0.0211 | 0.1378 |
| $Np^{4+}$ | 0.4206 | 19.805 | 2.8004 | 5.978 | −2.2436 | 4.985 | 0.0228 | 0.1408 |
| $Np^{5+}$ | 0.3692 | 18.190 | 3.1510 | 5.850 | −2.5446 | 4.916 | 0.0248 | 0.1515 |
| $Np^{6+}$ | 0.2929 | 17.561 | 3.4866 | 5.785 | −2.8066 | 4.871 | 0.0267 | 0.1698 |
| $Pu^{3+}$ | 0.3840 | 16.679 | 3.1049 | 5.421 | −2.5148 | 4.551 | 0.0263 | 0.1280 |
| $Pu^{4+}$ | 0.4934 | 16.836 | 1.6394 | 5.638 | −1.1581 | 4.140 | 0.0248 | 0.1242 |
| $Pu^{5+}$ | 0.3888 | 16.559 | 2.0362 | 5.657 | −1.4515 | 4.255 | 0.0267 | 0.1287 |
| $Pu^{6+}$ | 0.3172 | 16.051 | 3.4654 | 5.351 | −2.8102 | 4.513 | 0.0281 | 0.1382 |
| $Am^{2+}$ | 0.4743 | 21.776 | 1.5800 | 5.690 | −1.0779 | 4.145 | 0.0218 | 0.1253 |
| $Am^{3+}$ | 0.4239 | 19.574 | 1.4573 | 5.872 | −0.9052 | 3.968 | 0.0238 | 0.1054 |
| $Am^{4+}$ | 0.3737 | 17.862 | 1.3521 | 6.043 | −0.7514 | 3.720 | 0.0258 | 0.1113 |
| $Am^{5+}$ | 0.2956 | 17.372 | 1.4525 | 6.073 | −0.7755 | 3.662 | 0.0277 | 0.1202 |
| $Am^{6+}$ | 0.2302 | 16.953 | 1.4864 | 6.116 | −0.7457 | 3.543 | 0.0294 | 0.1323 |
| $Am^{7+}$ | 0.3601 | 12.730 | 1.9640 | 5.120 | −1.3560 | 3.714 | 0.0316 | 0.1232 |

Table 4.4.5.5. $\langle j_2 \rangle$ *form factors for 3d transition elements and their ions*

| Atom or ion | *A* | *a* | *B* | *b* | *C* | *c* | *D* | *e* |
|---|---|---|---|---|---|---|---|---|
| Sc | 10.8172 | 54.327 | 4.7353 | 14.847 | 0.6071 | 4.218 | 0.0011 | 0.1212 |
| $Sc^{+}$ | 8.5021 | 34.285 | 3.2116 | 10.994 | 0.4244 | 3.605 | 0.0009 | 0.1037 |
| $Sc^{2+}$ | 4.3683 | 28.654 | 3.7231 | 10.823 | 0.6074 | 3.668 | 0.0014 | 0.0681 |
| Ti | 4.3583 | 36.056 | 3.8230 | 11.133 | 0.6855 | 3.469 | 0.0020 | 0.0967 |
| $Ti^{+}$ | 6.1567 | 27.275 | 2.6833 | 8.983 | 0.4070 | 3.052 | 0.0011 | 0.0902 |
| $Ti^{2+}$ | 4.3107 | 18.348 | 2.0960 | 6.797 | 0.2984 | 2.548 | 0.0007 | 0.0640 |
| $Ti^{3+}$ | 3.3717 | 14.444 | 1.8258 | 5.713 | 0.2470 | 2.265 | 0.0005 | 0.0491 |
| V | 3.7600 | 21.831 | 2.4026 | 7.546 | 0.4464 | 2.663 | 0.0017 | 0.0556 |
| $V^{+}$ | 4.7474 | 23.323 | 2.3609 | 7.808 | 0.4105 | 2.706 | 0.0014 | 0.0800 |
| $V^{2+}$ | 3.4386 | 16.530 | 1.9638 | 6.141 | 0.2997 | 2.267 | 0.0009 | 0.0565 |
| $V^{3+}$ | 2.3005 | 14.682 | 2.0364 | 6.130 | 0.4099 | 2.382 | 0.0014 | 0.0252 |
| $V^{4+}$ | 1.8377 | 12.267 | 1.8247 | 5.458 | 0.3979 | 2.248 | 0.0012 | 0.0399 |
| Cr | 3.4085 | 20.127 | 2.1006 | 6.802 | 0.4266 | 2.394 | 0.0019 | 0.0662 |
| $Cr^{+}$ | 3.7768 | 20.346 | 2.1028 | 6.893 | 0.4010 | 2.411 | 0.0017 | 0.0686 |
| $Cr^{2+}$ | 2.6422 | 16.060 | 1.9198 | 6.253 | 0.4446 | 2.372 | 0.0020 | 0.0480 |
| $Cr^{3+}$ | 1.6262 | 15.066 | 2.0618 | 6.284 | 0.5281 | 2.368 | 0.0023 | 0.0263 |
| $Cr^{4+}$ | 1.0293 | 13.950 | 1.9933 | 6.059 | 0.5974 | 2.346 | 0.0027 | 0.0366 |
| Mn | 2.6681 | 16.060 | 1.7561 | 5.640 | 0.3675 | 2.049 | 0.0017 | 0.0595 |
| $Mn^{+}$ | 3.2953 | 18.695 | 1.8792 | 6.240 | 0.3927 | 2.201 | 0.0022 | 0.0659 |
| $Mn^{2+}$ | 2.0515 | 15.556 | 1.8841 | 6.063 | 0.4787 | 2.232 | 0.0027 | 0.0306 |
| $Mn^{3+}$ | 1.2427 | 14.997 | 1.9567 | 6.118 | 0.5732 | 2.258 | 0.0031 | 0.0336 |
| $Mn^{4+}$ | 0.7879 | 13.886 | 1.8717 | 5.743 | 0.5981 | 2.182 | 0.0034 | 0.0434 |
| Fe | 1.9405 | 18.473 | 1.9566 | 6.323 | 0.5166 | 2.161 | 0.0036 | 0.0394 |
| $Fe^{+}$ | 2.6290 | 18.660 | 1.8704 | 6.331 | 0.4690 | 2.163 | 0.0031 | 0.0491 |
| $Fe^{2+}$ | 1.6490 | 16.559 | 1.9064 | 6.133 | 0.5206 | 2.137 | 0.0035 | 0.0335 |
| $Fe^{3+}$ | 1.3602 | 11.998 | 1.5188 | 5.003 | 0.4705 | 1.991 | 0.0038 | 0.0374 |
| $Fe^{4+}$ | 1.5582 | 8.275 | 1.1863 | 3.279 | 0.1366 | 1.107 | −0.0022 | 0.0327 |
| Co | 1.9678 | 14.170 | 1.4911 | 4.948 | 0.3844 | 1.797 | 0.0027 | 0.0452 |
| $Co^{+}$ | 2.4097 | 16.161 | 1.5780 | 5.460 | 0.4095 | 1.914 | 0.0031 | 0.0581 |
| $Co^{2+}$ | 1.9049 | 11.644 | 1.3159 | 4.357 | 0.3146 | 1.645 | 0.0017 | 0.0459 |
| $Co^{3+}$ | 1.7058 | 8.859 | 1.1409 | 3.309 | 0.1474 | 1.090 | −0.0025 | 0.0462 |
| $Co^{4+}$ | 1.3110 | 8.025 | 1.1551 | 3.179 | 0.1608 | 1.130 | −0.0011 | 0.0374 |
| Ni | 1.0302 | 12.252 | 1.4669 | 4.745 | 0.4521 | 1.744 | 0.0036 | 0.0338 |
| $Ni^{+}$ | 2.1040 | 14.866 | 1.4302 | 5.071 | 0.4031 | 1.778 | 0.0034 | 0.0561 |
| $Ni^{2+}$ | 1.7080 | 11.016 | 1.2147 | 4.103 | 0.3150 | 1.533 | 0.0018 | 0.0446 |
| $Ni^{3+}$ | 1.4683 | 8.671 | 0.1794 | 1.106 | 1.1068 | 3.257 | −0.0023 | 0.0373 |
| $Ni^{4+}$ | 1.1612 | 7.700 | 1.0027 | 3.263 | 0.2719 | 1.378 | 0.0025 | 0.0326 |
| Cu | 1.9182 | 14.490 | 1.3329 | 4.730 | 0.3842 | 1.639 | 0.0035 | 0.0617 |
| $Cu^{+}$ | 1.8814 | 13.433 | 1.2809 | 4.545 | 0.3646 | 1.602 | 0.0033 | 0.0590 |
| $Cu^{2+}$ | 1.5189 | 10.478 | 1.1512 | 3.813 | 0.2918 | 1.398 | 0.0017 | 0.0429 |
| $Cu^{3+}$ | 1.2797 | 8.450 | 1.0315 | 3.280 | 0.2401 | 1.250 | 0.0015 | 0.0389 |
| $Cu^{4+}$ | 0.9568 | 7.448 | 0.9099 | 3.396 | 0.3729 | 1.494 | 0.0049 | 0.0330 |

Table 4.4.5.6. $\langle j_2 \rangle$ *form factors for 4d atoms and their ions*

| Atom or ion | *A* | *a* | *B* | *b* | *C* | *c* | *D* | *e* |
|---|---|---|---|---|---|---|---|---|
| Y | 14.4084 | 44.658 | 5.1045 | 14.904 | −0.0535 | 3.319 | 0.0028 | 0.1093 |
| Zr | 10.1378 | 35.337 | 4.7734 | 12.545 | −0.0489 | 2.672 | 0.0036 | 0.0912 |
| $Zr^{+}$ | 11.8722 | 34.920 | 4.0502 | 12.127 | −0.0632 | 2.828 | 0.0034 | 0.0737 |
| Nb | 7.4796 | 33.179 | 5.0884 | 11.571 | −0.0281 | 1.564 | 0.0047 | 0.0944 |
| $Nb^{+}$ | 8.7735 | 33.285 | 4.6556 | 11.605 | −0.0268 | 1.539 | 0.0044 | 0.0855 |
| Mo | 5.1180 | 23.422 | 4.1809 | 9.208 | −0.0505 | 1.743 | 0.0053 | 0.0655 |
| $Mo^{+}$ | 7.2367 | 28.128 | 4.0705 | 9.923 | −0.0317 | 1.455 | 0.0049 | 0.0798 |
| Tc | 4.2441 | 21.397 | 3.9439 | 8.375 | −0.0371 | 1.187 | 0.0066 | 0.0645 |
| $Tc^{+}$ | 6.4056 | 24.824 | 3.5400 | 8.611 | −0.0366 | 1.485 | 0.0044 | 0.0806 |
| Ru | 3.7445 | 18.613 | 3.4749 | 7.420 | −0.0363 | 1.007 | 0.0073 | 0.0533 |
| $Ru^{+}$ | 5.2826 | 23.683 | 3.5813 | 8.152 | −0.0257 | 0.426 | 0.0131 | 0.0830 |
| Rh | 3.3651 | 17.344 | 3.2121 | 6.804 | −0.0350 | 0.503 | 0.0146 | 0.0545 |
| $Rh^{+}$ | 4.0260 | 18.950 | 3.1663 | 7.000 | −0.0296 | 0.486 | 0.0127 | 0.0629 |
| Pd | 3.3105 | 14.726 | 2.6332 | 5.862 | −0.0437 | 1.130 | 0.0053 | 0.0492 |
| $Pd^{+}$ | 4.2749 | 17.900 | 2.7021 | 6.354 | −0.0258 | 0.700 | 0.0071 | 0.0768 |

Table 4.4.5.7. $\langle j_2 \rangle$ *form factors for rare-earth ions*

| Ion | *A* | *a* | *B* | *b* | *C* | *c* | *D* | *e* |
|---|---|---|---|---|---|---|---|---|
| $Ce^{2+}$ | 0.9809 | 18.063 | 1.8413 | 7.769 | 0.9905 | 2.845 | 0.0120 | 0.0448 |
| $Nd^{2+}$ | 1.4530 | 18.340 | 1.6196 | 7.285 | 0.8752 | 2.622 | 0.0126 | 0.0461 |
| $Nd^{3+}$ | 0.6751 | 18.342 | 1.6272 | 7.260 | 0.9644 | 2.602 | 0.0150 | 0.0450 |
| $Sm^{2+}$ | 1.0360 | 18.425 | 1.4769 | 7.032 | 0.8810 | 2.437 | 0.0152 | 0.0345 |
| $Sm^{3+}$ | 0.4707 | 18.430 | 1.4261 | 7.034 | 0.9574 | 2.439 | 0.0182 | 0.0510 |
| $Eu^{2+}$ | 0.8970 | 18.443 | 1.3769 | 7.005 | 0.9060 | 2.421 | 0.0190 | 0.0511 |
| $Eu^{3+}$ | 0.3985 | 18.451 | 1.3307 | 6.956 | 0.9603 | 2.378 | 0.0197 | 0.0447 |
| $Gd^{2+}$ | 0.7756 | 18.469 | 1.3124 | 6.899 | 0.8956 | 2.338 | 0.0199 | 0.0441 |
| $Gd^{3+}$ | 0.3347 | 18.476 | 1.2465 | 6.877 | 0.9537 | 2.318 | 0.0217 | 0.0484 |
| $Tb^{2+}$ | 0.6688 | 18.491 | 1.2487 | 6.822 | 0.8888 | 2.275 | 0.0215 | 0.0439 |
| $Tb^{3+}$ | 0.2892 | 18.497 | 1.1678 | 6.797 | 0.9437 | 2.257 | 0.0232 | 0.0458 |
| $Dy^{2+}$ | 0.5917 | 18.511 | 1.1828 | 6.747 | 0.8801 | 2.214 | 0.0229 | 0.0439 |
| $Dy^{3+}$ | 0.2523 | 18.517 | 1.0914 | 6.736 | 0.9345 | 2.208 | 0.0250 | 0.0476 |
| $Ho^{2+}$ | 0.5094 | 18.515 | 1.1234 | 6.706 | 0.8727 | 2.159 | 0.0242 | 0.0560 |
| $Ho^{3+}$ | 0.2188 | 18.516 | 1.0240 | 6.707 | 0.9251 | 2.161 | 0.0268 | 0.0503 |
| $Er^{2+}$ | 0.4693 | 18.528 | 1.0545 | 6.649 | 0.8679 | 2.120 | 0.0261 | 0.0413 |
| $Er^{3+}$ | 0.1710 | 18.534 | 0.9879 | 6.625 | 0.9044 | 2.100 | 0.0278 | 0.0489 |
| $Tm^{2+}$ | 0.4198 | 18.542 | 0.9959 | 6.600 | 0.8593 | 2.082 | 0.0284 | 0.0457 |
| $Tm^{3+}$ | 0.1760 | 18.542 | 0.9105 | 6.579 | 0.8970 | 2.062 | 0.0294 | 0.0468 |
| $Yb^{2+}$ | 0.3852 | 18.550 | 0.9415 | 6.551 | 0.8492 | 2.043 | 0.0301 | 0.0478 |
| $Yb^{3+}$ | 0.1570 | 18.555 | 0.8484 | 6.540 | 0.8880 | 2.037 | 0.0318 | 0.0498 |

Table 4.4.5.8. $\langle j_2 \rangle$ *form factors for actinide ions*

| Ion | *A* | *a* | *B* | *b* | *C* | *c* | *D* | *e* |
|---|---|---|---|---|---|---|---|---|
| $U^{3+}$ | 4.1582 | 16.534 | 2.4675 | 5.952 | −0.0252 | 0.765 | 0.0057 | 0.0822 |
| $U^{4+}$ | 3.7449 | 13.894 | 2.6453 | 4.863 | −0.5218 | 3.192 | 0.0009 | 0.0928 |
| $U^{5+}$ | 3.0724 | 12.546 | 2.3076 | 5.231 | −0.0644 | 1.474 | 0.0035 | 0.0477 |
| $Np^{3+}$ | 3.7170 | 15.133 | 2.3216 | 5.503 | −0.0275 | 0.800 | 0.0052 | 0.0948 |
| $Np^{4+}$ | 2.9203 | 14.646 | 2.5979 | 5.559 | −0.0301 | 0.367 | 0.0141 | 0.0532 |
| $Np^{5+}$ | 2.3308 | 13.654 | 2.7219 | 5.494 | −0.1357 | 0.049 | 0.1224 | 0.0553 |
| $Np^{6+}$ | 1.8245 | 13.180 | 2.8508 | 5.407 | −0.1579 | 0.044 | 0.1438 | 0.0585 |
| $Pu^{3+}$ | 2.0885 | 12.871 | 2.5961 | 5.190 | −0.1465 | 0.039 | 0.1343 | 0.0866 |
| $Pu^{4+}$ | 2.7244 | 12.926 | 2.3387 | 5.163 | −0.1300 | 0.046 | 0.1177 | 0.0490 |
| $Pu^{5+}$ | 2.1409 | 12.832 | 2.5664 | 5.152 | −0.1338 | 0.046 | 0.1210 | 0.0491 |
| $Pu^{6+}$ | 1.7262 | 12.324 | 2.6652 | 5.066 | −0.1695 | 0.041 | 0.1550 | 0.0502 |
| $Am^{2+}$ | 3.5237 | 15.955 | 2.2855 | 5.195 | −0.0142 | 0.585 | 0.0033 | 0.1120 |
| $Am^{3+}$ | 2.8622 | 14.733 | 2.4099 | 5.144 | −0.1326 | 0.031 | 0.1233 | 0.0727 |
| $Am^{4+}$ | 2.4141 | 12.948 | 2.3687 | 4.945 | −0.2490 | 0.022 | 0.2371 | 0.0502 |
| $Am^{5+}$ | 2.0109 | 12.053 | 2.4155 | 4.836 | −0.2264 | 0.027 | 0.2128 | 0.0414 |
| $Am^{6+}$ | 1.6778 | 11.337 | 2.4531 | 4.725 | −0.2043 | 0.034 | 0.1892 | 0.0387 |
| $Am^{7+}$ | 1.8845 | 9.161 | 2.0746 | 4.042 | −0.1318 | 1.723 | 0.0020 | 0.0379 |

Table 4.4.5.9. $\langle j_4 \rangle$ *form factors for 3d atoms and their ions*

| Atom or ion | *A* | *a* | *B* | *b* | *C* | *c* | *D* | *e* |
|---|---|---|---|---|---|---|---|---|
| Sc | 1.3420 | 10.200 | 0.3837 | 3.079 | 0.0468 | 0.118 | −0.0328 | 0.1343 |
| $Sc^{+}$ | 7.1167 | 15.487 | −6.6671 | 18.269 | 0.4900 | 2.992 | 0.0047 | 0.1624 |
| $Sc^{2+}$ | −1.6684 | 15.648 | 1.7742 | 9.062 | 0.4075 | 2.412 | 0.0042 | 0.1105 |
| Ti | −2.1515 | 11.271 | 2.5149 | 8.859 | 0.3555 | 2.149 | 0.0045 | 0.1244 |
| $Ti^{+}$ | −1.0383 | 16.190 | 1.4699 | 8.924 | 0.3631 | 2.283 | 0.0044 | 0.1270 |
| $Ti^{2+}$ | −1.3242 | 15.310 | 1.2042 | 7.899 | 0.3976 | 2.156 | 0.0051 | 0.0820 |
| $Ti^{3+}$ | −1.1117 | 14.635 | 0.7689 | 6.927 | 0.4385 | 2.089 | 0.0060 | 0.0572 |
| V | −0.9633 | 15.273 | 0.9274 | 7.732 | 0.3891 | 2.053 | 0.0063 | 0.0840 |
| $V^{+}$ | −0.9606 | 15.545 | 1.1278 | 8.118 | 0.3653 | 2.097 | 0.0056 | 0.1027 |
| $V^{2+}$ | −1.1729 | 14.973 | 0.9092 | 7.613 | 0.4105 | 2.039 | 0.0067 | 0.0719 |
| $V^{3+}$ | −0.9417 | 14.205 | 0.5284 | 6.607 | 0.4411 | 1.967 | 0.0076 | 0.0569 |
| $V^{4+}$ | −0.7654 | 13.097 | 0.3071 | 5.674 | 0.4476 | 1.871 | 0.0081 | 0.0518 |
| Cr | −0.6670 | 19.613 | 0.5342 | 6.478 | 0.3641 | 1.905 | 0.0073 | 0.0628 |
| $Cr^{+}$ | −0.8309 | 18.043 | 0.7252 | 7.531 | 0.3828 | 2.003 | 0.0073 | 0.0781 |
| $Cr^{2+}$ | −0.8930 | 15.664 | 0.5590 | 7.033 | 0.4093 | 1.924 | 0.0081 | 0.0631 |
| $Cr^{3+}$ | −0.7327 | 14.073 | 0.3268 | 5.674 | 0.4114 | 1.810 | 0.0085 | 0.0505 |
| $Cr^{4+}$ | −0.6748 | 12.946 | 0.1805 | 6.753 | 0.4526 | 1.800 | 0.0098 | 0.0644 |
| Mn | −0.5452 | 15.471 | 0.4406 | 4.902 | 0.2884 | 1.543 | 0.0059 | 0.0488 |
| $Mn^{+}$ | −0.7947 | 17.867 | 0.6078 | 7.704 | 0.3798 | 1.905 | 0.0087 | 0.0737 |
| $Mn^{2+}$ | −0.7416 | 15.255 | 0.3831 | 6.469 | 0.3935 | 1.800 | 0.0093 | 0.0577 |
| $Mn^{3+}$ | −0.6603 | 13.607 | 0.2322 | 6.218 | 0.4104 | 1.740 | 0.0101 | 0.0579 |
| $Mn^{4+}$ | −0.5127 | 13.461 | 0.0313 | 7.763 | 0.4282 | 1.701 | 0.0113 | 0.0693 |
| Fe | −0.5029 | 19.677 | 0.2999 | 3.776 | 0.2576 | 1.424 | 0.0071 | 0.0292 |
| $Fe^{+}$ | −0.5109 | 19.250 | 0.3896 | 4.891 | 0.2810 | 1.526 | 0.0069 | 0.0375 |
| $Fe^{2+}$ | −0.5401 | 17.227 | 0.2865 | 3.742 | 0.2658 | 1.424 | 0.0076 | 0.0278 |
| $Fe^{3+}$ | −0.5507 | 11.493 | 0.2153 | 4.906 | 0.3468 | 1.523 | 0.0095 | 0.0314 |
| $Fe^{4+}$ | −0.5352 | 9.507 | 0.1783 | 5.175 | 0.3584 | 1.469 | 0.0097 | 0.0360 |
| Co | −0.4221 | 14.195 | 0.2900 | 3.979 | 0.2469 | 1.286 | 0.0063 | 0.0400 |
| $Co^{+}$ | −0.4115 | 14.561 | 0.3580 | 4.717 | 0.2644 | 1.418 | 0.0074 | 0.0541 |
| $Co^{2+}$ | 0.4759 | 14.046 | 0.2747 | 3.731 | 0.2458 | 1.250 | 0.0057 | 0.0282 |
| $Co^{3+}$ | −0.4466 | 13.391 | 0.1419 | 3.011 | 0.2773 | 1.335 | 0.0093 | 0.0341 |
| $Co^{4+}$ | −0.4091 | 13.194 | −0.0194 | 3.417 | 0.3534 | 1.421 | 0.0112 | 0.0622 |
| Ni | −0.4428 | 14.485 | 0.0870 | 3.234 | 0.2932 | 1.331 | 0.0096 | 0.0554 |
| $Ni^{+}$ | −0.3836 | 13.425 | 0.3116 | 4.462 | 0.2471 | 1.309 | 0.0079 | 0.0515 |
| $Ni^{2+}$ | −0.3803 | 10.403 | 0.2838 | 3.378 | 0.2108 | 1.104 | 0.0050 | 0.0474 |
| $Ni^{3+}$ | −0.4014 | 9.046 | 0.2314 | 3.075 | 0.2192 | 1.084 | 0.0060 | 0.0323 |
| $Ni^{4+}$ | −0.3509 | 8.157 | 0.2220 | 2.106 | 0.1567 | 0.925 | 0.0065 | 0.0352 |
| Cu | −0.3204 | 15.132 | 0.2335 | 4.021 | 0.2312 | 1.196 | 0.0068 | 0.0457 |
| $Cu^{+}$ | −0.3572 | 15.125 | 0.2336 | 3.966 | 0.2315 | 1.197 | 0.0070 | 0.0397 |
| $Cu^{2+}$ | −0.3914 | 14.740 | 0.1275 | 3.384 | 0.2548 | 1.255 | 0.0103 | 0.0394 |
| $Cu^{3+}$ | −0.3671 | 14.082 | −0.0078 | 3.315 | 0.3154 | 1.377 | 0.0132 | 0.0534 |
| $Cu^{4+}$ | −0.2915 | 14.124 | −0.1065 | 4.201 | 0.3247 | 1.352 | 0.0148 | 0.0579 |

Table 4.4.5.10. $\langle j_4 \rangle$ *form factors for 4d atoms and their ions*

| Atom or ion | *A* | *a* | *B* | *b* | *C* | *c* | *D* | *e* |
|---|---|---|---|---|---|---|---|---|
| Y | −8.0767 | 32.201 | 7.9197 | 25.156 | 1.4067 | 6.827 | −0.0001 | 0.1031 |
| Zr | −5.2697 | 32.868 | 4.1930 | 24.183 | 1.5202 | 6.048 | −0.0002 | 0.0855 |
| $Zr^{+}$ | −5.6384 | 33.607 | 4.6729 | 22.338 | 1.3258 | 5.924 | −0.0003 | 0.0674 |
| Nb | −3.1377 | 25.595 | 2.3411 | 16.569 | 1.2304 | 4.990 | −0.0005 | 0.0615 |
| $Nb^{+}$ | −3.3598 | 25.820 | 2.8297 | 16.427 | 1.1203 | 4.982 | −0.0005 | 0.0724 |
| Mo | −2.8860 | 20.572 | 1.8130 | 14.628 | 1.1899 | 4.264 | −0.0008 | 0.0410 |
| $Mo^{+}$ | −3.2618 | 25.486 | 2.3596 | 16.462 | 1.1164 | 4.491 | −0.0007 | 0.0592 |
| Tc | −2.7975 | 20.159 | 1.6520 | 16.261 | 1.1726 | 3.943 | −0.0008 | 0.0657 |
| $Tc^{+}$ | −2.0470 | 19.683 | 1.6306 | 11.592 | 0.8698 | 3.769 | −0.0010 | 0.0723 |
| Ru | −1.5042 | 17.949 | 0.6027 | 9.961 | 0.9700 | 3.393 | −0.0010 | 0.0338 |
| $Ru^{+}$ | 1.6278 | 18.506 | 1.1828 | 10.189 | 0.8138 | 3.418 | −0.0009 | 0.0673 |
| Rh | −1.3492 | 17.577 | 0.4527 | 10.507 | 0.9285 | 3.155 | −0.0009 | 0.0483 |
| $Rh^{+}$ | −1.4673 | 17.957 | 0.7381 | 9.944 | 0.8485 | 3.126 | −0.0012 | 0.0487 |
| Pd | −1.1955 | 17.628 | 0.3183 | 11.309 | 0.8696 | 2.909 | −0.0006 | 0.0555 |
| $Pd^{+}$ | −1.4098 | 17.765 | 0.7927 | 9.999 | 0.7710 | 2.930 | −0.0006 | 0.0530 |

Table 4.4.5.11. $\langle j_4 \rangle$ *form factors for rare-earth ions*

| Ion | *A* | *a* | *B* | *b* | *C* | *c* | *D* | *e* |
|---|---|---|---|---|---|---|---|---|
| $Ce^{2+}$ | −0.6468 | 10.533 | 0.4052 | 5.624 | 0.3412 | 1.535 | 0.0080 | 0.0522 |
| $Nd^{2+}$ | −0.5416 | 12.204 | 0.3571 | 6.169 | 0.3154 | 1.485 | 0.0098 | 0.0519 |
| $Nd^{3+}$ | −0.4053 | 14.014 | 0.0329 | 7.005 | 0.3759 | 1.707 | 0.0209 | 0.0372 |
| $Sm^{2+}$ | −0.4150 | 14.057 | 0.1368 | 7.032 | 0.3272 | 1.582 | 0.0192 | 0.0319 |
| $Sm^{3+}$ | −0.4288 | 10.052 | 0.1782 | 5.019 | 0.2833 | 1.236 | 0.0088 | 0.0328 |
| $Eu^{2+}$ | −0.4145 | 10.193 | 0.2447 | 5.164 | 0.2661 | 1.205 | 0.0065 | 0.0516 |
| $Eu^{3+}$ | −0.4095 | 10.211 | 0.1485 | 5.175 | 0.2720 | 1.237 | 0.0131 | 0.0494 |
| $Gd^{2+}$ | −0.3824 | 10.344 | 0.1955 | 5.306 | 0.2622 | 1.203 | 0.0097 | 0.0363 |
| $Gd^{3+}$ | −0.3621 | 10.353 | 0.1016 | 5.310 | 0.2649 | 1.219 | 0.0147 | 0.0494 |
| $Tb^{2+}$ | −0.3443 | 10.469 | 0.1481 | 5.416 | 0.2575 | 1.182 | 0.0104 | 0.0280 |
| $Tb^{3+}$ | −0.3228 | 10.476 | 0.0638 | 5.419 | 0.2566 | 1.196 | 0.0159 | 0.0439 |
| $Dy^{2+}$ | −0.3206 | 12.071 | 0.0904 | 8.026 | 0.2616 | 1.230 | 0.0143 | 0.0767 |
| $Dy^{3+}$ | −0.2829 | 9.525 | 0.0565 | 4.429 | 0.2437 | 1.066 | 0.0092 | 0.0181 |
| $Ho^{2+}$ | −0.2976 | 9.719 | 0.1224 | 4.635 | 0.2279 | 1.005 | 0.0063 | 0.0452 |
| $Ho^{3+}$ | −0.2717 | 9.731 | 0.0474 | 4.638 | 0.2292 | 1.047 | 0.0124 | 0.0310 |
| $Er^{2+}$ | −0.2975 | 9.829 | 0.1189 | 4.741 | 0.2116 | 1.004 | 0.0117 | 0.0524 |
| $Er^{3+}$ | −0.2568 | 9.834 | 0.0356 | 4.741 | 0.2172 | 1.028 | 0.0148 | 0.0434 |
| $Tm^{2+}$ | −0.2677 | 9.888 | 0.0925 | 4.784 | 0.2056 | 0.990 | 0.0124 | 0.0396 |
| $Tm^{3+}$ | −0.2292 | 9.895 | 0.0124 | 4.785 | 0.2108 | 1.007 | 0.0151 | 0.0334 |
| $Yb^{2+}$ | −0.2393 | 9.947 | 0.0663 | 4.823 | 0.2009 | 0.965 | 0.0122 | 0.0311 |
| $Yb^{3+}$ | −0.2121 | 8.197 | 0.0325 | 3.153 | 0.1975 | 0.884 | 0.0093 | 0.0435 |

Table 4.4.5.12. $\langle j_4 \rangle$ *form factors for actinide ions*

| Ion | *A* | *a* | *B* | *b* | *C* | *c* | *D* | *e* |
|---|---|---|---|---|---|---|---|---|
| $U^{3+}$ | −0.9859 | 16.601 | 0.6116 | 6.515 | 0.6020 | 2.597 | −0.0010 | 0.0599 |
| $U^{4+}$ | −1.0540 | 16.605 | 0.4339 | 6.512 | 0.6746 | 2.599 | −0.0011 | 0.0471 |
| $U^{5+}$ | −0.9588 | 16.485 | 0.1576 | 6.440 | 0.7785 | 2.640 | −0.0010 | 0.0493 |
| $Np^{3+}$ | 0.9029 | 16.586 | 0.4006 | 6.470 | 0.6545 | 2.563 | −0.0004 | 0.0470 |
| $Np^{4+}$ | −0.9887 | 12.441 | 0.5918 | 5.294 | 0.5306 | 2.263 | −0.0021 | 0.0583 |
| $Np^{5+}$ | −0.8146 | 16.581 | −0.0055 | 6.475 | 0.7956 | 2.562 | −0.0004 | 0.0600 |
| $Np^{6+}$ | 0.6738 | 16.553 | −0.2297 | 6.505 | 0.8513 | 2.553 | −0.0003 | 0.0623 |
| $Pu^{3+}$ | −0.7014 | 16.369 | −0.1162 | 6.697 | 0.7778 | 2.450 | 0.0000 | 0.0546 |
| $Pu^{4+}$ | −0.9160 | 12.203 | 0.4891 | 5.127 | 0.5290 | 2.149 | −0.0022 | 0.0520 |
| $Pu^{5+}$ | −0.7035 | 16.360 | −0.0979 | 6.706 | 0.7726 | 2.447 | 0.0000 | 0.0610 |
| $Pu^{6+}$ | −0.5560 | 16.322 | −0.3046 | 6.768 | 0.8146 | 2.426 | 0.0001 | 0.0596 |
| $Am^{2+}$ | −0.7433 | 16.416 | 0.3481 | 6.788 | 0.6014 | 2.346 | 0.0000 | 0.0566 |
| $Am^{3+}$ | 0.8092 | 12.854 | 0.4161 | 5.459 | 0.5476 | 2.172 | −0.0011 | 0.0530 |
| $Am^{4+}$ | −0.8548 | 12.226 | 0.3037 | 5.909 | 0.6173 | 2.188 | −0.0016 | 0.0456 |
| $Am^{5+}$ | −0.6538 | 15.462 | −0.0948 | 5.997 | 0.7295 | 2.297 | 0.0000 | 0.0594 |
| $Am^{6+}$ | −0.5390 | 15.449 | −0.2689 | 6.017 | 0.7711 | 2.297 | 0.0002 | 0.0729 |
| $Am^{7+}$ | −0.4688 | 12.019 | −0.2692 | 7.042 | 0.7297 | 2.164 | −0.0011 | 0.0262 |

Table 4.4.5.13. $\langle j_6 \rangle$ *form factors for rare-earth ions*

| Ion | *A* | *a* | *B* | *b* | *C* | *c* | *D* | *e* |
|---|---|---|---|---|---|---|---|---|
| $Ce^{2+}$ | −0.1212 | 7.994 | −0.0639 | 4.024 | 0.1519 | 1.096 | 0.0078 | 0.0388 |
| $Nd^{2+}$ | −0.1600 | 8.009 | 0.0272 | 4.028 | 0.1104 | 1.068 | 0.0139 | 0.0363 |
| $Nd^{3+}$ | 0.0416 | 8.014 | −0.1261 | 4.040 | 0.1400 | 1.087 | 0.0102 | 0.0367 |
| $Sm^{2+}$ | 0.1428 | 6.041 | 0.0723 | 2.033 | 0.0550 | 0.513 | 0.0081 | 0.0450 |
| $Sm^{3+}$ | −0.0944 | 6.030 | −0.0498 | 2.074 | 0.1372 | 0.645 | −0.0132 | 0.0387 |
| $Eu^{2+}$ | −0.1252 | 6.049 | 0.0507 | 2.085 | 0.0572 | 0.646 | 0.0132 | 0.0403 |
| $Eu^{3+}$ | −0.0817 | 6.039 | −0.0596 | 2.120 | 0.1243 | 0.764 | −0.0001 | 0.0206 |
| $Gd^{2+}$ | −0.1351 | 5.030 | 0.0828 | 2.025 | 0.0315 | 0.503 | 0.0187 | 0.0453 |
| $Gd^{3+}$ | −0.0662 | 6.031 | −0.0850 | 2.154 | 0.1323 | 0.891 | 0.0048 | 0.0371 |
| $Th^{2+}$ | −0.0758 | 6.032 | −0.0540 | 2.158 | 0.1199 | 0.890 | 0.0051 | 0.0488 |
| $Tb^{3+}$ | −0.0559 | 6.031 | −0.1020 | 2.237 | 0.1264 | 1.107 | 0.0167 | 0.0170 |
| $Dy^{2+}$ | −0.0568 | 6.032 | −0.1003 | 2.240 | 0.1401 | 1.106 | 0.0109 | 0.0463 |
| $Dy^{3+}$ | −0.0423 | 6.038 | −0.1248 | 2.244 | 0.1359 | 1.200 | 0.0188 | 0.0350 |
| $Ho^{2+}$ | −0.0725 | 6.045 | −0.0318 | 2.243 | 0.0738 | 1.202 | 0.0252 | 0.0634 |
| $Ho^{3+}$ | −0.0289 | 6.050 | −0.1545 | 2.230 | 0.1550 | 1.260 | 0.0177 | 0.0351 |
| $Er^{2+}$ | 0.0648 | 6.056 | −0.0515 | 2.230 | 0.0825 | 1.264 | 0.0250 | 0.0409 |
| $Er^{3+}$ | −0.0110 | 6.061 | −0.1954 | 2.224 | 0.1818 | 1.296 | 0.0149 | 0.0455 |
| $Tm^{2+}$ | 0.0842 | 4.070 | 0.0807 | 0.849 | −0.2087 | 0.039 | 0.2095 | 0.0360 |
| $Tm^{3+}$ | 0.0727 | 4.073 | 0.0243 | 0.689 | 3.9459 | 0.002 | −3.9076 | 0.0502 |
| $Yb^{2+}$ | −0.0739 | 5.031 | 0.0140 | 2.030 | 0.0351 | 0.508 | 0.0174 | 0.0434 |
| $Yb^{3+}$ | −0.0345 | 5.007 | −0.0677 | 2.020 | 0.0985 | 0.549 | −0.0076 | 0.0359 |

Table 4.4.5.14. $\langle j_6 \rangle$ *form factors for actinide ions*

| Ion | *A* | *a* | *B* | *b* | *C* | *c* | *D* | *e* |
|---|---|---|---|---|---|---|---|---|
| $U^{3+}$ | −0.3797 | 9.953 | 0.0459 | 5.038 | 0.2748 | 1.607 | 0.0016 | 0.0345 |
| $U^{4+}$ | −0.1793 | 11.896 | −0.2269 | 5.428 | 0.3291 | 1.701 | 0.0030 | 0.0472 |
| $U^{5+}$ | −0.0399 | 11.891 | −0.3458 | 5.580 | 0.3340 | 1.645 | 0.0029 | 0.0444 |
| $Np^{3+}$ | −0.2427 | 11.844 | −0.1129 | 5.377 | 0.2848 | 1.568 | 0.0022 | 0.0368 |
| $Np^{4+}$ | −0.2436 | 9.599 | −0.1317 | 4.101 | 0.3029 | 1.545 | 0.0019 | 0.0500 |
| $Np^{5+}$ | −0.1157 | 9.565 | −0.2654 | 4.260 | 0.3298 | 1.549 | 0.0025 | 0.0495 |
| $Np^{6+}$ | −0.0128 | 9.569 | −0.3611 | 4.304 | 0.3419 | 1.541 | 0.0032 | 0.0520 |
| $Pu^{3+}$ | −0.0364 | 9.572 | −0.3181 | 4.342 | 0.3210 | 1.523 | 0.0041 | 0.0496 |
| $Pu^{4+}$ | −0.2394 | 7.837 | −0.0785 | 4.024 | 0.2643 | 1.378 | 0.0012 | 0.0414 |
| $Pu^{5+}$ | −0.1090 | 7.819 | −0.2243 | 4.100 | 0.2947 | 1.404 | 0.0015 | 0.0477 |
| $Pu^{6+}$ | −0.0001 | 7.820 | −0.3354 | 4.144 | 0.3097 | 1.403 | 0.0020 | 0.0513 |
| $Am^{2+}$ | −0.3176 | 7.864 | 0.0771 | 4.161 | 0.2194 | 1.339 | 0.0018 | 0.0374 |
| $Am^{3+}$ | −0.3159 | 6.982 | 0.0682 | 3.995 | 0.2141 | 1.188 | −0.0015 | 0.0281 |
| $Am^{4+}$ | −0.1787 | 7.880 | −0.1274 | 4.090 | 0.2565 | 1.315 | 0.0017 | 0.0419 |
| $Am^{5+}$ | −0.0927 | 6.073 | −0.2227 | 3.784 | 0.2916 | 1.372 | 0.0026 | 0.0485 |
| $Am^{6+}$ | 0.0152 | 6.079 | −0.3549 | 3.861 | 0.3125 | 1.403 | 0.0036 | 0.0732 |
| $Am^{7+}$ | 0.1292 | 6.082 | −0.4689 | 3.879 | 0.3234 | 1.393 | 0.0042 | 0.0475 |

in which $U(r)$ is the radial wavefunction for the unpaired electrons in the atom, $k$ is the length of the scattering vector, and $j_l(kr)$ is the $l$th-order spherical Bessel function.

Tables 4.4.5.1–4.4.5.8 give the coefficients in an analytical approximation to the $\langle j_0 \rangle$ magnetic form factors for the 3*d* and 4*d* transition series, the 4*f* electrons of rare-earth ions, and the 5*f* electrons of some actinide ions. The approximation has the form used by Forsyth & Wells (1959) but allowing three instead of two exponential terms:

$$\langle j_0(s) \rangle = A \exp(-as^2) + B \exp(-bs^2) + C \exp(-cs^2) + D, \quad (4.4.5.2)$$

where $s$ is the value of $(\sin\theta)/\lambda$ in $\text{Å}^{-1}$.

Tables 4.4.5.9–4.4.5.14 give coefficients in the approximation used by Lisher & Forsyth (1971) to the $\langle j_2 \rangle$, $\langle j_4 \rangle$, and $\langle j_6 \rangle$ form factors for the same series of atoms and ions, again using three rather than two exponential terms, *viz* for $l \neq 0$:

$$\langle j_l(s) \rangle = As^2 \exp(-as^2) + Bs^2 \exp(-bs^2) + Cs^2 \exp(-cs^2) + Ds^2. \quad (4.4.5.3)$$

For the transition-metal series, the coefficients of the approximation have been obtained by fitting to form factors calculated from the Hartree–Fock wavefunctions given by Clementi & Roetti (1974) in terms of Slater-type functions in the form

$$U(r) = \sum_{nj} N_{nl}\, r^2 A_{nlj} \exp(-a_{nlj}\, r) \quad (4.4.5.4)$$

by using the identity:

$$\int_0^\infty j_l(kr) r^n \exp(-pr) 4\pi r^2 \, dr = \frac{\pi^{3/2}\Gamma(n+l+3)k^l}{2^{l-1}\Gamma(l+3/2)(k^2+p^2)^{(n+l+3)/2}} \times {}_2F_1\left(\frac{n+l+3}{2}; \frac{l-n+3}{2}; l+\frac{3}{2}; \frac{k^2}{k^2+p^2}\right). \quad (4.4.5.5)$$

The form factors have been calculated from these relationships in the range $(\sin\theta)/\lambda = 0$ to $1.5\,\text{Å}^{-1}$ at intervals of $0.05\,\text{Å}^{-1}$, and the coefficients of the exponential expansion fitted by a least-squares procedure at the calculated points.

For the atoms of the rare-earth and actinide series, the wavefunctions and form factors have been calculated by Freeman & Desclaux (1979) and Desclaux & Freeman (1978) using Dirac–Fock theory. The constants given in Tables 4.4.5.3, 4.4.5.4, 4.4.5.7, 4.4.5.8, and 4.4.5.11–4.4.5.14 have been fitted to the results of these calculations. For the rare-earth ions, the form factors are given in the range $(\sin\theta)/\lambda = 0$ to $0.5\,\text{Å}^{-1}$ at intervals of $0.5\,\text{Å}^{-1}$ and in the range 0.5 to $1.2\,\text{Å}^{-1}$ at intervals of $0.1\,\text{Å}^{-1}$. For the actinide ions, the calculations extend to $1.5\,\text{Å}^{-1}$. All the values given in the publications cited were included in the fitting procedure. The accuracy with which the exponential expansions fit the theoretical form factors can be judged from the value of the parameter $e$ given in the tables, and defined by:

$$e = 100\left(\frac{\sum_i \delta_i^2}{N}\right)^{1/2}, \quad (4.4.5.6)$$

where $\delta_i$ is the difference between the $i$th fitted point and its theoretical value. The sum is over the $N$ points included in the fitting procedure.

### 4.4.6. Absorption coefficients for neutrons (By B. T. M. Willis)

The cross sections $\sigma$ discussed in Section 4.4.4 represent the area of each nucleus as seen by the neutron. To calculate the beam attenuation arising from absorption it is more convenient to use the macroscopic cross section $\Sigma$, which is the cross section per unit volume in units of $\text{cm}^{-1}$. $\Sigma$ is derived by multiplying $\sigma$ for the element by the number of atoms per unit volume. Thus, for element $j$, with density $\rho_j$ and atomic weight $A_j$,

$$\Sigma_j = N_A \rho_j \sigma_j / A_j,$$

where $N_A$ is Avogadro's number.

Table 4.4.6.1 gives the macroscopic absorption cross sections $\Sigma_a$ of the elements. They are tabulated for a neutron velocity $v = 2200\ \text{m s}^{-1}$, corresponding to a wavelength of 1.80 Å. The cross sections are larger at longer wavelengths (Section 4.4.4). Apart from a few exceptions, such as boron and cadmium, the absorption cross section is vastly smaller than for X-rays. The $1/e$ penetration depth ($l$) is listed separately – most metals, for example, have a penetration depth of several cm. The data in Table 4.4.6.1 have been derived from the review article by Hutchings & Windsor (1987).

Table 4.4.6.1. *Absorption of the elements for neutrons ($\lambda = 1.80$ Å)*

| Atom | $\Sigma_a$ ($\text{cm}^{-1}$) | $l$ (cm) | Atom | $\Sigma_a$ ($\text{cm}^{-1}$) | $l$ (cm) |
|---|---|---|---|---|---|
| H | 0.0141 | 0.288 | Rh | 10.544 | 0.092 |
| D | 0.0000 | 6.17 | Pd | 0.4687 | 1.29 |
| He | 0.0001 | 20.22 | Ag | 3.7120 | 0.249 |
| Li | 3.2698 | 0.300 | Cd | 116.80 | 0.008 |
| Be | 0.0009 | 1.059 | In | 7.4135 | 0.133 |
| B | 105.41 | 0.009 | Sn | 0.0231 | 4.87 |
| C | 0.0004 | 1.58 | Sb | 0.1689 | 3.20 |
| N | 0.0662 | 2.14 | Te | 0.1386 | 4.01 |
| O | 0.0001 | 5.52 | I | 0.1458 | 4.36 |
| F | 0.0003 | 6.82 | Xe | 0.3904 | 2.27 |
| Ne | 0.0017 | 8.71 | Cs | 0.2458 | 3.57 |
| Na | 0.0135 | 10.22 | Ba | 0.0189 | 13.39 |
| Mg | 0.0027 | 6.11 | La | 0.2402 | 2.00 |
| Al | 0.0139 | 9.48 | Ce | 0.0182 | 9.60 |
| Si | 0.0085 | 8.45 | Pr | 0.3333 | 2.46 |
| P | 0.0061 | 8.04 | Nd | 1.4763 | 0.496 |
| S | 0.0208 | 16.14 | Sm | 171.23 | 0.005 |
| Cl | 0.9109 | 0.731 | Eu | 95.715 | 0.010 |
| Ar | 0.0143 | 2.03 | Gd | 1474.1 | 0.000 |
| K | 0.0279 | 18.12 | Tb | 0.7334 | 1.05 |
| Ca | 0.0099 | 12.35 | Dy | 29.731 | 0.030 |
| Sc | 1.0906 | 0.491 | Ho | 2.0791 | 0.424 |
| Ti | 0.3453 | 1.74 | Er | 5.1861 | 0.182 |
| V | 0.3658 | 1.35 | Tm | 3.4919 | 0.269 |
| Cr | 0.2558 | 1.82 | Yb | 0.8513 | 0.717 |
| Mn | 1.0900 | 0.789 | Lu | 2.5889 | 0.354 |
| Fe | 0.2174 | 0.82 | Hf | 4.6648 | 0.195 |
| Co | 3.3440 | 0.260 | Ta | 1.1434 | 0.676 |
| Ni | 0.4104 | 0.475 | W | 1.1609 | 0.681 |
| Cu | 0.3202 | 1.00 | Re | 6.1692 | 0.143 |
| Zn | 0.0730 | 2.89 | Os | 1.1444 | 0.442 |
| Ga | 0.1480 | 2.04 | Ir | 30.064 | 0.032 |
| Ge | 0.1016 | 2.07 | Pt | 0.6843 | 0.682 |
| As | 0.2091 | 2.15 | Au | 5.8181 | 0.159 |
| Se | 0.4292 | 1.36 | Hg | 15.146 | 0.061 |
| Br | 0.1623 | 3.31 | Tl | 0.1200 | 2.15 |
| Kr | 0.3882 | 1.97 | Pb | 0.0056 | 2.68 |
| Rb | 0.0041 | 13.09 | Bi | 0.0009 | 3.84 |
| Sr | 0.0227 | 7.44 | Ra | 0.1706 | 2.95 |
| Y | 0.0388 | 3.66 | Th | 0.2244 | 1.68 |
| Zr | 0.0079 | 3.42 | Pa | 8.0405 | 0.118 |
| Nb | 0.0640 | 2.42 | U | 0.3650 | 1.26 |
| Mo | 0.1637 | 1.75 | Np | 9.0534 | 0.10 |
| Tc | 1.4281 | 0.542 | Pu | 14.481 | 0.069 |
| Ru | 0.1886 | 1.48 | Am | 2.5522 | 0.351 |

## References

### 4.1


Bonse, U. (1980). *X-ray sources. Characterization of crystal growth defects by X-ray methods*, edited by B. K. Tanner & D. K. Bowen, Chap. 11, pp. 298–319. New York: Plenum. [NATO Advanced Study Institute Series B63.]

Bordas, J. (1980). *A synchrotron radiation camera and data acquisition system for time resolved X-ray scattering studies. J. Phys. E*, **13**, 938–944.

Cowley, J. M. (1975). *Diffraction physics*, Chap. 1. Amsterdam: North-Holland.

Ertl, G. & Küppers, J. (1974). *Monographs in modern chemistry*, Vol. 4. *Energy electrons and surface chemistry*, edited by H. F. Ebel, Chap. 9, pp. 129–192. Weinheim: Verlag Chemie.

Feldman, C., Mayer, J. W. & Picraux, S. T. (1982). *Materials analysis by ion channeling*. London: Academic Press.

Frankel, R. D. & Forsyth, J. M. (1979). *Nanosecond X-ray diffraction from biological samples with a laser-produced plasma source. Science*, **204**, 622–624.

Grasselli, J. G., Snavely, M. K. & Bulkin, B. J. (1980). *Applications of Raman spectroscopy. Physics reports* 65, No. 4, pp. 231–344. Amsterdam: North-Holland.

Gyax, F. N., Kündig, W. & Meier, P. F. (1979). Editors. *Muon spin rotation*. Amsterdam: North-Holland.

Hansen, N. K. & Schneider, J. R. (1984). *Charge-density distribution of Be metal studied by γ-ray diffractometry. Phys. Rev. B*, **29**, 917–926.

Kaufmann, E. N. & Shenoy, G. K. (1981). Editors. *MRS symposia proceedings*, Vol. 3. *Nuclear and electron resonance spectroscopies applied to materials science*. New York: North-Holland.

Kunz, C. (1979). Editor. *Topics in current physics*, Vol. 10. *Synchrotron radiation, techniques and applications*. Berlin: Springer Verlag.

Kuz'min, R. N., Kolpakov, A. V. & Zhdanov, G. S. (1966). *Rassejanie messbauerovskovo izlutschenija kristallami. Kristallografiya*, **11**, 511–519. [English translation: *Sov. Phys. Crystallogr.* (1967), **11**, 457–465.]

Lee, P. A., Citrin, P. H., Eisenberger, P. & Kincaid, B. M. (1981). *Extended X-ray absorption fine structure – its strengths and limitations as a structural tool. Rev. Mod. Phys.* **53**, 769–806.

Marshall, W. & Lovesey, S. W. (1971). *Theory of thermal neutron scattering*. Oxford: Clarendon Press.

Parsons, D. F. (1980). Editor. *Ultrasoft X-ray microscopy: its application to biological and physical sciences*. New York: New York Academy of Sciences.

Plummer, E. W. & Eberhardt, W. (1982). *Advances in chemical physics*, Vol. XLIX. *Angle-resolved photoemission as a tool for the study of surfaces*, edited by I. Prigogine & S. I. Rice. New York: John Wiley.

Rosier, D. J. de & Klug, A. (1968). *Reconstruction of three dimensional structures from electron micrographs. Nature (London)*, **217**, 130–134.

Schneider, J. R. (1983). *Characterization of crystals by γ-ray and neutron diffraction methods. J. Cryst. Growth*, **65**, 660–671.

Siegel, R. W. (1980). *Positron annihilation spectroscopy. Annu. Rev. Mater. Sci.* **10**, 393–425.

Tanner, B. K. & Bowen, D. K. (1980). Editors. *Characterization of crystal growth defects by X-ray methods*. NATO Advanced Study Institute Series B63. New York: Plenum.

Windsor, C. G. (1981). *Pulsed neutron scattering*. London: Taylor and Francis.


### 4.2.1


Bailey, R. L. (1978). *The design and operation of magnetic liquid shaft seals*. In *Thermomechanics of magnetic fluids*, edited by B. Berkovsky. London: Hemisphere.

Buras, B. (1985). *The European Synchrotron Radiation Project. Nucl. Sci. Appl.* **2**, 127–143.

Buras, B. & Marr, G. V. (1979). Editors. *European Synchrotron Radiation Facility*. Suppl. III: *Instrumentation*. Strasbourg: ESF.

Buras, B. & Tazzari, S. (1984). Editors. *European Synchrotron Radiation Facility*. Geneva: ESRP c/o CERN.

Byer, R. L., Kuhn, K., Reed, M. & Trail, J. (1983). *Progress in high peak and average power lasers for soft X-ray production. Proc. SPIE*, **448**, 2–7.

Castaing, R. & Descamps, J. (1955). *Sur les bases physiques de l'analyse ponctuelle par spectrographie X. J. Phys. Radium*, **16**, 304–317.

Clay, R. E. (1934). *A 5 kW X-ray generator with a spinning target. Proc. Phys. Soc. London*, **46**, 703–712.

Cohen, E. R. & Taylor, B. N. (1987). *The 1986 adjustment of the fundamental physical constants. Rev. Mod. Phys.* **89**, 1121–1148.

Collins, C. B., Davanloo, F. & Bowen, T. S. (1986). *Flash X-ray source of intense nanosecond pulses produced at high repetition rates. Rev. Sci. Instrum.* **57**, 863–865.

Compton, A. H. & Allison, S. K. (1935). *X-rays in theory and experiment*. New York: Van Nostrand.

Cosslett, V. E. & Nixon, W. C. (1951). *X-ray shadow microscope. Nature (London)*, **168**, 24–25.

Cosslett, V. E. & Nixon, W. C. (1960). *X-ray microscopy*, pp. 217–222. Cambridge University Press.

Dyson, N. A. (1973). *X-rays in atomic and nuclear physics*. London: Longman.

Ehrenberg, W. & Spear, W. E. (1951). *An electrostatic focusing system and its application to a fine focus X-ray tube. Proc. Phys. Soc. London Sect. B*, **64**, 67–75.

Farge, Y. & Duke, P. J. (1979). Editors. *European Synchrotron Radiation Facility*. Suppl. 1: *The scientific case*. Strasbourg: ESF.

Fiorito, R. B., Rule, D. W., Piestrup, M. A., Li, Q., Ho, A. H. & Maruyama, X. K. (1993). *Parametric X-ray generation from moderate-energy electron beams. Nucl. Instrum. Methods*, B**79**, 758–761.

Forsyth, J. M. & Frankel, R. D. (1980). *Flash X-ray diffraction from biological specimens using a laser-produced plasma source*. Report No. 106. Laboratory for Laser Energetics, University of Rochester, USA.

Forsyth, J. M. & Frankel, R. D. (1984). *Experimental facility for nanosecond time-resolved low-angle X-ray diffraction experiments using a laser-produced plasma source. Rev. Sci. Instrum.* **55**, 1235–1242.

Fourme, R. (1992). *Sources X intenses et cristallographie biologique. Ann. Phys. (Leipzig)*, **17**, 247–255.

Frankel, R. D. & Forsyth, J. M. (1979). *Nanosecond exposure X-ray diffraction patterns from biological specimens using a laser plasma source. Science*, **204**, 622–624.

**4.2.1 (*cont.*)**


Frankel, R. D. & Forsyth, J. M. (1985). *Time-resolved X-ray diffraction study of photo stimulated purple membrane*. *Biophys. J.* **47**, 387–393.

Godwin, R. P. (1968). *Synchrotron radiation light source*. *Springer Tracts Mod. Phys.* **51**, 1–69.

Goldberg, M. (1961). *Intensités relatives des raies X du spectre L excité par bombardement électronique des éléments lourds*. *J. Phys. Radium*, **22**, 743–748.

Goldsztaub, S. (1947). *Tube à rayons X de grande brilliance à foyer ponctuel*. *CR Acad. Sci.* **224**, 458–459.

Green, M. (1963). *The target absorption correction in X-ray microanalysis*. *X-ray optics and X-ray microanalysis*, edited by H. Pattee, V. E. Cosslett & A. Engstrom, pp. 361–377. London: Academic Press.

Green, M. & Cosslett, V. E. (1968). *Measurement of K, L and M shell X-ray production efficiencies*. *Br. J. Appl. Phys. Ser.* 2, **1**, 425–436.

Guo, C.-L. & Wu, Y.-Q. (1985). *Empirical relationship between the characteristic X-ray intensity and the incident electron energy*. *Kexue Tongbao*, **30**, 1621–1627.

Helliwell, J. R. (1984). *Synchrotron X-radiation protein crystallography*. *Rep. Progr. Phys.* **47**, 1403–1497.

Hofmann, A. (1978). *Quasi-monochromatic synchrotron radiation from undulators*. *Nucl. Instrum. Methods*, **152**, 17–21.

Honkimaki, V., Sleight, J. & Suortti, P. (1990). *Characteristic X-ray flux from sealed Cr, Cu, Mo, Ag and W tubes*. *J. Appl. Cryst.* **23**, 412–417.

Huke, K. & Kobayakawa, M. (1989). *World-wide census of SR facilities*. *Rev. Sci. Instrum.* **60**, 2548–2561.

Ishimura, T., Shiraiwa, Y. & Sawada, M. (1957). *The input power limit of the cylindrical rotating anode of an X-ray tube*. *J. Phys. Soc. Jpn*, **12**, 1064–1070.

Jenkins, R., Manne, R., Robin, J. & Senemaud, C. (1991). *Nomenclature, symbols, units and their usuage in spectrochemical analysis. VIII Nomenclature system for X-ray spectroscopy*. *Pure Appl. Chem.* **63**, 735–746.

Kirkpatrick, P. & Wiedmann, L. (1945). *Theoretical continuous X-ray energy and polarization*. *Phys. Rev.* **67**, 321–339.

Koch, E. E. (1983). Editor. *Handbook on synchrotron radiation*. Amsterdam: North-Holland.

Kramers, H. A. (1923). *On the theory of X-ray absorption and of the continuous X-ray spectrum*. *Philos. Mag.* **46**, 836–871.

Kulenkampff, H. & Schmidt, L. (1943). *Die Energieverteilung im Spektrum der Röntgen Bremsstrahlung*. *Ann. Phys. (Leipzig)*, **43**, 494–512.

Kulipanov, G. N. & Strinskii, A. N. (1977). *Utilization of synchrotron radiation: current status and propsects*. *Usp. Fiz. Nauk,* **122**, 369–418. English translation: *Sov. Phys. Usp.* **20**, 559–586.

Kunz, C. (1979). Editor. *Synchrotron radiation*. Berlin: Springer.

Kusev, S. V., Raiko, V. I. & Skuratowski, I., Ya. (1992). *The status of beam lines for macromolecular crystallography at the Siberia-2 storage ring*. *Rev. Sci. Instrum.* **63**, 1055–1057.

Laclare, J. L. (1994). *Target specifications and performance of the ESRF source*. *J. Synchrotron Rad.* **1**, 12–18.

Lea, K. (1978). *Highlights of synchrotron radiation*. *Phys. Rep.* **43**, 337–375.

Maruyama, X. K., Di Nova, K., Snyder, D., Piestrup, M. A., Li, Q., Fiorito, R. B. & Rule, D. W. (1993). *A compact tunable X-ray source based on parametric X-ray generation by moderate-energy linacs*. *Proc. 1993 Particle Accelerator Conference*. *IEEE*, **2**, 1620–1622.

Metchnik, V. & Tomlin, S. G. (1963). *On the absolute intensity of emission of characteristic X radiation*. *Proc. Phys. Soc. London*, **81**, 956–964.

Müller, A. (1927). *Input limits of X-ray generators*. *Proc. R. Soc. London Ser. A*, **117**, 30–42.

Müller, A. (1929). *A spinning-target X-ray generator and its input limit*. *Proc. R. Soc. London Ser. A*, **125**, 507–516.

Müller, A. (1931). *Further estimates of the input limits of X-ray generators*. *Proc. R. Soc. London Ser. A*, **132**, 646–649.

Nagel, D. J. (1980). *Comparison of X-ray sources for exposure of photo resists*. *Ann. NY Acad. Sci*, **342**, 235–247.

Oosterkamp, W. J. (1948). *The heat dissipation in the anode of an X-ray tube*. *Philips Res.* **3**, 49–59, 161–173, 303–317.

Phillips, W. C. (1985). *X-ray sources*. *Methods Enzymol.* **114**, 300–316.

Piestrup, M. A., Boyers, D. G., Pincus, C. I., Harris, J. L., Maruyama, X. K., Bergstrom, J. C., Caplan, H. S., Silzer, R. M. & Skopik, D. M. (1991). *Quasimonochromatic X-ray source using photo-absorption edge transition radiation*. *Phys. Rev. A*, **43**, 3653–3661.

Piestrup, M. A., Moran, M. J., Boyers, D. G., Pincus, C. I., Kephart, J. O., Gearhart, R. A. & Maruyama, X. K. (1991). *Generation of hard X-rays from transition radiation using high-density foils and moderate-energy electrons*. *Phys. Rev. A*, **43**, 2387–2396.

Reed, S. J. B. (1975). *Electron microprobe analysis*. Cambridge University Press.

Rudakov, L. I., Baigarin, K. A., Kalinin, Y. G., Korolev, V. D. & Kumachov, M. A. (1991). *Pulsed-plasma-based X-ray source and new X-ray optics*. *Phys. Fluids B (Plasma Phys.)*, **3**, 2414–2419.

Sakurai, K. (1993). *High-intensity X-ray line-focal spot for laboratory EXAFS measurements*. *Rev. Sci. Instrum.* **64**, 267–268.

Sakurai, K. & Sakurai, H. (1994). *Comment on High intensity low tube-voltage X-ray source for laboratory EXAFS measurements*. *Rev. Sci. Instrum.* **65**, 2417–2418.

Schwinger, J. (1949). *On the classical radiation of accelerated electrons*. *Phys. Rev.* **75**, 1912–1925.

Scott, V. D. & Love, G. (1983). *Quantitative electron microprobe analysis*. Cambridge University Press.

Seka, W., Soures, J. M., Lewis, O., Bunkenburg, J., Brown, D., Jacobs, S., Mourou, X. & Zimmermann, J. (1980). *High-power phosphate-glass laser system: design and performance characteristics*. *Appl. Opt.* **19**, 409–419.

Seka, W., Soures, J. M., Lund, L. & Craxton, R. S. (1981). *GDL: a high-power 0.35 $\mu$m laser irradiation facility*. *IEEE J. Quantum Electron. QE*-**17**, 1689–1693.

Siegbahn, M. (1925). *The spectroscopy of X-rays*. Oxford University Press.

Stephenson, S. T. (1957). *The continuous X-ray spectrum*. *Handbuch der Physik*. XXX: *X-rays*, edited by S. Flügge, pp. 337–370. Berlin: Springer.

Stern, E. A. (1980). Editor. *Laboratory EXAFS facilities 1980*. *AIP Conf. Proc.* No. 64.

Stuhrmann, H. (1982). Editor. *Uses of synchrotron radiation in biology*. Esp. *Properties of synchrotron radiation*, Chap. 1, by G. Materlik. London: Academic Press.

Suller, V. P. (1992). *Review of the status of synchrotron radiation storage rings*. *Third European Particle Accelerator Conference*. *Editions Frontières*, **1**, 77–81.

Taylor, A. (1949). *A 5 kW crystallographic X-ray tube with a rotating anode*. *J. Sci. Instrum.* **26**, 225–229.

Taylor, A. (1956). *Improved demountable crystallographic rotating anode X-ray tube*. *Rev. Sci. Instrum.* **27**, 757–759.

### 4.2.1 (*cont.*)


Thompson, D. J. & Poole, M. W. (1979). Editors. *European Synchrotron Radiation Facility*. Suppl. II: *The machine*. Strasbourg: ESF.

Tohji, K., Udagawa, Y., Kawasaki, T. & Masuda, K. (1983). *Laboratory EXAFS spectrometer with a bent-crystal, a solid-state detector, and a fast detection system. Rev. Sci. Instrum.* **54**, 1482–1487.

Wilson, R. R. (1941). *A vacuum-tight sliding seal. Rev. Sci. Instrum.* **12**, 91–93.

Winick, H. (1980). *Properties of synchrotron radiation*. In *Synchrotron radiation research*, edited by H. Winick & S. Doniach. New York: Plenum.

Winick, H. & Bienenstock, A. (1978). *Synchrotron radiation research. Ann. Rev. Nucl. Sci.* **28**, 33–113.

Yaakobi, B., Boehli, T., Bourke, P., Conturie, Y., Craxton, R. S., Delettrez, J., Forsyth, J. M., Frankel, R. D., Goldman, L. M., McCrory, L. R., Richardson, M. C., Seka, W., Shvarts, D. & Soures, J. M. (1981). *Characteristics of target interaction with high-power UV laser radiation. Opt. Commun.* **39**, 175–179.

Yaakobi, B., Bourke, P., Conturie, Y., Delettrez, J., Forsyth, J. M., Frankel, R. D., Goldman, L. M., McCrory, L. R., Seka, W., Soures, J. M., Burek, A. J. & Deslattes, R. D. (1981). *High X-ray conversion efficiency with target irradiation by a frequency-tripled Nd:glass laser. Opt. Commun.* **38**, 196–200.

Yao, T. (1992). *Lanthanum hexaboride filament in an X-ray generator of a laboratory EXAFS facility. Rev. Sci. Instrum.* **63**, 2103–2104.

Yoshimatsu, M. & Kozaki, S. (1977). *High-brilliance X-ray sources. X-ray optics*, edited by H.-J. Queisser, Chap. 2. Berlin: Springer.


### 4.2.2


Arndt, U. W. (1992). *X-ray wavelengths. International Tables for Crystallography*, Vol. C, edited by A. J. C. Wilson, pp. 176–182. Dordrecht: Kluwer Academic Publishers.

Barreau, G. H., Börner, H. G., Egidy, T. V. & Hoff, R. W. (1982). *Precision measurement of X-ray energies, natural widths and intensities in the actinide region. Z. Phys.* A**308**, 209–213.

Basile, G., Bergamin, A., Cavagnero, G., Mana, G., Vittone, E. & Zosi, G. (1994). *Measurement of the silicon (220) lattice spacing. Phys. Rev. Lett.* **72**, 3133–3136.

Basile, G., Bergamin, A., Cavagnero, G., Mana, G., Vittone, E. & Zosi, G. (1995). *The (220) lattice spacing of silicon. IEEE Trans. Instrum. Meas.* **44**, 526–529.

Bearden, J. A. (1960). *Lead K absorption edge for $\mu$-meson mass determination. Phys. Rev. Lett.* **4**, 240–241.

Bearden, J. A. (1965). *Selection of W $K\alpha_1$ as the X-ray wavelength standard. Phys. Rev. B,* **137**, 455–461.

Bearden, J. A. (1967). *X-ray wavelengths. Rev. Mod. Phys.* **39**, 78–100.

Bearden, J. A., Henins, A., Marzolf, J. G., Sauder, W. C. & Thomsen, J. S. (1964). *Precision redetermination of standard reference wavelengths for X-ray spectroscopy. Phys. Rev. A,* **135**, 899–910.

Bearden, J. A., Thomsen, J. S., Burr, A. F., Yap, F. Y., Huffman, F. N., Henins, A. & Matthews, G. D. (1964). *Remeasurement of selected X-ray lines and reevaluation of all published wavelengths on a consistent and absolute scale.* Baltimore, Maryland: The Johns Hopkins University.

Becker, P., Dorenwendt, K., Ebeling, G., Lauer, R., Lucas, W., Probst, R., Rademacher, H.-J., Reim, G., Seyfried, P. & Siegert, H. (1981). *Absolute measurement of the (220) lattice plane spacing in a silicon crystal. Phys. Rev. Lett.* **46**, 1540–1543.

Becker, P., Seyfried, P. & Siegert, H. (1982). *The lattice parameter of highly pure silicon single crystals. Z. Phys.* B**48**, 17–21.

Beyer, H., Indelicato, P., Finlayson, H., Liesen, D. & Deslattes, R. D. (1991). *Measurement of the 1s Lamb-shift in hydrogenlike nickel. Phys. Rev. A,* **43**, 223–227.

Blundell, S. A. (1993*a*). *Ab initio calculations of QED effects of Li-like, Na-like and Cu-like ions. Phys. Scr.* T**46**, 144–149.

Blundell, S. A. (1993*b*). *Calculations of the screened self-energy and vacuum polarization in Li-like, Na-like and Cu-like ions. Phys. Rev. A*, **47**, 1790–1803.

Blundell, S. A., Johnson, W. R. & Sapirstein, J. (1990). *Improved many-body perturbation theory calculations of the $n=2$ states of lithiumlike uranium. Phys. Rev. A*, **41**, 1698–1700.

Blundell, S. A., Mohr, P. J., Johnson, W. R. & Sapirstein, J. (1993). *Evaluation of two-photon exchange graphs for highly charged heliumlike ions. Phys. Rev. A*, **48**, 2615–2626.

Bonse, U. & Hart, M. (1965). *An X-ray interferometer. Appl. Phys. Lett.* **6**, 155–156.

Borchert, G. L. (1976). *Precise energies of K-Röntgen-lines of Tm, Th, U and Pu. Z. Naturforsh. Teil A*, **31**, 102–104.

Borchert, G. L., Hansen, P. G., Jonson, B., Ravn, H. L. & Desclaux, J. P. (1980). *Comparison of the K X-ray energy ratios of high Z and low Z elements with relativistic SCF DF calculations. Atomic massses and fundamental constants*, edited by J. E. Nolen & W. Benenson, Vol. 6, pp. 189–201. New York: Plenum Press.

Burr, A. F. (1996). Personal communication.

Cardona, M. & Ley, L. (1978). *Photemission in Solids I. Top. Appl. Phys.* **26**, 265–276.

Cauchois, Y. & Hulubei, H. (1947). *Tables de constantes et données numeriques. I. Longueurs d'onde des emissions X et des discontinuites d'absorption X.* Paris: Herman.

Cauchois, Y. & Senemaud, C. (1978). *Tables internationales de constantes selectionnées. 18. Longeurs d'onde des emissions X et des discontinuités d'absorption X.* London: Pergamon Press.

Cohen, E. R. & Taylor, B. N. (1973). *The 1973 least-squares adjustment of the fundamental constants. J. Phys. Chem. Ref. Data*, **2**, 663–734.

Desclaux, J. P. (1975). *A multiconfiguration relativistic Dirac–Fock program. Comput. Phys. Commun.* **9**, 31–45.

Desclaux, J. P. (1993). *Relativistic multiconfiguration Dirac–Fock package. Methods and techniques in computational chemistry – 94*, Vol. A, edited by E. Clementi. Cagliary: STEF.

Deslattes, R. D. & Henins, A. (1973). *X-ray to visible wavelength ratios. Phys. Rev. Lett.* **31**, 972–975.

Deslattes, R. D. & Kessler, E. G. Jr (1985). *Experimental evaluation of inner-vacancy level energies for comparison with theory. Atomic inner-shell physics,* edited by B. Crasemann, pp. 181–235. New York: Plenum.

Deslattes, R. D., Tanaka, M., Greene, G. L., Henins, A. & Kessler, E. G. (1987). *Remeasurement of a silicon lattice period. IEEE Trans. Instrum. Meas.* IM-**36**, 166.

Fuggle, J. C., Burr, A. F., Watson, L. M., Fabian, D. J. & Lang, W. (1974). *X-ray photoelectron studies of thorium and uranium. J. Phys. F*, **4**, 335–342.

**4.2.2 (*cont.*)**


Fujimoto, Z., Fujii, K., Tanaka, M. & Nakayama, K. (1997). *Lattice measurement in silicon. IEEE Trans. Instrum. Meas.* **50**, 123–124.

Härtwig, J., Hölzer, G., Förster, E., Goetz, K., Wokulska, K. & Wolf, J. (1994). *Remeasurement of characteristic X-ray emission lines and their application to line profile analysis and lattice parameter determination. Phys. Status Solidi. A,* **143**, 23–34.

Härtwig, J., Hölzer, G., Wolf, J. & Förster, E. (1993). *Remeasurement of the profile of the characteristic Cu Kα emission line with high precision and accuracy. J. Appl. Cryst.* **26**, 539–548.

Henins, A. (1971). *Ruled grating measurements of the Al $K\alpha_{1,2}$ wavelength. Precision measurements and fundamental constants*, edited by D. N. Langenberg & B. N. Taylor, pp. 255–258. *Natl Bur. Stand. (US) Spec. Publ.* No. 343. Gaithersburg, Maryland: National Bureau of Standards.

Hölzer, G., Fritsch, M., Deutsch, M., Härtwig, J. & Förster, E. (1997). *$K\alpha_{1,2}$ and $K\beta_{1,3}$ X-ray emission lines of the 3d transition metals. Phys. Rev. A*, **56**, 4554–4568.

Indelicato, P. (1990). *Kα transitions in few-electron ions and in atoms. X-ray and inner-shell processes*, edited by T. A. Carlson, M. O. Krause & S. T. Manson, pp. 591–601. New York: American Institute of Physics.

Indelicato, P. & Desclaux, J. P. (1990). *Multiconfiguration Dirac–Fock calculations of transition energies with QED corrections in three-electron ions. Phys. Rev. A*, **42**, 5139–5149.

Indelicato, P., Gorceix, O. & Desclaux, J. P. (1987). *MCDF studies of two electron ions II: radiative corrections and comparison with experiment. J. Phys. B*, **20**, 651.

Indelicato, P. & Lindroth, E. (1992). *Relativistic effects, correlation, and QED corrections on Kα transitions in medium to very heavy atoms. Phys. Rev. A*, **46**, 2426–2436.

Indelicato, P. & Lindroth, E. (1996). *Current status of the relativistic theory of inner hole states in heavy atoms. Comments At. Mol. Phys.* **32**, 197–208.

Indelicato, P. & Mohr, P. J. (1990). *Electron screening correction to the self energy in high-Z atoms.* 12th International Conference on Atomic Physics, Ann Arbor, Michigan, USA.

Indelicato, P. & Mohr, P. J. (1991). *Quantum electrodynamic effects in atomic structure. Theor. Chim. Acta*, **80**, 207–214.

Johnson, W. R. & Soff, G. (1985). *The Lamb shift in hydrogenlike atoms, $1 \leq Z \leq 110$. At. Data Nucl. Data Tables*, **33**, 405.

Kessler, E. G. Jr, Deslattes, R. D. & Henins, A. (1979). *Wavelength of the W $K\alpha_1$ X-ray line. Phys. Rev. A*, **19**, 215–218.

Kim, Y. K., Baik, D. H., Indelicato, P. & Desclaux, J. P. (1991). *Resonance transition energies of Li-, Na-, and Cu-like ions. Phys. Rev. A*, **44**, 148–166.

Kraft, S., Stümpel, J., Becker, P. & Kuetgens, U. (1996). *High resolution X-ray absorption spectroscopy with absolute energy calibration for the determination of absorption edge energies. Rev. Sci. Instrum.* **67**, 681–687.

Lebugle, A., Axelsson, U., Nyholm, R. & Mårtensson, N. (1981). *Experimental L and M core level binding energies for the metals 22Ti to 30Zn. Phys Scr.* **23**, 825–827.

Lindgren, I., Persson, H., Salomonson, S. & Labzowsky, L. (1995). *Full QED calculations of two-photon exchange for heliumlike systems: analysis in the Coulomb and Feynman gauge. Phys. Rev. A*, **51**, 1167–1195.

Lindroth, E. & Indelicato, P. (1993). *Inner shell transitions in heavy atoms. Phys. Scr.* T**46**, 139–143.

Lindroth, E. & Indelicato, P. (1994). *High precision calculations of inner shell transitions in heavy elements. Nucl. Instrum. Methods*, B**87**, 222–226.

Lum, G. K., Wiegand, C. E., Kessler, E. G. Jr, Deslattes, R. D., Jacobs, L., Schwitz, W. & Seki, R. (1981). *Kaonic mass by critical absorption of kaonic-atom X-rays. Phys. Rev. D,* **23**, 2522–2532.

Mohr, P. J. (1974*a*). *Numerical evaluation of the 1S1/2 state radiative level shift. Ann. Phys. (Leipzig)*, **88**, 52–87.

Mohr, P. J. (1974*b*). *Self-energy radiative corrections in hydrogen-like systems. Ann. Phys. (Leipzig)*, **88**, 26–51.

Mohr, P. J. (1975). *Lamb shift in a strong Coulomb potential. Phys. Rev. Lett.* **34**, 1050–1052.

Mohr, P. J. (1982). *Self-energy of the $n = 2$ states in a strong Coulomb field. Phys. Rev. A*, **26**, 2338–2354.

Mohr, P. J. (1992). *Self-energy correction to one-electron energy levels in a strong Coulomb field. Phys. Rev. A*, **46**, 4421–4424.

Mohr, P. J. & Soff, G. (1993). *Nuclear size correction to the electron self-energy. Phys. Rev. Lett.* **70**, 158–161.

Mohr, P. J. & Taylor, B. N. (2000). *CODATA recommended values of the fundamental physical constants: 1998. Rev. Mod. Phys.* **72**, 351–495.

Mooney, T., Lindroth, E., Indelicato, P., Kessler, E. & Deslattes, R. D. (1992). *Precision measurements of K and L transitions in xenon: experiment and theory for the K, L and M levels. Phys. Rev. A*, **45**, 1531–1543.

Mooney, T. M. (1996). Personal communication.

Nyholm, R., Berndtsson, A. & Mårtensson, N. (1980). *Core level binding energies for the elements Hf to Bi ($Z = 72$–$83$). J. Phys. C*, **13**, L1091–l1096.

Nyholm, R. & Mårtensson, N. (1980). *Core level binding energies for the elements Zr–Te ($Z = 40$–$52$). J. Phys. C,* **13**, L279–L284.

Parratt, L. G. (1959). *Electronic band structure of solids by X-ray spectroscopy. Rev. Mod. Phys.* **31**, 616–645.

Powell, C. J. (1995). *Elemental binding energies for X-ray photelectron spectroscopy. Appl. Surf. Sci.* **89**, 141–149.

Rieck, C. D. (1962). *Tables relating to the production, wavelengths, and intensities of X-rays. International tables for X-ray crystallography*, Vol. III, edited by C. H. MacGillavry & G. D. Rieck, pp. 59–72. Birmingham: Kynoch Press.

Schwarzenbach, D., Abrahams, S. C., Flack, H. D., Prince, E. & Wilson, A. J. C. (1995). *Statistical descriptors in crystallography. II. Report of a Working Group on Expression of Uncertainty in Measurement. Acta Cryst.* A**51**, 565–569.

Schweppe, J., Deslattes, R. D., Mooney, T. & Powell, C. J. (1994). *Accurate measurement of Mg and Al $K\alpha_{1,2}$ X-ray energy profiles. J. Electron Spectrosc. Relat. Phenom.* **67**, 463–478.

Schweppe, J. E. (1995). Personal communication.

Soff, G. & Mohr, P. J. (1988). *Vacuum polarization in a strong external field. Phys. Rev. A*, **38**, 5066–5075.

Taylor, B. N. & Kuyatt, C. E. (1994). *Guidelines for evaluating and expressing the uncertainty of NIST measurement results. NIST Technical Note* No. 1297. Gaithersburg, MD: National Institute of Standards and Technology.

Thomsen, J. S. & Burr, A. F. (1968). *Biography of the x-unit – the X-ray wavelength scale. Am. J. Phys.* **36**, 803–810.

Uehling, E. A. (1935). *Polarization effects in the positron theory. Phys. Rev.* **48**, 55–63.

**4.2.2 (*cont.*)**

Wichmann, E. H. & Kroll, N. M. (1956). *Vacuum polarization in a strong Coulomb field. Phys. Rev.* **101**, 843–859.

**4.2.3**

Alvarez, L. W., Crawford, F. S. & Stevenson, M. L. (1958). *Elastic scattering of 1.6 MeV gamma rays from H, Li, C and Al nuclei. Phys. Rev.* **112**, 1267–1273.

Azaroff, L. V. & Pease, D. M. (1974). *X-ray absorption spectra. X-ray spectroscopy*, edited by L. V. Azaroff, Chap. 6, pp. 284–337. New York: McGraw-Hill.

Bertin, E. P. (1975). *Principles and practice of X-ray spectrometric analysis*. New York: Plenum.

Bianconi, A., Incoccia, L. & Stipcich, S. (1983). Editors. *EXAFS and near edge structure*. Berlin: Springer.

Bowen, D. K., Stock, S. R., Davies, S. T., Pantos, E., Birnbaum, H. R. & Chen, H. (1984). *Topographic EXAFS. Nature (London)*, **309**, 336–338.

Bunker, G., Hasnain, S. S. & Sayers, D. E. (1990). *Report of the International Workshops on Standards and Criteria in XAFS*. In *X-ray absorption spectroscopy*, edited by S. S. Hasnain. London: Ellis Horwood.

Caballero, A., Villain, F., Dexpert, H., Le Peltier, F. & Lynch, J. (1993). *Characterization by in situ EXAFS spectroscopy of $Pt/Al_2O_3$ and $PtRe/Al_2O_3$ catalysts under reaction conditions. Jpn. J. Appl. Phys.* **32**, Suppl. 32–2, 439–441.

Chipman, D. R. (1969). *Conversion of relative intensities to an absolute scale. Acta Cryst.* A**25**, 209–214.

Citrin, P. H., Eisenberger, P. & Hewitt, R. (1978). *Extended X-ray absorption fine structure of surface atoms on single crystal substrates: iodine absorbed on Ag(111). Phys. Rev. Lett.* **41**, 309–312.

Cohen, E. R. & Taylor, B. N. (1987). *The 1986 adjustment of the fundamental physical constants. Rev. Mod. Phys.* **89**, 1121–1148.

Cooper, M. J. (1985). *Compton scattering and electron momentum determination. Rep. Prog. Phys.* **48**, 415–481.

Creagh, D. C. (1985). *Theoretical and experimental techniques for the determination of X-ray dispersion corrections. Aust. J. Phys.* **38**, 371–404.

Creagh, D. C. (1987*a*). *The resolution of discrepancies in tables of photon attenuation coefficients. Nucl. Instrum. Methods*, A**255**, 1–16.

Creagh, D. C. (1987*b*). *The X-ray anomalous dispersion corrections and their use for the characterization of materials*. In *Progress in crystal growth and characterization*, Vol. 14, edited by P. Krishna, Chap. 7, pp. 1–46. Oxford: Pergamon Press.

Creagh, D. C. & Hubbell, J. H. (1987). *Problems associated with the measurement of X-ray attenuation coefficients. I. Silicon. Acta Cryst.* A**43**, 102–112.

Crozier, E. D. & Seary, A. J. (1980). *Asymmetric effects in the extended X-ray absorption fine structure. Analysis of solid and liquid zinc. Can. J. Phys.* **58**, 1388–1399.

Dreier, P., Rabe, P., Matzfeld, W. & Niemann, W. (1984). *Anomalous X-ray scattering factors calculated from experimental absorption factor. J. Phys. C*, **17**, 3123–3136.

Durham, P. J. (1983). *Multiple scattering calculations of XANES. EXAFS and near edge structure*, edited by A. Bianconi, L. Incoccia & S. Stipcich, pp. 37–43. Berlin: Springer.

Fricke, H. (1920). *The K-characteristic absorption frequencies for the chemical elements magnesium to chromium. Phys. Rev.* **16**, 202–212.

Fuoss, P. H., Eisenberger, P., Warburton, W. K. & Bienenstock, A. (1981). *Application of differential anomalous X-ray scattering to structural studies of amorphous materials. Phys. Rev. Lett.* **46**, 1537–1540.

Gerstenberg, H. & Hubbell, J. H. (1982). *Comparison of experimental with theoretical photon attenuation cross sections between 10 eV and 100 GeV. Nuclear data for science and technology*, edited by K. H. Bockhoff, pp. 1007–1009. Amsterdam: North-Holland.

Gerward, L. (1981). *X-ray attenuation coefficients and atomic photoelectric absorption cross sections of silicon. J. Phys. B*, **14**, 3389–3395.

Gerward, L. (1982). *X-ray attenuation coefficients of copper in the energy range 5 to 50 keV. Z. Naturforsch. Teil A*, **37**, 451–459.

Gerward, L. (1983). *X-ray attenuation coefficients of carbon in the energy range 5 to 50 keV. Acta Cryst.* A**39**, 322–325.

Gerward. L., Thuesen, G., Stibius-Jensen, M. & Alstrup, I. (1979). *X-ray anomalous scattering factors for silicon and germanium. Acta Cryst.* A**35**, 852–857.

Gurman, S. J. (1988). *The small atom approximation in EXAFS and surface EXAFS. J. Phys. C*, **21**, 3699–3717.

Gurman, S. J. (1995). *Interpretation of EXAFS data. J. Synchrotron Rad.* **2**, 56–63.

Hasnain, S. S. (1990). *X-ray absorption fine structure*. London: Ellis Horwood.

Hastings, J. B., Eisenberger, P., Lengeler, B. & Perlman, M. L. (1975). *Local structure determination at high dilution: internal oxidation at 75 ppm Fe in Cu. Phys. Rev. Lett.* **43**, 1807–1810.

Helliwell, J. R. (1984). *Synchrotron X-radiation protein crystallography. Rep. Prog. Phys.* A**7**, 1403–1497.

Hertz, G. (1920). *Über die Absorptionsgrenzen in den L-Serie. Z. Phys.* **3**, 19–27.

Hida, M., Wada, N., Maeda, H., Hikaru, T., Tsu, Y. & Kamino, N. (1985). *An EXAFS investigation on the lattice relaxation of Ni fine particles prepared by gas evaporation. Jpn. J. Appl. Phys.* **24**, L3–L5.

Hubbell, J. H. (1969). *Phonon cross sections, attenuation coefficients, and energy absorption coefficients from 10 keV to 100 GeV*. Report NRDS-NBS29. National Institute of Standards and Technology, Gaithersburg, MD, USA.

Hubbell, J. H., Gerstenberg, H. M. & Saloman, E. B. (1986). *Bibliography of photon total cross section (attenuation coefficient) measurements 10 eV to 13.5 GeV*. Report NBSIR 86-3461. US Department of Commerce, Gaithersburg, MD, USA.

Hubbell, J. H., McMaster, W. H., Del Grande, N. K. & Mallett, J. H. (1974). *X-ray cross sections and attenuation coefficients. International tables for X-ray crystallography,* Vol. IV, edited by J. A. Ibers & W. C. Hamilton, pp. 47–70. Birmingham: Kynoch Press. (Present distributor Kluwer Academic Publishers, Dordrecht.)

Hubbell, J. H. & Øverbø, I. (1979). *Relativistic atomic form factors and photon coherent scattering cross sections. J. Phys. Chem. Ref. Data*, **8**, 69–105.

*International Tables for X-ray Crystallography* (1974). Vol. IV. Birmingham: Kynoch Press. (Present distributor Kluwer Academic Publishers, Dordrecht.)

Jennings, L. D. (1984). *The polarization ratio of crystal monochromators. Acta Cryst.* A**40**, 12–16.

**4.2.3 (*cont.*)**


Joy, D. C. & Maher, D. (1985). *Quantitative electron energy loss spectroscopy: an introduction to the power of Kevex Elstar software*. *Kevex Analyst*, **10**, 6–9.

Kostarev, A. L. (1941). *Theory of the fine structure of X-ray absorption spectra in solids*. *Zh. Eksper Teor. Fiz.* **11**, 60–73.

Kostarev, A. L. (1949). *Elucidation of the super-fine structure of X-ray absorption spectra in solids*. *Zh. Eksper. Teor. Fiz.* **19**, 413–420.

Kronig, R. de L. (1932*a*). *Zur Theorie der Feinstruktur in den Röntgenabsorptionspecktren II. Z. Phys.* **75**, 191–210.

Kronig, R. de L. (1932*b*). *Zur Theorie der Feinstruktur in den Röntgenabsorptionspecktren III. Z. Phys.* **75**, 468–475.

Kuroda, H., Ohta, T., Murata, T., Udagawa, Y. & Nomura, M. (1992). *XAFS VII: Proceedings of the Seventh Conference on X-ray Absorption Fine Structure*. *Jpn. J. Appl. Phys.* **32**, Suppl. 32–2.

Kutzler, F. W., Natoli, C. R., Misemer, D. K., Doniach, S. & Hodgson, K. O. (1981). *Use of one electron theory for the interpretation of near edge structure in K-shell X-ray absorption spectra of transition metal complexes*. *J. Chem. Phys.* **73**, 3274–3288.

Leapman, R. D. & Cosslet, V. E. (1976). *Extended fine structure above the X-ray edge in electron energy loss spectra*. *J. Phys. D*, **9**, L29–L31.

Lee, P. A. (1981). *Theory of extended X-ray absorption fine structure*. *EXAFS spectroscopy: techniques and applications*, edited by B. K. Teo & D. C. Joy, Chap. 2, pp. 5–13. New York: Plenum.

Lee, P. A. & Beni, G. (1977). *New method for the calculation of atomic phase shifts: application to extended X-ray absorption fine structure (EXAFS) in molecules and crystals*. *Phys. Rev. B*, **15**, 2862–2883.

Lee, P. A., Citrin, P. H., Eisenberger, P. & Kincaid, B. M. (1981). *Extended X-ray absorption fine structure – its strengths and limitations as a structural tool*. *Rev. Mod. Phys.* **53**, 769–787.

Lengeler, B., Materlik, G. & Müller, J. E. (1983). *Near edge structure in cerium and cerium compounds*. *EXAFS and near edge structure*, edited by A. Bianconi, L. Incoccia & S. Stipcich, pp. 150–153. Berlin: Springer.

Lereboures, B., Dürr, J., d'Huysser, A., Bonelle, J. P. & Lenglet, M. (1980). *Phys. Status Solidi*, **62**, K175.

Lytle, F. W., Sayers, D. E. & Stern, E. A. (1989). *Report of the International Workshops on Standards and Criteria in XAFS*. In *X-ray absorption spectroscopy*. *Physica (Utrecht)*, **B158**, 701–722.

Lytle, F. W., Stern, E. A. & Sayers, D. E. (1975). *Extended X-ray-absorption fine-structure technique II. Experimental practice and selected results*. *Phys. Rev. B*, **11**, 4825–4835.

Marcus, M., Powers, L. S., Storm, A. R., Kincaid, B. M. & Chance, B. (1980). *Curved-crystal (LiF) X-ray focusing array for fluorescence EXAFS in dilute samples*. *Rev. Sci. Instrum.* **51**, 1023–1029.

Martens, G. & Rabe, P. (1980). *EXAFS studies on superficial regions by means of total reflection*. *Phys. Status Solidi A*, **58**, 415–425.

Materlik, G., Bedzyk, M. J. & Frahm, A. (1984). Report SR-84-07. DESY, Hamburg, Germany.

Mustre de Leon, J., Stern, E. A., Sayers, D. E., Ma, Y. & Rehr, J. J. (1988). *XAFS V: Proceedings of the Fifth International Conference on X-ray Absorption Fine Structure*. Amsterdam: North-Holland.

Natoli, C. R. (1990). *Multichannel multiple scattering theory with general potentials*. *Phys. Rev. B*, **42**, 1944–1968.

Natoli, C. R., Misemer, D. K., Doniach, S. & Kutzler, F. W. (1980). *First principles calculation of X-ray absorption edge structure in molecular clusters*. *Phys. Rev. A*, **22**, 1104–1108.

Nordfors, B. (1960). *The statistical error in X-ray absorption measurements*. *Ark. Fys.* **18**, 37–47.

Norman, D., Durham, P. J. & Pendry, J. B. (1983). *The absorption of oxygen on nickel (001) studied by XANES*. *EXAFS and near edge structure*, edited by A. Bianconi, L. Incoccia & S. Stipcich, pp. 144–146. Berlin: Springer.

Oyanagi, H., Ihara, H., Matsushita, T., Hirabayashi, M., Terada, N., Tokumoto, M., Senzaki, K., Kimura, T. & Yao, T. (1987). *Short range order in high $T_c$ superconductors $Ba_xY_{1-x}CuO_{3-y}$ and $Sr_xLa_{2-x}CuO_{4-7}$*. *Jpn. J. Appl. Phys.* **26**, L828–L831.

Oyanagi, H., Martini, M., Saito, M. & Haga, K. (1995). *Nineteen element high purity Ge solid state detector array for fluorescence X-ray absorption fine structure studies*. Submitted to *Rev. Sci. Instrum.*

Oyanagi, H., Matsushita, T., Tanoue, H., Ishiguro, T. & Kohra, K. (1985). *Fluorescence-detected X-ray absorption spectroscopy applied to structural characterization of very thin films: ion-beam-induced modification of thin Ni layers on Si (100)*. *Jpn. J. Appl. Phys.* **24**, 610–619.

Oyanagi, H., Takeda, T., Matsushita, T., Ishiguro, T. & Sasaki, A. (1986). *Local structure in InGaAsP I quaternary alloys*. *J. Phys. (Paris)*, **28**, Suppl. 12, C8, 423–426.

Pantos, E. (1982). *The SRS program library documentation*. Daresbury: SRC.

Papatzacos, P. & Mort, K. (1975). *Delbrück scattering calculations*. *Phys. Rev. D*, **12**, 206–221.

Parratt, L. G., Porteus, I. O., Schnopper, H. W. & Watanabe, T. (1959). *X-ray absorption coefficients and geometrical collimation of the beam*. *Rev. Sci. Instrum.* **30**, 344–347.

Pendry, J. B. (1983). *The transition region between XANES and EXAFS*. *EXAFS and near edge structure*, edited by A. Bianconi, L. Incoccia & S. Stipcich, pp. 4–10. Berlin: Springer.

Petiau, J. & Calas, G. (1983). *EXAFS for inorganic systems*, pp. 127–129. Daresbury: SRC.

Rehr, J. J. & Albers, R. C. (1990). *Phys. Rev. B*, **41**, 8139–8144.

Riggs, P. J., Mei, R., Yocum, C. F. & Penner-Hahn, J. E. (1993). *The characterization of the Mn site in the photosynthetic oxygen evolving complexes: the effect of hydroxylamine and hydroquinone on the XAFS*. *Jpn. J. Appl. Phys.* **32**, Suppl. 32–2, 527–529.

Saloman, E. B. & Hubbell, J. H. (1986). *X-ray attenuation coefficients (total cross sections): comparison of the data base with the experimental values of Henke and the theoretical values of Schofield for energies between 0.1–100 keV*. Report NBSIR 86–3431. US Department of Commerce, Gaithersburg, MD, USA.

Sawada, M., Tsutsumi, K., Shiraiwa, T., Ishimura, T. & Obashi, M. (1959). *Some contributions to the X-ray spectroscopy of solid state*. *Annu. Rep. Sci. Works Osaka Univ.* **7**, R–87.

Sayers, D. E., Lytle, F. W. & Stern, E. A. (1970). *Point scattering theory of X-ray K absorption fine structure*. *Adv. X-ray Anal.* **13**, 248–256.

Schmidt, V. V. (1961*a*). *Contribution to the theory of the temperature dependence of the fine structure of X-ray absorption spectra*. *Bull. Acad. Sci. USSR Phys. Ser.* **25**, 988–993.

### 4.2.3 (*cont.*)


Schmidt, V. V. (1961*b*). *On the effect of the temperature dependence of the fine structure of X-ray absorption spectra*. *J. Exp. Theor. Phys.* **12**, 886–890.

Schmidt, V. V. (1963). *Contributions to the theory of the dependence of the fine structure of X-ray absorption spectra II. Case of high temperatures*. *Bull. Acad. Sci. USSR Phys. Ser.* **27**, 392–397.

Scofield, J. H. (1973). *Theoretical photoionization cross sections from 1 to 1500 keV*. Report UCRL-51326. Lawrence Livermore Laboratory, Livermore, CA, USA.

Sears, V. F. (1983). *Optimum sample thickness for total cross section measurements*. *Nucl. Instrum. Methods*, **213**, 561–562.

Sevillano, E., Meuth, H. & Rehr, J. J. (1978). *Extended X-ray absorption fine structure Debye Waller factors. I. Monatomic crystals*. *Phys. Rev. B*, **20**, 4908–4911.

Shulman, R. G., Weisenberger, P., Teo, B. K., Kincaid, B. M. & Brown, G. S. (1978). *Fluorescence X-ray absorption studies of rubendoxin and its compounds*. *J. Mol. Biol.* **124**, 305–315.

Sinfelt, J. H., Via, G. H. & Lytle, F. W. (1980). *Structures of biometallic clusters. Extended X-ray absorption fine structure (EXAFS) studies of Ru–Cu clusters*. *J. Chem. Phys.* **72**, 4832–4843.

Sorenson, L. B., Cross, J. O., Newville, M., Ravel, B., Rehr, J. J., Stragier, H., Bouldin, C. E. & Woicik, J. C. (1994). *Diffraction anomalous fine structure: unifying X-ray diffraction and X-ray absorption with DAFS. Diffraction anomalous fine structure*, edited by G. Materlik, C. J. Sparks & K. Fischer, pp. 389–420. Amsterdam: North Holland.

Stern, E. A., Bunker, B. & Heald, A. (1981). *Understanding the causes of non-transferability of EXAFS amplitude*. *EXAFS spectroscopy: techniques and applications*, edited by B. K. Teo & D. C. Joy, pp. 59–79. New York: Plenum.

Stern, E. A., Sayers, D. E. & Lytle, F. W. (1975). *Extended X-ray absorption fine structure technique. III. Determination of physical parameters*. *Phys. Rev. B*, **11**, 4836–4846.

Stohr, J., Denley, D. & Perfettii, P. (1978). *Surface extended X-ray absorption fine structure in the soft X-ray region: study of an oxidized Al surface*. *Phys. Rev. B*, **18**, 4132–4135.

Templeton, D. H. & Templeton, L. K. (1982). *X-ray dichroism and polarized anomalous scattering of the uranyl ion*. *Acta Cryst.* A**38**, 62–67.

Templeton, D. H. & Templeton, L. K. (1985). *X-ray dichroism and anomalous scattering of potassium tetrachloroplatinate*. *Acta Cryst.* A**41**, 133–142.

Templeton, D. H. & Templeton, L. K. (1986). *X-ray birefringence and forbidden reflections in sodium bromate*. *Acta Cryst.* A**42**, 478–481.

Teo, B. K. (1981). *EXAFS spectroscopy: techniques and applications*, edited by B. K. Teo & D. C. Joy, Chap. 3, pp. 13–59. New York: Plenum.

Teo, B. K. & Joy, D. C. (1981). Editors. *EXAFS spectroscopy: techniques and applications*. New York: Plenum.

Teo, B. K. & Lee, P. A. (1979). *Ab initio calculations of amplitude and phase functions for extended X-ray absorption fine structure spectroscopy*. *J. Am. Chem. Soc.* **101**, 2815–2832.

Teo, B. K., Lee, P. A., Simons, A. L., Eisenberger, P. & Kincaid, B. M. (1977). *EXAFS. Approximation, parameterization and chemical transferability of amplitude function*. *J. Am. Chem. Soc.* **99**, 3854–3856.

Winick, H. & Doniach, S. (1980). Editors. *Synchrotron radiation research*. New York: Plenum.

Woodruff, D. P. (1986). *Fine structure in ionization cross sections and applications to surface science*. *Rep. Prog. Phys.* **49**, 683–723.

Yamaguchi, T., Mitsunaga, T., Yoshida, N., Wakita, H., Fujiwara, M., Matsushita, T., Ikeda, S. & Nomura, M. (1993). *XAFS study with an in situ electrochemical cell on manganese Schiff base complexes as a model of a photosystem*. *Jpn. J. Appl. Phys.* **32**, Suppl. 32-2, 533–535.


### 4.2.4


Allen, S. J. M. (1935). *X-rays in theory and experiment*, edited by A. H. Compton & S. K. Allison, pp. 799–806. New York: Van Nostrand.

Allen, S. J. M. (1969). *Handbook of chemistry and physics*, edited by R. C. Weast, pp. E143–E144. Cleveland: The Chemical Rubber Co.

Band, I. M., Kharitonov, Yu. I. & Trzhaskovskaya, M. B. (1979). *Photoionization cross sections and photoelectron angular distributions for X-ray line energies in the range 0.132–4.509 keV*. *At. Data Nucl. Data Tables*, **23**, 443–505.

Creagh, D. C. (1987). *Resolution of discrepancies in tables of photon attenuation cross sections*. *Nucl. Instrum. Methods*, A**255**, 38–42.

Creagh, D. C. (1990). *An evaluation of tabulations of X-ray attenuation coefficients: the new versus the old*. *Nucl. Instrum. Methods*, A**295**, 417–439.

Creagh, D. C. & Hubbell, J. H. (1987). *Problems associated with the measurement of X-ray attenuation coefficients. I. Silicon*. *Acta Cryst.* A**43**, 102–112.

Creagh, D. C. & Hubbell, J. H. (1990). *Problems associated with the measurement of X-ray attenuation coefficients. II. Carbon*. *Acta Cryst.* A**46**, 402–408.

Cromer, D. T. (1969). *Anomalous dispersion corrections computed from self consistent field relativistic Dirac–Slater wavefunctions*. *J. Chem. Phys.* **50**, 4857–4859.

Cromer, D. T. & Liberman, D. (1970). *Relativistic calculation of anomalous scattering for X-rays*. *J. Chem. Phys.* **53**, 1891–1898.

Cromer, D. T. & Mann, J. B. (1967). *Compton scattering factors for spherically symmetric free atoms*. *J. Chem. Phys.* **47**, 1892–1893.

Cromer, D. T. & Waber, J. T. (1974). *Atomic scattering factors for X-rays*. Section 2.2. *International tables for X-ray crystallography*, Vol. IV, edited by J. A. Ibers & W. C. Hamilton, pp. 71–147. Birmingham: Kynoch Press. (Present distributor Kluwer Academic Publishers, Dordrecht.)

De Marco, J. J. & Suortti, P. (1971). *Effect of scattering on the attenuation of X-rays*. *Phys. Rev. B*, **4**, 1028–1033.

Doyle, P. A. & Turner, P. S. (1968). *Relativistic Hartree–Fock X-ray and electron scattering factors*. *Acta Cryst.* A**24**, 390–397.

Gerward, L. (1986). *Empirical absorption equations for use in X-ray spectrometric analysis*. *X-ray Spectrom.* **15**, 29–33.

Heinrich, K. F. J. (1966). *X-ray absorption uncertainty*. *The electron microprobe*, edited by T. D. McKinley, K. F. J. Heinrich & D. B. Wittrey, pp. 296–377. New York: John Wiley.

Henke, B. L., Lee, P., Tanaka, T. J., Shimambukuro, R. L. & Fujikawa, B. K. (1982). *Low-energy X-ray interaction coefficients: photoabsorption, scattering and reflection*. *At. Data Nucl. Data Tables*, **27**, 1–144.

**4.2.4 (*cont.*)**

Hubbell, J. H., Gerstenberg, H. M. & Saloman, E. B. (1986). *Bibliography of photon total cross section (attenuation coefficient) measurements 10 eV to 13.5 GeV*. Report NBSIR 86–3461. National Institute of Standards and Technology, Gaithersburg, MD, USA.

Hubbell, J. H., McMaster, W. H., Del Grande, N. K. & Mallett, J. H. (1974). *X-ray cross sections and attenuation coefficients. International tables for X-ray crystallography*, Vol. IV, pp. 47–70. Birmingham: Kynoch Press. (Present distributor Kluwer Academic Publishers, Dordrecht.)

Hubbell, J. H. & Øverbø, I. (1979). *Relativistic atomic form factors and photon coherent scattering cross sections. J. Phys. Chem. Ref. Data*, **8**, 69–105.

Hubbell, J. H., Veigele, W. J., Briggs, E. A., Brown, R. T., Cromer, D. T. & Howerton, R. J. (1975). *Atomic form factors, incoherent scattering functions and photon scattering cross sections. J. Phys. Chem. Ref. Data*, **4**, 471–538.

Jackson, D. F. & Hawkes, D. J. (1981). *X-ray attenuation coefficients of elements and mixtures. Phys. Rep.* **70**, 169–233.

Kane, P. P., Kissel, L., Pratt, R. H. & Roy, S. C. (1986). *Elastic scattering of $\gamma$-rays and X-rays by atoms. Phys. Rep.* **150**, 75–159.

Kissel, L., Roy, S. C. & Pratt, R. H. (1980). *Rayleigh scattering by neutral atoms 100 eV to 10 MeV. Phys. Rev. A*, **22**, 1970–2004.

Koch, B., MacGillavry, C. H. & Milledge, H. J. (1962). *Absorption. International tables for X-ray crystallography*, Vol. III, Section 2.2, pp. 157–192. Birmingham: Kynoch Press.

Leroux, J. & Thinh, T. P. (1977). *Revised tables of X-ray mass attenuation coefficients*. Quebec: Corporation Scientifique Claisse, Inc.

Levinger, J. S. (1952). *Small angle coherent scattering of gammas by bound electrons. Phys. Rev.* **87**, 656–662.

Liebhafsky, H. A., Pfeiffer, H. G., Winslow, E. H. & Zemany, P. D. (1960). *X-ray absorption and emission analytical chemistry*, pp. 313–317. New York: John Wiley.

McMaster, W. H., Del Grande, N. K., Mallett, J. H. & Hubbell, J. H. (1969/1970). *Compilation of X-ray cross sections*. Report UCRL-50174. (Section I, 1970; Section II, 1969; Section III, 1969; Section IV 1969.) Lawrence Livermore National Laboratory, Livermore, CA, USA.

Montenegro, E. C., Baptista, G. B. & Duarte, P. W. E. P. (1978). *K and L X-rays mass attenuation coefficients for low-Z materials. At. Data Nucl. Data Tables*, **22**, 131–177.

Øverbø, I. (1977). *The Coulomb correction to electron pair production by intermediate-energy photons. Phys. Lett. B*, **71**, 412–414.

Øverbø, I. (1978). *Large-q form factors for light atoms. Phys. Scr.* **17**, 547–549.

Pirenne, M. H. (1946). *The diffraction of X-rays and electrons by free molecules*. Cambridge University Press.

Plechaty, E. F., Cullen, E. E. & Howerton, R. J. (1981). *Tables and graphs of photon-interaction cross sections from 0.1 keV to 100 MeV*. Derived from the LLL Evaluated-Nuclear-Data Library. Report UCRL-50400, Vol. 6, Rev. 3. Lawrence Livermore National Laboratory, Livermore, CA, USA.

Saloman, E. B. & Hubbell, J. H. (1986). *X-ray attenuation coefficients (total cross sections): comparison of the experimental data base with the recommended values of Henke and the theoretical values of Scofield for energies between 0.1–100 keV*. Report NBSIR 86–3431. National Institute of Standards and Technology, Gaithersburg, MD, USA.

Saloman, E. B. & Hubbell, J. H. (1987). *Critical analysis of soft X-ray cross section data. Nucl. Instrum. Methods*, A**255**, 38–42.

Saloman, E. B., Hubbell, J. H. & Scofield, J. H. (1988). *At. Data Nucl. Data Tables*, **38**, 1–197.

Sano, H., Ohtaka, K. & Ohtsuki, Y. H. (1969). *Normal and abnormal absorption coefficients of X-rays. J. Phys. Soc. Jpn*, **27**, 1254–1261.

Schaupp, D., Schumacher, M., Smend, F., Rullhausen, P. & Hubbell, J. H. (1983). *Small-angle Rayleigh scattering of photons at high energies: tabulations of relativistic HFS modified atomic form factors. J. Phys. Chem. Ref. Data*, **12**, 467–512.

Scofield, J. H. (1973). *Theoretical photoionization cross sections from 1 to 1500 keV*. UCRL-51326. Lawrence Livermore National Laboratory, Livermore, CA, USA.

Scofield, J. H. (1986). Personal communication to E. B. Saloman and J. H. Hubbell. *Calculated photoeffect values 0.1 to 1.0 keV*. [Presented in Saloman & Hubbell (1986) and Saloman *et al.* (1988).]

Storm, E. & Israel, H. I. (1970). *Photon cross sections from 0.001 to 100 MeV for elements 1 through 100. Nucl. Data Tables*, A**7**, 565–681.

Theisen, R. & Vollath, D. (1967). *Tables of X-ray mass attenuation coefficients*. Düsseldorf: Verlag Stahleisen.

Veigele, W. J. (1973). *Photon cross sections from 0.1 keV to 1 MeV for elements $Z = 1$ to $Z = 94$. At. Data*, **5**, 51–111.

Victoreen, J. A. (1949). *The calculation of X-ray mass absorption coefficients. J. Appl. Phys.* **20**, 1141–1147.

Yeh, J. J. & Lindau, I. (1985). *Atomic subshell photoionization cross sections and asymmetry parameters: $1 \leq Z \leq 103$. At. Data Nucl. Data Tables*, **32**, 1–156.

**4.2.5**

Balaic, D. X., Barnea, Z., Nugent, K. A., Garrett, R. F., Varghese, J. N. & Wilkins, S. W. (1996). *Protein crystal diffraction patterns using a capillary-focused synchrotron X-ray beam. J. Synchrotron Rad.* **3**, 289–295.

Balaic, D. X. & Nugent, K. A. (1995). *The X-ray optics of tapered capillaries. Appl. Opt.* **34**, 7263–7272.

Balaic, D. X., Nugent, K. A., Barnea, Z., Garrett, R. & Wilkins, S. W. (1995). *Focusing of X-rays by total external reflection from a paraboloidally tapered glass capillary. J. Synchrotron Rad.* **2**, 296–299.

Beaumont, J. H. & Hart, M. (1973). *Multiple-Bragg reflection monochromators for synchrotron radiation. J. Phys. E,* **7**, 823–829.

Berman, L. E. & Hart, M. (1991). *Adaptive crystal optics for high power synchrotron sources. Nucl. Instrum. Methods,* A**302**, 558–562.

Bilderback, D. H., Thiel, D. J., Pahl, R. & Brister, K. E. (1994). *X-ray applications with glass-capillary optics. J. Synchrotron Rad.* **1**, 37–42.

Bonse, U. & Hart, M. (1965). *Tailless X-ray single-crystal reflection curves obtained by multiple reflection. Appl. Phys. Lett.* **7**, 238–240.

Brodsky, A. (1982). Editor. *Handbook of radiation measurement and protection*, Vols. 1 and 2. Florida: CRC Press.

### 4.2.5 (*cont.*)


Creagh, D. C. & Garrett, R. F. (1995). *Testing of a sagittal focusing monochromator at BL 20B at the Photon Factory*. *Access to major facilities program*, edited by J. W. Boldeman, pp. 251–252. Sydney: ANSTO.

Delf, B. W. (1961). *The effect of absorption in the β-filter on the mean wavelength of X-ray emission lines*. *Proc. Phys. Soc. London*, **78**, 305–306.

Engström, P., Rindby, A. & Vincze, L. (1996). *Capillary optics*. *ESRF Newsletter,* **26**, 30–31.

Freund, A. K. (1993). *Thin is beautiful*. *ESRF Newsletter,* **19**, 11–13.

Fukumachi, T., Nakano, Y. & Kawamura, T. (1986). *Energy dependence of X-ray reflectivity from multi-layer mirrors. X-ray instrumentation for the Photon Factory: dynamic analyses of micro-structures in matter*, edited by S. Hosoya, Y. Iitaka & H. Hashizume, pp. 25–34. Japan: Photon Factory.

Giles, C., Vettier, C., de Bergevin, F., Grubel, G., Goulon, J. & Grossi, F. (1994). *X-ray polarimetry with phase plates*. *ESRF Newsletter,* **21**, 16–17.

Grey, D. (1996). *Instrumentation developments and observations in hard X-ray astronomy*. PhD thesis. The University of New South Wales, Australia.

Hanfland, M., Häusermann, D., Snigirev, A., Snigireva, I., Ahahama, Y. & McMahon, M. (1994). *Bragg–Fresnel lens for high pressure studies*. *ESRF Newsletter,* **22**, 8–9.

Hart, M. (1971). *Bragg reflection X-ray optics*. *Rep. Prog. Phys.* **34**, 435–490.

Hart, M. & Rodrigues, A. R. D. (1978). *Harmonic-free single-crystal monochromators for neutrons and X-rays*. *J. Appl. Cryst*. **11**, 248–253.

Hashizume, H. (1983). *Asymmetrically grooved monolithic crystal monochromators for suppression of harmonics in synchrotron X-radiation*. *J. Appl. Cryst*. **16**, 420–427.

Holt, S. A., Brown, A. S., Creagh, D. C. & Leon, R. (1997). *The application of grazing incidence X-ray diffraction and specular reflectivity to the structural investigation of multiple quantum well and quantum dot semiconductor devices*. *J. Synchrotron Rad*. **4**, 169–174.

Jennings, L. D. (1981). *Extinction, polarization and crystal monochromators*. *Acta Cryst*. A**37**, 584–593.

Kikuta, S. (1971). *X-ray crystal monochromators using successive asymmetric diffractions and their applications to measurements of diffraction curves. II. Type 1 collimator*. *J. Phys. Soc. Jpn,* **30**, 222–227.

Kikuta, S. & Kohra, K. (1970). *X-ray crystal collimators using successive asymmetric diffractions and their applications to measurements of diffraction curves. I. General considerations on collimators*. *J. Phys. Soc. Jpn,* **29**, 1322–1328.

Kumakov, M. A. & Komarov, F. F. (1990). *Multiple reflection from surface X-ray optics*. *Phys. Rep*. **191**(5), 284–350.

Matsushita, T., Ishikawa, T. & Oyanagi, H. (1986). *Sagitally focusing double-crystal monochromator with constant exit height at the Photon Factory*. *Nucl. Instrum. Methods*, A**246**, 377–379.

Matsushita, T., Kikuta, S. & Kohra, K. (1971). *X-ray crystal monochromators using successive asymmetric diffractions and their applications to measurements of diffraction curves. III. Type II collimators*. *J. Phys. Soc. Jpn*, **30**, 1136–1144.

Oshima, K., Harada, J. & Sakabe, N. (1986). *Curved crystal monochromator. X-ray instrumentation for the Photon Factory: dynamic analyses of micro-structures in matter*, edited by S. Hosoya, Y. Iitaka & H.Hashizume, pp. 35–41. Japan: Photon Factory.

OSMIC (1996). Catalogue. *A new family of collimating and focusing optics for X-ray analysis*. OSMIC, Michigan, USA.

Peele, A. G., Nugent, K. A., Rode, A. V., Gabel, K., Richardson, M. C. M., Strack, R. & Siegmund, W. (1996). *X-ray focusing with lobster-eye optics: a comparison of theory with experiment*. *Appl. Opt*. **35**, 4420–4425.

Siemens (1996*a*). *Parallel beam optics for measurements of samples with irregularly shaped surfaces*. Laboratory Report X-ray Analysis, DXRD, 13. Karlsruhe: Siemens.

Siemens (1996*b*). *Goebel mirrors for X-ray reflectometry investigations*. Laboratory Report X-ray Analysis, DXRD, 14. Karlsruhe: Siemens.

Siemens (1996*c*) *Grazing incidence diffraction with Goebel mirrors*. Laboratory Report X-ray Analysis, DXRD, 15. Karlsruhe: Siemens.

Snigirev, A. (1994). *Bragg–Fresnel optics: new fields of applications*. *ESRF Newsletter,* **22**, 20–21.

Stephens, P. W., Eng, P. J. & Tse, T. (1992). *Construction and performance of a bent crystal X-ray monochromator*. *Rev. Sci. Instrum*. **64**, 374–378.

Sussini, J. & Labergerie, D. (1995). *Bi-morph piezo-electric mirror: a novel active mirror*. *Synchrotron Rad. News,* **8**, 21–26.

Warren, B. E. (1968). *X-ray diffraction*. New York: Addison-Wesley.

Young, R. A. (1963). *Balanced filters for X-ray diffractometry*. *Z. Kristallogr*. **118**, 233–247.

Young, R. A. (1993). *The Rietveld method*. Oxford University Press.


### 4.2.6


Agarwal, B. K. (1979). *X-ray spectroscopy*, p. 215. Berlin: Springer-Verlag.

Akhiezer, A. I. & Berestetsky, V. B. (1957). *Quantum electrodynamics*. TESE, Oak Ridge, Tennessee, USA.

Aldred, P. J. E. & Hart, M. (1973*a*). *The electron distribution in silicon. I. Experiment*. *Proc. R. Soc. London Ser. A*, **332**, 233–238.

Aldred, P. J. E. & Hart, M. (1973*b*). *The electron distribution in silicon. II. Theoretical interpretation*. *Proc. R. Soc. London Ser. A*, **332**, 239–254.

Aristov, V. V., Shmytko, I. M. & Shulakov, E. V. (1977). *Dynamical contrast of the topographic image of a crystal with continuous X-radiation*. *Acta Cryst*. A**33**, 412–418.

Begum, R., Hart, M., Lea, K. R. & Siddons, D. P. (1986). *Direct measurements of the complex X-ray atomic scattering factors for elements by X-ray interferometry at the Daresbury synchrotron radiation source*. *Acta Cryst*. A**42**, 456–463.

Bijvoet, J. M., Peerdeman, A. F. & Van Bommel, A. J. (1951). *Determination of the absolute configuration of optically active compounds by means of X-rays*. *Nature (London)*, **168**, 271.

Blume, M. (1994). *Magnetic effects in anomalous dispersion. Resonant anomalous X-ray scattering*, edited by G. Materlik, C. J. Sparks & K. Fischer, pp. 495–512. Amsterdam: North Holland.

Bonse, U. & Hart, M. (1965). *Tailless X-ray single crystal reflection curves obtained by multiple reflection*. *Appl. Phys. Lett*. **1**, 238–242.

Bonse, U. & Hart, M. (1966*a*). *A Laue-case X-ray interferometer*. *Z. Phys*. **188**, 154–162.

Bonse, U. & Hart, M. (1966*b*). *An X-ray interferometer with Bragg-case beam splitting*. *Z. Phys*. **194**, 1–17.

**4.2.6 (*cont.*)**


Bonse, U. & Hart, M. (1966*c*). *Moire patterns of atomic planes obtained by X-ray interferometry*. *Z. Phys.* **190**, 455–467.

Bonse, U. & Hart, M. (1966*d*). *Small single X-ray scattering by spherical particles*. *Z. Phys.* **189**, 151–165.

Bonse, U. & Hart, M. (1970). *Interferometry with X-rays*. *Phys. Today*, **23**(8), 26–31.

Bonse, U. & Hartmann-Lotsch, I. (1984). *Kramers–Kronig correlation of measured f′(E) and f″(E) values*. *Nucl. Instrum. Methods*, **222**, 185–188.

Bonse, U., Hartmann-Lotsch, I. & Lotsch, H. (1983*a*). *Interferometric measurement of absorption $\mu(E)$ and dispersion $f'(E)$ at the K edge of copper*. *EXAFS and near edge structure*, edited by A. Bianconi, I. Incoccia & A. S. Stipcich, pp. 376–377. Berlin: Springer.

Bonse, U., Hartmann-Lotsch, I. & Lotsch, H. (1983*b*). *The X-ray interferometer for high resolution measurement of anomalous dispersion at HASYLAB*. *Nucl. Instrum. Methods*, **208**, 603–604.

Bonse, U. & Hellkötter, H. (1969). *Interferometrische Messung des Brechungsindex für Röntgenstrahlen*. *Z. Phys.* **223**, 345–352.

Bonse, U. & Henning, A. (1986). *Measurement of polarization isotropy of the anomalous forward scattering amplitude at the niobium K-edge in $LiNbO_3$*. *Nucl. Instrum. Methods*, A**246**, 814–816.

Bonse, U. & Materlik, G. (1972). *Dispersionskorrektur für Nickel nahe der K-Absorptionskante*. *Z. Phys.* **253**, 232–239.

Bonse, U. & Materlik, G. (1975). *Dispersion correction measurements by X-ray interferometry*. *Anomalous scattering*, edited by S. Ramaseshan & S. C. Abrahams, pp. 107–109. Copenhagen: Munksgaard.

Brown, G. E., Peierls, R. E. & Woodward, J. B. (1955). *The coherent scattering of $\gamma$-rays by K electrons in heavy atoms: method*. *Proc. R. Soc. London Ser. A*, **227**, 51–63.

Brysk, H. & Zerby, C. D. (1968). *Photoelectric cross sections in the keV range*. *Phys. Rev.* **171**, 292–298.

Buras, B. & Tazzari, S. (1985). *The European Synchrotron Radiation Facility*. *Report of the ESRP*, pp. 6–32. European Synchrotron Radiation Project, CERN, LEP Division, Geneva, Switzerland.

Chantler, C. T. (1994). *Towards improved form factor tables*. *Resonant anomalous X-ray scattering*, edited by G. Materlik, C. J. Sparks & K. Fischer, pp. 61–79. Amsterdam: North Holland.

Chantler, C. T. (1995). *Theoretical form factor, attenuation and scattering tabulation for $Z = 1$–$92$ from $1$–$10\,eV$ to $E = 0.4$–$1.0\,MeV$*. *J. Phys. Chem. Ref. Data*, **24**, 71–643.

Chapuis, G., Templeton, D. H. & Templeton, L. K. (1985). *Solving crystal structures using several wavelengths from conventional sources*. *Anomalous scattering by holmium*. *Acta Cryst.* A**41**, 274–278.

Cole, H. & Stemple, N. R. (1962). *Effect of crystal perfection and polarity on absorption edges seen in Bragg diffraction*. *J. Appl. Phys.* **33**, 2227–2233.

Creagh, D. C. (1970). *On the measurement of X-ray dispersion corrections using X-ray interferometers*. *Aust. J. Phys.* **23**, 99–103.

Creagh, D. C. (1977). *Determination of the mass attenuation coefficients and the anomalous dispersion corrections for calcium at X-ray wavelengths from I $K\alpha_1$ to Cu $K\alpha_1$*. *Phys. Status Solidi A*, **39**, 705–715.

Creagh, D. C. (1978). *A new device for the precise measurement of X-ray attenuation coefficients and dispersion corrections*. *Advances in X-ray analysis*, Vol. 21, edited by C. S. Barrett & D. E. Leyden, pp. 149–153. New York: Plenum.

Creagh, D. C. (1980). *X-ray interferometer measurements of the anomalous dispersion correction $f'(\omega,0)$ for some low Z elements*. *Phys. Lett. A*, **77**, 129–132.

Creagh, D. C. (1982). *On the use of photoelectric attenuation coefficients for the determination of the anomalous dispersion coefficient f′ for X-rays*. *Phys. Lett. A*, **103**, 52–56.

Creagh, D. C. (1984). *The real part of the forward scattering factor for aluminium*. Unpublished.

Creagh, D. C. (1985). *Theoretical and experimental techniques for the determination of X-ray anomalous dispersion corrections*. *Aust. J. Phys.* **38**, 371–404.

Creagh, D. C. (1986). *The X-ray anomalous dispersion of materials*. In *Recent advances in X-ray characterization of materials*, edited by P. Krishna, Chap. 7. Oxford: Pergamon Press.

Creagh, D. C. (1990). *Tables of X-ray dispersion corrections and attenuation coefficients: the new versus the old*. *Nucl. Instrum. Methods*, A**295**, 417–434.

Creagh, D. C. (1993). *f′: its present and its future*. *Ind. J. Phys.* **67**B, 511–525.

Creagh, D. C. & Cookson, D. J. (1995). *Diffraction anomalous fine structure study of basic zinc sulphate and basic zinc sulphonate*. In *Photon Factory Activity Report 1994*, edited by K. Nasu. National Laboratory for High Energy Physics, Tsukuba 93-0305, Japan.

Creagh, D. C. & Hart, M. (1970). *X-ray interferometric measurements of the forward scattering amplitude of lithium fluoride*. *Phys. Status Solidi*, **37**, 753–758.

Creagh, D. C. & Hubbell, J. H. (1987). *Problems associated with the measurement of X-ray attenuation coefficients*. *I. Silicon*. *Acta Cryst.* A**43**, 102–112.

Creagh, D. C. & Hubbell, J. H. (1990). *Problems associated with the measurement of X-ray attenuation coefficients*. *II. Carbon*. *Acta Cryst.* A**46**, 402–408.

Cromer, D. T. & Liberman, D. A. (1970). *Relativistic calculation of anomalous scattering factors for X-rays*. *J. Chem. Phys.* **53**, 1891–1898.

Cromer, D. T. & Liberman, D. A. (1981). *Anomalous dispersion calculations near to and on the long-wavelength side of an absorption edge*. *Acta Cryst.* A**37**, 267–268.

Cromer, D. T. & Liberman, D. A. (1983). *Calculation of anomalous scattering factors at arbitrary wavelengths*. *J. Appl. Cryst.* **16**, 437.

Cromer, D. T. & Waber, J. T. (1974). *Atomic scattering factors for X-rays*. *International tables for X-ray crystallography*, Vol. IV, edited by J. A. Ibers & W. C. Hamilton, Chap. 2.2, pp. 71–147. Birmingham: Kynoch Press. (Present distributor Kluwer Academic Publishers, Dordrecht.)

Cusatis, C. & Hart, M. (1975). *Dispersion correction measurements by X-ray interferometry*. *Anomalous scattering*, edited by S. Ramaseshan & S. C. Abrahams, pp. 57–68. Copenhagen: Munksgaard.

Cusatis, C. & Hart, M. (1977). *The anomalous dispersion corrections for zirconium*. *Proc. R. Soc. London Ser. A*, **354**, 291–302.

Deutsch, M. & Hart, M. (1982). *Wavelength energy shape and structure of the Cu $K\alpha_1$ X-ray emission line*. *Phys. Rev. B*, **26**, 5550–5567.

Deutsch, M. & Hart, M. (1984*a*). *Noninterferometric measurement of the X-ray refractive index of beryllium*. *Phys. Rev. B*, **30**, 643–646.

**4.2.6 (*cont.*)**


Deutsch, M. & Hart, M. (1984*b*). *X-ray refractive-index measurement in silicon and lithium fluoride*. *Phys. Rev. B*, **30**, 640–642.

Deutsch, M. & Hart, M. (1985). *A new approach to the measurement of X-ray structure amplitudes determined by the Pendellösung method*. *Acta Cryst.* A**41**, 48–55.

Dreier, P., Rabe, P., Malzfeldt, W. & Niemann, W. (1984). *Anomalous X-ray scattering factors calculated from experimental absorption factor*. *J. Phys. C*, **7**, 3123–3136.

Engel, D. H. & Sturm, M. (1975). *Experimental determination of f″ for heavy atoms*. *Anomalous scattering*, edited by S. Ramaseshan & S. C. Abrahams, pp. 93–100. Copenhagen: Munksgaard.

Fermi, E. (1928). *Eine statistiche Methode zur Bestimmung einiger geschaften des Atoms und ihre Anwendung auf die Theorie des periodische Systems der Elemente*. *Z. Phys.* **48**, 73–79.

Fock, V. (1930). *Näherungsmethode zur Lösung des quantenmechanischen Mehrkörperproblems*. *Z. Phys.* **61**, 126–148.

Freund, A. (1975). *Anomalous scattering of X-rays in copper*. *Anomalous scattering,* edited by S. Ramaseshan & S. C. Abrahams, pp. 69–86. Copenhagen: Munksgaard.

Fuoss, P. H. & Bienenstock, A. (1981). *X-ray anomalous scattering factors – measurements and applications*. *Inner-shell and X-ray physics of atoms and solids*, edited by D. J. Fabian, A. Kleinpoppen & L. M. Watson, pp. 875–884. New York: Plenum.

Gavrila, M. (1981). *Photon atom elastic scattering in inner-shell and X-ray physics of atoms and solids*, edited by B. Craseman. New York: Plenum.

Gerward, L. (1982). *X-ray attenuation coefficients of copper in the energy range 5 to 50 keV*. *Z. Naturforsch. Teil A*, **37**, 451–459.

Gerward, L. (1983). *X-ray attenuation coefficients of carbon in the energy range 5 to 20 keV*. *Acta Cryst.* A**39**, 322–325.

Gerward, L., Thuesen, G., Stibius-Jensen, M. & Alstrup, I. (1979). *X-ray anomalous scattering factors for silicon and germanium*. *Acta Cryst.* A**35**, 852–857.

Grimvall, G. & Persson, E. (1969). *Absorption of X-rays in germanium*. *Acta Cryst.* A**25**, 417–422.

Hart, M. (1968). *An ångström ruler*. *J. Phys. D*, **1**, 1405–1408.

Hart, M. (1985). *Private communication*.

Hart, M. (1994). *Polarizing X-ray optics and anomalous dispersion in chiral systems*. *Resonant anomalous X-ray scattering*, edited by G. Materlik, C. J. Sparks & K. Fischer, pp. 103–118. Amsterdam: North Holland.

Hart, M. & Siddons, D. P. (1981). *Measurements of anomalous dispersion corrections made from X-ray interferometers*. *Proc. R. Soc. London Ser. A*, **376**, 465–482.

Hartree, D. R. (1928). *The wavemechanics of an atom with a non-Coulomb central field*. *Proc. Cambridge Philos. Soc.* **24**, 89–132.

Hashimoto, H., Kozaki, S. & Ohkawa, T. (1965). *Observations of Pendellösung fringes and images of dislocations by X-ray shadow micrographs of silicon crystals*. *Appl. Phys. Lett.* **6**, 16–17.

Helliwell, J. R. (1984). *Synchrotron X-radiation protein crystallography*. *Rep. Prog. Phys.* **47**, 1403–1497.

Hendrickson, W. A. (1994). *MAD phasing for macromolecular structures*. *Resonant anomalous X-ray scattering*, edited by G. Materlik, C. J. Sparks & K. Fischer, pp. 159–173. Amsterdam: North Holland.

Henke, B. L., Lee, P., Tanaka, T. J., Shimambukuro, R. L. & Fujikawa, B. K. (1982). *Low-energy interaction coefficients: photoabsorption, scattering, and reflection*. *At. Data Nucl. Data Tables*, **27**, 1–144.

Hönl, H. (1933*a*). *Zur Dispersions theorie der Röntgenstrahlen*. *Z. Phys.* **84**, 1–16.

Hönl, H. (1933*b*). *Atomfactor für Röntgenstrahlen als Problem der Dispersionstheorie (K-Schale)*. *Ann. Phys. (Leipzig)*, **18**, 625–657.

Hosoya, S. (1975). *Anomalous scattering measurements and amplitude and phase determinations with continuous X-rays*. *Anomalous scattering*, edited by S. Ramaseshan & S. C. Abrahams, pp. 275–287. Copenhagen: Munksgaard.

Hubbell, J. H., Veigele, W. J., Briggs, E. A., Brown, R. T., Cromer, D. T. & Howerton, R. J. (1975). *Atomic form factors, incoherent scattering functions and photon scattering cross section*. *J. Chem. Phys. Ref. Data*, **4**, 471–538.

*International Tables for Crystallography* (1995). Vol. B. Dordrecht: Kluwer Academic Publishers.

*International Tables for X-ray Crystallography* (1974). Vol. IV. Birmingham: Kynoch Press. (Present distributor Kluwer Academic Publishers, Dordrecht.)

Ishida, K. & Katoh, H. (1982). *Use of multiple reflection diffraction to measure X-ray refractive index*. *Jpn. J. Appl. Phys.* **21**, 1109.

James, R. W. (1955). *The optical principles of the diffraction of X-rays*. Ithaca: Cornell University Press.

Karle, J. (1980). *Anomalous dispersion and the use of triplet phase invariants*. *Int. J. Quantum. Chem.* **7**, 357–367.

Karle, J. (1984*a*). *Rules for evaluating triplet phase invariants by use of anomalous dispersion data*. *Acta Cryst.* A**40**, 366–379.

Karle, J. (1984*b*). *The relative scaling of multiple wavelength anomalous dispersion data*. *Acta Cryst.* A**40**, 1–4.

Karle, J. (1984*c*). *Triplet phase invariants from and exact algebraic analysis of anomalous dispersion*. *Acta Cryst.* A**40**, 526–532.

Karle, J. (1985). *Many algebraic formulas for the evaluation of triplet phase invariants from isomorphous replacement and anomalous dispersion data*. *Acta Cryst.* A**41**, 182–189.

Katoh, H., Shimakura, H., Ogawa, T., Hattori, S., Kobayashi, Y., Umezawa, K., Ishikawa, T. & Ishida, K. (1985*a*). *Measurement of X-ray refractive index by multiple reflection diffractometer*. Activity Report, KEK, Tsukuba, Japan.

Katoh, H., Shimakura, H., Ogawa, T., Hattori, S., Kobayashi, Y., Umezawa, K., Ishikawa, T. & Ishida, K. (1985*b*). *Measurement of the X-ray anomalous scattering of the germanium K-edge with synchrotron radiation*. *J. Phys. Soc. Jpn*, **54**, 881–884.

Kirfel, A. (1994). *Anisotropy of anomalous scattering in single crystals*. *Resonant anomalous X-ray scattering*, edited by G. Materlik, C. J. Sparks & K. Fischer, pp. 231–256. Amsterdam: North Holland.

Kissel, L. (1977). *Rayleigh scattering: elastic scattering by bound electrons*. PhD thesis, University of Pittsburgh, PA, USA.

Kissel, L. & Pratt, R. H. (1985). *Rayleigh scattering: elastic photon scattering by bound electrons*. In *Atomic inner-shell physics*, edited by B. Craseman. New York: Plenum.

Kissel, L., Pratt, R. H., Kane, P. P. & Roy, S. C. (1985). *Elastic scattering of X-rays and γ-rays by atoms*. Sandia Report SANDE5-0501J. Sandia, Albuquerque, NM, USA.

Kissel, L., Pratt, R. H. & Roy, S. C. (1980). *Rayleigh scattering by neutral atoms, 100 eV to 10 MeV*. *Phys. Rev. A*, **22**, 1970–2004.

**4.2.6 (*cont.*)**


Kohn, W. & Sham, L. S. (1965). *Self consistent equations including exchange and correlation effects. Phys. Rev. A*, **140**, 1133–1138.

Lengeler, B. (1994). *Experimental determination of the dispersion correction f′(E) to the atomic scattering factor. Resonant anomalous X-ray scattering*, edited by G. Materlik, C. J. Sparks & K. Fischer, pp. 35–69. Amsterdam: North Holland.

Liberman, D., Waber, J. T. & Cromer, D. T. (1965). *Self-consistent field Dirac–Slater wavefunctions for atoms and ions. I. Comparison with previous calculations. Phys. Rev. A*, **137**, 27–34.

Morgenroth, W., Kirfel, A. & Fischer, K. (1994). *Computing kinematic diffraction intensities with anomalous scatterers – 'forbidden' axial reflections in space groups up to orthorhombic symmetry. Resonant anomalous X-ray scattering*, edited by G. Materlik, C. J. Sparks & K. Fischer, pp. 257–264. Amsterdam: North Holland.

Nelms, A. T. & Oppenheimer, I. (1955). *J. Res. Natl Bur. Stand.* **55**, 53–62.

Philips, J. C. & Hodgson, K. O. (1985). *Single-crystal X-ray diffraction and anomalous scattering using synchrotron radiation. Synchrotron radiation research*, edited by H. Winick & S. Doniach, pp. 565–604. New York: Plenum.

Philips, J. C., Templeton, D. H., Templeton, L. K. & Hodgson, K. O. (1978). *L-III edge anomalous X-ray scattering by cesium measured with synchrotron radiation. Science*, **201**, 257–259.

Pratt, R. H., Kissel, L. & Bergstrom, P. M. Jr (1994). *New relativistic S-matrix results for scattering – beyond the anomalous factors/beyond impulse approximation. Resonant anomalous X-ray scattering*, edited by G. Materlik, C. J. Sparks & K. Fischer, pp. 9–34. Amsterdam: North Holland.

Price, P. F., Maslen, E. N. & Mair, S. L. (1978). *Electron-density studies. III. A re-evaluation of the electron distribution in crystalline silicon. Acta Cryst.* A**34**, 183–193.

Ramaseshan, S. & Abrahams, S. C. (1975). *Anomalous scattering*. Copenhagen: Munksgaard.

Roy, S. C., Kissel, L. & Pratt, R. H. (1983). *Elastic photon scattering at small momentum transfer and validity of form-factor theories. Phys. Rev. A*, **27**, 285–290.

Roy, S. C. & Pratt, R. H. (1982). *Validity of non relativistic dipole approximation for forward Rayleigh scattering. Phys. Rev. A*, **26**, 651–653.

Schaupp, D., Schumacher, M., Smend, F., Rullhausen, P. & Hubbell, J. H. (1983). *Small-angle Rayleigh scattering of photons at high energies: tabulations of relativistic HFS modified atomic form factors. J. Phys. Chem. Ref. Data*, **12**, 467–511.

Scofield, J. (1973). *Theoretical photoionization cross sections from 1 to 1500 keV*. Report UCRL-51326. Lawrence Livermore National Laboratory, Livermore, USA.

Siddons, P. & Hart, M. (1983). *Simultaneous measurements of the real and imaginary parts of the X-ray anomalous dispersion using X-ray interferometers. EXAFS and near edge structure*, edited by A. Branconi, L. Incoccia & S. Stipcich, pp. 373–375. Berlin: Springer.

Smith, D. Y. (1987). *Anomalous X-ray scattering: relativistic effects in X-ray dispersion analysis. Phys. Rev. A*, **35**, 3381–3387.

Sorenson, L. O. (1994). *Diffraction anomalous fine structure*, edited by G. Materlik, C. J. Sparks & K. Fischer, pp. 389–420. Amsterdam: North Holland.

Stanglmeier, F., Lengeler, B., Weber, W., Gobel, H. & Schuster, M. (1992). *Determination of the dispersive correction f′(E) to the atomic form factor from X-ray reflection. Acta Cryst.* A**48**, 626–639.

Stearns, D. G. (1984). *Broadening of extended X-ray absorption fine structure ensuing from the finite lifetime of the K hole. Philos. Mag.* **49**, 541–558.

Stibius-Jensen, M. (1979). *Some remarks on the anomalous scattering factors for X-rays. Phys. Lett. A*, **74**, 41–44.

Stibius-Jensen, M. (1980). *Atomic X-ray scattering factors for forward scattering beyond the dipole approximation*. Personal communication.

Storm, E. & Israel, H. (1970). *Photon cross sections from 0.001 to 100 MeV for elements 1 through 100. Nucl. Data Tables*, A**7**, 565–681.

Suortti, P., Hastings, J. B. & Cox, D. E. (1985). *Powder diffraction with synchrotron radiation. II. Dispersion factors of Ni. Acta Cryst.* A**41**, 417–420.

Takama, T., Iwasaki, N. & Sato, S. (1980). *Measurement of X-ray Pendellösung intensity beats in diffracted white radiation from silicon wafers. Acta Cryst.* A**36**, 1025–1030.

Takama, T., Kobayashi, K., Hyogah, H., Wittono, G. & Sato, S. (1984). *Atomic scattering factors of Zn determined from measurement of Pendellösung intensity beats using white radiation. Jpn. J. Appl. Phys.* **23**, 11–14.

Takama, T., Kobayashi, K. & Sato, S. (1982). *Determination of the atomic scattering factor of aluminium by the Pendellösung-beat measurement using white radiation. Trans. Jpn. Inst. Met.* **23**, 153–160.

Takama, T. & Sato, S. (1982). *Atomic scattering factors of copper determined by Pendellösung beat measurements using white radiation. Philos. Mag.* **45**, 615–626.

Takama, T. & Sato, S. (1984). *Determination of the atomic scattering factors of germanium by means of the Pendellösung beat measurement using white radiation. Jpn. J. Appl. Phys.* **20**, 1183–1190.

Templeton, D. H. (1994). *X-ray resonance, then and now. Resonant anomalous X-ray scattering*, edited by G. Materlik, C. J. Sparks & K. Fischer, pp. 1–7. Amsterdam: North Holland.

Templeton, D. H. & Templeton, L. K. (1978). *Cesium hydrogen tartrate and anomalous dispersion of cesium. Acta Cryst.* A**34**, 368–373.

Templeton, D. H. & Templeton, L. K. (1985). *Tensor X-ray optical properties of the bromate ion. Acta Cryst.* A**41**, 133–142.

Templeton, D. H., Templeton, L. K., Philips, J. C. & Hodgson, K. O. (1980). *Anomalous scattering of X-rays by cesium and cobalt measured with synchrotron radiation. Acta Cryst.* A**36**, 436–442.

Thomas, L. H. (1927). *The calculation of atomic fields. Proc. Cambridge Philos. Soc.* **23**, 542–548.

Wagenfeld, H. (1975). *Theoretical computations of X-ray dispersion corrections. Anomalous scattering*, edited by S. Ramaseshan & S. C. Abrahams, pp. 12–23. Copenhagen: Munksgaard.

Waller, I. (1928). *Über eine verallgemeinerte Streuringsformel. Z. Phys.* **51**, 213–231.

Wang, M. S. (1986). *Relativistic dispersion relation for X-ray anomalous scattering factor. Phys. Ref. A*, **34**, 636–637.

Wang, M. S. & Pratt, R. H. (1983). *Importance of bound–bound transitions in the dispersion relation for calculation of soft-X-ray forward Rayleigh scattering from light elements. Phys. Rev. A*, **28**, 3115–3116.

### 4.2.6 (*cont.*)

Zachariasen, W. H. (1945). *Theory of X-ray diffraction in crystals*. New York: Dover.

### 4.3.1

Bethe, H. A. (1928). *Theorie der Beugung von Elektronen an Kristallen*. *Ann. Phys (Leipzig)*, **87**, 55–129.

Blackman, M. (1939). *On the intensities of electron diffraction rings*. *Proc. R. Soc. London Ser A*, **173**, 68–82.

Coulthard, M. A. (1967). *A relativistic Hartree–Fock atomic field calculation*. *Proc. Phys. Soc.* **91**, 44–49.

Cowley, J. M. & Moodie, A. F. (1957). *The scattering of electrons by atoms and crystals. I. A new theoretical approach*. *Acta Cryst.* **10**, 609–619.

Cromer, D. T. & Waber, J. T. (1974). *Atomic scattering factors for X-rays*. *International tables for X-ray crystallography*, Vol. IV, Section 2.2. Birmingham: Kynoch Press. (Present distributor Kluwer Academic Publishers, Dordrecht.)

Doyle, P. A. & Turner, P. S. (1968). *Relativistic Hartree–Fock X-ray and electron scattering factors*. *Acta Cryst.* A**24**, 390–397.

Fox, A. G., O'Keefe, M. A. & Tabbernor, M. A. (1989). *Relativistic Hartree–Fock X-ray and electron atomic scattering factors at high angles*. *Acta Cryst.* A**45**, 786–793.

Fujiwara, K. (1959). *Application of higher-order Born approximation to multiple elastic scattering of electrons in crystals*. *J. Phys. Soc. Jpn*, **14**, 1513–1524.

Fujiwara, K. (1961). *Relativistic dynamical theory of electron diffraction*. *J. Phys. Soc. Jpn*, **16**, 2226–2238.

Ibers, J. A. (1958). *Atomic scattering amplitudes for electrons*. *Acta Cryst.* **11**, 178–183.

*International Tables for Crystallography* (1992). Vol. B. Dordrecht: Kluwer Academic Publishers.

*International Tables for X-ray Crystallography* (1974). Vol. IV. Birmingham: Kynoch Press. (Present distributor Kluwer Academic Publishers, Dordrecht.)

MacGillavry, C. H. (1940). *Zur Prufung der Dynamischen Theorie der Elektronenbeugung an Kristallgitter*. *Physica (Utrecht)*, **7**, 329–343.

Mann, J. B. (1968). Los Alamos Scientific Laboratory Report LA3691, p. 168.

Peng, L. M. & Cowley, J. M. (1988). *Errors arising from numerical use of the Mott formula in electron image simulation*. *Acta Cryst.* A**44**, 1–5.

Rez, D., Rez, P. & Grant, I. (1994). *Dirac–Fock calculations of X-ray scattering factors and contributions to the mean inner potential for electron scattering*. *Acta Cryst.* A**50**, 481–497.

### 4.3.2

Bird, D. M. & King, Q. A. (1990). *Absorptive form factors for high-energy electron diffraction*. *Acta Cryst.* A**46**, 202–208.

Doyle, P. A. & Turner, P. S. (1968). *Relativistic Hartree–Fock X-ray and electron scattering factors*. *Acta Cryst.* A**24**, 390–397.

Fox, A. G., O'Keefe, M. A. & Tabbernor, M. A. (1989). *Relativistic Hartree–Fock X-ray and electron atomic scattering factors at high angles*. *Acta Cryst.* A**45**, 786–793.

Peng, L.-M. (1998). *Electron scattering factors of ions and their parameterization*. *Acta Cryst.* A**54**, 481–485.

Peng, L. M., Ren, G., Dudarev, S. L. & Whelan, M. J. (1996). *Robust parameterization of elastic and absorptive electron atomic scattering factors*. *Acta Cryst.* A**52**, 257–276.

Rez, D., Rez, P. & Grant, I. (1994). *Dirac–Fock calculations of X-ray scattering factors and contributions to the mean inner potential for electron scattering*. *Acta Cryst.* A**50**, 481–497.

Weickenmeier, A. & Kohl, H. (1991). *Computation of absorptive form factors for high-energy electron diffraction*. *Acta Cryst.* A**47**, 590–597.

### 4.3.3

Arnesen, S. P. & Seip, H. M. (1966). *Studies on the failure of the first Born approximation in electron diffraction. V. Molybdenum- and tungsten hexacarbonyl*. *Acta Chem. Scand.* **20**, 2711–2727.

Bartell, L. S. (1975). *Modification of Glauber theory for dynamic scattering of electrons by polyatomic molecules*. *J. Chem. Phys.* **63**, 3750–3755.

Bartell, L. S. & Brockway, L. O. (1953). *The investigation of electron distribution in atoms by electron diffraction*. *Phys Rev.* **90**, 833–838.

Bartell, L. S. & Gavin, R. M. Jr (1964). *Effects of electron correlation in X-ray and electron diffraction*. *J. Am. Chem. Soc.* **86**, 3493–3498.

Bartell, L. S. & Miller, B. (1980). *Extension of Glauber theory to account for intratarget diffraction in multicenter scattering*. *J. Chem. Phys.* **72**, 800–807.

Bartell, L. S. & Wong, T. C. (1972). *Three-atom scattering in gas-phase electron diffraction: a tractable limiting case*. *J. Chem. Phys.* **56**, 2364–2367.

Bethe, H. A. (1930). *Zur Theorie des Durchgangs Schneller Korpuskularstrahlen durch Materie*. *Ann. Phys. (Leipzig)*, **5**, 325–400.

Biggs, F., Mendelsohn, L. B. & Mann, J. B. (1975). *Hartree–Fock Compton profiles for the elements*. *At. Data Nucl. Data Tables*, **16**, 210–309.

Bonham, R. A. (1965*a*). *Multiple elastic intramolecular scattering in gas electron diffraction*. *J. Chem. Phys.* **43**, 1103–1109.

Bonham, R. A. (1965*b*). *Corrections to the incoherent scattering factor for electrons and X-rays*. *J. Chem. Phys.* **43**, 1460–1464.

Bonham, R. A. (1966). *Dynamic effects in gas electron diffraction*. *Trans. Am. Crystallogr. Assoc.* **2**, 165–172.

Bonham, R. A. (1967). *Some new relations connecting molecular properties and electron and X-ray diffraction intensities*. *J. Phys. Chem.* **71**, 856–862.

Bonham, R. A. & Cox, H. L. Jr (1967). *40-kV elecron scattering fom Ne, Ar, Kr, and Xe measured by the sector-microphotometer electron-diffraction method*. *J. Chem. Phys.* **47**, 3508–3517.

Bonham, R. A. & Fink, M. (1974). *High energy electron scattering*, Chaps. 5 and 6. New York: Van Nostrand Reinhold.

Bonham, R. A. & Iijima, T. (1965). *Preliminary electron-diffraction study of $H_2$ at small scattering angles*. *J. Chem. Phys.* **42**, 2612–2614.

Bonham, R. A. & Su, L. S. (1966). *Use of Hellman–Feynman and hyperviral theorems to obtain anharmonic vibration–rotation expectation values and their application to gas diffraction*. *J. Chem. Phys.* **45**, 2827–2831.

**4.3.3 (*cont.*)**


Breitenstein, M., Endesfelder, A., Meyer, H. & Schweig, A. (1984). *CI calculations of electron-scattering cross sections for some linear molecules*. *Chem. Phys. Lett.* **108**, 430–434.

Breitenstein, M., Endesfelder, A., Meyer, H., Schweig, A. & Zittlau, W. (1983). *Electron correlation effects in electron scattering cross-section calculations of $N_2$*. *Chem. Phys. Lett.* **97**, 403–409.

Breitenstein, M., Mawhorter, R. J., Meyer, H. & Schweig, A. (1984). *Theoretical study of potential-energy differences from high-energy electron scattering cross sections of $CO_2$*. *Phys. Rev. Lett.* **53**, 2398–2401.

Breitenstein, M., Mawhorter, R. J., Meyer, H. & Schweig, A. (1986). *Vibrational effects on electron–molecule scattering for polyatomics in the first Born approximation: $H_2O$*. *Mol. Phys.* **57**, 81–88.

Bunge, C. F., Barrientos, J. & Bunge, A. V. (1993). *Roothaan–Hartree–Fock ground-state atomic wave functions: Slater-type orbital expansions and expectation values*. *At. Data Nucl. Data Tables*, **53**, 113–162.

Bunyan, P. J. (1963). *The effect of multiple elastic scattering in gas electron diffraction*. *Proc. Phys. Soc.* **82**, 1051–1057.

Coffman, D., Fink, M. & Wellenstein, H. (1985). *Elastic small-angle electron scattering by He, Ne, and Ar at 35 keV*. *Phys. Rev. Lett.* **55**, 1392–1394.

Epstein, J. & Stewart, R. F. (1977). *X-ray and electron scattering from diatomic molecules in the first Born approximation*. *J. Chem. Phys.* **66**, 4057–4064.

Fink, M., Bonham, R. A., Lee, J. S. & Ng, E. W. (1969). *Large angle scattering from $N_2$ with 40 keV electrons*. *Chem. Phys. Lett.* **4**, 347–351.

Fink, M. & Kessler, J. (1966). *Absolute Wirkungsquerschnitte für Elektronenstreuung um Kleine Winkel. Experimente sum Gültigkeitsbereich der Ersten Bornschen Näherung*. *Z. Phys.* **196**, 1–15.

Geiger, J. (1964). *Streuung von 25 keV-Elektronen an Gasen. II. Streuung an Neon, Argon, Krypton und Xenon*. *Z. Phys.* **177**, 138–145.

Gjønnes, J. (1964). *A dynamic effect in electron diffraction by molecules*. *Acta Cryst.* **17**, 1075–1076.

Glauber, R. & Schomacher, V. (1953). *The theory of electron diffraction*. *Phys. Rev.* **89**, 667–671.

Hanson, H. P. (1962). *Experimental f values and electron diffraction amplitudes for bromine*. *J. Chem. Phys.* **36**, 1043–1049.

Heisenberg, W. (1931). *Über die Inkohärente Streuung von Röntgenstrahlen*. *Phys. Z.* **32**, 737–740.

Hilderbrandt, R. L. & Kohl, D. A. (1981). *A variational treatment of the effects of vibrational anharmonicity on gas-phase electron diffraction intensities. Part I. Molecular scattering function*. *J. Mol. Struct. Theochem.* **85**, 25–36.

Hoerni, J. A. (1956). *Multiple elastic scattering in electron diffraction by molecules*. *Phys. Rev.* **102**, 1530–1533.

Horota, F., Kakuta, N. & Shibata, S. (1981). *High energy electron scattering by diborane*. *J. Phys. B*, **14**, 3299–3304.

Iijima, T., Bonham, R. A. & Ando, T. (1963). *The theory of electron scattering from molecules. I. Theoretical development*. *J. Phys. Chem.* **67**, 1472–1474.

Karle, I. L. & Karle, J. (1950). *Internal motion and molecular structure studies by electron diffraction. III. Structure of $CH_2CF_2$ and $CF_2CF_2$*. *J. Chem. Phys.* **18**, 963–971.

Kelley, M. H. & Fink, M. (1982*a*). *The molecular structure of dimolybdenum tetraacetate*. *J. Chem. Phys.* **76**, 1407–1416.

Kelley, M. H. & Fink, M. (1982*b*). *The temperture dependence of the molecular structure parameters in $SF_6$*. *J. Chem. Phys.* **77**, 1813–1817.

Kessler, J. (1959). *Einzelstreuung Mittelschneller Elektronen an Schweren Atomkernen*. *Z. Phys.* **155**, 350–367.

Ketkar, S. N. & Fink, M. (1985). *Structure of dichromium tetraacetate by gas-phase electron diffraction*. *J. Am. Chem. Soc.* **107**, 338–340.

Kimura, M., Schomaker, V., Smith, D. & Weinstock, B. (1968). *Electron-diffraction investigation of the hexafluorides of tungsten, osmium, iridium, uranium, neptunium, and plutonium*. *J. Chem. Phys.* **48**, 4001–4012.

Kohl, D. A. & Arvedson, M. (1980). *Elastic electron scattering from molecular potentials*. *J. Chem. Phys.* **73**, 3818–3822.

Kohl, D. A. & Bartell, L. S. (1969). *Electron densities from gas-phase electron diffraction intensities. II. Molecular Hartree–Fock cross sections*. *J. Chem. Phys.* **51**, 2896–2904.

Kohl, D. A. & Bonham, R. A. (1967). *Effect of bond formation on electron scattering cross sections for molecules*. *J. Chem. Phys.* **47**, 1634–1646.

Kohl, D. A. & Hilderbrandt, R. L. (1981). *A variational treatment of the effects of vibrational anharmonicity on gas-phase electron diffraction intensities. Part II. Temperature dependence*. *J. Mol. Struct. Theochem.* **85**, 325–335.

Liu, J. W. & Smith, V. H. (1977). *A critical study of high energy electron scattering from $H_2$*. *Chem. Phys. Lett.* **45**, 59–63.

McClelland, J. J. & Fink, M. (1985). *Electron correlation and binding effects in measured electron-scattering cross sections of $CO_2$*. *Phys. Rev. Lett.* **54**, 2218–2221.

McLean, A. D. & McLean, R. S. (1981). *Roothaan–Hartree–Fock atomic wave functions: Slater basis-set expansions for $Z = 55$–$92$*. *At. Data Nucl. Data Tables*, **26**, 197–381.

Mawhorter, R. J. & Fink, M. (1983). *The vibrationally averaged, temperture-dependent structure of polyatomic molecules. II. $SO_2$*. *J. Chem. Phys.* **79**, 3292–3296.

Mawhorter, R. J., Fink, M. & Archer, B. T. (1983). *The vibrationally averaged, temperature-dependent strucure of polyatomic molecules. I. $CO_2$*. *J. Chem. Phys.* **79**, 170–174.

Melkanov, M. A., Sawada, T. & Raynal, J. (1966). *Nuclear optical model calculations*. *Meth. Comput. Phys.* **6**, 1–80.

Miller, B. R. & Fink, M. (1981). *Mean amplitudes of vibration of $SF_6$ and intramolecular multiple scattering*. *J. Chem. Phys.* **75**, 5326–5328.

Miller, B. R. & Fink, M. (1985). *The vibrationally averaged, temperature-dependent structure of polyatomic molecules. III. $NO_2$*. *J. Chem. Phys.* **83**, 939–944.

Morse, P. M. (1932). *Unelastische Streuung von Kathodenstrahlen*. *Phys. Z.* **33**, 443–445.

Mott, N. I. & Massey, H. S. W. (1965). *The theory of atomic collisions*, 3rd ed., Chap. IX, Section 4, equations (22) and (23). Oxford University Press.

Numerov, B. V. (1924). *A method of extrapolation of perturbations*. *Mon. Not. R. Astron. Soc.* **84**, 592–601.

Peixoto, E. M. A., Bunge, C. F. & Bonham, R. A. (1969). *Elastic and inelastic electron scattering by He and Ne atoms in their ground states*. *Phys. Rev.* **181**, 322–328.

Pulay, P., Mawhorter, R. J., Kohl, D. A. & Fink, M. (1983). *Ab initio Hartree–Fock calculation of the elastic electron scattering cross section of sulphur hexafluoride*. *J. Chem. Phys.* **79**, 185–191.

Ross, A. W. & Fink, M. (1986). *Atomic scattering factor and spin polarization calculations*. *Phys. Rev.* **85**, 6810–6811.

Sasaki, H., Konaka, S., Iijima, T. & Kimura, M. (1982). *Small-angle electron scattering and electron density in carbon dioxide*. *Int. J. Quantum Chem.* **21**, 475–485.

**4.3.3 (*cont.*)**

Schäfer, L. & Seip, H. M. (1967). *Studies on the failure of the first Born approximation in electron diffraction. VI. Ruthenium tetraoxide. Acta Chem. Scand.* **21**, 737–744.

Schomaker, V. & Glauber, R. (1952). *The Born approximation in electron diffraction. Nature (London)*, **170**, 290–291.

Seip, H. M. (1965). *Studies on the failiure of the first Born approximation in electron diffraction. I. Uranium hexafluoride. Acta Chem. Scand.* **19**, 1955–1968.

Seip, H. M. & Seip, R. (1966). *Studies on the failure of the first Born approximation in electron diffraction. IV. Molybdenum- and tungsten hexafluoride. Acta Chem. Scand.* **20**, 2698–2711.

Seip, H. M. & Stølevik, V. (1966). *Studies on the failure of the first Born approximation in electron diffraction. II. Osmium tetraoxide. III. Tellurium hexafluoride. Acta Chem. Scand.* **20**, 385–394, 1535–1545.

Shibata, S., Hirota, F., Kakuta, N. & Muramatsu, T. (1980). *Electron distribution in water by high-energy electron scattering. Int. J. Quantum Chem.* **18**, 281–285.

Tavard, C. & Bonham, R. A. (1969). *Quantum-mechanical formulas for the inelastic scattering of fast electrons and their Compton line shape. Nonrelativistic approximation. J. Chem. Phys.* **50**, 1736–1747.

Tavard, C., Rouault, M. & Roux, M. (1965). *Diffraction des rayons X et des électrons par les molécules. III. Une méthode de detémination des densités électroniques moléculaires. J. Chim. Phys.* **62**, 1410–1417.

Tavard, C. & Roux, M. (1965). *Calcul des intensités de diffraction de rayons X et de électrons par les molécules. C. R. Acad. Sci.* **260**, 4933–4936.

Thakkar, A. J. & Smith, V. H. Jr (1978). *Form factors and total scattering intensities for the helium-like ions from explicitly correlated wavefunctions. J. Phys. B*, **11**, 3803–3820.

Wang, J., Esquivel, R. O., Smith, V. H. Jr & Bunge, C. (1995). *Accurate elastic and inelastic scattering factors from He to Ne using correlated wavefunctions. Phys. Rev. A*, **51**, 3812–3818.

Wang, J., Sagar, R. P., Schmider, H. & Smith, V. H. Jr (1993). *X-ray elastic and inelastic scattering factors for neutral atoms $Z = 2 - 92$. At. Data Nucl. Data Tables*, **53**, 233–269.

Wang, J., Tripathi, A. N. & Smith, V. H. Jr (1994). *Chemical binding and electron correlation effects in X-ray and high energy electron scattering. J. Chem. Phys.* **101**, 4842–4854.

Wong, T. C. & Bartell, L. S. (1973). *Three atom scattering in gas-phase electron diffraction. II. A general treatment. J. Chem. Phys.* **58**, 5654–5660.

Xie, S.-D., Fink, M. & Kohl, D. A. (1984). *Basis set dependence of ab initio SCF elastic, Born, electron scattering cross sections for $C_2H_4$. J. Chem. Phys.* **81**, 1940–1942.

Yates, A. C. (1970). *Relativistic effects in high-energy inelastic electron–atom collisions. Chem. Phys. Lett.* **6**, 49–53.

Yates, A. C. (1971). *A program for calculating relativistic elastic electron–atom collision data. Comput. Phys. Commun.* **2**, 175–179.

Yates, A. C. & Bonham, R. A. (1969). *Use of relativistic electron scattering factors in electron diffraction analysis. J. Chem. Phys.* **50**, 1056–1058.

**4.3.4**

Ahn, C. C. & Krivanek, O. L. (1982). *An EELS atlas*. Available from Center for Solid State Science, Arizona State University, Tempe, AZ 85287, USA.

Ahn, C. C. & Rez, P. (1985). *Inner shell edge profiles in electron energy loss spectroscopy. Ultramicroscopy*, **17**, 105–116.

Altarelli, M. & Smith, S. Y. (1974). *Superconvergence and sum rules for the optical constants: physical meaning, comparison with experiment and generalization. Phys Rev. B*, **9**, 1290–1298.

Batson, P. E. (1986). *High energy resolution electron spectrometer for a 1 nm spatial analysis. Rev. Sci. Instrum* **57**, 43–48.

Batson, P. E. (1987). *Spatially resolved interband spectroscopy. Physical aspects of microscopic characterization of materials*, edited by J. Kirschner, K. Murata & J. A. Venables, pp. 189–195. *Scanning Microscopy*, Suppl. I.

Batson, P. E. (1989). *High resolution energy-loss spectroscopy. Ultramicroscopy*, **28**, 32–39.

Batson, P. E. & Silcox, J. (1983). *Experimental energy loss function, $Im[-1/\varepsilon(q, \omega)]$, for aluminium. Phys. Rev. B*, **27**, 5224–5239.

Berger, S. D. & McMullan, D. (1989). *Parallel recording for an electron spectrometer on a scanning transmission electron microscope. Ultramicroscopy*, **28**, 122–125.

Bethe, H. A. (1930). *Zur Theorie des Durchgangs schneller Korpuskularstrahlen durch Materie. Ann. Phys. (Leipzig)*, **5**, 325–400.

Bianconi, A., Fritsch, E., Calas, G. & Petiau, J. (1985). *X-ray absorption near edge structure of 3d transition elements in tetrahedral coordination: the effect of bond length variation. Phys. Rev. B*, **32**, 4292–4295.

Boersch, H. (1954). *Experimentelle Bestimmung der Energieverteilung in thermisch ausgelosten Elektronenstrahlen. Z. Phys.* **139**, 115–146.

Bross, H. (1978*a*). *Anisotropy of plasmon dispersion in Al. Phys. Lett. A*, **64**, 418–420.

Bross, H. (1978*b*). *Pseudopotential theory of the dielectric function of Al – the volume plasmon dispersion. J. Phys. F*, **8**, 2631–2649.

Brydson, R., Sauer, H., Engel, W., Thomas, J. M., Zeitler, E., Kosugi, N. & Kuroda, H. (1989). *Electron energy loss and X-ray absorption spectroscopy of rutile and anatase: a test of structural sensitivity. J. Phys. Condens. Matter,* **1**, 797–812.

Castaing, R. & Henry, L. (1962). *Filtrage magnétique des vitesses en microscopie électronique. C. R. Acad. Sci. Sér. B*, **255**, 76–78.

Chen, C. H. & Silcox, J. (1971). *Detection of optical surface guided modes in thin graphite films by high energy electron scattering. Phys. Rev. Lett.* **35**, 390–393.

Colliex, C. (1984). *Electron energy loss spectroscopy in the electron microscope. Advances in optical and electron microscopy,* Vol. 9, edited by V. E. Cosslett & R. Barer, pp. 65–177. London: Academic Press.

Colliex, C. (1985). *An illustrated review on various factors governing the high spatial resolution capabilities in EELS microanalysis. Ultramicroscopy*, **18**, 131–150.

Colliex, C., Gasgnier, M. & Trebbia, P. (1976). *Analysis of the electron excitation spectra in heavy rare earth metals, hydrides and oxides. J. Phys. (Paris)*, **27**, 397–406.

Colliex, C., Manoubi, T., Gasgnier, M. & Brown, L. M. (1985). *Near edge structures on EELS core-loss edges. Scanning Electron Microsc.* **2**, 489–512.

Colliex, C., Maurice, J. L. & Ugarte, D. (1989). *Frontiers of analytical electron microscopy with special reference to cluster and interface problems. Ultramicroscopy*, **29**, 31–43.

Craven, A. J. & Buggy, T. W. (1981). *Design considerations and performance of an analytical STEM. Ultramicroscopy*, **7**, 27–37.

**4.3.4 (*cont.*)**


Crewe, A. V. (1977*a*). *Post specimen optics in the STEM. I. General information. Optik (Stuttgart)*, **47**, 299-312.

Crewe, A. V. (1977*b*). *Post specimen optics in the STEM. II. Optik (Stuttgart)*, **47**, 371–380.

Daniels, J., Festenberg, C. V., Raether, H. & Zeppenfeld, K. (1970). *Optical constants of solids by electron spectroscopy. Springer tracts in modern physics*, Vol. 54, pp. 78–135. New York: Springer-Verlag.

Disko, M. M., Krivanek, O. L. & Rez, P. (1982). *Orientation dependent extended fine structure in EELS. Phys. Rev. B*, **25**, 4252–4255.

Durham, J. P., Pendry, J. B. & Hodges, C. H. (1981). *XANES: determination of bond angles and multi-atom correlations in ordered and disordered systems. Solid State Commun.* **8**, 159–162.

Egerton, R. F. (1978). *Formulae for light element analysis by electron energy loss spectrometry. Ultramicroscopy*, **3**, 243–351.

Egerton, R. F. (1979). *K-shell ionization cross sections for use in microanalysis. Ultramicroscopy*, **4**, 169–179.

Egerton, R. F. (1980*a*). *The use of electron lenses between a TEM specimen and an electron spectrometer. Optik (Stuttgart)*, **56**, 363–376.

Egerton, R. F. (1980*b*). *Design of an aberration-corrected electron spectrometer for the TEM. Optik (Stuttgart)*, **57**, 229–242.

Egerton, R. F. (1986). *Electron energy loss spectroscopy in the electron microscope*. New York/London: Plenum.

Egerton, R. F. & Crozier, P. A. (1987). *A compact parallel recording. J. Microsc.* **148**, 157.

Enge, H. A. (1967). *Deflecting magnets. Focusing of charged particles*, Vol. 2, edited by A. Septier, pp. 203–264. New York: Academic Press.

Engel, W., Sauer, H., Zeitler, E., Brydson, R., Williams, B. G. & Thomas, J. M. (1988). *Electron energy loss spectroscopy and the crystal chemistry of rhodizite. J. Chem. Soc. Faraday Trans. 1*, **84**, 617–629.

Fano, U. (1961). *Effects of configuration interaction on intensities and phase shifts. Phys. Rev.* **124**, 1966–1978.

Fink, J. & Kisker, E. (1980). *A method for rapid calculation of electron trajectories in multielement electrostatic cylinder lenses. Rev. Sci. Instrum.* **51**, 918–920.

Fink, J. & Leising, G. (1986). *Momentum dependent dielectric functions of oriented trans-polyacetylen. Phys. Rev. B*, **34**, 5320–5328.

Fink, J., Müller-Heinzerling, T., Pflüger, J., Scheerer, B., Dischler, B., Koidl, P., Bubenzer, A. & Sah, R. E. (1984). *Investigation of hydrocarbon-plasma-generated carbon films by EELS. Phys. Rev. B*, **30**, 4713–4718.

Fischer, D. W. (1970). *Molecular orbital interpretation of the soft X-ray $L_{23}$ emission and absorption spectra from some titanium and vanadium compounds. J. Appl. Phys.* **41**, 3561–3569.

Gibbons, P. C., Ritsko, J. J. & Schnatterly, S. E. (1975). *Inelastic electron scattering spectrometer. Rev. Sci. Instrum.* **46**, 1546–1554.

Grunes, L. A., Leapman, R. D., Wilker, C. N., Hoffmann, R. & Kunz, A. B. (1982). *Oxygen K near-edge fine structure: an electron energy-loss investigation with comparisons to new theory for selected 3d transition-metal oxides. Phys. Rev. B*, **25**, 7157–7173.

Hagemann, H. J., Gudat, W. & Kunz, C. (1975). *Optical constants from the far infrared to the X-ray region: Mg, Al, Cu, Ag, Au, Bi, C, and $Al_2O_3$. J. Opt. Soc. Am.* **65**, 742–748.

Hartl, W. A. M. (1966). *Die Filterlinse als Monochromator für schnelle Elektronen. Z. Phys.* **191**, 487–502.

Heine, V. (1980). *Electronic structure from the point of view of the local atomic environment. Solid State Phys.* **35**, 1–127.

Hillier, J. & Baker, R. F. (1944). *Microanalysis by means of electrons. J. Appl. Phys.* **15**, 663–675.

Hitchcock, A. P. (1982). *Bibliography of atomic and molecular inner-shell excitation studies. J. Electron Spectrosc. Relat. Phenom.* **25**, 245–275. [Updated copies of this bibliography are available from the author on request.]

Hofer, F., Golob, P. & Brunegger, A. (1988). *EELS quantification of the elements Sr to W by means of $M_{45}$ edges. Ultramicroscopy*, **25**, 81–84.

Hohberger, H. I., Otto, A. & Petri, E. (1975). *Plasmon resonance in Al, devations from quadratic dispersion observed. Solid State Commun.* **16**, 175–179.

Ibach, H. & Mills, D. L. (1982). *Electron energy-loss spectroscopy and surface vibrations*. New York: Academic Press.

Inokuti, M. (1971). *Inelastic collisions of fast charged particles with atoms and molecules. The Bethe theory revisited. Rev. Mod. Phys.* **43**, 297–344; *Addenda: Rev. Mod. Phys.* **50**, 23–26.

Inokuti, M. (1979). *Electron scattering cross sections pertinent to electron microscopy. Ultramicroscopy*, **3**, 423–427.

Isaacson, M. (1972*a*). *Interaction of 24 keV electrons with the nucleic acid bases, adenine, thymine and uracil. I. Outer shell excitation. J. Chem. Phys.* **56**, 1803–1812.

Isaacson, M. (1972*b*). *Interaction of 25 keV electsons with the nucleic acid bases, adenine, thymine and uracil. II. Inner shell excitation and inelastic scattering cross section. J. Chem. Phys.* **56**, 1813–1818.

Isaacson, M. & Johnson, D. (1975). *The microanalysis of light elements using transmitted energy-loss electrons. Ultramicroscopy*, **1**, 33–52.

Janssen, R. W. & Sankey, O. F. (1987). *Ab inito linear combination of pseudo-atomic orbital scheme for the electronic properties of semiconductors. Results for ten materials. Phys. Rev. B*, **36**, 6520–6531.

Johnson, D. E. (1979). *Basic aspects of energy-loss spectrometer systems. Ultramicroscopy*, **3**, 361–365.

Johnson, D. E. (1980). *Post specimen optics for energy loss spectrometry. Scanning Electron. Microsc.* **1**, 33–40.

Johnson, D. W. (1975). *A Fourier method for numerical Kramers–Kronig analysis. J. Phys. A*, **8**, 490–495.

Johnson, D. W. & Spence, J. C. H. (1974). *Determination of the single scattering probability distribution from plural scattering data. J. Phys. D*, **7**, 771–780.

Jouffrey, B., Sevely, J., Zanchi, G. & Kihn, Y. (1985). *Characteristic energy losses with high energy electrons up to 2.5 MeV. Scanning Electron Microsc.* **3**, 1063–1070.

Keil, P. (1968). *Elektronen-Energieverlustmessungen und Berechnung optischer Konstanten. I. Festes Xenon. Z. Phys.* **214**, 251–265.

Killat, U. (1974). *Optical properties of $C_6H_{12}$, $C_6H_{10}$, $C_6H_8$, $C_6H_6$, $C_7H_8$, $C_6H_5Cl$ and $C_5H_5N$ in the solid and gaseous state derived from electron energy losses. J. Phys. C*, **7**, 2396–2408.

Klemperer, O. (1965). *Electron beam spectroscopy. Rev. Prog. Phys.* **28**, 77–111.

Kliewer, K. & Fuchs, R. (1974). *Theory of dynamical properties of dielectric surfaces. Adv. Chem. Phys.* **27**, 355–541.

**4.3.4 (*cont.*)**


Krahl, D. & Herrmann, K. H. (1980). *Experiments with an imaging energy filter in the CTEM. Micron*, **11**, 287–289.

Krivanek, O. L., Ahn, C. C. & Keeney, R. B. (1987). *Parallel detection electron spectrometer using quadrupole lens. Ultramicroscopy*, **22**, 103–115.

Krivanek, O. L., Manoubi, T. & Colliex, C. (1985). *Sub 1 eV resolution EELS at energy losses greater than 1 keV. Ultramicroscopy*, **18**, 155–158.

Krivanek, O. L. & Swann, P. R. (1981). *An advanced electron energy loss spectrometer. Quantitative microanalysis with high spatial resolution*, pp. 136–140. London: The Metals Society.

Kröger, E. Z. (1970). *Transition radiation, Čerenkov radiation and energy losses of relativistic charged particles traversing thin foils at oblique incidence. Z. Phys.* **235**, 403–421.

Kuyatt, C. E. & Simpson, J. A. (1967). *Electron monochromator design. Rev. Sci. Instrum.* **38**, 103–111.

Landau, L. & Lifchitz, E. (1966). *Mécanique quantique. Théorie non relativiste*, pp. 632–690. Moscow: Editions Mir.

Leapman, R. D., Grunes, L. A. & Fejes, P. L. (1982). *Study of the $L_{23}$ edges in the 3d transition metals and their oxides by electron energy loss spectroscopy with comparisons to theory. Phys. Rev. B*, **26**, 614–635.

Leapman, R. D., Rez, P. & Mayers, D. F. (1980). *K, L and M shell generalized oscillator strengths and ionization cross sections for fast electron collisions. J. Chem. Phys.* **72**, 1232–1243.

Leapman, R. D. & Swyt, C. R. (1988). *Separation of overlapping core edges in EELS spectra by mutiple least-squares fitting. Ultramicroscopy*, **26**, 393–404.

Lindhard, J. (1954). *On the properties of a gas of charged particles. Dan. Vidensk. Selsk. Mat. Fys. Medd.* **28**, 1–57.

Lindner, T., Sauer, H., Engel, W. & Kambe, K. (1986). *Near-edge structure in electron energy loss spectra of MgO. Phys. Rev. B*, **33**, 22–24.

Livingood, J. J. (1969). *The optics of dipole magnets*. New York: Academic Press.

Lytle, F. W., Greegor, R. B. & Panson, A. Y. (1988). *Discussion of X-ray asorption near edge structure: application to Cu in the high $T_c$ superconductors $La_{1.8}Sr_{0.2}Cu_4$ and $YBa_2Cu_3O_7$. Phys. Rev. B*, **37**, 1550–1562.

Maher, D. M. (1979). *Elemental analysis using inner-shell excitations: a microanalytical technique for materials characterization. Introduction to analytical electron microscopy*, edited by J. J. Hren, J. I. Goldstein & D. C. Joy, pp. 259–294. New York: Plenum.

Manoubi, T., Rez, P. & Colliex, C. (1989). *Quantitative electron energy loss spectroscopy on $M_{45}$ edges in rare earth oxides. J. Electron Spectrosc. Relat. Phenom.* **50**, 1–18.

Manoubi, T., Tence, M., Walls, M. G. & Colliex, C. (1990). *Curve fitting methods for quantitative analysis in EELS. Microsc. Microanal. Microstruct.* **1**, 23–39.

Manzke, R. (1980). *Wavevector dependence of the volume plasmon of GaAs and InSb. J. Phys. C*, **13**, 911–917.

Maslen, V. M. & Rossouw, C. J. (1983). *The inelastic scattering matrix element and its application to electron energy loss spectroscopy. Philos. Mag.* A**47**, 119–130.

Metherell, A. J. F. (1971). *Energy analysing and energy selecting electron microscopes. Adv. Opt. Electron Microsc.* **4**, 263–361.

Mory, C. & Colliex, C. (1989). *Elemental analysis near the single-atom detection level by processing sequences of energy-filtered images. Ultramicroscopy*, **28**, 339–346.

Mott, N. F. & Massey, H. S. W. (1952). *The theory of atomic collisions*, pp. 224–248. Oxford: Clarendon Press.

Müller, J. E., Jepsen, O. & Wilkins, J. W. (1982). *X-ray absorption spectra: K edges of 3d transition metals, L edges of 3d and 4d metals and M edges of palladium. Solid State Commun.* **42**, 365–368.

Parker, N. W., Utlaut, M. & Isaacson, M. S. (1978). *Design of magnetic spectrometers with second order aberrations corrected. Optik (Stuttgart)*, **51**, 333–351.

Pearce-Percy, H. T. (1978). *The design of spectrometers for energy loss spectroscopy. Scanning Electron Microsc.* **1**, 41–51.

Powell, C. J. (1976). *Cross sections for ionization of inner-shell electrons by electrons. Rev. Mod. Phys.* **48**, 33–47.

Powell, C. J. (1984). *Inelastic scattering of electrons in solids. Electron beam interactions with solids for microscopy, microanalysis and micro-lithography*, edited by D. F. Kyser, H. Niedrig, D. E. Newbury & R. Shimizu, pp. 19–31. Chicago: SEM, Inc,.

Powell, C. J. (1989). *Cross sections for inelastic electron scattering in solids. Ultramicroscopy*, **28**, 24–31.

Raether, H. (1965). *Electron energy loss spectroscopy. Springer Tracts Mod. Phys.* Vol. 38, pp. 85–170. Berlin: Springer.

Raether, H. (1980). *Excitation of plasmons and interband transitions by electrons. Springer Tracts in Modern Physics*, Vol. 88. Berlin: Springer.

Rao, C. N., Thomas, J. M., Williams, B. G. & Sparrow, T. G. (1984). *Determination of the number of d-electron states in transition metal compounds. J. Phys. Chem.* **88**, 5769–5770.

Rask, J. H., Miner, B. A. & Buseck, P. (1987). *Determination of manganese oxidation states in solids by EELS. Ultramicroscopy*, **21**, 321–326.

Reimer, L. & Rennekamp. R. (1989). *Imaging and recording of multiple scattering effects by angular resolved electron energy loss spectroscopy. Ultramicroscopy*, **28**, 258–265.

Rez, P. (1989). *Inner shell spectroscopy: an atomic view. Ultramicroscopy*, **28**, 16–23.

Ritchie, R. H. (1957). *Plasmon losses by fast electrons in thin films. Phys. Rev.* **106**, 874–881.

Rose, H. & Plies, E. (1974). *Entwurf eines fehlerarmen magnetischen Energie Analysators. Optik (Stuttgart)*, **40**, 336–341.

Rose, H. & Spehr, R. (1980). *On the theory of the Boersch effect. Optik (Stuttgart)*, **57**, 339–364.

Sayers, D. E., Stern, E. A. & Lytle, F. W. (1971). *New technique for investigating noncrystalline structures: Fourier analysis of the extended X-ray absorption fine structure. Phys. Rev. Lett.* **27**, 1204–1207.

Schattschneider, P. (1983). *A performance test of the recovery of single energy loss profiles via matrix analysis. Ultramicroscopy*, **11**, 321–322.

Schattschneider, P. (1989). *The dielectric description of inelastic electron scattering. Ultramicroscopy*, **28**, 1–15.

Scheinfein, M. & Isaacson, M. S. (1984). *Design and performance of second order aberration corrected spectrometers for use with the scanning transmission electron microscope. Scanning Electron Microsc.* **4**, 1681–1696.

Scheinfein, M. & Isaacson, M. S. (1986). *Electronic and chemical analysis of fluoride interface structures at subnanometer spatial resolution. J. Vac. Sci. Technol.* B**4**, 326–332.

Schnatterly, S. E. (1979). *Inelastic electron scattering spectroscopy. Solid State Phys.* **14**, 275–358.

Schröder, B. & Geiger, J. (1972). *Electron spectrometric study of amorphous germanium and silicon in the two phonon region. Phys. Rev. Lett.* **28**, 301–303.

### 4.3.4 (*cont.*)


Sevely, J. (1985). *Voltage dependence in electron energy loss spectroscopy*. *Inst. Phys. Conf. Ser.* **78**, 155–160.

Shiles, E., Sazaki, T., Inokuti, M. & Smith, D. Y. (1980). *Self consistency and sum-rule tests in the Kramers Kronig analysis of optical data: applications to aluminium*. *Phys. Rev. B*, **22**, 1612–1628.

Shuman, H. (1980). *Correction of the second order aberrations of uniform field magnetic sections*. *Ultramicroscopy*, **5**, 45–53.

Shuman, H. & Kruit, P. (1985). *Quantitative data processing of parallel recorded electron energy-loss spectra with low signal to background*. *Rev. Sci. Instrum.* **56**, 231–239.

Shuman, H. & Somlyo, A. P. (1987). *Electron energy loss analysis of near-trace-element concentrations of calcium*. *Ultramicroscopy*, **21**, 23–32.

Spence, J. C. H. (1979). *Uniqueness and the inversion problem of incoherent multiple scattering*. *Ultramicroscopy*, **4**, 9–12.

Spence, J. C. H. (1981). *The crystallographic information in localized characteristic-loss electron images and diffraction patterns*. *Ultramicroscopy*, **7**, 59–64.

Spence, J. C. H. (1988). *Inelastic electron scattering: Parts I and II*. *High resolution transmission electron microscopy and associated techniques*, edited by P. R. Buseck, J. M. Cowley & L. Eyring, pp. 129–189. Oxford University Press.

Spence, J. C. H. & Tafto, J. (1983). *ALCHEMI: a new technique for locating atioms in small crystals*. *J. Microsc.* **130**, 147–154.

Stohr, J., Sette, F. & Johnson, A. L. (1984). *Near edge X-ray absorption fine structure studies of chemisorbed hydrocarbons: bond lengths with a ruler*. *Phys. Rev. Lett.* **53**, 1684–1687.

Strauss, M. G., Naday, Y., Sherman, I. S. & Zaluzec, N. J. (1987). *CCD base parallel detection system for EELS spectroscopy and imaging*. *Ultramicroscopy*, **22**, 117–124.

Sturm, K. (1982). *Electron energy loss in simple metals and semiconductors*. *Adv. Phys.* **31**, 1–64.

Swyt, C. R. & Leapman, R. D. (1982). *Plural scattering in electron energy loss analysis*. *Scanning Electron Microsc.* **1**, 73–82.

Taft, E. A. & Philipp, H. R. (1965). *Optical properties of graphite*. *Phys. Rev. A*, **138**, 197–202.

Tafto, J. & Krivanek, O. L. (1982). *Site specific valence determination by EELS*. *Phys. Rev. Lett.* **48**, 560–563.

Tafto, J. & Zhu, J. (1982). *Electron energy-loss near edge structure (ELNES), A potential technique in the studies of local atomic arrangements*. *Ultramicroscopy*, **9**, 349–354.

Teo, B. K. & Joy, D. C. (1981). *EXAFS spectroscopy techniques and applications*. New York: Plenum.

Thole, B. T., van der Laan, G., Fuggle, J. C., Sawatsky, G. A., Karnatak, R. C. & Esteva, J. M. (1985). *3d X-ray absorption lines and the $3d^9 4f^{n+1}$ multiplets of the lanthanides*. *Phys. Rev. B*, **32**, 5107–5118.

Tossel, J. A., Vaughan, D. J. & Johnson, K. H. (1974). *The electronic structure of rutile, wustite and hematite from molecular orbital calculations*. *Am. Mineral.* **59**, 319–334.

Trebbia, P. (1988). *Unbiased method for signal estimation in EELS. Concentration measurements and detection limits in quantitative analysis: methods and programs*. *Ultramicroscopy*, **24**, 399–408.

Venghaus, H. (1975). *Redetermination of the dielectric function of graphite*. *Phys. Status Solidi B*, **71**, 609–614.

Von Festenberg, C. (1968). *Retardierungseffekte im Energieverlustspektrum von GaP*. *Z. Phys.* **214**, 464.

Vvedensky, D. D., Saldin, D. K. & Pendry, J. B. (1985). *Azimuthal and polar angle dependence in XANES of low symmetry adsorption sites*. *Surf. Sci.* **162**, 909–912.

Wehenkel, C. (1975). *Mise au point d'une nouvelle méthode d'analyse quantitative des spectres de pertes d'énergie d'électrons rapides diffusés dans la direction du faisceau incident: application à l'étude des métaux nobles*. *J. Phys. (Paris)*, **36**, 199–207.

Weng, X. D. & Rez, P. (1989). *Multiple scattering approach to oxygen K near edge structures in EELS spectroscopy of alkaline earths*. *Phys. Rev. B*, **39**, 7405–7412.

Weng, X. D., Rez, P. & Ma, H. (1989). *Carbon K-shell near-edge structure: multiple scattering and band theory calculations*. *Phys. Rev. B*, **40**, 4175–4178.

Weng, X. D., Rez, P. & Sankey, O. F. (1989). *Pseudo-atomic orbital band theory applied to EELS near edge structures*. *Phys. Rev. B*, **40**, 5694–5704.

Wien, W. (1897). *Vert. Deutschen Phys. Res.* **16**, 165.

Williams, B. G. & Bourdillon, A. J. (1982). *Localised Compton scattering using EELS*. *J. Phys. C*, **15**, 6881–6890.

Williams, B. G., Sparrow, T. G. & Egerton, R. F. (1984). *Electron Compton scattering from solids*. *Proc. R. Soc. London Ser. A*, **393**, 409–422.

Zaanen, J., Sawatsky, G. A., Fink, J., Speier, W. & Fuggle, J. C. (1985). *$L_{23}$ absorption spectra of the lighter 3d transition metals*. *Phys. Rev. B*, **32**, 4905–4913.

Zanchi, G., Perez, J. P. & Sevely, J. (1975). *Adaptation of magnetic filtering device on a one megavolt electron microscope*. *Optik (Stuttgart)*, **43**, 495–501.

Zanchi, G., Sevely, J. & Jouffrey, B. (1977). *Second order image aberration of a one megavolt magnetic filter*. *Optik (Stuttgart)*, **48**, 173–192.

Zimmermann, S. (1976). *The dielectric function of InSb determined by electron energy losses*. *J. Phys. C*, **9**, 2643–2649.


### 4.3.5


Barrett, C. S. & Massalski, T. B. (1980). *Structure of metals*, 3rd revised ed. Oxford: Pergamon Press.

Bernal, J. D. (1926). *On the interpretation of X-ray single-crystal rotation photographs*. *Proc. R. Soc. London Ser. A*, **113**, 117–160.

Bunge, H.-J. (1982). *Texture analysis in materials science*. London: Butterworth.

Gritsaenko, G. S., Zvyagin, B. B., Boyarskaya, R. V., Gorshkov, A. I., Samotoin, N. D. & Frolova, K. E. (1969). *Methods of electron microscopy of minerals*. Moscow: Nauka.

Guinier, A. (1956). *Théorie et technique de la radiocristallographie,* 2nd ed. Paris: Dunod.

Kakudo, M. & Kasai, N. (1972). *X-ray diffraction by polymers*. Tokyo: Kodanska; Amsterdam: Elsevier.

Krinary, G. A. (1975). *On the possibilities to use oriented specimens for recording of non-basal X-ray reflexions of fine-grained layer silicates*. *Crystal chemistry of minerals and geological problems*, pp. 132–138. Moscow: Nauka.

Mamy, J. & Gaultier, J.-P. (1976). *Evolution structurale de la montmorillonite associée au phénomène de fixation irréversible du potassium*. *An. Agron.* **27**(1), 1–16.

Méring, J. (1949). *L'interférence des rayons X dans les systèmes à stratification désordonnée*. *Acta Cryst.* **2**, 371–377.

Pinsker, Z. G. (1953). *Electron diffraction*. London: Butterworth.

**4.3.5 (*cont.*)**

Plançon, A., Rousseaux, F., Tchoubar, D., Tchoubar, C., Krinari, G. & Drits, V. A. (1982). *Recording and calculation of hk rod intensities in case of diffraction by highly oriented powders of lamellar samples. J. Appl. Cryst.* **15**, 509–512.

Vainshtein, B. K. (1964). *Structure analysis by electron diffraction*. Oxford: Pergamon Press.

Warren, B. E. (1941). *X-ray diffraction in random layer lattices. Phys. Rev.* **59**, 693–698.

Wilson, A. J. C. (1949). *Diffraction by random layers: ideal line profiles and determination of structure amplitudes from observed line profiles. Acta Cryst.* **2**, 245–251.

Wilson, A. J. C. (1962). *X-ray optics,* 2nd ed. London: Methuen.

Zhukhlistov, A. P., Avilov, A. S., Ferraris, G., Zvyagin, B. B. & Plotnikov, V. P. (1997). *Statistical distribution of hydrogen over three positions in brucite $Mg(OH)_2$ structure from electron diffractometry data. Crystallogr. Rep.* **42**, 774–777.

Zvyagin, B. B. (1967). *Electron diffraction analysis of clay mineral structures*. New York: Plenum.

Zvyagin, B. B., Vrublevskaya, Z. V., Zhukhlistov, A. P., Sidorenko, O. V., Soboleva, S. V. & Fedotov, A. F. (1979). *High-voltage electron diffraction in the study of layered minerals*. Moscow: Nauka.

Zvyagin, B. B., Zhukhlistov, A. P. & Plotnikov, V. P. (1996). *The development of electron diffractometry of minerals. Structural studies of crystals (For the 75th birthday of B. K. Vainshtein)*, pp. 225–234. Moscow: Nauka Physmathgis.

**4.3.6.1**

Cowley, J. M. (1975). *Diffraction physics*. New York: North-Holland.

Goodman, P. & Moodie, A. F. (1974). *Numerical evaluation of N-beam wave functions in electron scattering by the multislice method. Acta Cryst.* A**30**, 280–290.

**4.3.6.2**

*International Tables for Crystallography* (1996). Vol. B. Dordrecht: Kluwer Academic Publishers.

Hirsch, P. B., Howie, A., Nicholson, R. B., Pashley, D. W. & Whelan, M. J. (1977). *Electron microscopy of thin crystals*. New York: Krieger.

Howie, A. & Basinski, Z. S. (1968). *Approximations of the dynamical theory of diffraction contrast. Philos. Mag.* **17**, 1039–1063.

Humphreys, C. J. & Hirsch, P. B. (1968). *Absorption parameters in electron diffraction theory. Philos. Mag.* **18**, 115–122.

Jones, P. M., Rackham, G. M. & Steeds, J. W. (1977). *High-order Laue zone electron diffraction. Proc. R. Soc. London Ser. A*, **354**, 192–222.

Pendry, J. B. (1974). *Low energy electron diffraction*. New York: Academic Press.

**4.3.7**

Ackermann, I. (1948). *Observations on the dynamical interference phenomena in convergent electron beams. II. Ann. Phys. (Leipzig)*, **2**, 41–54.

Andersson, B. (1975). *Structure analysis of the γ-phase in the vanadium oxide system by electron diffraction studies. Acta Cryst.* A**31**, 63–70.

Ando, Y., Ichimiya, A. & Uyeda, R. (1974). *A determination of values and signs of the 111 and 222 structure factors of silicon. Acta Cryst.* A**30**, 600–601.

Bird, D. M. (1990). *Absorption in high-energy electron diffraction from non-centrosymmetrical crystals. Acta Cryst.* A**46**, 208–214.

Bird, D. M. & Saunders, M. (1992). *Inversion of convergent-beam electron diffraction patterns. Acta Cryst.* A**48**, 555–562.

Blake, R. G., Jostsons, A., Kelly, P. M. & Napier, J. G. (1978). *The determination of extinction distances and anomalous absorption coefficients by scanning electron microscopy. Philos. Mag.* A**37**, 1–16.

Buxton, B. F. (1976). *Bloch waves in high order Laue zone effects in high energy electron diffraction. Proc. R. Soc. London Ser. A*, **300**, 335–361.

Cowley, J. M. (1961). *Diffraction intensities from bent crystals. Acta Cryst.* **14**, 920–926.

Dorset, D. L. (1991). *Is electron crystallography possible? The direct determination of organic crystal structures. Ultramicroscopy*, **38**, 23–40.

Dorset, D. L., Jap, B. K., Ho, M. M. & Glaeser, R. M. (1979). *Direct phasing of electron diffraction data from organic crystals: the effect of n-beam dynamical scattering. Acta Cryst.* A**35**, 1001–1009.

Fox, A. G. & Fisher, R. M. (1988). *A summary of low-angle X-ray atomic scattering factors measured by the critical voltage effect in high energy electron diffraction. Aust. J. Phys.* **41**, 461–468.

Fox, A. G. & Tabbernor, M. A. (1991). *The bonding charge density of β′NiAl″. Acta Metall.* **39**, 669–678.

Fujiyoshi, Y., Mizusaki, T., Morikawa, K., Yamagishi, H., Aoki, Y., Kihara, H. & Harada, Y. (1991). *Development of a superfluid helium stage for high-resolution electron microscopy. Ultramicroscopy*, **38**, 241–251.

Fukuhara, A. (1966). *Many-ray approximation in the dynamical theory of electron diffraction. J. Phys. Soc. Jpn*, **21**, 2645–2662.

Gjønnes, J. & Høier, R. (1971). *The application of non-systematic many-beam dynamic effects to structure-factor determination. Acta Cryst.* A**27**, 313–316.

Gjønnes, K. & Bøe, N. (1994). *Refinement of temperature factors and charge distributions in $YBa_2Cu_3O_7$ and $YBa_2(Cu,Co)_3O_7$ from CBED intensities. Micron Microsc. Acta*, **25**, 29–44.

Glazer, J., Ramesh, R., Hilton, M. R. & Sarikaya, M. (1985). *Comparison of convergent beam electron diffraction methods for determination of foil thickness. Philos. Mag.* A**52**, 59–63.

Goodman, P. (1976). *Examination of the graphite structure using convergent-beam electron diffraction. Acta Cryst.* A**32**, 793–798.

Goodman, P. & Lehmpfuhl, G. (1967). *Electron diffraction study of MgO h00 systematic interactions. Acta Cryst.* **22**, 14–24.

Høier, R. (1972). *Displaced lines in Kikuchi patterns. Phys. Status Solidi A*, **11**, 597–610.

Høier, R., Bakken, L. N., Marthinsen, K. & Holmestad, R. (1993). *Structure factor determination in non-centrosymmetrical crystals by a two-dimensional CBED-based multi-parameter refinement method. Ultramicroscopy,* **49**, 159–170.

Holmestad, R., Weickenmeier, A. L., Zuo, J. M., Spence, J. C. H. & Horita, Z. (1993). *Debye–Waller factor measurement in TiAl from HOLZ reflections. Electron microscopy and analysis 1993,* pp. 141–144. Bristol: IOP Publishing.

**4.3.7 (*cont.*)**

Howie, A. (1963). *Inelastic scattering of electrons by crystals. I. The theory of small angle inelastic scattering*. *Proc. R. Soc. London Ser. A*, **271**, 268–287.

Kambe, K. (1957). *Study of simultaneous reflections in electron diffraction by crystals*. *J. Phys. Soc. Jpn*, **12**, 13–36.

Kelly, P. M., Jostsons, A., Blake, R. G. & Napier, J. G. (1975). *The determination of foil thickness by scanning transmission electron microscopy*. *Phys. Status Solidi A*, **31**, 771–780.

Kogiso, M. & Takahashi, H. (1977). *Group-theoretical method in the many-beam theory in electron diffraction*. *J. Phys Soc. Jpn*, **42**, 223–229.

Krahl, D., Pätzold, H. & Swoboda, M. (1990). *An aberration-minimized imaging energy filter of simple design*. Proceedings of 12th International Conference on Electron Microscopy 1990, Vol. 2, pp. 60–61.

Krivanek, O. L., Gubbens, A. J., Dellby, N. & Meyer, C. E. (1991). *Design and first applications of a post-column imaging filter*. *Microsc. Microanal. Microstruct. (France)*, **3**, 187–199.

Krivanek, O. L., Mooney, P. E., Fan, G. Y., Leber, M. L. & Meyer, C. E. (1991). *Slow-scan CCD cameras for transmission electron microscopy*. *Electron microscopy and analysis 1991*, pp. 523–526. Bristol: IOP Publishing.

Kühlbrandt, W., Wang, D. N. & Fujiyoshi, Y. (1994). *Atomic model of plan light-harvesting complex by electron crystallography*. *Nature (London)*, **367**, 614–621.

Lehmpfuhl, G. (1974). *Dynamical interaction of electron waves in a perfect single crystal*. *Z. Naturforsch. Teil A*, **27**, 424–433.

Ma, Y., Rømming, C., Lebech, B. & Gjønnes, J. (1992). *Structure refinement of $Al_3Zr$ using single-crystal X-ray diffraction, powder neutron diffraction and CBED*. *Acta Cryst.* B**48**, 11–16.

Marthinsen, K., Holmestad, R. & Høier, R. (1994). *Analytical filtering of low-angle inelastic scattering contributions to CBED contrast*. *Ultramicroscopy*, **55**, 268–275.

Matsuhata, H. & Gjønnes, J. (1994). *Bloch-wave degeneracies and non-systematic critical voltage: a method for structure-factor determination*. *Acta Cryst.* A**50**, 107–115.

Matsuhata, H. & Steeds, J. W. (1987). *Observation of accidental Bloch-wave degeneracies of zone-axis critical voltge*. *Philos. Mag.* B**55**, 39–54.

Matsuhata, H., Tomokiyo, Y., Watanabe, H. & Eguchi, T. (1984). *Determination of the structure factors of Cu and $Cu_3Au$ by the intersecting Kikuchi-line method*. *Acta Cryst.* B**40**, 544–549.

Mori, N., Oikawa, T. & Harada, Y. (1990). *Development of the imaging plate for the transmission electron microscope and its characteristics*. *J. Electron Microsc. (Japan)*, **39**, 433–436.

Olsen, A., Goodman, P. & Whitfield, H. (1985). *$Tl_3SbS_3$, $Tl_3SbSe_3$, $Tl_3Sb_{3-x}Se_x$ and $Tl_3Sb_yAs_{1-y}Se_3$*. *J. Solid State Chem.* **60**, 305–315.

Saunders, M., Bird, D. M., Midgley, P. A. & Vincent, R. (1994). *Structure factor refinement by zone-axis CBED pattern matching*. Proceedings of 13th International Congress on Electron Microscopy, Paris, France, 17–22 July 1994, Vol. 1, pp. 847–848.

Spargo, A. E. C. (1994). *Electron crystallography and crystal structure*. Proceedings of 13th International Congress on Electron Microscopy, Paris, France, 17–22 July 1994, Vol. 1, pp. 959–960.

Spence, J. C. H. & Zuo, J. M. (1992). *Electron microdiffraction*. New York: Plenum.

Steeds, J. W. (1984). *Further development in the analysis of convergent beam electron diffraction (CBED) data. EMAG 1983. Inst. Phys. Conf. Ser.* No. 69, pp. 31–36.

Taftø, J. & Gjønnes, J. (1985). *The intersecting Kikuchi line technique: critical voltage at any voltage*. *Ultramicroscopy,* **17**, 329–334.

Taftø, J. & Metzger, T. H. (1985). *Large-angle convergent-beam electron diffraction; a simple technique for the study of modulated structures with application to $V_2D$*. *J. Appl. Cryst.* **18**, 110–113.

Tanaka, M. & Tsuda, K. (1990). *Determination of positional parameters by convergent-beam electron diffraction*. Proceedings of 12th International Congress on Electron Microscopy 1990, Vol. 2, pp. 518–519.

Terasaki, O., Watanabe, D. & Gjønnes, J. (1979). *Determination of crystal structure factor of Si by the intersecting-Kikuchi-line method*. *Acta Cryst.* A**35**, 895–900.

Unwin, P. N. T. & Henderson, R. J. (1975). *Three-dimensional model of purple membrane obtained by electron microscopy*. *Mol. Biol.* **94**, 425–430.

Vincent, R., Bird, D. M. & Steeds, J. W. (1984). *Structure of AuGeAs determined by convergent beam electron diffraction. II. Refinement of structural parameters*. *Philos. Mag.* A**50**, 765–786.

Vincent, R. & Midgley, P. A. (1994). *Double conical beam-rocking system for measurement of integrated electron diffraction intensities*. *Ultramicroscopy*, **53**, 271–284.

Voigt-Martin, I. G., Yan, D. H., Gilmore, C. J., Shankland, K. & Bricogne, G. (1994). *The use of maximum entropy and likelihood ranking to determine the crystal structure of 4-[4′-(N-dimethylamino)benzylidene]pyrazolidine-3,5-dione at 1.4 Å resolution from electron diffraction and high-resolution electron microscopy image data*. *Ultramicroscopy*, **56**, 271–288.

Voss, R., Lehmpfuhl, G. & Smith, D. J. (1980). *Influence of doping on the crystal potential of silicon investigated by the convergent beam electron diffraction technique*. *Z. Naturforsch. Teil A*, **35**, 973–984.

Watanabe, D., Uyeda, R. & Fukuhara, A. (1969). *Determination of the atomic form factor by high–voltage electron diffraction*. *Acta Cryst.* A**25**, 138–140.

Zou, X. D., Sukharev, Y. & Hovmöller, S. (1993). *ELD – a computer program for extracting intensities from electron diffraction patterns*. *Ultramicroscopy,* **49**, 147–158.

Zuo, J. M., Høier, R. & Spence, J. C. H. (1989). *Three-beam and many-beam theory in electron diffraction and its use for structure-factor phase determination in non-centrosymmetrical crystal structures*. *Acta Cryst.* A**45**, 839–851.

Zuo, J. M., Spence, J. C. H., Downs, J. & Mayer, J. (1993). *Measurement of individual structure-factor phases with tenth-degree accuracy: the 00.2 reflection in BeO studied with electron and X-ray diffraction*. *Acta Cryst.* A**49**, 422–429.

**4.3.8**

Alexander, H., Spence, J. C. H., Shindo, D., Gottschalk, H. & Long, N. (1986). *Forbidden reflection lattice imaging for the determination of kink densities on partial dislocations*. *Philos. Mag.* A**53**, 627–643.

Anstis, G. R., Lynch, D. F., Moodie, A. F. & O'Keefe, M. A. (1973). *n-Beam lattice imges. III. Upper limits of ionicity in $W_4Nb_{26}P_{77}$*. *Acta Cryst.* A**29**, 138–147.

d'Anterroches, C. & Bourret, A. (1984). *Atomic structure of [011] and [001] near-coincident tilt boundaries in germanium and silicon*. *Philos. Mag.* A**49**, 783–807.

**4.3.8 (*cont.*)**


Binnig, G., Rohrer, H., Gerber, C. & Weibel, E. (1983). *Direct imaging of semiconductor surfaces. Phys. Rev. Lett.* **50**, 120–123.

Budinger, T. F. & Glaeser, R. M. (1976). *Measurement of focus and spherical aberration of an electron microscope objective lens. Ultramicroscopy*, **2**, 31–41.

Cherns, D. (1974). *Direct resolution of surface steps by transmission electron microscopy. Philos. Mag.* **30**, 549–557.

Cockayne, D. J. H. & Gronsky, R. (1981). *Lattice fringe imaging of modulated structures. Philos. Mag.* A**44**, 159–175.

Cowley, J. M. (1959). *The electron-optical imaging of crystal lattices. Acta Cryst.* **12**, 367–375.

Cowley, J. M. (1969). *Image contrast in transmission scanning electron microscope. Appl. Phys. Lett.* **15**, 58–59.

Cowley, J. M. (1981). *Diffraction physics*, 2nd ed. New York: North-Holland.

Cowley, J. M. (1988). *Electron microscopy of crystals with time-dependent perturbations. Acta Cryst.* A**44**, 847–853.

Cowley, J. M. (1992). *Coherent convergent beam diffraction. Electron diffraction techniques*, Vol. 1, edited by J. M. Cowley, pp. 439–464. Oxford University Press.

Cowley, J. M. (1994). *Applications of electron holography*. In *Handbook of advanced materials testing*, edited by N. P. Cheremisinoff & P. N. Cheremisinoff. New York: Marcel Dekker, Inc.

Cowley, J. M. & Iijima, S. (1972). *Electron microscope image contrast for thin crystals. Z. Naturforsch. Teil A,* **27**, 445–451.

Cowley, J. M. & Moodie, A. F. (1960). *Fourier images IV: the phase grating. Proc. Phys. Soc. (London)*, **76**, 378–384.

Cowley, J. M., Spence, J. C. & Smirnov, V. V. (1997). *The enhancement of electron microscope resolution by the use of atomic focusers. Ultramicroscopy*, **68**, 135–148.

Crewe, A. V. & Wall, J. (1970). *A scanning microscope with 5 Å resolution. J. Mol. Biol.* **48**, 375–393.

Daberkow, I., Herrman, K., Liu, L. & Rau, W. (1991). *Performance of electron image converters with YAG and CCD. Ultramicroscopy*, **38**, 215–224.

Desseaux, J., Renault, A. & Bourret, A. (1977). *Multibeam lattice images from germanium oriented in (001). Philos Mag.* **35**, 357–363.

Dorset, D. L. (1994). *Electron crystallography of organic molecules. Adv. Electron. Electron Phys.* **88**, 111–197.

Dorset, D. L. (1995). Editor. *Structural electron crystallography*. New York/London: Plenum Press.

Dorset, D. L., McCourt, M. P., Fryer, J. R., Tivol, W. F. & Turner, J. N. (1994). *The tangent formula in electron crystallography. Phase determination of copper perchlorophthalocyanine. Microsc. Soc. Am. Bull.* **24**, 398–404.

Downing, K. H., Meisheng, H., Wenk, H. R. & O'Keefe, M. A. (1990). *Resolution of oxygen atoms in staurolife by three dimensional transmission electron microscopy. Nature (London)*, **348**, 525.

Endoh, H., Hashimoto, H. & Makita, Y. (1994). *Theoretical and observed images of impurity atoms formed by L-shell ionization. Ultramicroscopy*, **56**, 108–120.

Fejes, P. L. (1977). *Approximations for the calculation of high-resolution electron-microscope images of thin films. Acta Cryst.* A**33**, 109–113.

Fields, P. M. & Cowley, J. M. (1978). *Computed electron microscope images of atomic defects in f.c.c. metals. Acta Cryst.* A**34**, 103–112.

Fitzgerald, J. D. & Johnson, A. W. S. (1984). *A simplified method of electron microscope voltage measurement. Ultramicroscopy*, **12**, 231–236.

Frank, J. (1975). *A practical resolution criterion in optics and electron microscopy. Optik (Stuttgart)*, **43**, 25–34.

Frank, J. (1980). *The role of correlation techniques in computer image processing. Computer processing of electron microscope images. Topics in current physics*, Vol. 13, edited by P. W. Hawkes, p. 187. Berlin/Heidelberg/New York: Springer Verlag.

Fryer, J. R. & Gilmore, C. J. (1992). *Structure determination by electron crystallography. Trans. Am. Crystallogr. Assoc.* **28**, 57–75.

Fu, Z. Q., Huang, D. X., Li, F. H., Li, J. Q., Zhao, Z. X., Cheng, T. Z. & Fan, H. F. (1994). *Incommensurate modulation in minute crystals revealed by combining high-resolution electron microscopy and electron diffraction. Ultramicroscopy*, **54**, 229–236.

Fujiyoshi, Y., Ishizuka, K., Tsuji, M., Kobayashi, T. & Uyeda, N. (1983). *Charge density distribution from high resolution molecular images*. Proceedings of the 17th International Conference on High Voltage Electron Microscopy, p. 21.

Fukuhara, A. (1966). *Many-ray approximation in the dynamical theory of electron diffraction. J. Phys. Soc. Jpn*, **21**, 2645–2662.

Gabor, D. (1948). *A new microscope principle. Nature (London)*, **161**, 777–778.

Gabor, D. (1949). *Microscopy of reconstructed wavefronts. Proc. R. Soc. London Ser. A*, **197**, 454–487.

Grinton, G. R. & Cowley, J. M. (1971). *Phase and amplitude contrast in electron micrographs of biological materials. Optik (Stuttgart)*, **34**, 221–233.

Haider, M. & Zach, J. (1995). *Multipole correctors. Proceedings of Microscopy and Microanalysis*, edited by G. Bailey, pp. 596–567. New York: Jones and Bigell.

Hashimoto, H., Mannami, M. & Naiki, T. (1961). *Theory of lattice images. Philos. Trans. R. Soc. London*, **253**, 459–489.

Hirsch, P. B., Howie, A., Nicholson, R. B., Pashley, D. W. & Whelan, M. J. (1977). *Electron microscopy of thin crystals*, p. 190. London: Butterworth.

Horiuchi, S. (1982). *Reduction in a niobium tungsten bronze. J. Appl. Cryst.* **15**, 323–329.

Howie, A. (1979). *Image contrast and localized signal selection techniques. J. Micros. (Oxford)*, **117**, 11–23.

Iijima, S. (1977). *High resolution electron microscopy of phase objects: observation of small holes and steps on graphite crystals. Optik (Stuttgart)*, **47**, 437–452.

*International Tables for Crystallography* (1992). Vol. B. Dordrecht: Kluwer Academic Publishers.

Ishizuka, K. (1982). *Multislice formula for inclined illumination. Acta Cryst.* A**38**, 773–779.

Jap, B. K. & Glaeser, R. M. (1978). *The scattering of high energy electrons. Acta Cryst.* A**34**, 94–102.

Kambe, K. (1982). *Visualization of Bloch waves of high energy electrons in high resolution electron microscopy. Ultramicroscopy*, **10**, 223–228.

Kirkland, A., Saxton, W., Chau, K., Tsuno, K. & Kawasaki, M. (1995). *Super-resolution by aperture synthesis. Ultramicroscopy*, **57**, 355–374.

Kobayashi, T., Fujiyoshi, Y. & Uyeda, N. (1982). *The observation of molecular orientations in crystal defects and the growth mechanism of thin phthalocyanine films. Acta Cryst.* A**38**, 356–362.

**4.3.8 (*cont.*)**


Koike, H., Kobayashi, K., Ozawa, S. & Yagi, K. (1989). *High resolution reflection electron microscopy of Si(111) $7 \times 7$ surfaces using a high voltage electron microscope*. *Jpn. J. Appl. Phys.* **28**, 861–865.

Komoda, T. (1964). *On the resolution of the lattice image in the electron microscope*. *Optik (Stuttgart)*, **21**, 94–110.

Krivanek, O. L. (1976). *A method for determining the coefficient of spherical aberration from a single electron micrograph*. *Optik (Stuttgart)*, **45**, 97–101.

Krivanek, O. L., Dellby, N., Spence, A. J., Camps, R. A. & Brown, L. M. (1997). *Aberration correction in the STEM*. *Proc EMAG 1997*, edited by S. McVitie. London: Institute of Physics.

Krivanek, O. L. & Mooney, P. E. (1993). *Applications of slow-scan CCD cameras in HREM*. *Ultramicroscopy*, **49**, 95–108.

Larsen, P. K. & Dobson, P. J. (1988). Editors. *Reflection high energy electron diffraction and reflection electron imaging of surfaces*. *NATO ASI Series*. New York/London: Plenum Press.

Lichte, H. (1991). *Electron image plane off-axis holography of atomic structures*. *Adv. Opt. Electron Microsc.* **12**, 25–91.

Lovey, F. C., Coene, W., Van Dyck, D., Van Tendeloo, G., Van Landuyt, J. & Amelinckx, S. (1984). *HREM imaging conditions for stacking sequences in 18R martensite of Cu–Al alloys*. *Ultramicroscopy*, **15**, 345–356.

Lynch, D. F., Moodie, A. F. & O'Keefe, M. A. (1975). *n-Beam lattice images. V. The use of the charge-density approximation in the interpretation of lattice images*. *Acta Cryst.* A**31**, 300–307.

Marks, L. (1986). *High resolution electron microscopy of surfaces*. In *Topics in current physics*, Vol. 41. *Structure and dynamics of surfaces. I*, edited by W. Schommers & P. Von Blackenhagen. Berlin/Heidelberg: Springer Verlag.

Menter, J. W. (1956). *The resolution of crystal lattices*. *Proc. R. Soc. London Ser. A*, **236**, 119.

Möllenstedt, G. & Düker, H. (1956). *Beobachtungen und Messungen an Biprisma-Interferenzen mit Elektronenwellen*. *Z. Phys.* **145**, 377–397.

Moodie, A. F. & Warble, C. E. (1967). *The observation of primary step growth in magnesium oxide by direct transmission electron microscopy*. *Philos. Mag.* **16**, 891–904.

Nagakura, S., Nakamura, Y. & Suzuki, T. (1982). *Forbidden reflection intensity in electron diffraction and its influence on the crystal structure image*. *Jpn. J. Appl. Phys.* **21**, L449–L451.

Nellist, P., McCallum, B. & Rodenburg, J. (1995). *Resolution beyond the information limit in STEM*. *Nature (London)*, **374**, 630–632.

O'Keefe, M. A., Spence, J. C. H., Hutchinson, J. L. & Waddington, W. G. (1985). *Proc. 43rd EMSA Meeting*, p. 64. San Francisco: San Francisco Press. [See also H. Hashimoto in *Ultramicroscopy* (1985), **18**, 19–32.]

Olsen, A. & Spence, J. C. H. (1981). *Distinguishing dissociated glide and shuffle set dislocations by high resolution electron microscopy*. *Philos. Mag.* A**43**, 945–965.

Orchowski, A., Rau, W. D. & Lichte, H. (1995). *Electron holography surmounts resolution limit of electron microscopy*. *Phys. Rev. Lett.* **74**, 399.

Pennycook, S. J. & Jesson, D. E. (1991). *High-resolution Z-contrast imaging of crystals*. *Ultramicroscopy*, **37**, 14–38.

Pirouz, P. (1974). *Effects of absorption on lattice images*. *Optik (Stuttgart)*, **54**, 69–74.

Saxton, W. O. (1978). *Computer techniques for image processing in electron microscopy*, pp. 9–19. New York: Academic Press.

Saxton, W. O. (1980*a*). *Recovery of specimen information for strongly scattering objects*. In *Computer processing of electron microscopy images*. *Topics in current physics*, Vol. 13, edited by P. W. Hawkes, p. 35. Berlin/Heidelberg/New York: Springer Verlag.

Saxton, W. O. (1980*b*). *Correction of artifacts in linear and nonlinear high resolution electron micrographs*. *J. Microsc. Spectrosc. Electron*, **5**, 665–674.

Scherzer, O. (1949). *The theoretical resolution limit of the electron microscope*. *J. Appl. Phys.* **20**, 20–29.

Schiske, P. (1975). *Phase determination from a focal series and the corresponding diffraction pattern in electron microscopy for strongly scattering objects*. *J. Phys. D*, **8**, 1372–1386.

Self, P. G., O'Keefe, M. A., Buseck, P. R. & Spargo, A. E. C. (1983). *Practical computation of amplitudes and phases in electron diffraction*. *Ultramicroscopy*, **11**, 35–52.

Shindo, D., Hiraga, K., Oikawa, T. & Mori, N. (1990). *Quantification of electron diffraction with imaging plate*. *J. Electron Microsc.* **39**, 449–453.

Smith, D. J., Bursill, L. A. & Wood, G. J. (1985). *Non-anomalous high-resolution imaging of crystalline materials*. *Ultramicroscopy*, **16**, 19–32.

Smith, D. J., Saxton, W. O., O'Keefe, M. A., Wood, G. J. & Stobbs, W. M. (1983). *The importance of beam alignment and crystal tilt in high resolution electron microscopy*. *Ultramicroscopy*, **11**, 263–282.

Spence, J. C. H. (1988). *High resolution electron microscopy*, 2nd ed. New York: Oxford University Press.

Spence, J. C. H. (1998). *Direct inversion of dynamical electron difffraction patterns to structure factors*. *Acta Cryst.* A**54**, 7–18.

Spence, J. C. H. & Lynch, J. (1982). *STEM microanalysis and inelastic imaging in crystals*. *Ultramicroscopy*, **9**, 267–278.

Spence, J. C. H., O'Keefe, M. A. & Iijima, S. (1978). *On the thickness periodicity of atomic-resolution images of dislocation cores*. *Philos. Mag.* A**38**, 463–482.

Takayanagi, K. (1984). *Surface structure imaging by electron microscopy*. *J. Microsc.*, **136**, 287–298.

Tonomura, A. (1992). *Electron-holographic interference microscopy*. *Adv. Phys.* **41**, 59–103.

Treacy, M. M. J. & Rice, S. B. (1989).*Catalyst particle sizes from Rutherford scattered intensities*. *J. Microsc.* **156**, 211–234.

Unwin, P. N. T. & Henderson, R. (1975). *Molecular structure determination by electron microscopy of unstained crystalline specimens*. *J. Mol. Biol.* **94**, 425–440.

Van Dyck, D. (1980). *Fast computational procedures for the simulation of structure images in complex or disordered crystals*. *J. Microsc.* **119**, 141.

Van Dyck, D., Op de Beeck, M. & Coene, W. M. J. (1994). *Information in electron microscopy*. *Microsc. Soc. Am. Bull.* **24**, 427–437.

Voss, R., Lehmpfuhl, G. & Smith, D. J. (1980). *Influence of doping on the crystal potential of silicon*. *Z. Naturforsch. Teil A*, **35**, 973–984.

Wade, R. H. & Frank, J. (1977). *Electron microscope transfer functions for partially coherent axial illumination*. *Optik (Stuttgart)*, **49**, 81–92.

Williams, D. B. & Carter, C. B. (1996). *Transmission electron microscopy*. New York: Plenum Press.

Wilson, A. R., Spargo, A. E. C. & Smith, D. J. (1982). *The characterisation of instrumental parameters in the high resolution electron microscope. Optik (Stuttgart)*, **61**, 63–78.
Yagi, K. (1993). *RHEED and REM*. In *Electron diffraction techniques*, Vol. 2, edited by J. M. Cowley. IUCr/Oxford University Press.
Yagi, K. & Cowley, J. M. (1978). *Electron microscopy study of ordering of potassium ions in cubic $KSbO_3$. Acta Cryst.* A**34**, 625–634.
Zakharov, N. D., Pasemann, M. & Rozhanski, V. N. (1982). *Observations of point defects in silicon by means of dark-field lattice plane imaging. Phys. Status Solidi A*, **71**, 275–281.
Zuo, J. M., Spence, J. C. H. & O'Keefe, M. A. (1988). *Bonding in GaAs. Phys. Rev. Lett.* **61**, 353–356.

### 4.4.2

Abrahams, K., Steinsvoll, O., Bongaarts, P. J. M. & De Lange, P. W. (1962). *Reversal of the spin of polarized thermal neutrons without depolarization. Rev. Sci. Instrum.* **33**, 524–529.
Agamalyan, M. M., Drabkin, G. M. & Sbitnev, V. I. (1988). *Spatial spin resonances of polarized neutrons. A tunable slow neutron filter. Phys. Rep.* **168**, 265–303.
Alefeld, B. (1972). *Neutronen-Rückstreuspektrometer. Kerntechnik,* **14**, 15–17.
Alefeld, B., Duppich, J., Schärpf, O., Schirmer, A., Springer, T. & Werner, K. (1988). *The new neutron guide laboratory at the FRJ-2 reactor in the KFA Jülich and its special beam forming devices. Thin film neutron optical devices: mirrors, supermirrors, multilayer monochromators, polarizers, and beam guides*, edited by C. F. Majkrzak, pp. 75–83. *SPIE Proc.* No. 983. Bellingham, WA: SPIE.
Alvarez, L. W. & Bloch, F. (1940). *A quantitative determination of the neutron moment in absolute nuclear magnetons. Phys. Rev.* **57**, 111–122.
Anderson, I. S. (1988). *Neutron beam focusing using supermirrors. Thin film neutron optical devices: mirrors, supermirrors, multilayer monochromators, polarizers, and beam guides*, edited by C. F. Majkrzak, pp. 84–92. *SPIE Proc.* No. 983. Bellingham, WA: SPIE.
Anderson, I. S. & Høghøj, P. (1996). *New developments in Ni/Ti multilayers*. ILL 1996 Annual Report, pp. 84–85. Institut Laue–Langevin, Grenoble, France
Bacon, G. E. & Lowde, R. D. (1948). *Secondary extinction and neutron crystallography. Acta Cryst.* **1**, 303–314.
Badurek, G. & Rauch, H. (1978). *Experimental capability study of non-conventional methods in neutron time-of-flight analysis. Neutron Inelastic Scattering Proceedings*, Vol. I, pp. 211–227. Vienna: IAEA.
Bednarski, S., Dobrzynski, L. & Steinsvoll, O. (1980). *Experimental test on $Fe_3Si(Mn)$ and $Li_{.5}Fe_{2.5}O_4$ crystals as polarizers for slow neutrons. Phys. Scr.* **21**, 217–219.
Blanc, Y. (1983). *Le spectrometre à temps de vol IN6: characteristiques techniques et performances*. ILL Internal Report No. 83BL21G. Institut Laue–Langevin, Grenoble, France.
Bonse, U. & Hart, M. (1965). *Tailless X-ray single crystal reflection curves obtained by multiple reflection. Appl. Phys. Lett.* **7**, 238–240.
Bouchiat, M. A., Carver, T. R. & Varnum, C. M. (1960). *Nuclear polarization in $^3$He gas induced by optical pumping and dipolar exchange. Phys. Rev. Lett.* **5**, 373–375.
Brockhouse, B. N. (1958). *Bull. Am. Phys. Soc.* **3**, 233.
Bührer, W. (1994). *Triple axis instrument with doubly focusing ('zoom') monochromator and horizontally focusing analyser: seven years experience. Nucl. Instrum. Methods*, A**338**, 44–52.
Carlile, C. J., Hey, P. D. & Mack, B. J. (1977). *High-efficiency Soller slit collimators for thermal neutrons. J. Phys. E,* **10**, 543–546.
Chen, H., Sharov, V. A., Mildner, D. F. R., Downing, R. G., Paul, R. L., Lindstrom, R. M., Zeissler, C. J. & Xiao, Q. F. (1995). *Prompt gamma activation analysis enhanced by a neutron focusing capillary lens. Nucl. Instrum. Methods*, B**95**, 107–114.
Chen-Mayer, H. H., Mildner, D. F. R., Sharov, V. A., Ullrich, J. B., Ponomarev, I. Yu. & Downing, R. G. (1996). *Monolithic polycapillary neutron focusing lenses: experimental characterizations. J. Phys. Soc. Jpn,* **65**, Suppl. A, 319–321.
Christ, J. & Springer, T. (1962). *Über die Entwicklung eines Neutronenleiters am FRM-Reaktor. Nukleonik,* **4**, 23–25.
Chupp, T. E., Coulter, K. P., Hwang, S. R., Smith, T. B. & Welsh, R. C. J. (1996). *Progress toward a spin exchange pumped $^3$He neutron spin filter. J. Neutron Res.* **5**, 11–24.
Colegrove, F. D., Schearer, L. D. & Walters, K. (1963). *Polarization of $^3$He gas by optical pumping. Phys. Rev.* **132**, 2561–2572.
Colwell, J. F., Miller, P. H. & Whittemore, W. L. (1968). *A new high-efficiency time-of-flight system. Neutron inelastic scattering*, Vol. II, IAEA Conference Proceedings, pp. 429–437. Vienna: IAEA.
Copley, J. R. D. (1991). *Transmission properties of a counter-rotationg pair of disk choppers. Nucl. Instrum. Methods*, A**303**, 332–341.
Currat, R. (1973). *The efficiency of vertically bent neutron monochromators. Nucl. Instrum. Methods*, **107**, 21–28.
Dabbs, J. W. T., Roberts, L. D. & Bernstein, S. (1955). *Direct polarization of $^{115}$In nuclei; J value for 1.456 eV resonance.* Report ORNL-CF-55-5-126. Oak Ridge National Laboratory, TN, USA.
Dash, J. G. & Sommers, H. S. (1953). *A high transmission slow neutron velocity selector. Rev. Sci. Instrum.* **24**, 91–96.
Delapalme, A., Schweizer, J., Couderchon, G. & Perrier de la Bathie, R. (1971). *Étude de l'alliage Heusler ($Cu_2MnAl$) comme monochromateur de neutrons polarizés. Nucl. Instrum. Methods*, **95**, 589–594.
Drabkin, G. M., Okorokov, A. I., Schebetov, A. F., Borovilova, N. V., Kugasov, A. G., Kudriashov, V. A., Runov, V. V. & Korneev, D. A. (1976). *Multilayer Fe–Co mirror polarizing neutron guide. Nucl. Instrum. Methods*, **133**, 453–456.
Drabkin, G. M., Zabidarov, E. I., Kasman, Ya. A. & Okorokov, A. I. (1969). *Investigation of a phase transition in nickel with polarized neutrons. Sov. Phys. JETP*, **29**, 261–266.
Egelstaff, P. A., Cocking, S. J. & Alexander, T. K. (1961). *A four-rotor thermal-neutron analyser. Inelastic scattering of neutrons in solids and liquids*, pp. 165–177. Vienna: IAEA.
Egorov, A. I., Lobashov, V. M., Nazarenko, V. A., Porsev, G. D. & Serebrov, A. P. (1974). *Production, storage, and polarization of ultracold neutrons. Sov. J. Nucl. Phys.* **19**, 147–152.
Elsenhans, O., Böni, P., Friedli, H. P., Grimmer, H., Buffat, P., Leifer, K., Söchtig, J. & Anderson, I. S. (1994). *Development of Ni/Ti multilayer supermirrors for neutron optics. Thin Solid Films*, **246**, 110–119.

**4.4.2 (*cont.*)**


Forsyth, J. B. (1979). *Magnetic neutron scattering and the chemical bond. At. Energy Rev.* **17**, 345–412.

Forte, M. & Zeyen, C. M. E. (1989). *Neutron optical spin-orbit rotation in dynamical diffraction. Nucl. Instrum. Methods*, A**284**, 147–150.

Freeman, F. F. & Williams W. G. (1978). *A $^{149}$Sm polarizing filter for thermal neutrons. J. Phys. E*, **11**, 459–467.

Freund, A. K. (1975). *A neutron monochromator system consisting of deformed crystals with anisotropic mosaic structure. Nucl. Instrum. Methods*, **124**, 93–99.

Freund, A. K. (1976). *Progress in neutron monochromator development at the Institut Laue–Langevin. Conference on Neutron Scattering*. Report CONF-760601-p2, pp. 1143–1150. Oak Ridge National Laboratory, TN, USA.

Freund, A. K. (1983). *Cross sections of materials used as neutron monochromators and filters. Nucl. Instrum. Methods*, **213**, 495–501.

Freund, A. K. (1985). *On the wavelength dependence of neutron monochromator reflectivities. Nucl. Instrum. Methods*, A**238**, 570–571.

Freund, A. K. & Forsyth, J. B. (1979). *Materials problems in neutron devices. Neutron scattering*, edited by G. Kostorz, pp. 462–507. New York: Academic Press.

Freund, A. K., Guinet, P., Maréschal, J., Rustichelli, F. & Vanoni, F. (1972). *Cristaux á gradient de maille. J. Cryst. Growth*, **13/14**, 726.

Freund, A. K., Pynn, R., Stirling, W. G. & Zeyen, C. M. E. (1983). *Vertically focusing Heusler alloy monochromators for polarized neutrons. Physica (Utrecht) B*, **120**, 86–90.

Frey, F. (1974). *A packet of ideal-crystalline lamellae as neutron monochromator. Nucl. Instrum. Methods*, **115**, 277–284.

Gähler, R. & Golub, R. (1987). *A high resolution neutron spectrometer for quasielastic scattering on the basis of spin-echo and magnetic resonance. Z. Phys. B*, **65**, 269–273.

Glinka, C. J., Rowe, J. M. & LaRock, J. G. (1986). *The small-angle neutron scattering spectrometer at the National Bureau of Standards. J. Appl. Cryst.* **19**, 427–439.

Hamelin, B., Anderson, I., Berneron, M., Escoffier, A., Foltyn, T. & Hehn, R. (1997). *Nucl. Instrum. Methods.* Submitted.

Hautecler, S., Legrand, E., Vansteelandt, L., d'Hooghe, P., Rooms, G., Seeger, A., Schalt, W. & Gobert, G. (1985). *Mibemol: a six chopper TOF spectrometer installed on a neutron guide at the Orphée reactor.* Proceedings of the Conference on Neutron Scattering in the Nineties, Jülich, pp. 211–215. Vienna: IAEA.

Hayes, C., Lartigue, C., Copley, J. R. D., Alefeld, B., Mezei, F., Richter, D. & Springer, T. (1996). *The focusing mirror at the ILL spin-echo spectrometer IN15; experimental results. J. Phys. Soc. Jpn*, **65**, Suppl. A, 312–315.

Hayter, J. B. & Mook, H. A. (1989). *Discrete thin-film multilayer design for X-ray and neutron supermirrors. J. Appl. Cryst.* **22**, 35–41.

Hayter, J. B., Penfold, J. & Williams, W. G. (1978). *Compact polarizing Soller guides for cold neutrons. J. Phys. E*, **11**, 454–458.

Hiismäki, P. (1997). *Modulation spectroscopy of neutrons with diffractometry applications.* Singapore: World Science Publishing.

Hines, W. A., Menotti, A. H., Budnick, J. L., Burch, T. J., Litrenta, T., Niculescu, V. & Raj, K. (1976). *Magnetization studies of binary and ternary alloys based on $Fe_3Si$. Phys. Rev. B*, **13**, 4060–4068.

Hock, R., Vogt, T., Kulda, J., Mursic, Z., Fuess, H. & Magerl, A. (1993). *Neutron backscattering on vibrating silicon crystals – experimental results on the neutron backscattering spectrometer IN10. Z. Phys. B*, **90**, 143–153.

Høghøj, P., Anderson, I. S., Ebisawa, T. & Takeda, T. (1996). *Fabrication and performance of a large wavelength band multilayer monochromator. J. Phys. Soc. Jpn*, **65**, Suppl. A, 296–298.

Hossfeld, F., Amadori, R. & Scherm, R. (1970). Proceedings of Instrumentation for Neutron Inelastic Scattering, IAEA, Vienna, Austria, p. 117.

Hughes, D. J. & Burgy, M. T. (1951). *Reflection of neutrons from magnetized mirrors. Phys. Rev.* **81**, 498–506.

Korneev, D. A. & Kudriashov, V. A. (1981). *Experimental determination of the characteristics of a spin-flipper with a prolonged working area. Nucl. Instrum. Methods*, **179**, 509–513.

Lushchikov, V. I., Taran, Yu. V. & Shapiro, F. L. (1969). *Polarized proton target as neutron polarizer. Sov. J. Nucl. Phys.* **10**, 669–677.

Magerl, A., Liss, K.-D., Doll, C., Madar, R. & Steichele, E. (1994). *Will gradient crystals become available for neutron diffraction? Nucl. Instrum. Methods*, A**338**, 83–89.

Magerl, A. & Wagner, V. (1994). Editors. *Focusing neutron optics. Nucl. Instrum. Methods*, A**338**, 1–150.

Maier-Leibnitz, H. (1967). *Einige Vorschläge für die Verwendung von zusammengesetzten Monochromatorkristallen fur Neutronenbeugungs- und Streumessungen. Ann. Acad. Sci. Fenn. Ser. A*, **267**, 3–17.

Maier-Leibnitz, H. (1969). Summer School on Neutron Physics, Alushta. Dubna: Joint Institute of Nuclear Physics.

Maier-Leibnitz, H. & Rustichelli, F. (1968). German Patent No. 1816542.

Maier-Leibnitz, H. & Springer, T. (1963). *The use of neutron optical devices on beam-hole experiments. J. Nucl. Energy A/B*, **17**, 217–225.

Majkrzak, C. F., Nunez, V., Copley, J. R. D., Ankner, J. F. & Greene, G. C. (1992). *Supermirror transmission polarizers for neutrons. Neutron optical devices and applications*, edited by C. F. Majkrzak & J. L. Wood, pp. 90–106. *SPIE Proc.* No. 1738. Bellingham, WA: SPIE.

Majkrzak, C. F. & Shirane, G. (1982). *Polarized neutron spectrometer developments and experiments at Brookhaven. J. Phys. (Paris)*, **43**, C7, 215–220.

Marx, D. (1971). *Microguides for neutrons. Nucl. Instrum. Methods*, **94**, 533–536.

May, C., Klimanek, P. & Magerl, A. (1995). *Plastic bending of thin beryllium blades for neutron monochromators. Nucl. Instrum. Methods*, A**357**, 511–518.

Meardon, B. H. & Wroe, H. (1977). Report RL-77-059/A. Rutherford Laboratory, Oxon, England.

Meister, H. & Weckerman, B. (1972). *A high resolution time focusing spectrometer for quasi-elastic neutron scattering.* Proceedings of the Symposium on Inelastic Neutron Scattering of Neutrons in Solids and Liquids. Vienna: IAEA.

Meister, H. & Weckerman, B. (1973). *Neutron collimators with plates of self-contracting foils. Nucl. Instrum. Methods*, **108**, 107–111.

Mezei, F. (1972). *Neutron spin-echo: a new concept in polarized thermal neutron techniques. Z. Phys.* **255**, 146–160.

Mezei, F. (1976). *Novel polarized neutron devices: supermirror and spin component amplifier. Commun. Phys.* **1**, 81–85.

**4.4.2 (*cont.*)**


Mezei, F. (1988). *Very high reflectivity supermirrors and their applications. Thin film neutron optical devices: mirrors, supermirrors, multilayer monochromators, polarizers, and beam guides*, edited by C. F. Majkrzak, pp. 10–17. *SPIE Proc.* No. 983. Bellingham, WA: SPIE.

Mildner, D. F. R. (1994). *Neutron focusing optics for low-resolution small-angle scattering. J. Appl. Cryst.* **27**, 521–526.

Mücklich, F. & Petzow, G. (1993). *Development of beryllium single crystal material for monochromator applications. Mineral processing & extractive metallurgy review, beryllium – issue*. New York: Gordon and Breach.

Nunes, A. C. (1974). *A focusing low-angle neutron diffractometer. Nucl. Instrum. Methods*, **119**, 291–293.

Pickart, S. J. & Nathans, R. (1961). *Unpaired spin density in ordered $Fe_3Al$. Phys. Rev.* **123**, 1163–1171.

Reed, R. E., Bolling, E. D. & Harmon, H. E. (1973). Solid State Division Report, pp. 129–131. Oak Ridge National Laboratory, TN, USA.

Riste, T. (1970). *Singly bent graphite monochromators for neutrons. Nucl. Instrum. Methods*, **86**, 1–4.

Rossbach, M., Schärpf, O., Kaiser, W., Graf, W., Schirmer, A., Faber, W., Duppich, J. & Zeisler, R. (1988). *The use of focusing supermirror neutron guides to enhance cold neutron fluence rates. Nucl. Instrum. Methods*, B**35**, 181–190.

Schaerpf, O. (1975). *Magnetic neutron guide tube for polarization of thermal neutrons with $P = 97\%$ irrespective of wavelength. J. Phys. E*, **8**, 268–269.

Schaerpf, O. (1989). *Properties of beam bender type neutron polarizers using supermirrors. Physica (Utrecht) B*, **156&157**, 639–646.

Schaerpf, O. & Stuesser, N. (1989). *Recent progress in neutron polarizers. Nucl. Instrum. Methods*, A**284**, 208–211.

Schärpf, O. (1980). *Neutron spin echo. Lecture notes in physics*, Vol. 128, edited by F. Mezei, pp. 27–52. Heidelberg: Springer-Verlag.

Schärpf, O. & Capellmann, H. (1993). *The xyz-difference method with polarized neutrons and the separation of coherent, spin-incoherent, and magnetic scattering cross sections in a multidetector. Phys. Status Solidi A*, **135**, 359–379.

Schefer, J., Medarde, M., Fischer, S., Thut, R., Koch, M., Fischer, P., Staub, U., Horisberger, M., Böttger, G. & Dönni, A. (1996). *Sputtering method for improving neutron composite germanium monochromators. Nucl. Instrum. Methods*, A**372**, 229–232.

Schelten, J. & Alefeld, B. (1984). *Backscattering spectrometer with adapted Q-resolution at the pulsed neutron source*. Report No. 1954, pp. 378–389. KFA Jülich, Germany.

Scherm, R., Dolling, G., Ritter, R., Schedler, E., Teuchert, W. & Wagner, V. (1977). *A variable-curvature analyser crystal for three axis spectrometers. Nucl. Instrum. Methods*, **143**, 77–85.

Scherm, R. H. & Kruger, E. (1994). *Bragg optics – focusing in real and k space. Nucl. Instrum. Methods*, A**338**, 1–8.

Schmatz, W., Springer, T., Schelten, J. & Ibel, K. (1974). *Neutron small-angle scattering: experimental techniques and applications. J. Appl. Cryst.* **7**, 96–116.

Schoenborn, B. P., Caspar, D. L. D. & Kammerer, O. F. (1974). *A novel neutron monochromator. J. Appl. Cryst.* **7**, 508–510.

Sears, V. F. (1997). *Bragg reflection in mosaic crystals. Acta Cryst.* A**53**, 35–54.

Shapiro, S. M. & Chesser, N. J. (1972). *Characteristics of pyrolytic graphite as an analyser and higher order filter in neutron scattering experiments. Nucl. Instrum. Methods*, **101**, 183–186.

Steinberger, J. & Wick, G. C. (1949). *On the polarization of slow neutrons. Phys. Rev.* **76**, 994–995.

Surkau, R., Becker, J., Ebert, M., Grossman, T., Heil, W., Hofmann, D., Humblot, H., Leduc, M., Otten, E. W., Rohe, D., Siemensmeyer, K., Steiner, M., Tasset, F. & Trautmann, N. (1997). *Realization of a broad band neutron spin filter with compressed, polarized $^3He$ gas. Nucl. Instrum. Methods*, A**384**, 444–450.

Tasset, F. & Resouche, E. (1995). *Optimum transmission for a $^3He$ neutron polarizer. Nucl. Instrum. Methods*, A**359**, 537–541.

Turchin, V. F. (1965). *Slow neutrons*. Jerusalem: Israel Program for Scientific Translations.

Turchin, V. F. (1967). Deposited Paper, Atomic Energy 22.

Vogt, T., Passell, L., Cheung, S. & Axe, J. D. (1994). *Using wafer stacks as neutron monochromators. Nucl. Instrum. Methods*, A**338**, 71–77.

Wagner, V., Friedrich, H. & Wille, P. (1992). *Performance of a high-tech neutron velocity selector. Physica (Utrecht), B* **180&181**, 938–940.

Wagshul, M. E. & Chupp, T. E. (1994). *Laser optical pumping of high-density Rb in polarized $^3He$ targets. Phys. Rev. A*, **49**, 3854–3869.

Williams, W. G. (1988). *Polarised neutrons. Oxford Series on Neutron Scattering in Condensed Matter*, Vol. 1. Oxford: Clarendon Press.

Wright, A. F., Berneron, M. & Heathman, S. P. (1981). *Radial collimator system for reducing background noise during neutron diffraction with area detectors. Nucl. Instrum. Methods*, **180**, 655–658.

Zachariasen, W. H. (1945). *Theory of X-ray diffraction in crystals*. New York: Wiley.

Zeyen, C. M. E. & Rem, P. C. (1996). *Optimal Larmor precession magnetic field shapes: application to neutron spin echo three-axis spectrometry. Meas. Sci. Tech.* **7**, 782–791.


**4.4.3**


Bjerrum Møller, H. & Nielson, M. (1970). *Proceedings of IAEA panel meeting on instrumentation for neutron inelastic scattering research*. Vienna: IAEA.

Caglioti, G., Paoletti, A. & Ricci, F. P. (1960). *On resolution and luminosity of a neutron diffraction spectrometer for single crystal analysis. Nucl. Insrum. Methods*, **9**, 195–198.

Chesser, N. J. & Axe, J. D. (1973). *Derivation and experimental verifiation of the normalised resolution function for inelastic neutron scattering. Acta Cryst.* A**29**, 160–169.

Cooper, M. J. (1968). *The resolution function in neutron diffractometry. IV. Application of the resolution function to the measurement of Bragg peaks. Acta Cryst.* A**24**, 624–627.

Cooper, M. J. & Nathans, R. (1967). *The resolution function in neutron diffractometry. I. The resolution function of a neutron diffractometer and its application to phonon measurements. Acta Cryst.* **23**, 357–367.

Cooper, M. J. & Nathans, R. (1968). *The resolution function in neutron diffractometry. II. Experimental determination and properties of the 'elastic two-crystal' resolution function. Acta Cryst.* A**24**, 619–624.

### 4.4.3 (*cont.*)


Dorner, B. (1972). *The normalization of the resolution function for inelastic neutron scattering and its applications*. *Acta Cryst*. A**28**, 319–327.

Mitchell, P. W., Cowley, R. A. & Higgins, S. A. (1984). *The resolution fuction of triple-axis neutron spectrometers in the limit of small scattering angles*. *Acta Cryst*. A**40**, 152–160.

Nielsen, M. & Bjerrum Møller, H. (1969). *Resolution of a triple-axis spectrometer*. *Acta Cryst*. A**25**, 547–550.

Pynn, R. (1975). *Lorentz factor for triple-axis spectrometers*. *Acta Cryst*. B**31**, 2555–2556.

Pynn, R. (1984). *Reactor based neutron scattering instrumentation*. *Rev. Sci. Instrum*. **55**, 837–848.

Pynn, R., Fujii, Y. & Shirane, G. (1983). *The resolution function of a perfect-crystal three-axis X-ray spectrometer*. *Acta Cryst*. A**39**, 38–46. [There is an omission in equation (*A*3) of this reference; the relation $X_3 = k/\alpha_A$ should be added.]

Robinson, R. A., Pynn, R. & Eckert, J. (1985). *An improved constant-Q spectrometer for pulsed neutron sources*. *Nucl. Instrum. Methods*, A**241**, 312–324.

Stedman, R. (1968). *Energy resolution and focusing in inelastic scattering experiments*. *Rev. Sci. Instrum*. **39**, 878–883.

Steinsvoll, O. (1973). *The resolution function of a hybrid neutron spectrometer*. *Nucl. Instrum. Methods*, **106**, 453–459.

Tindle, G. L. (1984). *A new instrumental factor in triple-axis spectrometry and Bragg reflectivity measurements*. *Acta Cryst*. A**40**, 103–107.

Werner, S. A. (1971). *Choice of scans in neutron diffraction*. *Acta Cryst*. A**27**, 665–669.

Werner, S. A. & Pynn, R. (1971). *Resolution effects in the measurement of phonons in sodium metal*. *J. Appl. Phys*. **42**, 4736–4749.


### 4.4.4


Bacon, G. E. (1975). *Neutron diffraction*, 3rd ed. Oxford: Clarendon Press.

Glättli, H. & Goldman, M. (1987). *Nuclear magnetism. Methods of experimental physics*, Vol. 23, *Neutron scattering* Part C, edited by K. Sköld & D. L. Price, pp. 241–286. New York: Academic Press.

Klein, A. G. & Werner, S. A. (1983). *Neutron optics*. *Rep. Prog. Phys*. **46**, 259–335.

Koester, L. (1977). *Neutron scattering lengths and fundamental neutron interactions*. *Springer Tracts in Modern Physics*, Vol. 80, pp. 1–55. Berlin: Springer Verlag.

Koester, L., Rauch, H. & Seymann, E. (1991). *Neutron scattering lengths: a survey of experimental data and methods*. *At. Data Nucl. Data Tables*, **49**, 65–120.

Koester, L., Waschkowski, W. & Meier, J. (1988). *Experimental study on the electric polarizability of the neutron*. *Z. Phys*. A**329**, 229–234.

Lynn, J. E. & Seegar, P. A. (1990). *Resonance effects in neutron scattering lengths of rare-earth nuclides*. *At. Data Nucl. Data Tables*, **44**, 191–207.

Mughabghab, S. F. (1984). *Neutron cross sections*, Vol. 1, Part *B: Z = 61–100*. New York: Academic Press.

Mughabghab, S. F., Divadeenam, M. & Holden, N. E. (1981). *Neutron cross sections*, Vol. 1, Part *A: Z = 1–60*. New York: Academic Press.

Sears, V. F. (1984). *Thermal-neutron scattering lengths and cross sections for condensed-matter research*. Report AECL-8490. Atomic Energy of Canada Limited, Chalk River, Ontario, Canada.

Sears, V. F. (1985). *Local-field refinement of neutron scattering lengths*. *Z. Phys*. A**321**, 443–449.

Sears, V. F. (1986*a*). *Electromagnetic neutron–atom interactions*. *Phys. Rep*. **141**, 281–317.

Sears, V. F. (1986*b*). *Neutron scattering lengths and cross sections*. *Methods of experimental physics*, Vol. 23, *Neutron scattering*, Part *A*, edited by K. Sköld & D. L. Price, pp. 521–550. New York: Academic Press.

Sears, V. F. (1989). *Neutron optics*. Oxford University Press.

Sears, V. F. (1992*a*). *Scattering lengths for neutrons*. *International tables for crystallography*, Vol. C, edited by A. J. C. Wilson, pp. 383–391. Dordrecht: Kluwer Academic Publishers.

Sears, V. F. (1992*b*). *Neutron scattering lengths and cross sections*. *Neutron News*, **3**, 26–37.

Sears, V. F. (1996). *Correction of neutron scattering lengths for electromagnetic interactions*. *J. Neutron Res*. **3**, 53–62.

Werner, S. A. & Klein, A. G. (1986). *Neutron optics*. *Methods of experimental physics*, Vol. 23, *Neutron scattering*, Part *A*, edited by K. Sköld & D. L. Price, pp. 259–337. New York: Academic Press.

Young, H. D. (1962). *Statistical treatment of experimental data*. New York: McGraw–Hill.


### 4.4.5


Clementi, E. & Roetti, C. (1974). *Roothan–Hartree–Fock atomic wavefunctions*. *At. Data Nucl. Data Tables*, **14**, 177–478.

Desclaux, J. P. & Freeman, A. J. (1978). *Dirac–Fock studies of some electronic properties of actinide ions*. *J. Magn. Magn. Mater*. **8**, 119–129.

Forsyth, J. B. & Wells, M. (1959). *On an analytic approximation to the atomic scattering factor*. *Acta Cryst*. **12**, 412–414.

Freeman, A. J. & Desclaux, J. P. (1979). *Dirac–Fock studies of some electronic properties of rare-earth ions*. *J. Magn. Magn. Mater*. **12**, 11–21.

Lisher, E. J. & Forsyth, J. B. (1971). *Analytic approximations to form factors*. *Acta Cryst*. A**27**, 545–549.


### 4.4.6


Hutchings, M. T. & Windsor, C. G. (1987). *Industrial applications of neutron scattering*. In *Methods of experimental physics*, Vol. 23, Part C, edited by K. Sköld & D. L Price. New York: Academic Press.